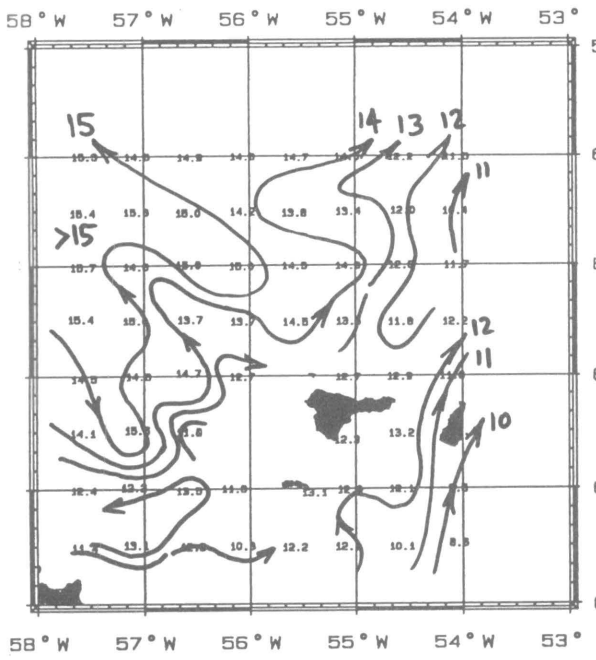

AMLR 92, SURVEY A
DYNAMIC HEIGHT (200 db)
19 JAN to 02 FEB 1992

FIGURE 1-A

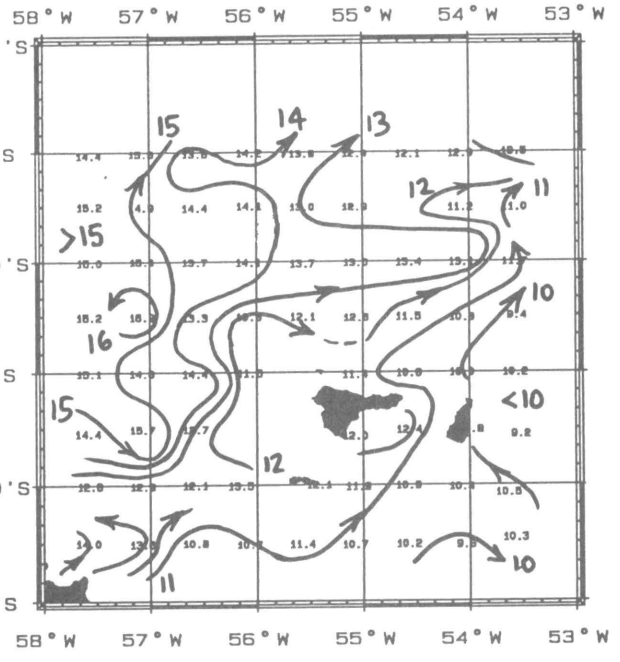

AMLR 92, SURVEY D
DYNAMIC HEIGHT (200 db)
28 FEB to 10 MAR 1992

FIGURE 1-B

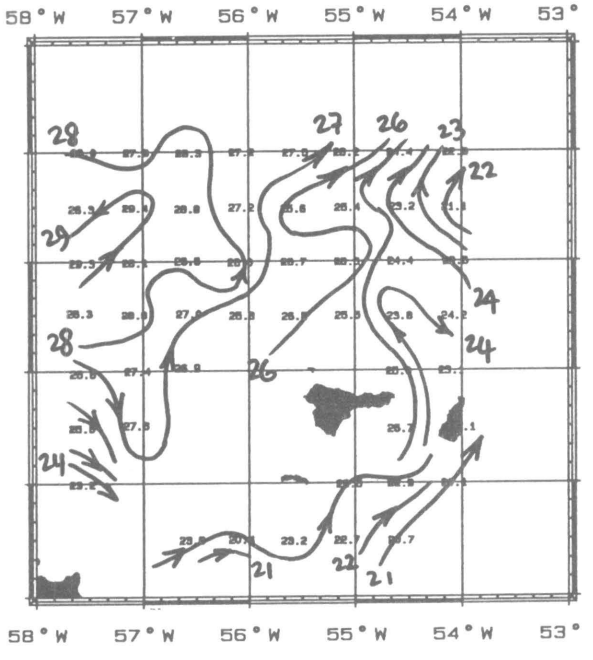

AMLR 92, SURVEY A
DYNAMIC HEIGHT (500 db)
19 JAN to 02 FEB 1992

FIGURE 1-C

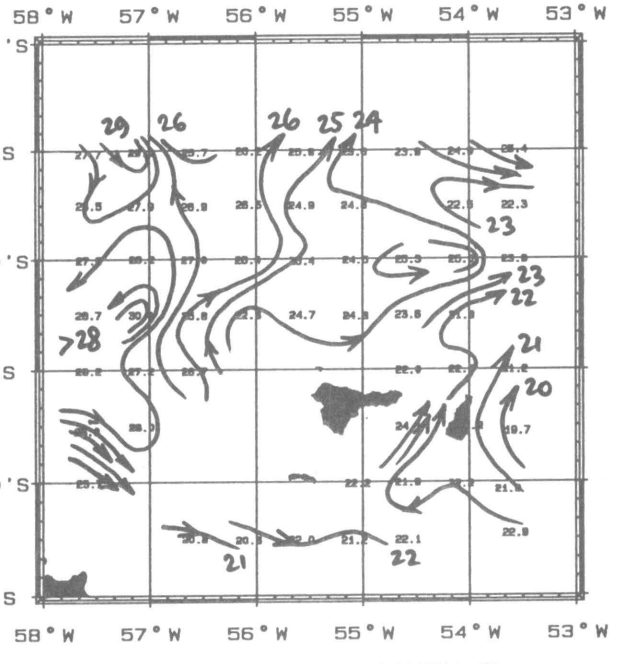

AMLR 92, SURVEY D
DYNAMIC HEIGHT (500 db)
28 FEB to 10 MAR 1992

FIGURE 1-D

Figure 1. Dynamic heights and geostrophic flow during the two large-scale surveys of AMLR 1991-1992. *(A)* Surface relative to 200 decibar, survey A; *(B)* surface relative to 200 decibar, survey D; *(C)* surface relative to 500 decibar, survey A; *(D)* surface relative to 500 decibar, survey B.

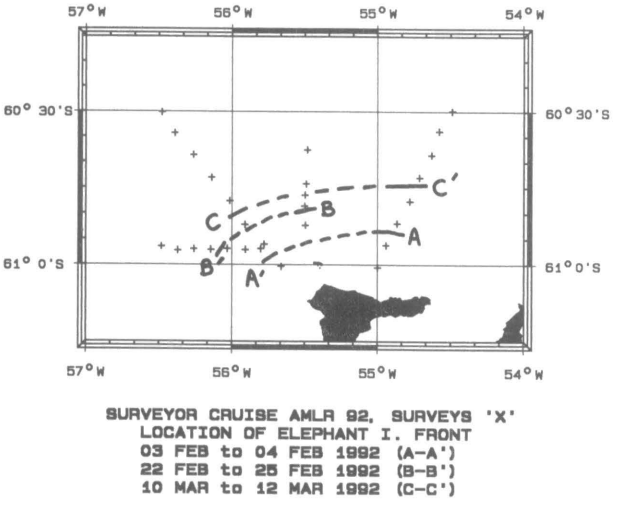

Figure 2. Location of frontal boundaries north of Elephant Island from cross-shell CTD transects.

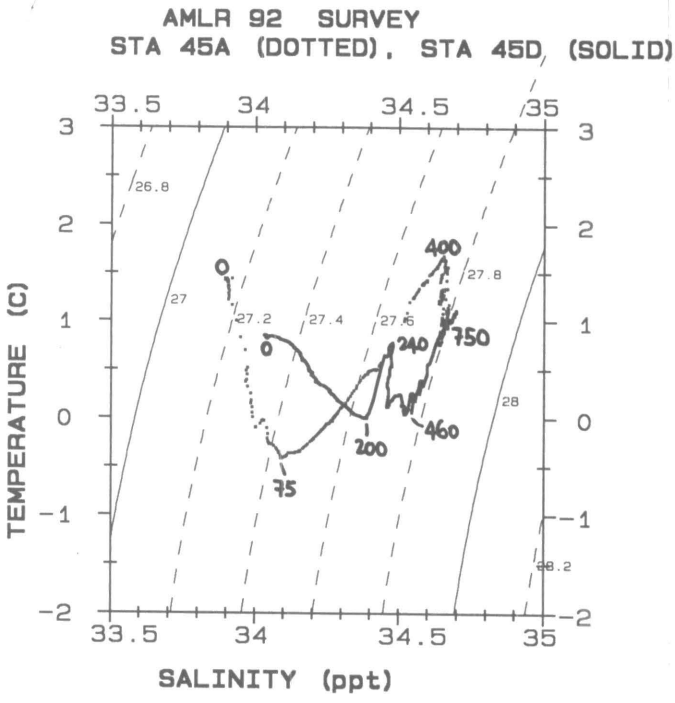

Figure 3. T/S relationship of water column at station 45 on 26 January and 3 March 1992. Depth of major T/S inversions are annotated on the curves.

phy of the surface water at Elephant Island, Antarctica. *Continental Shelf Research.*

Helbling, E. W., A. F. Amos, N. Silva, V. Villafane, and O. Holm-Hansen. In press. Phytoplankton distribution and abiotic measurements over a frontal system north of Elephant Island, Antarctica. *Antarctic Science.*

Holm-Hansen, O., V. E. Villafane, and E. W. Helbling. 1992. AMLR program: Phytoplankton abundance and rates of primary production around Elephant Island area. *Antarctic Journal of the U.S.,* this issue.

Loeb, V. and V. Siegal. 1992. AMLR program: Krill stock structure in the Elephant Island area. *Antarctic Journal of the U.S.,* this issue.

Niiler, P. P., A. F. Amos, and J. -H. Hu. 1991. Water masses and 200m relative geostrophic circulation in the western Bransfield Strait region. *Deep Sea Research,* 38(8/9):943-959.

Rosenberg, J., R. P. Hewitt, and R. S. Holt. 1992. The U.S. AMLR program: 1991-1992 field season activities. *Antarctic Journal of the U.S.,* this issue.

AMLR program: A comparison between the summer meteorological conditions at Seal Island and those over the adjacent waters of the Drake Passage

A. F. Amos

Marine Science Institute
University of Texas at Austin
Port Aransas, Texas 78373

Seal Island is the largest of a small group of islands located north of Elephant Island, the northernmost of the South Shetland Islands (see Rosenberg et al. for location map). It is the site of an annual study of seals and penguins by the Antarctic Marine Living Resource (AMLR) program (Croll et al. this issue). The waters of the adjacent continental shelf and the Drake Passage are the primary study area of the AMLR program's fieldwork aboard the National Oceanic and Atmospheric Administration (NOAA) ship *Surveyor.* The University of Texas's program in physical oceanography is part of the AMLR multidisciplinary study of the distribution of krill (*Euphausia superba*). Our work has two major tasks: to study the hydrography of the upper water column as it relates to the observed distribution of the biological organisms (Helbling et al. in press; Amos and Lavender this issue) and to monitor the surface meteorological conditions that may affect the water structure (Amos this issue).

To accomplish the second task, continuous measurements of winds, air temperature, humidity, pressure, solar radiation parameters, sea temperature, salinity, beam transmission, and chlorophyll fluorescence are made while the ship is under way. This year a Coastal Climate automatic weather station was installed on Seal Island and operated from mid-December 1991 to mid-March 1992. Weather data were of interest for the seal and

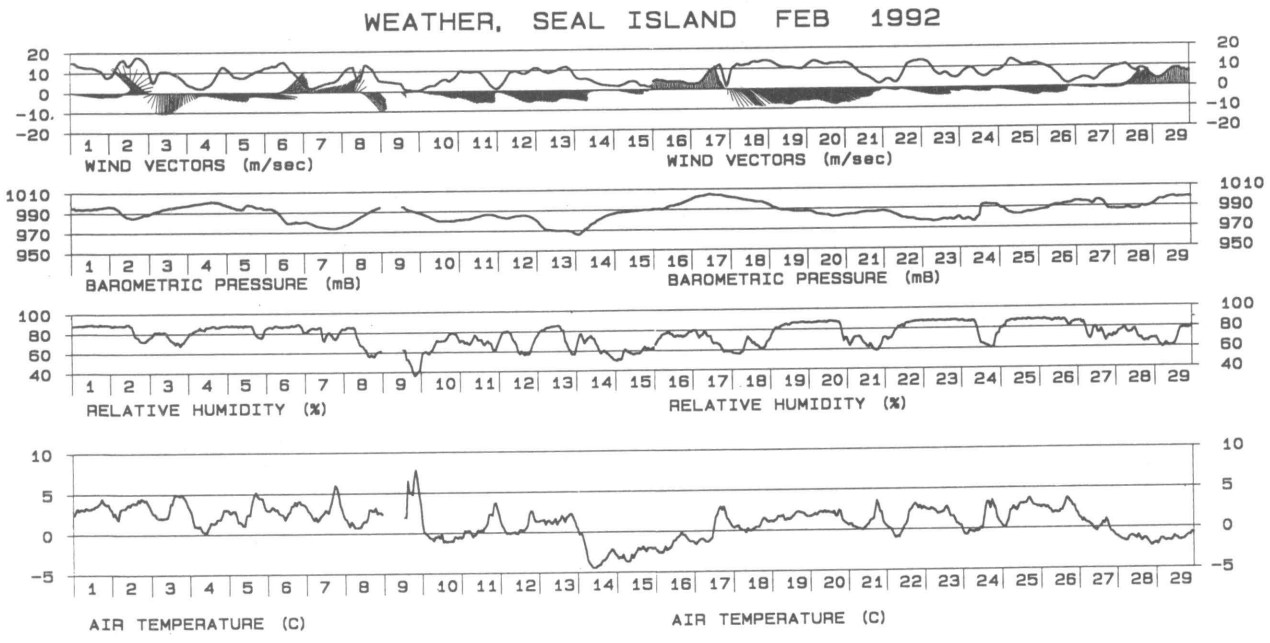

Figure 1. Time series weather data, Seal Island, February 1992. Top trace: wind speed and wind vectors (m.sec^{1}); north is up. Second trace: barometric pressure, reduced to sea level (mb). Third trace: relative humidity (percent). Bottom trace: air temperature (°C).

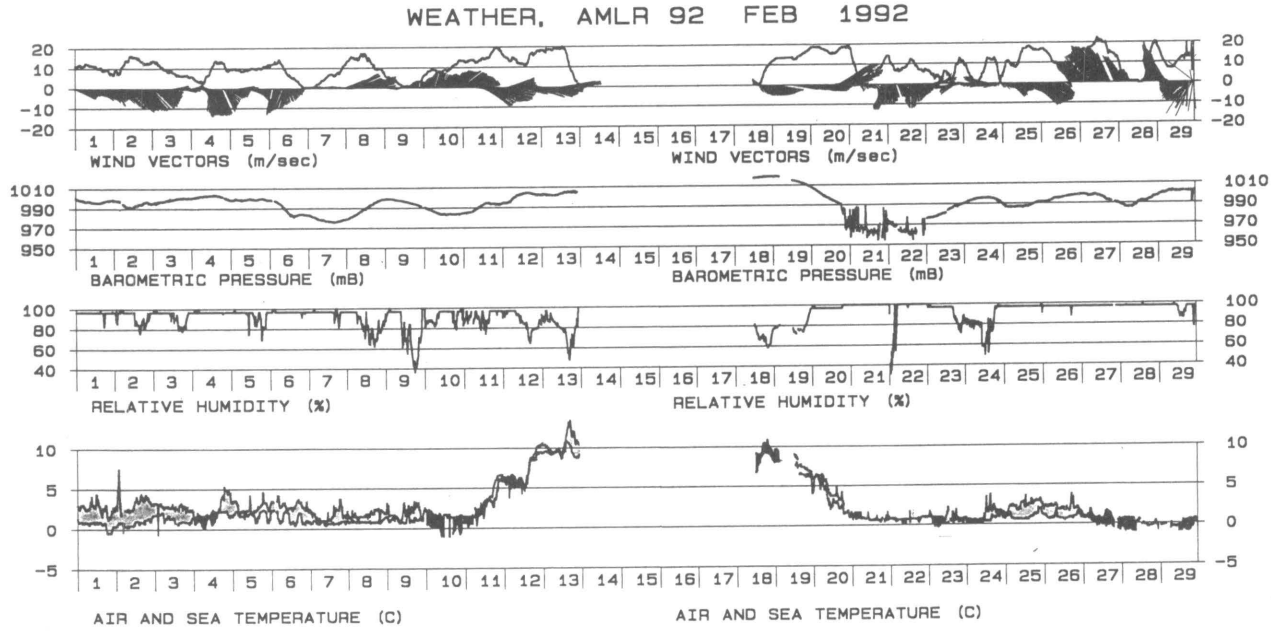

Figure 2. Time series weather data from AMLR underway equipment aboard *Surveyor*, February 1992. Traces as in figure 1, except bottom trace: air and sea temperature (°C); *gray shading*: air temperature greater than sea temperature; *solid shading*: air temperature greater than sea temperature. Gap in trace is when *Surveyor* was in port (Punta Arenas, Chile). Noise on pressure and humidity traces on 21 and 22 February is due to electronic interference.

penguin studies and also provided a comparison between a stationary "island" station and *Surveyor*'s traveling "oceanic" station. The Seal Island Zeno weather station is located at an altitude of 120 meters at 60° 59.1′ S 55° 23.1′ W on an unobstructed hill above the encampment. The parameters measured were wind speed and direction, air temperature, humidity, and barometric pressure. In the Zeno, data are recorded internally at 10-minute intervals using a microprocessor. The Seal Island crew downloaded data into a portable PC at approximately 2-week intervals.

Aboard *Surveyor*, a Coastal Climate Weatherpak shipboard weather system provides wind and air temperature data. The sensors are located 35 meters above sea level. Data from the ship's Global Positioning Satellite (GPS) navigation system and

Mean and extreme conditions on Seal Island and *Surveyor*

	Air temperature (°C)			Humidity (%)			Barometer (mb)			Winds (m.sec^{-1})		
	Max	Min	Mean	Max	Min	Mean	Max	Min	Mean	Max	Min	Mean
SEAL I	9.1	-3.0	1.63	93	31	81.5	1016.1	973.6	991.9	19.6	0.0	3.1/060
(date)	2/09	3/06		*	2/09		3/03	2/07		2/02	*	
SURVEYOR	6.7	-4.0	2.21	100	68	94.4	1017.4	974.2	994.0	23.7	1.0	3.8/117
(date)	1/18	2/10		**	2/10		3/02	2/07				

Note: Reading was obtained on several dates; **occurred on many dates. Mean wind directions are those to which the wind is blowing.

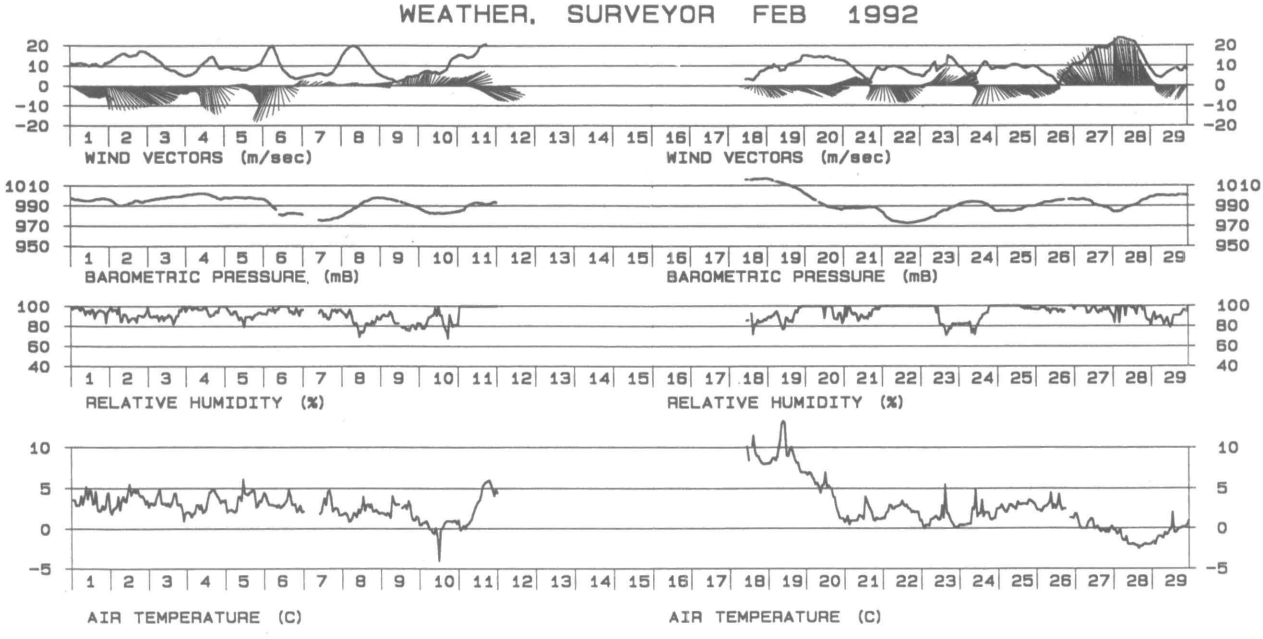

Figure 3. Time-series weather data from deck watch observations aboard *Surveyor*, February 1992. Traces as figure 1.

thermosalinograph are output to a shipwide local area network (LAN). Information is extracted from the LAN by a PC program developed by the author to integrate these data with data from several different environmental sensors for storage and real-time display and plotting. *Surveyor*'s deck watch also manually records weather data on a standard deck log and daily weather observation sheet. Wind data are read from the Weatherpak display, but wet and dry bulb temperatures are obtained from a standard sling psychrometer and barometric pressure from the ship's aneroid barometer.

I compare here the February 1992 weather data from the Seal Island (figure 1) with those from the AMLR underway system (figure 2) and also with the data collected by *Surveyor*'s deck watch (figure 3). These data have not yet been fully corrected. During February, *Surveyor* returned to Chile between legs 1 and 2, so comparable data were collected in the vicinity of Seal Island only from 1 through 10 February and 21 through 29 February. The most obvious similarity is in the atmospheric pressures which, when reduced to sea level for all three barometers (altitudes: Seal Island, 120 meters; AMLR, 10 meters; *Surveyor*, 10 meters), are identical within a millibar or so, with occasional phase lags of about an hour between the pressure measured on the ship and the pressure measured on Seal Island. Differences can be seen in air temperature—with a much greater diurnal range on Seal Island than over the Drake Passage—lower humidity and wind speed, and directional variability. The table lists the mean and extreme conditions on Seal Island and *Surveyor* during the time the ship was near Elephant Island.

Surface humidity is important in remote satellite sensing, global climate (Liu et al. 1992), and ocean-atmosphere heat flux calculations (Hsu and Blanchard 1989). Over the southern ocean, few reliable humidity measurements have been made. One problem is the difficulty of measuring humidity in the near-freezing, near-saturation conditions encountered in antarctic seas. Our humidity sensor output on *Surveyor* frequently limited at 97.2 percent and stayed there for hours or even days. At first we believed that the sensor was malfunctioning, but comparisons between psychrometer readings that frequently showed both thermometers reading the same (i.e., 100 percent relative humidity) confirmed saturation (figures 2 and 3). Likewise, the humidity sensor atop the Seal Island hill appeared to limit at 93 percent (figure 1). These data will be used to explore ocean-atmosphere exchange processes, the effect of winds on the surface circulation, and the location of fronts that may bound krill populations. The Seal Island weather station was left in place, recording at 1-hour intervals. It will be recovered in December 1992.

This work was supported by NOAA award NA27FR001-10 to the UTMSI. I wish to thank the officers and crew of the NOAA ship *Surveyor*, the bridge watch who collected the data used in figure 3, lead electronic technician Mark May, and electronic technician Frank Gomes. I am also grateful to Margaret Lavender (legs 1 and 2) and Jeff Heimann (leg 1), who kept the still-capricious weather system going on their watches. Many thanks to Peter Boveng, Mike Goebel, and Don Croll, who climbed the slippery hill several times to download the Seal Island data.

References

Amos, A. F. 1991. AMLR program: Meteorological conditions in the vicinity of Elephant Island. *Antarctic Journal of the U.S.*, 26:213-215.

Amos, A. F. and M. K. Lavender. 1991. AMLR program: Water masses in the vicinity of Elephant Island. *Antarctic Journal of the U.S.*, 26:210-213.

Amos, A. F. and M. K. Lavender. 1992. AMLR program: Dynamics of the summer hydrographic regime at Elephant Island. *Antarctic Journal of the U.S.*, this issue.

Croll, S. A., P. L. Boveng, M. E. Goebel, J. K. Jansen, S. C. Manley, H. D. Douglas, and J. L. Bengtson. 1992. AMLR program: Penguin and fur seal studies on Seal Island, South Shetland Islands. *Antarctic Journal of the U.S.*, this issue.

Helbling, E. W., A. F. Amos, N. Silva, V. Villafañe, and O. Holm-Hansen. In press. Phytoplankton distribution and abiotic measurements over a frontal system north of Elephant Island, Antarctica. *Antarctic Science.*

Hsu, S. S., and B. W. Blanchard. 1989. The relationship between total precipitable water and surface-level humidity over the sea surface: A further evaluation. *Journal of Geophysical Research*, 94(C10):14,539-14,545.

Liu, W. T., W. Tang, and F. J. Wentz. 1992. Precipitable water and surface humidity over global oceans from Special Sensor Microwave Imager and European Center for Medium Range Weather Forecasts. *Journal of Geophysical Research*, 97(C2):2,251-2,264.

Rosenberg, Jane E., Roger P. Hewitt, and Rennie S. Holt. 1992. The U.S. AMLR program: 1991-1992 field season activities. *Antarctic Journal of the U.S.*, this issue.

Palmer long-term ecological research (LTER): An overview of the 1991-1992 season

ROBIN M. ROSS AND
LANGDON B. QUETIN

Marine Science Institute
University of California at Santa Barbara
Santa Barbara, California 93106

Long-term ecological research (LTER) recognizes that some ecological phenomena occur on time scales of decades or centuries, and that investigations on these time scales are not routinely supported by funding agencies. Without an understanding of interannual variability over the long term, interpretation of ecological experiments and distinguishing long-term trends from cyclic changes in natural ecosystems are difficult. The LTER Network, sponsored by the National Science Foundation, has grown during the last decade to a total of 18 sites in ecosystems ranging from tall grass prairies to tundra. To facilitate comparison and the ability to construct ecological generalities, all sites are required to set up research efforts in five core areas:

(1) pattern and control of primary production;

(2) spatial and temporal distribution of populations representing trophic structures;

(3) pattern and control of organic matter accumulation;

(4) pattern of inorganic inputs and movements of nutrients; and

(5) pattern and frequency of disturbance to the research site.

The Palmer LTER, established in October of 1990, focuses on the pelagic marine ecosystem in the Antarctic, and the ecological processes which link the extent of annual pack ice to the biological dynamics of different trophic levels. Pack ice may be a major physical factor affecting the structure and function of polar biota. Interannual cycles and/or trends in the annual extent of pack ice are hypothesized to impact all levels of the food web, from total annual primary production to breeding success in seabirds. In the region around Palmer Station (64°40' S 64° W) west of the Antarctic Peninsula, the maximum extent of pack ice varies from near zero to halfway across Drake Passage (Quetin and Ross 1991), and appears to vary on a 6- to 8-year cycle. Satellite data on the maximum extent of pack ice in the Weddell Sea sector shows cold winters with heavy ice pack in 1973, and 1980 and 1981 (Zwally et al. 1983; Smith et al. 1988), and personal observations (Palmer Station personnel, Quetin and Ross) confirm that winters of 1980 and 1981, and 1986 and 1987, had heavy ice cover in the region around Palmer Station.

The overall objectives of the Palmer LTER are

(1) to document interannual variability in the development and extent of annual pack ice;

(2) to document interannual variability in life-history parameters of primary producers and populations of key species from different trophic levels, and to quantify the processes underlying this natural variation;

(3) to construct models that

- Link the ecosystem processes to the physical environmental variables,
- Simulate the spatial/temporal relationships between representative populations, and
- Predict and validate the impacts of altered periodicities in the annual extent of pack ice on ecosystem dynamics.

The Palmer LTER is presently composed of five components led by principal investigators from two universities (see table). Each year the core LTER measurements will include results from a sampling program based at Palmer Station throughout the austral spring and summer, and an annual cruise covering a mesoscale study region of about 400 kilometers by 200 kilometers. Two cruises are planned for the austral fall and austral spring of 1993 to define the temporal/spatial variability in biological, chemical, optical, and physical characteristics of the mesoscale study region, and to study processes underlying the interactions between ice cover and the marine ecosystem.

Some preliminary results from the first field season are presented in accompanying articles in this series. During our first season the Palmer LTER staged two major research efforts: an austral spring cruise on the R/V *Polar Duke* from 7 to 21 November 1991, and a nearshore monitoring and experimental program centered at Palmer Station from 15 October 1991 to 7 March 1992.

Components of the Palmer LTER

Research area	Principal investigator(s)
Remote sensing, climatology, environmental optics, hydrography, and bio-optical modeling of primary production	Ray Smith (Department of Geography, University of California at Santa Barbara)
Phytoplankton and inorganic nutrient dynamics; photosynthetic regulation of bio-optical modeling of primary production	Barbara Prezelin (Department of Biological Sciences, University of California at Santa Barbara)
Distribution, abundance and ecological physiology of secondary producers; biological/physical modeling	Robin Ross and Langon Quetin (Marine Science Institute, University of California at Santa Barbara)
Seabird population dynamics and reproductive ecology; population modeling	William Fraser and Wayne Trivelpiece (Center for Coastal Physical Oceanography, Old Dominion University)
Oceanic circulation, biological/physical and population modeling	Eileen Hofmann and John Klinck (Center for Coastal Physical Oceanography, Old Dominion University)

During the austral spring cruise, mesoscale variability of hydrographic and optical characteristics of the water column, phytoplankton biomass, photosynthetic potential and community composition, and distribution, abundance, and physiological condition of selected secondary producers (particularly antarctic krill, *Euphausia superba*) was successfully documented (Dallmann Bay, Palmer Basin, and Renaud transect lines, Waters and Smith). Heavy ice cover and westerly winds locked the ship in ice a few miles from Palmer Station for the first 4 days of the cruise, and also prevented the ship from occupying the inshore stations on both the Palmer Basin and Renaud lines.

The annual nearshore program (within 2 nautical miles of the station) includes research on the hydrography, chemistry, and biology of waters surrounding Palmer Station, and the population dynamics and ecology of Adélie penguins and south polar skuas that nest on nearby islands. This year heavy ice cover in early spring made Zodiac operations difficult, slowing some aspects of the nearshore research program, although scuba divers successfully collected young antarctic krill from under the ice for assays of physiological condition. Once Arthur Harbor cleared of pack ice in early December, access to the seabird colonies improved, and weekly surveys of the nearshore waters with well-equipped Zodiacs (transects in Waters and Smith) began. To add essential information to the Palmer LTER long-term data base, an automatic weather station was installed on the end of Bonaparte Point to the southeast of Palmer Station. Additional automatic weather stations will be installed at locations throughout the mesoscale study region as funding and logistical support permits.

This work was supported by National Science Foundation grant DPP 90-901127, and is Palmer LTER Publication No. 3.

References

Quetin, L. B. and R. M. Ross. 1991. Behavioral and physiological characteristics of the antarctic krill, *Euphausia superba*. *American Zoologist*, 31(1):117-146.

Ross, R. M. and L. B. Quetin. 1991. Ecological physiology of larval euphausiids, *Euphausia superba* (Euphausiacea). *Memoirs of the Queensland Museum*, 31:321-333.

Smith, W. O., N. K. Keene, and J. C. Comiso. 1988. Interannual variability in estimated primary productivity of the antarctic marginal ice zone. In D. Sahrhage (Ed.), *Antarctic Ocean and Resources Variability*. Berlin: Springer-Verlag, 131-9.

Waters, K. and R. Smith. 1992. Palmer LTER: A sampling grid for the Palmer LTER program. *Antarctic Journal of the U.S.*, this issue.

Zwally, H. J., C. L. Parkinson, and J. C. Comiso. 1983. Variability of antarctic sea ice and changes in carbon dioxide. *Science*, 220:1,005-1,012.

Palmer LTER: A sampling grid for the Palmer LTER program

KIRK J. WATERS AND RAYMOND C. SMITH

Center for Remote Sensing and Environmental Optics
and
Department of Geography
University of California at Santa Barbara
Santa Barbara, California 93106

The antarctic long-term ecological research (LTER) program will focus on the palegic marine ecosystem and the ecological processes which link the extent of annual pack ice to the biological dynamics of different trophic levels. The Palmer LTER site is centered near Palmer Station, Anvers Island midway down the Antarctic Peninsula (64°40' S 64°03' W) and will include a long-term comprehensive measurement program of this ice dominated system. Like other LTERs the Palmer LTER will investigate phenomena that occur on time scales of years to decades in order to separate long-term (decadal) systematic trends from interannual variability in physical conditions and populations. In order to structure our long-term monitoring we created a sampling grid analogous to the well-known CalCOFI grid along the west coast of North America. The PalLTER grid is west of the Antarctic Peninsula and covers an area of 900 kilometers (roughly parallel to the peninsula) by 200 kilometers (on- to offshore) (figure 1). Within this grid, cardinal lines spaced every 100 kilometers along the peninsula and cardinal points spaced every 20 kilometers on to offshore will comprise basic sampling stations (table 1). Imbedded within this large-scale or peninsula grid is a finer-scale grid specific to the immediate area of Palmer Station (figure 2, table 2). It is anticipated that other investigators working in this area may wish to reference their work to this PalLTER grid as a long-term data base is developed for this region.

The need for fixed geographic station locations that could be visited repeatedly over time scales of many years and the desire for a regularly spaced grid to simplify modeling computations motivated our effort. The difficulty in laying out such a grid in a polar region where lines of longitude rapidly converge complicated the problem. The recognition that increased use of Geographical Position Systems (GPS) would lead to outdated navigation charts leads us to base the grid on GPS positions.

We defined the PalLTER grid using a universal transverse Mercator (UTM) projection for zone minus 20 with the Geodetic Reference System 1980 (GRS80) spheriod (cf. Maling 1992). A UTM grid provides a coordinate system that is roughly Cartesian near the center point. By rotating the UTM grid by 50 degrees counterclockwise about a point near Palmer Station at 64°56' S 64°24' W), we obtain a grid that is approximately parallel to the peninsula in this region. Designating X as the axis running parallel to the peninsula for the rotated grid, and Y as the axis running perpendicular to the peninsula, we define LTER coordinates/stations as xxx.yyy where xxx is the distance along the X axis in kilometers and yyy is the distance along the Y axis in kilometers. We set the center point of the UTM grid (64°56' S 64°24' W) as station 600.040, thus completely defining all stations.

The conversion from UTM coordinates to latitude-longitude is done with the program PLANE-PC developed for interactive grid coordinates conversion by Jack Waananen, U.S. Geological

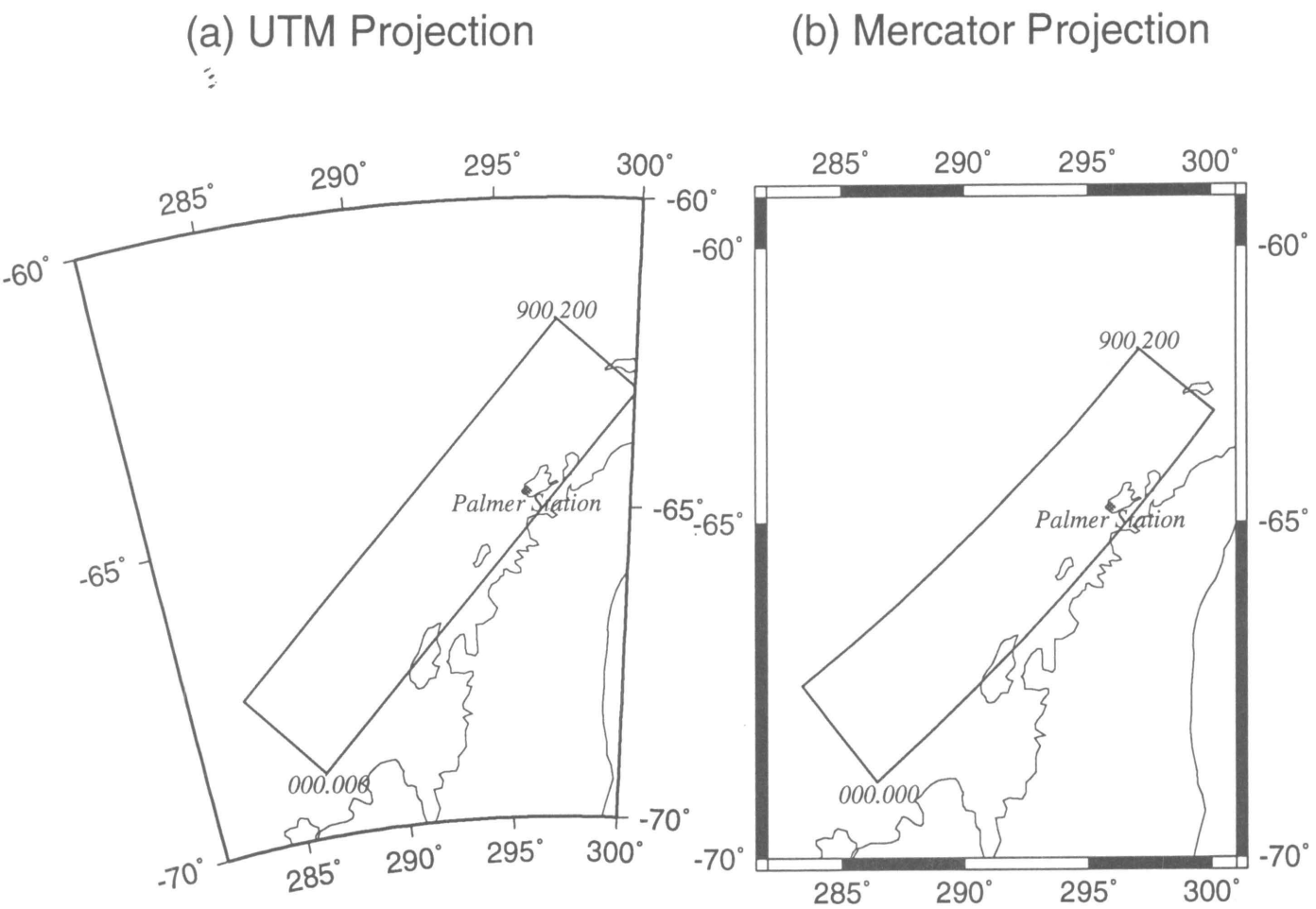

Figure 1. The Palmer peninsular area is shown on both UTM and Mercator projections. The PalLTER grid region is outlined.

Survey (USGS), Reston, Virginia (version of 6/17/86 program available from USGS). Additional programs were written to perform the coordinate rotation and provide input files for the PLANE-PC program. All programs were recompiled in a UNIX environment and piped together so that an input LTER station number gives an output latitude-longitude.

Thus defined, the PalLTER grid has coordinates, for our interests, from 000.000 to 900.200. Figure 1 illustrates the difference between the UTM projection used for the grid layout and a standard Mercator projection typically used for nautical charts where we show the PalLTER grid boundaries on both projections. The curvature of the boundary shown on the Mercator projection shows the difficulty of laying out a regularly spaced grid using a standard nautical chart. A finer grid, consistent with the cardinal lines and points given in table 1, is easily produced via the computer programs and is available upon request.

Fine-scale sampling positions near Palmer Station were selected to provide a set of fixed station locations within the Zodiac boating range of the station and with some selected to be along the normal in/out access route of research vessels visiting the station. These stations are not on a regular grid and are designated alphabetically (figure 2). Sampling of stations A-J by a Zodiac is done weekly from Palmer Station; stations K-O are sampled by Zodiac if a potential rescue ship is at the station; stations E1-E4 are sampled infrequently from a ship of opportunity. We designate this set of stations near Palmer station as the Palmer grid.

We found the nautical charts for this area (Defense Mapping Agency Stock #29AHA29123, last update 1977) to be systematically offset compared to GPS satellite positions. GPS positions are 51 seconds of longitude (690 meters) west of charted positions. The chart in figure 2 has been redrawn from the original so that landmarks, sampling stations, and GPS positions are consistent. Palmer grid stations locations shown on this chart and their GPS coordinates are listed in table 2. This chart is unofficial and should not be used for navigation purposes. We use a Trimble Pathfinder GPS to locate the stations from the Zodiac. We also give the LTER grid coordinates for the Palmer grid stations in table 2.

This work was supported by National Science Foundation grant DPP 90-11927 (R.C.S.), and is Palmer LTER Publication No. 4. We gratefully acknowledge the help of Professor Waldo Tobler in designing this grid.

Reference

Maling, D. H. 1992. *Coordinate Systems and Map Projections*, 2nd edition. New York: Pergamon Press.

Table 1. LTER grid coordinates/stations

Grid number	Latitude S	Longitude W	Grid number	Latitude S	Longitude W
000.000	68°58.047'	73°33.648'	500.080	65°21.409'	66°27.834'
000.020	68°49.820'	73°52.797'	500.100	65°14.029'	66°46.558'
000.040	68°41.559'	74°11.711'	500.120	65°06.611'	67°05.107'
000.060	68°33.265'	74°30.393'	500.140	64°59.156'	67°23.485'
000.080	68°24.939'	74°48.847'	500.160	64°51.665'	67°41.692'
000.100	68°16.583'	75°07.077'	500.180	64°44.138'	67°59.730'
000.120	68°08.196'	75°25.086'	500.200	64°36.576'	68°17.601'
000.140	67°59.779'	75°42.877'	600.000	65°10.122'	63°45.505'
000.160	67°51.333'	76°00.455'	600.020	65°03.081'	64°04.837'
000.180	67°42.859'	76°17.822'	600.040	64°56.000'	64°24.000'
000.200	67°34.358'	76°34.982'	600.060	64°48.878'	64°42.994'
100.000	68°22.795'	71°42.302'	600.080	64°41.717'	65°01.821'
100.020	68°14.778'	72°01.648'	600.100	64°34.516'	65°20.483'
100.040	68°06.727'	72°20.768'	600.120	64°27.277'	65°38.981'
100.060	67°58.641'	72°39.667'	600.140	64°20.000'	65°57.315'
100.080	67°50.521'	72°58.347'	600.160	64°12.685'	66°15.489'
100.100	67°42.368'	73°16.811'	600.180	64°05.334'	66°33.503'
100.120	67°34.183'	73°35.063'	600.200	63°57.947'	66°51.358'
100.140	67°25.966'	73°53.105'	700.000	64°28.921'	62°24.124'
100.160	67°17.718'	74°10.941'	700.020	64°22.057'	62°43.318'
100.180	67°09.441'	74°28.573'	700.040	64°15.150'	63°02.353
100.200	67°01.133'	74°46.005'	700.060	64°08.203'	63°21.230
200.000	67°46.319'	69°56.667'	700.080	64°01.215'	63°39.949
200.020	67°38.510'	70°16.130'	700.100	63°54.188'	63°58.513'
200.040	67°30.664'	70°35.377'	700.120	63°47.121'	64°16.922'
200.060	67°22.781'	70°54.414'	700.140	63°40.016'	64°35.178'
200.080	67°14.863'	71°13.242'	700.160	63°32.872'	64°53.281'
200.100	67°06.911'	71°31.863'	700.180	63°25.692'	65°11.234'
200.120	66°58.924'	71°50.281'	700.200	63°18.474'	65°29.037'
200.140	66°50.905'	72°08.499'	800.000	63°47.008'	61°06.757'
200.160	66°42.852'	72°26.518'	800.020	63°40.312'	61°25.784'
200.180	66°34.768'	72°44.343'	800.040	63°33.574'	61°44.662'
200.200	66°26.652'	73°01.974'	800.060	63°26.794'	62°03.391'
300.000	67°08.723'	68°16.460'	800.080	63°19.974'	62°21.973'
300.020	67°01.115'	68°35.970'	800.100	63°13.113'	62°40.409'
300.040	66°53.469'	68°55.276'	800.120	63°06.212'	62°58.699'
300.060	66°45.785'	69°14.382'	800.140	62°59.273'	63°16.845'
300.080	66°38.065'	69°33.289'	800.160	62°52.294'	63°34.847'
300.100	66°30.309'	69°52.001'	800.180	62°45.278'	63°52.708'
300.120	66°22.517'	70°10.518'	800.200	62°38.225'	64°10.427'
300.140	66°14.690'	70°28.844'	900.000	63°04.445'	59°53.146'
300.160	66°06.829'	70°46.982'	900.020	62°57.910'	60°11.983'
300.180	65°58.935'	71°04.932'	900.040	62°51.333'	60°30.680'
300.200	65°51.008'	71°22.698'	900.060	62°44.715'	60°49.238'
400.000	66°30.100'	66°41.390'	900.080	62°38.055'	61°07.658'
400.020	66°22.688'	67°00.888'	900.100	62°31.354'	61°25.941'
400.040	66°15.237'	67°20.194'	900.120	62°24.614'	61°44.087'
400.060	66°07.747'	67°39.310'	900.140	62°17.833'	62°02.097'
400.080	66°00.218'	67°58.239'	900.160	62°11.014'	62°19.972'
400.100	65°52.653'	68°16.981'	900.180	62°04.157'	62°37.714'
400.120	65°45.051'	68°35.540'	900.200	61°57.261'	62°55.322'
400.140	65°37.413'	68°53.917'			
400.160	65°29.739'	69°12.114'			
400.180	65°22.031'	69°30.133'			
400.200	65°14.289'	69°47.976'			
500.000	65°50.540'	65°11.167'			
500.020	65°43.317'	65°30.603'			
500.040	65°36.054'	65°49.859'			
500.060	65°28.751'	66°08.935'			

Cardinal lines (every 100 kilometers along the peninsula) and points (every 20 kilometers on- or offshore) are shown for the PalLTER grid. The locations of the Palmer grid stations are given in terms of latitude-longitude and LTER grid coordinates.

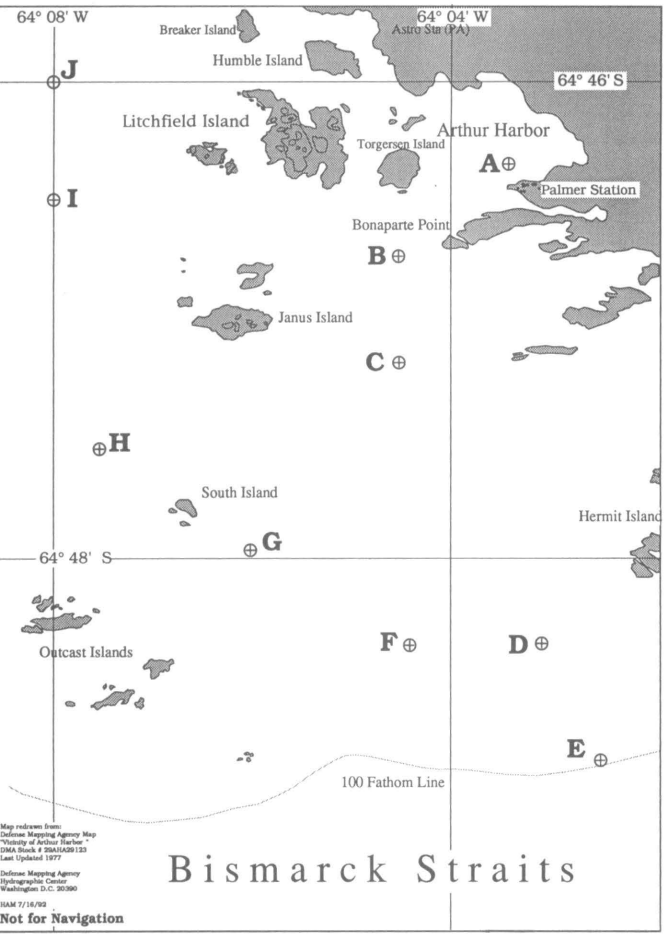

Figure 2. The PalLTER grid in relation to Palmer Station. The chart latitude-longitude marks have been redrawn so as to agree with GPS positions. The GPS and USGS benchmark at the tip of Bonaparte Point agree. The GPS readings are 51 seconds west (roughly 690 meters) with respect to the chart. This chart is unofficial and should NOT be used for navigation.

Table 2. LTER Palmer grid stations

Station ID	Latitude S	Longitude W	LTER grid
A	64° 46.45'	64° 03.27'	624.039
B	64° 46.77'	64° 04.35'	624.040
C	64° 47.30'	64° 04.35'	622.039
D	64° 48.40'	64° 03.06'	622.037
E	64° 48.90'	64° 02.43'	622.036
F	64° 48.40'	64° 04.35'	621.037
G	64° 48.00'	64° 06.00'	622.039
H	64° 47.3()'	64° 07.60'	621.040
I	64° 46.50'	64° 08.00'	622.042
J	64° 46.00'	64° 08.00'	622.042
K	64° 50.51'	64° 02.94'	619.034
L	64° 51.97'	64° 03.07'	617.033
M	64° 53.01'	64° 03.14'	615.031
N	64° 53.91'	64° 06.0()'	614.032
0	64° 52.60'	64° 08.30'	613.035
E1	64° 53.00'	64° 09.71'	613.035
E2	64° 52.92'	64° 39.16'	597.053
E4	64° 56.00'	64° 24.00'	600.040

Palmer LTER: Upper-ocean circulation in the LTER region from historical sources

EILEEN E. HOFMANN, CATHY M. LASCARA, AND JOHN M. KLINCK

Center for Coastal Physical Oceanography
Crittenton Hall
Old Dominion University
Norfolk, Virginia 23529

The long-term ecological research program (LTER) sampling region encompasses an area long the Antarctic Peninsula that is roughly 900 kilometers alongshore and 200 kilometers offshore. This region includes portions of Bransfield Strait, Gerlache Strait, and the Bellingshausen Sea and is influenced by adjacent areas such as Drake Passage, the Weddell Sea, and Marguerite Bay. The Antarctic Circumpolar Current forms the northern boundary of the study region.

Historical descriptions of water mass distributions and circulation patterns are available for selected portions of the LTER region. These previous studies were either concentrated on subareas within the LTER study area or were at the periphery of the LTER region. The purpose of this paper is to synthesize the existing hydrographic and current observations to provide a description of the major circulation features in the LTER study region. This circulation pattern is shown schematically in figure 1 and is described below.

The circulation of the northern section of the LTER region is based on descriptions from Bransfield Strait. A dynamic topography map (relative to 1800 decibars) constructed from data collected during the R/V *Discovery* cruises (Clowes 1934) shows flow from Drake Passage into Bransfield Strait through the gap (maximum 500 meters, figure 2) between Smith and Snow Islands. This flow continues to the northeast along the southern side of the South Shetland Islands and at the eastern end of Bransfield Strait turns north to exit between King George Island and Elephant Island or continues eastward towards the Weddell Sea.

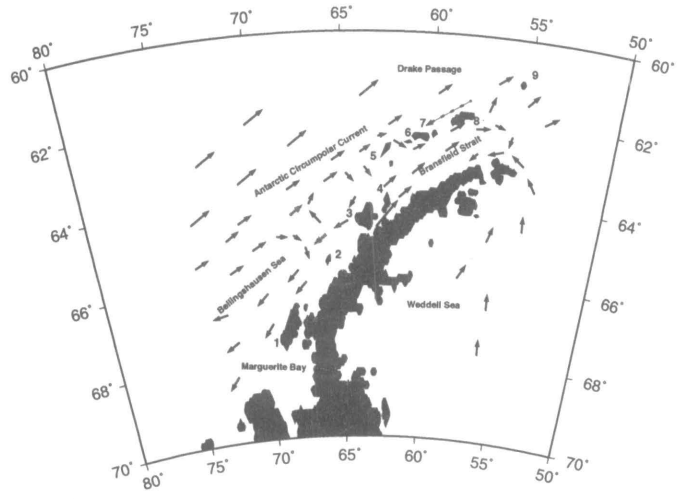

Figure 1. Schematic of the circulation in the upper 200-300 meters in the LTER study region. Circulation patterns were derived from the sources discussed in the text. The Polar Slope Current is indicated by the *dotted arrow*. The *vectors with lighter shading* in the eastern Bellingshausen Sea represent the possibility of a single cyclonic gyre in this region. Islands are identified as: *1*, Adelaide; *2*, Renaud; *3*, Anvers; *4*, Brabant; *5*, Smith; *6*, Snow; *7*, Livingston; *8*, King George; *9*, Elephant. Gerlache Strait is between Anvers and Brabant Islands and the Antarctic Peninsula.

A recent analysis of historical temperature data from the Bransfield Strait (Capella et al 1992a) indicates that Circumpolar Deep Water (CDW) enters the Strait from Drake Passage between Smith and Snow Islands. This water mass, which is characterized by temperature greater than 0 °C, is found throughout Drake Passage and the Bellinghausen Sea between 200 and 700 meters (Sievers and Nowlin 1984). Inside the Strait, CDW is found along the southern side of the Islands and between King George and Elephant Islands. Thus, the climatological temperature distributions support the circulation described between Clowes (1934). Additionally, in 1979 a First GARP (Global Atmospheric Research Program) Global Experiment buoy drifted from Drake Passage between Smith and Snow Islands into the Strait and continued eastward to about 55° W, which is in agreement with the circulation proposed by Clowes (1934) and Capella et al. (1992a). However, the buoy then turned and drifted to the west (Klinck 1991), suggesting the presence of a cyclonic gyre in the surface waters of the Bransfield Strait.

To the north of the South Shetland Islands, below 200-300 meters, is the westward flowing Polar Slope Current (Nowlin and Zenk 1988). This current, which is thought to originate in the Weddell Sea, is narrow (10 kilometers) and cold (less than 0 °C) and flows counter to the predominant surface flow in that region.

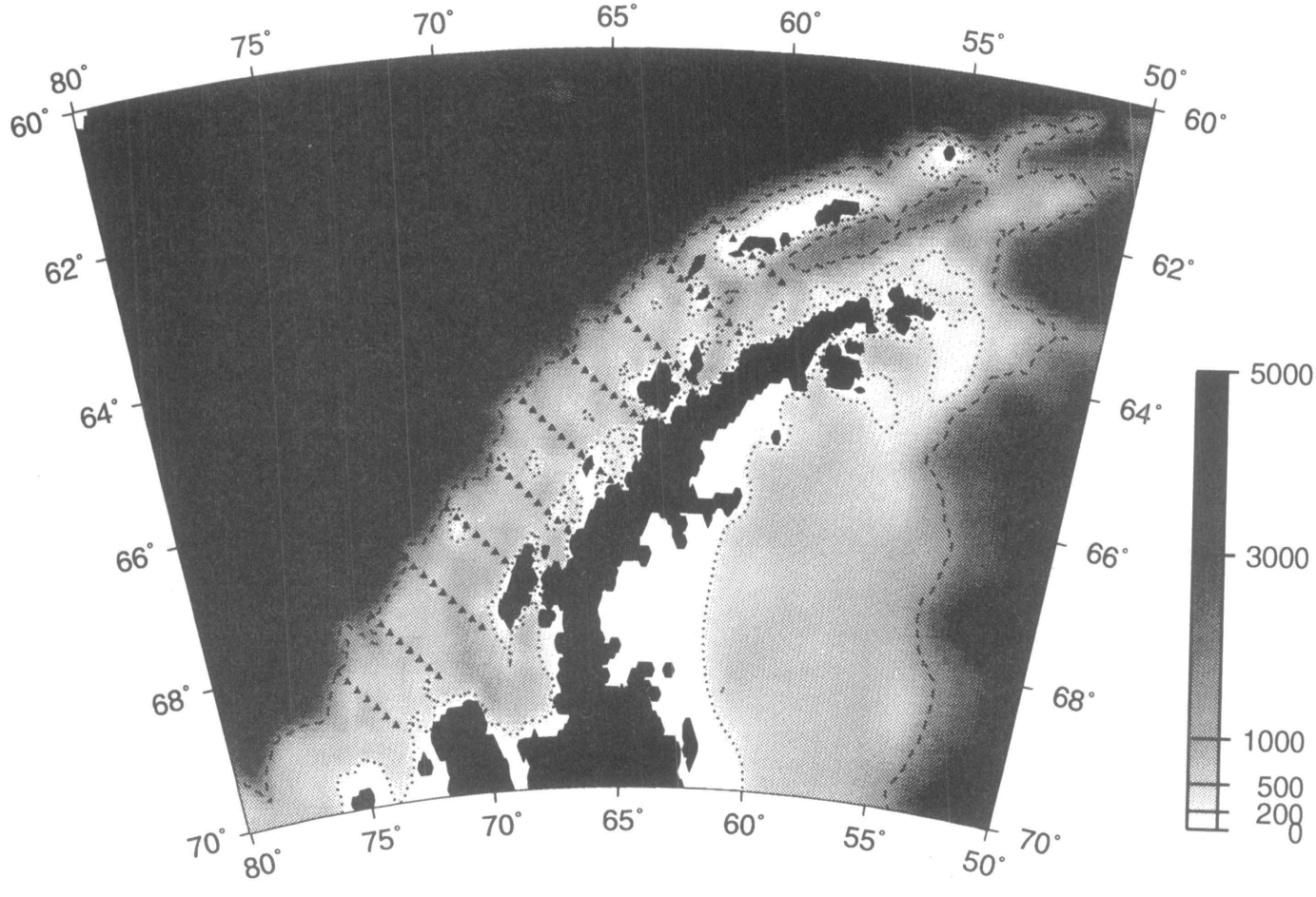

Figure 2. The LTER hydrographic grid. Hydrographic stations are indicated by *triangles*. Depth in meters is indicated by the *shading*. The 200 and 1,000 meter isobaths are indicated by the *dotted* and *dashed lines*, respectively. The bathymetric contours are from the ETOPO5 bathymetry data set, which is available through the National Center for Atmospheric Research in Boulder, Colorado.

The circulation of the central and southern sections of the LTER region is based on descriptions from hydrographic surveys and surface drifter studies in the Gerlache Strait and eastern Bellingshausen Sea made as part of the Research on Coastal Ecosystem Rates (RACER) program (Huntley et al. 1990). The dynamic topography maps (relative to 200 decibars) and drifter trajectories show that surface flow in the Gerlache is northeast along the axis of the Strait and exists to the northeast into the southern reaches of the Bransfield Strait (Amos et al. 1990; Niiler et al. 1990). Similarly, the surface flow in the near-shore coastal waters off Brabant Island appears to be to the north towards Bransfield Strait (Amos et al. 1990; Niiler et al. 1991). This northward flow turns southeastwards as it enters the southwest portion of Bransfield Strait. However, the circulation in this region is complex and likely has seasonal variations. For example, a westward surface flow has been observed in this region (Stein 1982). Similarly, seasonal variations are associated with flow from the Weddell Sea into the Bransfield Strait (Capella et al. 1992b).

Hydrographic surveys conducted in the eastern Bellingshausen Sea as part of the Biological Investigations of Marine Antarctic Systems and Stocks (BIOMASS) program show southward flow offshore of Anvers Island (Stein 1982, 1988) and between and Anvers and Renaud Islands (Kock and Stein 1978). More recently Stein (1991) presented dynamic topography contours (relative to 200 decibars) constructed from a larger scale hydrographic survey which suggest that the circulation in the upper water column consists of two cyclonic gyres: one near Anvers and Brabant Islands and one near Adelaide Island. This is similar to the circulation pattern presented in Stein (1988). However, given the spatial resolution of the measurement used by Stein (1991), it is equally possible that there is only a single cyclonic gyre in the Bellingshausen Sea. In fact, the trajectory traced by a FGGE buoy that drifted through the Bellingshausen Sea in 1979 (Klinck 1991) supports a single cyclonic gyre. This possibility is indicated by the dashed line in figure 1.

One of the goals of the LTER study is to define the large-scale distribution of water masses and circulation in a region of sufficient size to encompass areas that could potentially contribute larvae of *Euphausia superba* to the region around Palmer Basin. Previous studies (e.g., Capella et al. 1992b) have shown that *E.superba* larvae can be transported considerable distances (hundreds of kilometers) from their spawning area. In the LTER region, potential source sites of *E.superba* larvae are Marguerite Bay, the eastern Bellingshausen Sea, Gerlache Strait, and Bransfield Strait. This then defines the north and south extent of the hydrographic sampling grid. The across-shelf extent of the grid must be sufficient to include CDW, which is believed to be important to reproducing *E.superba* (Hofmann et al. 1992).

Given these requirements, the LTER hydrographic survey grid (figure 2) was designed with an along-shelf spacing of 100 kilometers and an across-shelf station spacing of 20 kilometers. Most across-shelf transects extend offshore beyond the 1,000-meter isobath and terminate inshore of the 200-meter isobath. It should be stressed that this is the basic hydrographic grid. Modifications will be made as needed to accommodate sampling requirements. In particular, stations may be added in certain regions to better define circulation features. We anticipate sampling the entire grid during an LTER cruise scheduled for austral fall (March-April) 1993.

We thank T. Whitworth for comments on the schematic circulation pattern. This work was supported by National Science Foundation grant DPP 90-11927 and is Palmer LTER publication No. 5.

References

Amos, A. F., S. S. Jacobs, and J. H. Hu. 1990. RACER: Hydrography of the surface waters during the spring bloom in the Gerlache Strait. *Antarctic Journal of the U.S.*, 25(5):131-134.

Capella, J. E., R. M. Ross, L. B. Quetin, and E. E. Hofmann. 1992a. A note on the thermal structure of the upper ocean in the Bransfield Strait-South Shetland Islands region. *Deep-Sea Research*, 39(7-8):1,221-1,229.

Capella, J. E., L. B. Quetin, E. E. Hofmann, and R. M. Ross. 1992b. Models of the early life history of *Euphausia superba*-Part II. Lagrangian calculations. *Deep-Sea Research*, 39(7-8):1,201-1,220.

Clowes, A. I. J. 1934. Hydrography of the Bransfield Strait. *Discovery Reports*, 9:1-64.

Hofmann, E. E., J. E. Capella, R. M. Ross, and L. B. Quetin. 1992. Models of the early life history of *Euphausia superba*-Part I. Temperature dependence during the descent-ascent cycle. *Deep-Sea Research*, 39(7-8):911-941.

Huntley, M. E., D. M. Karl, P. O. Niiler, and O. Holm-Hansen. 1990. Research on Antarctic Coastal Ecosystem Rates (RACER): An interdisciplinary field experiment. *Deep-Sea Research*, 38:911-41.

Klinck, J. M. 1991. Large scale physical structure of the southern ocean. In *GLOBEC: Southern Ocean Program, GLOBEC Workshop on Southern Ocean Marine Animal Populations and Climate Change*. GLOBEC Report Number 5, 74-83.

Kock, K. H. and M. Stein. 1978. Krill and hydrographic conditions off the Antarctic Peninsula. *Meeresforschung*, 26:79-95.

Niiler, P. P., A. Amos, and J. H. Hu. 1991. Water masses and 200 m relative geostrophic circulation in the western Bransfield Strait region. *Deep-Sea Research*, 38:943-959.

Niiler, P., J. Illeman, and J. H. Hu. 1990. RACER: Lagrangian drifter observations of surface circulation in the Gerlache and Bransfield Straits. *Antarctic Journal of the U.S.*, 25(5):134-7.

Nowlin, W. D., Jr. and W. Zenk. 1988. Westward bottom currents along the margin of the South Shetland Island Arc. *Deep-Sea Research*, 35:269-301.

Sievers, H. A. and W. D. Nowlin, Jr. 1984. The stratification and water masses at Drake Passage. *Journal of Geophysical Research*, 89:10,489-10,514.

Stein, M. 1982. Fischereiozeanographische Untersuchungen während FIBEX 1981. *Archiv für Fischereiwissenschaft*, 33:35-51.

Stein, M. 1988. Variation of geostrophic circulation off the Antarctic Peninsula and in the southwest Scotia Sea, 1975-1985. In D. Sahrhage (Ed.), *Antarctic ocean and resources variability*. Berlin: Springer-Verlag, 81-91.

Stein, M. 1991. Variability of local upwelling off the Antarctic Peninsula, 1986-1990. *Archiv für Fischereiwissenschaft*, in press.

Palmer LTER program: Spatial variability in phytoplankton distribution and surface photosynthetic potential within the peninsula grid, November 1991

Barbara B. Prezelin, Nicholas P. Boucher, Mark Moline, Elise Stephens, Keith Seydel, and Kai Scheppe

Marine Science Institute
University of California at Santa Barbara
Santa Barbara, California 93106

As part of the long-term ecological research program (LTER) 1991 austral spring cruise, which defined the biological, chemical, optical, and physical properties of marginal ice zone (MIZ) west of the Antarctic Peninsula (Waters and Smith 1993), we resolved the mesoscale variability in phytoplankton biomass, photosynthetic potential, and community composition. Preliminary results of three transects completed across the MIZ on the R/V *Polar Duke* are presented here. Figure 1*A* and 1*B* respectively, indicate station (Sta) locations and discrete depths sampled with a bio-optical profiling system (BOPS II) (Smith et al. 1992).

Due to strong westerly winds, the pack ice was compressed during this cruise and the edge of the MIZ was especially sharp (figure 1C). Phytoplankton communities beneath the ice pack west of Palmer Station (Sta 600.020 and 600.040) were sampled 7-9 November; the 700 line was transected out of the ice on 14-15 November; the 500 line was transected into the ice on 16-17 November; the outermost station of the 600 line was sampled on 16 November; and the remainder of the 600 line was transected into the ice on 18 November.

Rates of light-saturated photosynthesis (P_{max}) were determined from photosynthesis-irradiance relationships measured on bluegreen light photosynthetrons, using procedures detailed elsewhere (Prezelin and Glover 1991). Reverse-phase high-pressure liquid chromatography (HPLC) procedures were followed to determine phytoplankton pigmentation in replicate one liter samples filtered on 0.4 micrometer nylon 47 millimeter Nuclepore filters and extracted in 3 milliliter 90 percent acetone for 24

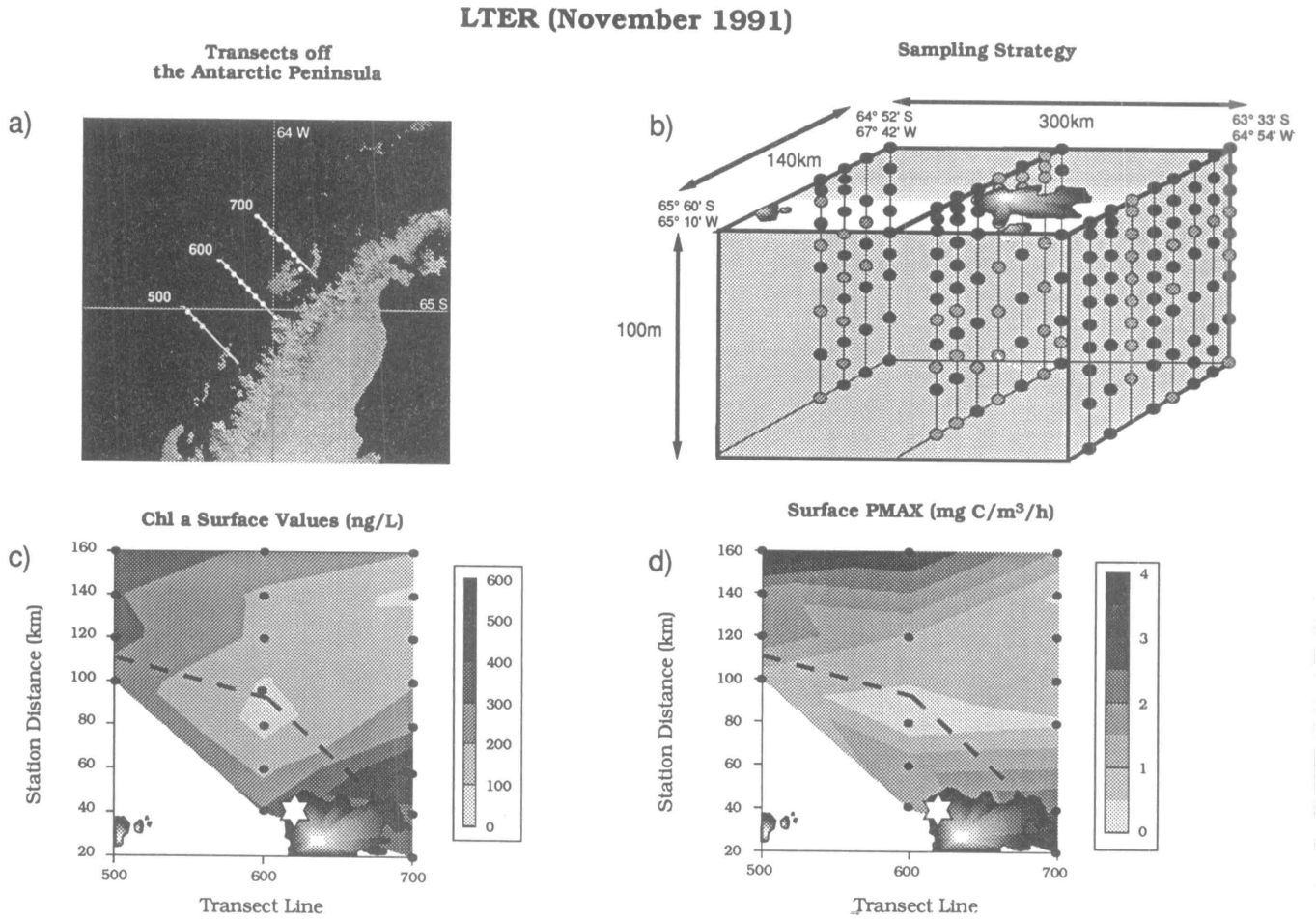

Figure 1. LTER grid, November 1991 (*A*) location of three transects west of the Palmer Peninsula; (*B*) vertical distribution of chemical (all *circles*; includes pigmentation and inorganic nutrients) and productivity (*black circles* only) discrete samples collected with the BOPS II (Smith et al. 1992); (*C* and *D*) surface contour plot of distribution of volumetric chlorophyll *a* and P_{max}, respectively, with station locations (shown as *black circles*), the edge of the MIZ (*dashed line*) and the location of Palmer Station (*star*).

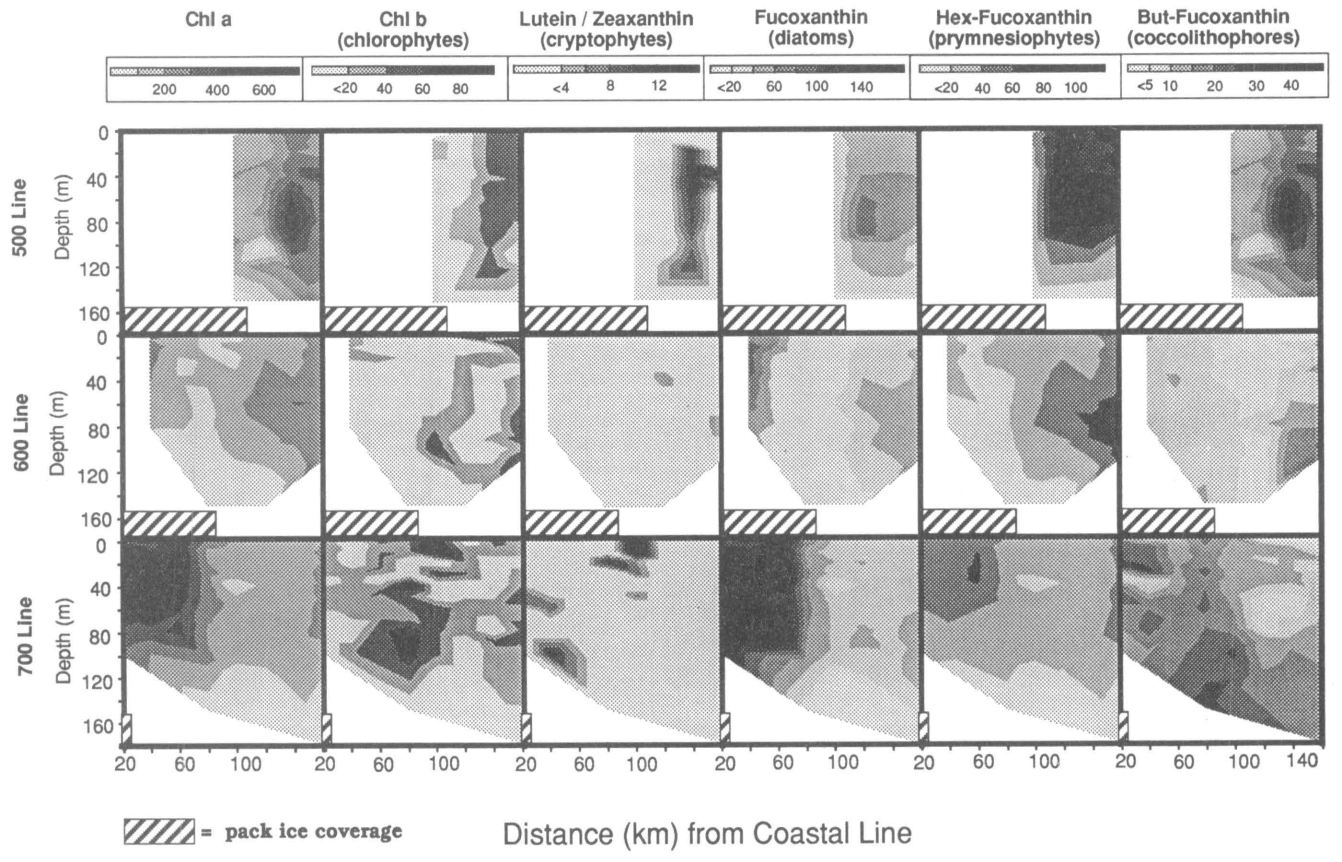

Figure 2. A comparison of contour plots for HPLC pigment distribution along the 500 line (*upper panels*), the 600 line (*middle panels*), and the 700 line (*lower panels*) during November 1991. Pigment concentrations are expressed as ng/L, and the phytoplankton group that each pigment chemotaxonomic marker represents is given in parentheses. Pack ice coverage (*slashed bar*) is indicated at the bottom of each panel.

hours in the dark (-20 °C). Following previously described procedures (Bidigare et al. 1989), pigment separation was carried out with a Hitachi L-6200A liquid chromatograph equipped with a Radial-PAK C18 column (8 × 100 millimeter column; 5 µ particles) and a Hitachi L-4250 UV/VIS Variable Wavelength Detector (436 nanometer). Individual HPLC peak areas were quantified with the aid of Hitachi D-6000 software. Peak identities of the algal extracts are determined by comparing their retention times with pure pigment standards and extracts prepared from standard plant materials of known pigment composition. Diode array spectroscopy (Beckmann DU-64) from 350 to 550 nanometer confirmed identities of the major pigments.

The spatial distribution of plant biomass and volumetric P_{max} in surface waters of the LTER grid are shown in figures 1 *C* and *D*, respectively. Results indicate that surface plant biomass and productivity was low but quite variable, showing a tendency to covary within the mesoscale grid. Moreover, a comparison of the three transects indicate that while elevated Chl biomass are found along the MIZ, this is not always the case. Note that the lowest levels of plant biomass and primary productivity were located at the ice edge of the 600 line (figure 1 *C* and *D*).

We have used the presence of key chlorophyll and carotenoid pigments as chemotaxonomic markers for different phytoplankton groups and the distribution of their *in situ* concentrations to define the spatial variability in phytoplankton distribution and the relative abundance in various ocean regimes (Smith et al. 1987, 1992). A comparison of contour plots for the most abundant pigment markers along the three LTER transects is presented in figure 2 that indicates diverse communities of phytoplankton existed at discrete locations within the grid. For instance, plant biomass (chl-*a*) was especially high in subsurface waters at the edge of the MIZ in the relatively shallow waters of the Dallmann Bay (inshore on the 700 line). Under the ice, a diatom (fucoxathin)-dominated community was evident and appeared shoreward of a mixed community of chlorophytes (chl-*b*) and coccolithophorids (but-fucoxanthin). While prymnesiophytes (hex-fucoxanthin) such as *Phaeocystis* spp. were present, they appeared concentrated in the open surface waters that entered the Dallmann Bay from the Gerlache Strait. Equally high chlorophyll *a* concentrations were found in subsurface waters over a topographical rise near the end of the Renaud Line (the 500 line), about 40 kilometers offshore the edge of the pack ice. In contrast to the Dallmann Bay, prymnesiophytes appeared to dominate mixed phytoplankton communities, where pigment markers for diatoms, coccolithophorids, chlorophytes, and perhaps cyanobacteria (zeaxanthin) were evident in lesser amount.

It is clear that HPLC technology and the sampling strategy employed during the first field season of the antarctic LTER pro-

gram were successful in documenting the mesoscale variability in phytoplankton communities along the MIZ. The data base is being further analyzed with respect to bottom topography, ocean circulation, and macronutrient availability within the same region to better define the physical and chemical variables that may regulate the mesoscale variability in phytoplankton distribution and the community structure in antarctic waters within a given season.

This study is reported in Palmer LTER publication number 6 and was supported by National Science Foundation grant DPP 90-11927. We gratefully acknowledge the HPLC training and pigment standards generously provided by R. Bidigare and M. Ondrusek of the University of Hawaii.

References

Bidigare, R. R., O. Schofield, and B. B. Prezelin. 1989. Influence of zeaxanthin on quantum yield of photosynthesis of *Synechococcus* clone WH7803 (DC2). *Marine Ecology Progress Series*, 56:177-88.

Prezelin, B. B. and H. E. Glover. 1991. Variability in time/space estimates of phytoplankton biomass and productivity in the Sargasso Sea. *Journal of Plankton Research*, 13S:45-67.

Smith, R. C., R. R. Bidigare, B. B. Prezelin, K. S. Baker, and J. M. Brooks. 1987. Optical characterization of primary production across a coastal front. *Marine Biology*, 96:575-91.

Smith, R. C., B. B. Prezelin et al. 1992. Ozone depletion: Ultraviolet radiation and phytoplankton biology in antarctic waters. *Science*, 255:952-59.

Waters, K. J. and R. C. Smith. 1993. A sampling grid for the antarctic LTER Program. *Antarctic Journal of the U.S.*, this issue.

Palmer LTER program: Biomass and community composition of Euphausiids within the peninsula grid, November 1991 cruise

Langdon B. Quetin, Robin M. Ross,
Barbara B. Prezelin, Karen L. Haberman,
Karen L. Hacecky, and Timothy Newberger

Marine Science Institute
University of California at Santa Barbara
Santa Barbara, California 93106

During the Palmer long-term ecological research program (LTER) cruise on the R/V *Polar Duke* in mid-November 1991, we investigated the distribution, abundance, and community composition of the zooplanktonic and nektonic community along three transects that each intersected the ice edge. Ice cover has been cited by various investigators as one of the primary determinants of the structure and function of the antarctic ecosystem. The data from the November 1991 cruise allowed us to investigate the validity of this presumption for larger, secondary producers during the austral spring west of the Antarctic Peninsula. This note is a preliminary look at some of this data. Abundance and community composition of two dominant euphausiids were compared to observations of ice cover and to measurements of phytoplankton standing-stock determined by high-pressure liquid chromatography techniques used at the same stations by other members of the Palmer LTER (see Prezelin et al. this issue). Measurements at 10-meter intervals were integrated over the top 100 meters of the water column to estimate food availability for grazers in milligrams of chlorophyll *a* per square meter.

At each station along the three transects surveyed (see Ross and Quetin), we did oblique tows with a 2-meter square trawl

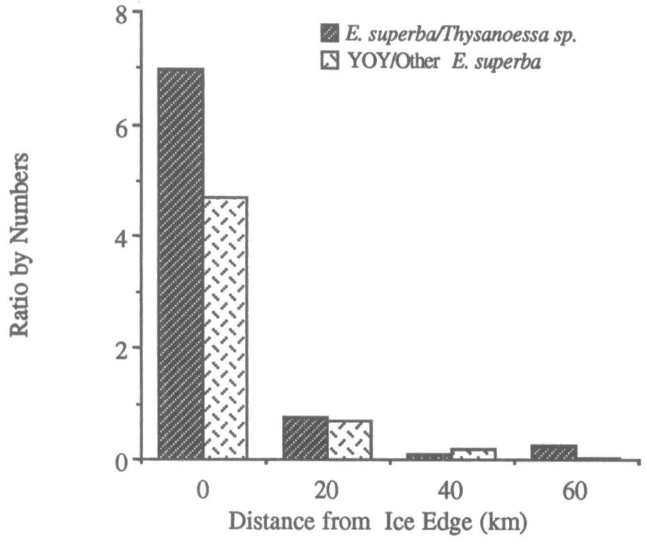

Figure 1. Catch volume (*solid black bars*) (milliliters per cubic meter times 300) at stations along the three transect lines sampled during the 7 to 21 November 1991 Palmer LTER cruise with phytoplankton standing stock integrated over the top 100 meters (*speckled bars*) (milligrams per meter squared). *Shaded area* was ice-covered during the cruise.

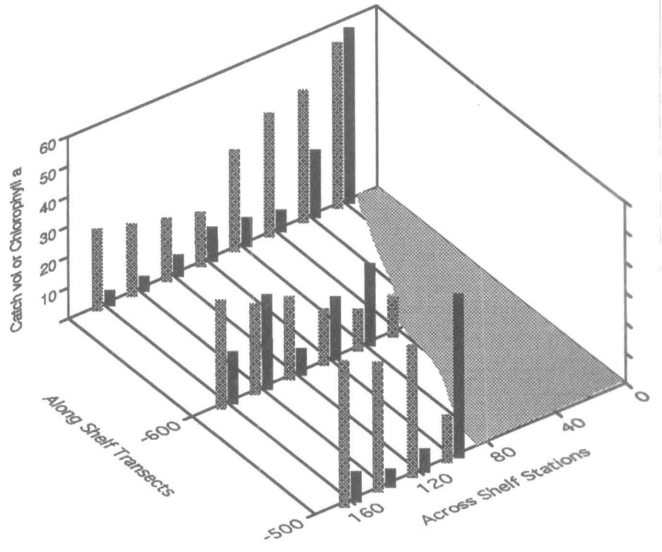

Figure 2. Catch composition in relation to distance from the ice edge: ratio of two euphausiid species (*E.superba* and *Thysanoessa* sp.) and ratio of young-of-the-year (YOY) to all older age groups of *E.superba*.

with 1,000 micrometer (μm) mesh. An Oceanics flowmeter monitored the volume of water passing through the net. Target depth was usually 300 meters, but varied somewhat with bottom depth. The volume of the cod end contents was measured with a graduated cylinder before the catch was preserved in 10 percent formalin. Catch per unit effort (catch volume) was calculated as milliliters of organisms per cubic meter of seawater filtered. Catch volume was greatest near the ice edge, and twice as high near the ice edges on the Renaud (500 line) and Dallmann Bay (700 line) transects than the Palmer Basin (600 line) transect (figure 1). Although large-volume catches were associated with high-standing stocks of phytoplankton on the Dallmann Bay line, this correlation was not consistent for the other two transects (figure 1). One difference in the two areas of highest phytoplankton biomass observed during this cruise is that diatoms dominated the phytoplankton assemblage near the ice edge on the Dallmann Bay transect, where antarctic krill were abundant, but prymnesiophytes dominated on the open ocean end of the Renaud transect (see Prezelin et al. this issue), where krill were in low abundance. Weber and El Sayed (1985) found high phytoplankton concentrations in areas with few schools of antarctic krill. In this preliminary analysis (during a transition period in the season) neither a positive nor a negative correlation between krill abundance and total phytoplankton biomass is clear.

Preserved samples from the Renaud transect have been examined: Two euphausiids, *Euphausia superba* and *Thysanoessa* sp., were identified and counted. Individual *E.superba* were categorized as to stage (Fraser 1936) or sex under a dissecting microscope, and were measured for total length with digital calipers from the tip of the rostrum to the end of the uropods. Furcilia larvae, juveniles, and subadults less than about 20 millimeters were young-of-the-year that survived the winter. Larger antarctic krill, called *others*, included both mature and immature individuals with secondary sex characteristics. The community composition was not homogeneous. Relative proportions of the two species and life stage within *E.superba* changed with distance from the ice edge (figure 2). At the ice edge *E.superba*, a herbivore, outnumbered the omnivore *Thysanoessa* sp. by a factor of seven and young-of-the-year *E.superba* dominated the community. A similar dominance of the ice-edge population of *E.superba* by young-of-the-year was found in the austral spring in the Weddell Sea (Daly and Macaulay 1988). As we moved away from the ice edge, the euphausiid community became equally divided between the herbivore and the omnivore by 20 kilometers, with *Thysanoessa* sp. increasingly outnumbering *E.superba* as we moved into open water. Mature antarctic krill far outnumbered young-of-the-year 40 to 60 kilometers seaward of the ice edge.

The patterns in both abundance, species composition, and life-stage distribution within a species all show definite associations with the ice edge, supporting the idea that ice has a role in the structure and function of communities of secondary producers, especially antarctic krill. The interaction of phytoplankton community composition and the major grazer awaits further investigation.

We gratefully acknowledge the assistance of all personnel on this antarctic cruise: Cathy Lascara, Mark Talkovic, and Vance Vredenberg 5-22 November 1991; Tom Moylan and Langdon Quetin, early October to mid-December 1991; and Tim Newberger, mid-October 1991 to mid-March 1992. This research was supported in part by National Science Foundation grant DPP 90-901127. This report is Palmer LTER publication number 7.

References

Daly, K. L. and M. C. Macaulay. 1988. Abundance and distribution of krill in the ice edge zone of the Weddell Sea, austral spring 1983. *Deep-Sea Research*, 35:21-41.

Fraser, R. C. 1936. On the development and distribution of the young stages of krill (*Euphausia superba*). *Discovery Reports*, 14:1-192.

Prezelin, B. B., N. P. Boucher, M. Moline, K. Seydell, and K. Scheppe. 1993. Spatial variability of phytoplankton distribution and surface photosynthetic potential within the Palmer LTER program: Peninsula grid, November 1991. *Antarctic Journal of the U.S.*, this issue.

Weber, L. H. and S. Z. El Sayed. 1985. Spatial variability of phytoplankton and the distribution and abundance of krill in the Indian Sector of the southern ocean. In W. R. Siegfried, P. R. Condy, and R. M. Laws (Eds.), *Antarctic nutrient cycles and food webs*. Berlin: Springer-Verlag, 284-293.

Palmer LTER: Temporal variability in HPLC pigmentation and inorganic nutrient distribution in surface waters adjacent to Palmer Station, December 1991-February 1992

Barbara B. Prezelin, Mark Moline, Keith Seydel, and Kai Scheppe

Department of Biological Sciences

and

Marine Science Institute
University of California at Santa Barbara
Santa Barbara, California 93106

A set of nearfield stations were established in waters adjacent to Palmer Station in the austral spring of 1991 (Kirk and Smith 1993). A range of hydrographic, optical, chemical, and biological properties of the water columns at these sites were repeatedly characterized during late austral spring and summer (December 1991-March 1992). The data will be used to define patterns and scales of variability for food-chain parameters in the area surrounding important nesting and fledgling sites for large populations of antarctic seabirds. Here, we present our preliminary data on the temporal variability and possible succession of phytoplankton communities within surface waters of the Palmer grid and their correspondance with changes in the availability of major plant nutrients.

A zodiac-based sampling strategy was used to collect water samples at five stations (stations A-E) along a transect line from Arthur Harbor out to the 100-Fathom Line (figure 1). At each station, surface samples were collected with a 5-liter GoFlo bottle, transferred to a black bottle, and returned to the laboratory where samples were filtered to determine pigmentation by high-performance liquid chromatography (HPLC). The filtrates of replicate

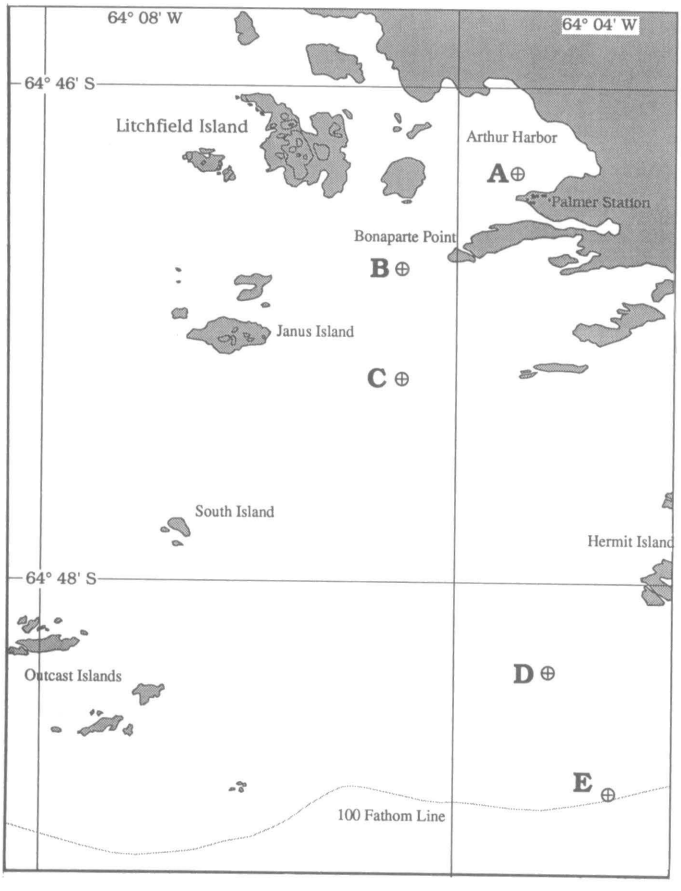

Figure 1. Location of transect stations (after Defense Mapping Agency Map "Vicinity of Arthur Harbor").

CHN samples were deep frozen, transported to the University of California at Santa Barbara, and analyzed at the Marine Science Analytical Laboratories for inorganic nutrient content (Johnson et al. 1985). All HPLC analyses were completed in the field, following procedures outlined in Prezelin et al. (1993a). Some plant pigments are found only in select groups of phytoplankton and can be used as chemotaxonomic markers. Changes in their abundance may indicate a change in the abundance of phytoplankton group (e.g., Smith et al. 1987, 1992). The significance, range of abundance, and mean concentration (± standard deviation) of pigment markers evident in the present field study are summarized in the table.

The frequency of sampling is shown in figure 2a as an overlay on a contour plot of temporal/spatial variability in surface chlorophyll *a* distribution. It is evident that a series of blooms (with chlorophyll *a* values greater than 15,000 nanograms per liter) occurred between mid-December and mid-January, with earlier blooms being lower in intensity and spread along a greater distance of the transect line than the last, very intense bloom that occurred off Bonaparte Point. Prior to the blooms, inorganic nutrients were abundant (figures 2j-l), and phytoplankton communities appeared dominated by prymnesiophytes and dinoflagellates (figures 2e and 2j).

The initiation of the bloom series was coincident with melting of the pack ice, decreasing ice coverage, and a differential rate of decline in surface-water nutrient concentrations (figures 2j-21). Large changes in the ratio of available nitrate:$Si(OH)_4$:PO_4 were observed during the period of bloom events and, as has been reported for other antarctic regions (cf. Sommer 1986, 1988; Smith et al. 1992), appeared to be an important determinant of short-term variability in phytoplankton distribution and community composition observed at the long-term ecological research program (LTER) nearfield stations. Diatoms (figure 2d) dominated the first observed bloom, at a time when silicate (figure 2k) and phosphate (figure 21) levels fell sharply, while prymnesiophytes

Comparision of the range and mean concentrations of chemotaxonomic pigment markers present in the surface waters off Palmer Station between December 1991 and mid-February 1992

Pigment	Chemotaxonomic marker for	Range (ng/L) Min. Max.	*Mean ± SD (ng/L)
Chlorophyll *a*	plant biomass	488 to 29,214	4,339 ± 3,068
Chlorophyll *b*	chlorophytes and/or prasinophytes	nd to 1,731	217 ± 94
Chlorophyll *c*	chromophytes	nd to 811	58 ± 105
Fucoxanthin	diatoms	nd to 28,672	3,332 ± 1,212
19' Hexanoyl-fucoxanthin	prymnesiophytes	nd to 374	60 87
Peridinin	dinoflagellates	nd to 160	36 ± 43
Butanoyl-fucoxanthin	chrysophytes	nd to 72	20 ± 14
Alloxanthin	cryptophytes	nd to 7,117	859 ± 316
Zeaxanthin	cyanobacteria	nd to 460	53 ± 16
Prasinoxanthin	prasinophytes	nd to 7,117	172 ± 97

nd = not detectable
* mean of all samples in which pigments were detectable

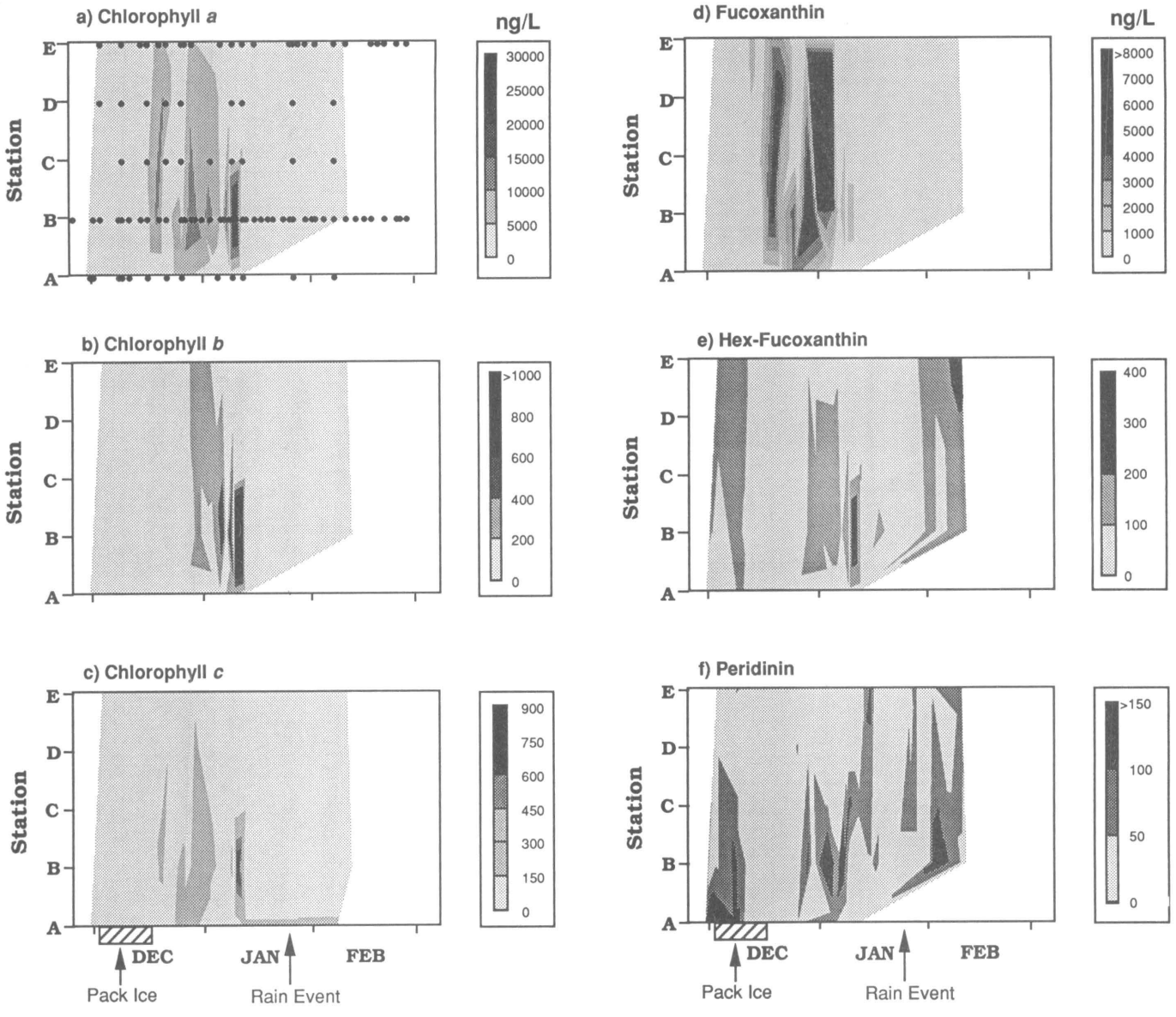

Figure 2a-f. Contour plots of the spatial and temporal variability in pigment and inorganic nutrient distribution along the transect line between December 1991 and March 1992. Only surface data is reported.

(figure 2e) and dinoflagellates (figure 2f) became less abundant. The only other significant phytoplankton group to increase appears to be prasinophytes (figure 2i). In subsequent blooms, we observed major increases in prymnesiophytes, dinoflagellates, cryptophytes (figure 2g), and cyanobacteria (figure 2h).

An intense but localized bloom near Palmer in mid-January was not dominated by diatoms, but rather by prymnesiophytes, cyanobacteria, and cryptophytes. The demise of the bloom series was sudden, coincident with a period of heavy rain and with the presence of a larger area of glacial flowering in the waters between station A-C. We observed an associated increase in nitrate and phosphate levels, with silicate abundance relatively unchanged (figures 2j-l). Depth profiles (not shown) also revealed evidence that diatom populations sank out of surface waters. It appears that within a few weeks of the demise of the first series of blooms, the abundance of prymnesiophytes and dinoflagellates was increasing again (figures 2a-f), and perhaps advecting in from offshore waters in late February/early March (data not shown).

The results indicate that significant changes in phytoplankton abundances and community composition can and do occur on time scales less than a week. Analyses of pigmentation data, in combination with nutrient, optical, and physical data, as well as photophysiological data on phytoplankton photosynthetic properties, should provide significant insight into the mechanisms of food-web dynamics and some aspects of biogeochemical cycling in the LTER nearfield sampling grid.

This report represents Palmer LTER publication #8 and was supported by National Science Foundation grant DPP 90-11927. Special thanks is given to Nicolas Boucher and Allen Matlick for their technical assistance.

References

Johnson, K. S., R. L. Petty, and J. Thomsen. 1985. Flow injection analysis for seawater micronutrients. In A. Zirino (Ed.), *Mapping strategies in chemical oceanography. Advances in Chemistry Series* (American Chemical Society), 209:7-30.

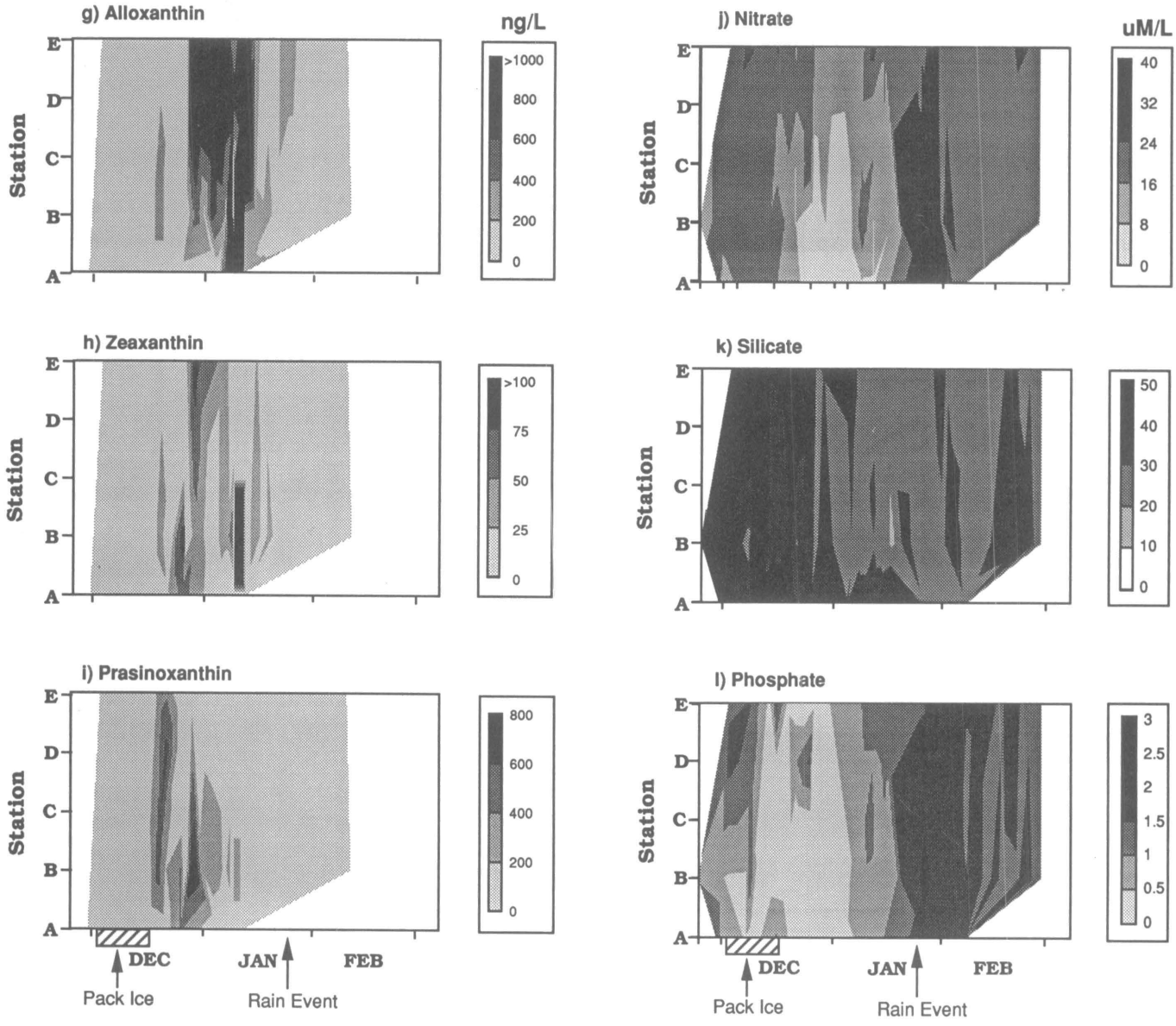

Figure 2g-l. Contour plots of the spatial and temporal variability in pigment and inorganic nutrient distribution along the transect line between December 1991 and March 1992. Only surface data is reported.

Prezelin, B. B., N. P. Boucher, M. Moline, E. Stephens, K. Seydel, and K. Scheppe. 1993. Palmer LTER: Spatial variability in phytoplankton distribution and surface photosynthetic potential within the peninsula grid, November 1991. *Antarctic Journal of the U.S.,* this issue.

Smith, R. C., R. R. Bidigare, B. B. Prezelin, K. S. Baker, and J. M. Brooks. 1987. Optical characterization of primary production across a coastal front. *Marine Biology,* 96:575-591.

Smith, R. C., B. B. Prezelin et al. 1992. Ozone depletion: Ultraviolet radiation and phytoplankton biology in antarctic waters. *Science,* 255:952-959.

Sommer, U. 1988. The species composition of antarctic phytoplankton interpreted in terms of Tilman's competition theory. *Oecologia,* 77:464-467.

Sommer, U. and H. H. Stabel. 1986. Near surface nutrient and phytoplankton distribution in the Drake Passage during early December. *Polar Biology,* 6:107-110.

Waters, K. J. and R. C. Smith 1993. Palmer LTER: A sampling grid for the antarctic LTER Program. *Antarctic Journal of the U.S.,* this issue.

Palmer LTER: Seabird research undertaken during 1991-1992 at Palmer Station, Antarctic Peninsula

WILLIAM R. FRASER, WAYNE Z. TRIVELPIECE,
BRENT R. HOUSTON, AND DONNA R. PATERSON

Polar Oceans Research Group
Center for Coastal and Physical Oceanography
Old Dominion University
Norfolk, Virginia 23529

The long-term ecological research (LTER) program at Palmer Station proposes to investigate how interannual variability in winter pack ice affects the physical and biological processes that link various trophic levels in the marine environment. To represent upper-trophic-level predators, we selected Adélie penguins (*Pygoscelis adeliae*) and south polar skuas (*Catharacta maccormicki*), two of the area's dominant consumers in terms of both abundances and biomass. Approximately 12,000 pairs of Adélie penguins and 750 pairs of south polar skuas breed on islands within 2.5 kilometers of Palmer Station. These species were also attractive as LTER representative species because of the availability of long-term, comparative data sets. South polar skuas, for example, have been the subject of various studies at Palmer Station since the mid-1970s (Parmelee et al. 1977), while Adélie penguins have been intensively studied in the area since 1987 (Fraser and Ainley 1988) as part of the CCAMLR (Convention for the Conservation of Antarctic Marine Living Resources) Ecosystem Monitoring Program (CEMP). The U.S. component of CEMP, known as AMLR (Antarctic Marine Living Resources), is funded through NOAA (National Oceanic and Atmospheric Administration) and managed by the National Marine Fisheries Service (NMFS). AMLR shares many objectives with the LTER and continued cost-sharing is expected to facilitate long-term data collection on Adélies that will be mutually beneficial to both programs.

Our approach capitalizes on long-term research on a host of ecological variables that in these seabirds are likely to be sensitive indicators of change in the marine system (table 1). This approach is ultimately designed to test the following four hypotheses:

- Winter-over survival and physiological conditions of adult Adélie penguins upon their return to the natal rookery to breed is a function of winter and early spring food availability in the pack ice and of the location of winter pack ice relative to the rookeries (extant of winter pack ice). Adult winter-over survival, physiological condition, and the percent of young birds that attempt to breed will be higher when pack ice extent is greater during winter.
- Breeding success of Adélie penguins, barring the effects of spring snow conditions and catastrophic summer storms, is linked to the extent of sea ice because of its effects on spring and summer food availability. During cold summers, krill (*Euphausia superba*) availability will be higher. As a result, breeding success (chicks creched per pair) and chick fledgling weights will increase, while the duration of foraging trip will decrease.
- Physiological conditions of south polar skuas during the pre-egg stage is a function of the availability of the antarctic silverfish (*Pleuragramma antarcticum*) within the skua spring foraging range. Territory occupancy will be earlier and more constant, and the onset of reproduction earlier when silverfish are more available.
- Breeding success in south polar skuas will exhibit different cycles than those of Adélie penguins. Recruitment in their primary prey, the antarctic silverfish, negatively affected by heavy pack ice during the spring cold years. Because south polar skuas primarily eat subadult silverfish, their breeding success will be a function of ice conditions 8-10 years before the current breeding season.

Although the LTER is in its second year of funding by the National Science Foundation, 1991-1992 was the first year of field

Table 1. Parameters for which data sets are being developed as part of the LTER seabird component. SS and SF refer to 1991-1992 sample sizes (number of breeding pairs) and sampling frequency, respectively. SF is coded as 1) sampled daily; 2) every two days; 3) every three days; 5) every five days; 6) once per season; 7) twice per season; 8) every 20 minutes (automatic data logging devices); 9) opportunistically. ND indicates the parameter was not measured; * before a number indicates the number of independent N used rather than the number of breeding pairs.

Parameter	Adélie Penguins SS	Adélie Penguins SF	South Polar Skuas SS	South Polar Skuas SF
Reproductive biology				
Breeding population size	9,319	6	736	6
Arrival dates/chronology	200	1	55	1
Onset of reproduction	200	1	55	1
Egg weights and volume	50	6	55	3
Ratio of 1:2 chick broods	3,030	7	55	3
Chick growth	50	5	*66	3
Chicks fledged/pair	200	2	55	3
Chicks fledged/colony	*7,072	7	ND	
Chicks fledging weights	*391	2	ND	
Chick fledging chronology	*391	2	*66	3
Breeding colony	200	2	55	3
Foraging ecology				
Adult diet composition	ND	55	9	
Chick diet composition	40	5	*66	9
Prey caloric value	40	5	ND	
Prey characteristics	40	5	55	9
Foraging trip duration	40	8	15	8
Ptylochronology	*20	6		ND
Demographic studies				
Adult overwinter survival	200	1	70	1
Annual cohort survival	*77	2	736	6
Recruitment	*28	2	736	6
Cohort banding	*1,000	6	*66	3

Table 2. Aspects of the ecology of Adélie penguins and south polar skuas during the 1990-1991 and 1991-1992 breeding seasons. ND indicates the parameter was not measured.

	Adélie Penguins 1990-1991	Adélie Penguins 1991-1992	South Polar Skuas 1990-1991	South Polar Skuas 1991-1992
Percent breeding pairs with eggs by 20 Nov. (Adélies) and 20 Dec. (skuas)	61	72	48	30
Chicks fledged/pair	1.00	1.39	1.21	1.22
Percent 2-chick broods	54	70	82	79
Mean foraging trip duration (hrs) during peak chick growth	32.54	14.69	ND	ND
Mean fledging weights (kg)	3.10	3.16	ND	ND

work under this award. As a result, our research activities focused primarily on expanding the scope of our ongoing work on seabirds under the AMLR and other awards to accommodate the hypotheses being tested by our LTER component. These activities included the development of additional study sites, increasing sample sizes and sampling frequency of some parameters to better represent Palmer seabird populations, and adding several research protocols to the suite of data being collected to provide a more comprehensive look at aspects of these species' behavior, demography, foraging ecology, and reproductive biology (table 1).

Our field work began on 13 October 1991 and ended on 7 March 1992. Some preliminary results of this first LTER field season are shown in table 2, which compares aspects of the ecology of Adélie penguins and south polar skuas during summers following cold (1991; heavy sea ice development) and warm (1990; light sea ice development) winters. In contrast to south polar skuas, Adélie breeding success and foraging efficiency improved during the summer season following the 1991 winter. Although heavy ice during the spring after the 1991 winter delayed reproduction in skuas (table 2), breeding success was not affected, indicating the availability of silverfish did not change (cf. Trivelpiece et al. 1990). This would suggest that approximately 8-10 years prior to the 1991 winter, sea-ice conditions were light and favored high silverfish recruitment. That such winter conditions did in fact occur a decade ago has been shown by Fraser et al. (1992), who also discuss how changing sea-ice conditions might influence the biology of Adélie penguins. These very preliminary data thus suggest that our LTER component's hypotheses are both testable and appropriate as a vehicle for guiding our research.

This research was supported by National Science Foundation grants DPP 89-18324, DPP 90-11927, and DPP 91-03429. Additional support was received from NOAA/NMFS.

References

Fraser, W. R. and D. G. Ainley. 1988. United States seabird research undertaken as part of the CCAMLR ecosystem monitoring program at Palmer Station 1987-1988. Research report submitted to the National Marine Fisheries Service, La Jolla, California.

Fraser, W. R., W. Z. Trivelpiece, D. G. Ainley, and S. G. Trivelpiece. 1992. Increases in antarctic penguin populations: Reduced competition with whales or a loss of sea ice due to environmental warming. *Polar Biology*, 11:525-531.

Parmelee, D. F., W. R. Fraser, and D. R. Neilson. 1977. Birds of the Palmer Station area. *Antarctic Journal of the U.S.*, 12:14-21.

Trivelpiece, W. Z., D. G. Ainley, W. R. Fraser, and S. G. Trivelpiece. 1990. Skua survival. *Nature*, 345:211.

Palmer LTER program: Hydrography and optics within the peninsula grid, November 1991 cruise

Raymond C. Smith, Karen S. Baker, Kelley K. Hwang, David Menzies, and Kirk J. Waters

Center for Remote Sensing and Environmental Optics
and
Department of Geography
University of California at Santa Barbara
Santa Barbara, California 93106

The Palmer long-term ecological research (LTER) program focuses on marine ecosystem processes that link physical forcing, especially the annual advance and retreat of pack ice, to biological factors at different levels of the food web. The abundance and distribution of phytoplankton biomass and primary production include contributions from open water, the marginal ice zone, and ice algae. Controls on phytoplankton production reflect the space/time variability in ice cover, turbulent mixing, nutrient availability, and solar irradiance. We selected the LTER sampling strategy to elucidate the relative importance of these mechanisms, and our hydrographic and bio-optical observations provide data necessary to quantify linkages between the physical and biological components of the system. During the Palmer LTER cruise on the R/V *Polar Duke* in mid-November 1991, we used the bio-optical profiling system (BOPS II) (Smith et al. 1984; Smith et al.) to sample and define the physical, optical, chemical, and biological characteristics of the marginal ice zone in the large-scale area surrouding Palmer Station. We carried out transects along the Renaud (500), Palmer basin (600), and Dallmann Bay (700) lines of the PalLTER Peninsula grid (Waters and Smith 1991). Here we present preliminary hydrographic and optical results which complement the LTER phytoplankton (Prezelin et al. 1991) and krill work (Quetin et al. 1991).

Figure 1 is a defense meterological satellite program (DMSP), optical line scanner image showing ice cover in LTER cruise area at the start of the cruise. The ice edge was compacted, the pack ice snow covered, and the concentration of large icebergs relatively high. The image shows open water in portions of the Gerlache and Bismarck Straits.

Temperature, conductivity, and sigma-t as a function of depth are shown for each transect line in figure 2. Also shown is the approximate location of the ice edge. Ship observations are consistent with the satellite image. On the Renaud I (500) line the compacted ice edge was near and seaward of station 500.100, which was snow-covered and rafted pack ice. Open and ice-free water was to the northwest, with many large icebergs to the southeast toward the Peninsula. On the Palmer basin line there was open water to the southeast near the Bismarck Strait, snow-covered and rafted pack ice (within which the R/V *Polar Duke* was held fast for four days) between stations 600.040 and 600.060, and

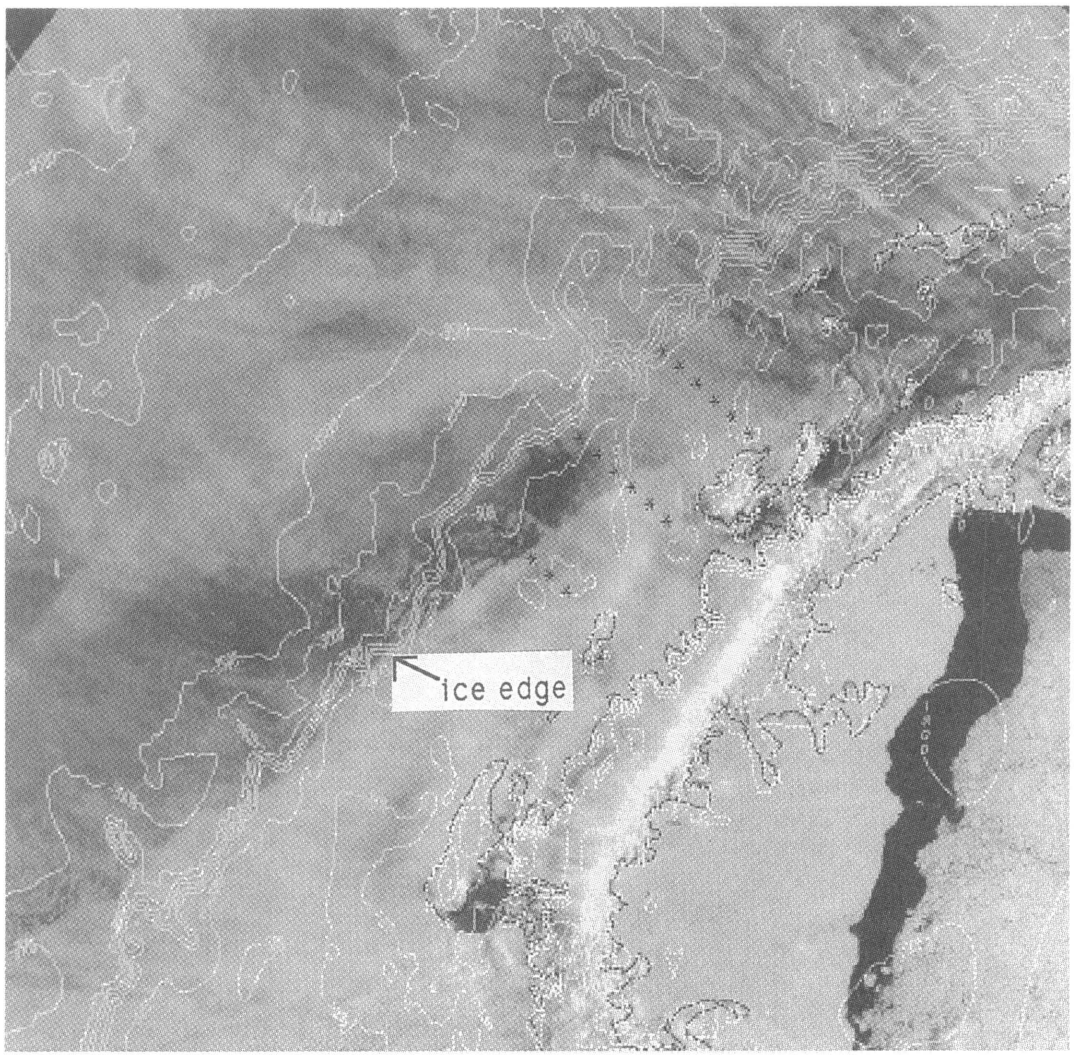

Figure 1. Defense Meterological Satellite Program, Optical Line Scanner (DMSP/OLS) image from 7 November 1991 (1023z) of the Antarctic Peninsula (coast simplified and outlines in black) and the Palmer area during the LTER cruise on the R/V *Polar Duke*. Small arrow points to the compacted ice edge to the west of the Antarctic Peninsula. Station points are shown as black asterisks and bottom topography as white lines with depth in meters.

ice-free water northwest of stations 600.080. The Dallmann Bay line had snow-covered and heavily rafted pack ice and icebergs near station 700.020, with open water in Schollaert Channel and ice-free water at all stations farther northwest.

The beam attenuation coefficient (660 nanometers), stimulated fluorescence, and downwelling irradiance at 488 nanometers as a function of depth are shown in figure 3. Beam c, often characteristic of biogenic particulate matter (Bishop et al. 1992), and fluorescence, an indicator of chl-*a*, show spatial coherence and are consistent with HPLC chl-*a* observations (Prezelin et al. 1991). Elevated values of pigment biomass appear to be associated with the marginal ice zone along the Renaud and Dallmann lines. The Palmer basin line, with open water at each end and a wind-compacted ice edge, had relatively low pigment biomass.

We are analyzing these data further with respect to the coupling between ice-edge dynamics, circulation, optical properties, nutrient distribution, and biological variability. Our goal is to define and model this coupling, using full spectral bio-optical models (Smith et al. 1987; Smith et al. 1989; Bidigare et al. 1992).

This work was supported by National Science Foundation grant DPP 90-11927 (RCS) and is Palmer LTER Publication No. 10. Bob Whritner, Manager of the Arctic and Antarctic Research Center, Scripps Institution of Oceanography, kindly provided the satellite image.

References

Bidigare, R. R., B. B. Prezelin, and R. C. Smith. 1992. Bio-optical models and the problems in scaling. In P. G. Falkowski (Ed.), *Primary Productivity and Biogeochemical Cycles in the Sea.* New York: Plenum Press, in press.

Bishop, J. K. B., R. C. Smith, and K. S. Baker. 1992. Springtime distribution and variability of biogenic particulate matter in Gulf Stream warm-core ring 82B and surrounding N.W. Atlantic waters. *Deep-Sea Research,* 39(1A):S295-S325.

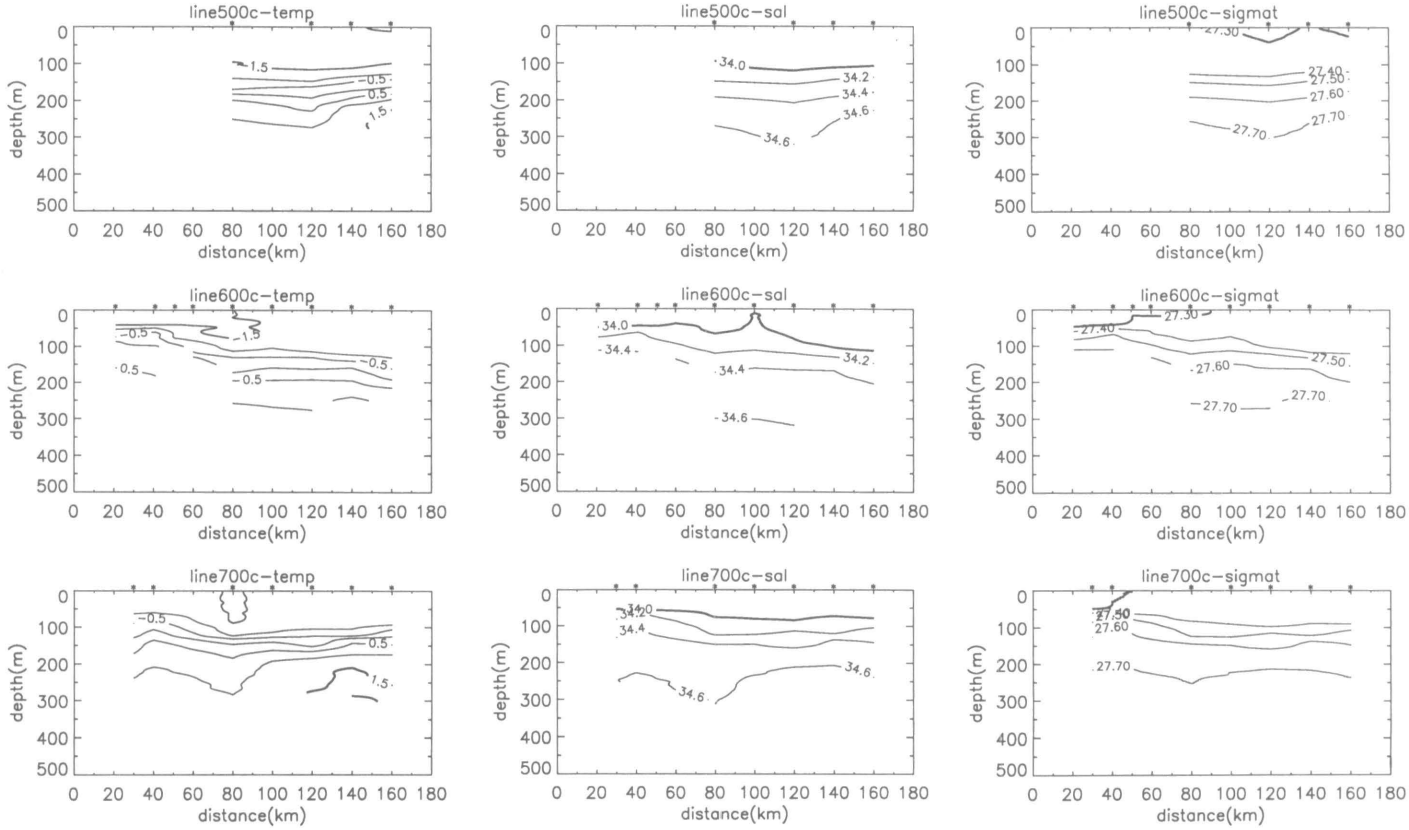

Figure 2. Temperature (degrees Celsius), salinity (percent), sigma-t (kilogram per cubic meter) vs. depth (meters) for transects along the Renaud I (500), Palmer basin (600) and Dallmann Bay (700) lines. Along these lines the approximate location of the ice edge was at grid locations 500.100, 600, 080, 700.025.

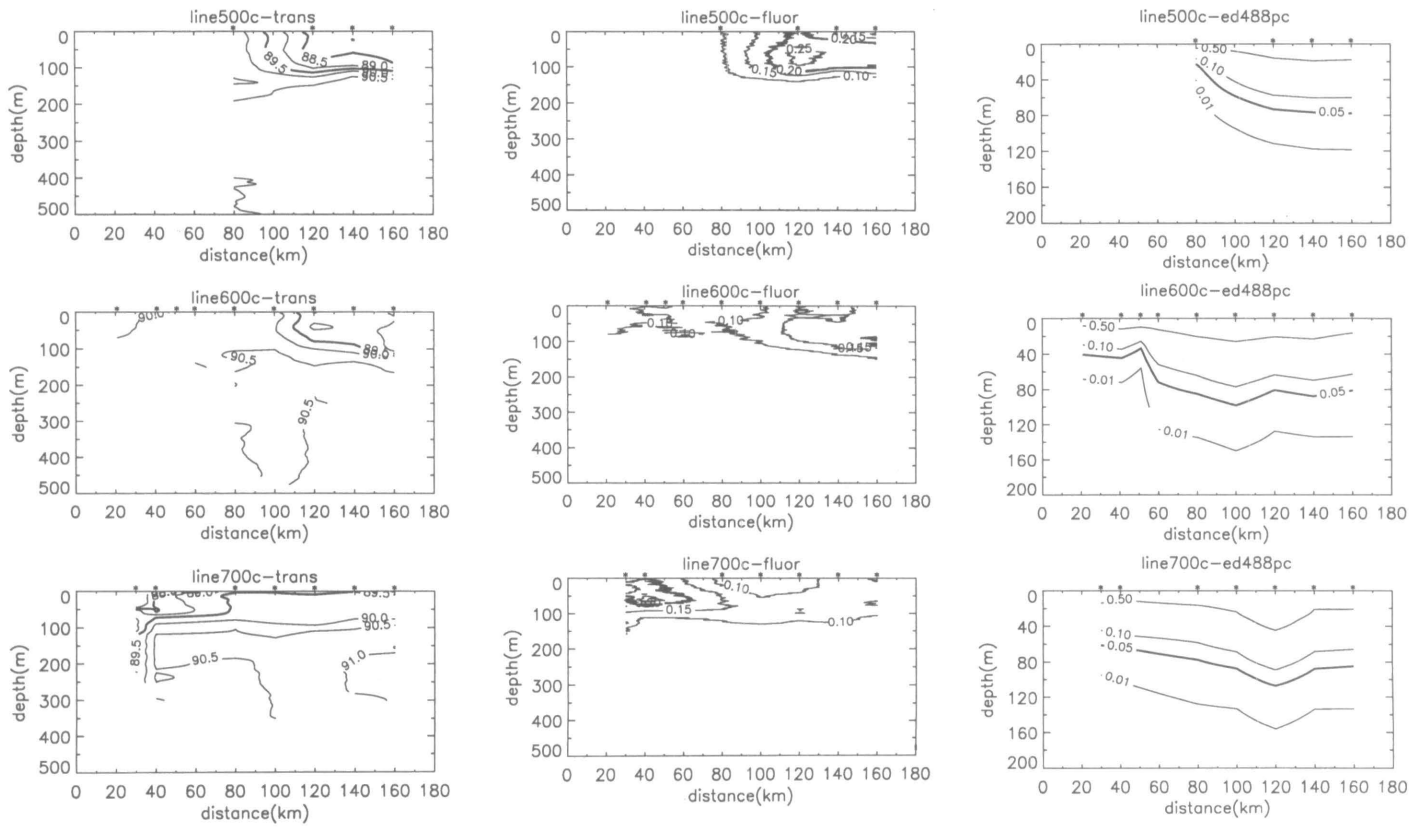

Figure 3. Beam transmittance (percent per meter), stimulated fluorescence (relative), and downwelling irradiance at 488 nanometers (per square meter per nanometer) vs. depth (meters) for transects along the Renaud, Palmer, and Dallmann lines. Scale as for figure 2.

Prezelin, B. B., N. P. Boucher, M. Moline, E. Stephens, K. Keydel, and K. Scheppe. 1992. Palmer LTER: Spatial variability in phytoplankton distribution and surface photosynthetic potential with the peninsula grid, November 1991. *Antarctic Journal of the U.S.*, this issue.
Quetin, L. B., R. M. Ross, B. Prezelin, K. L. Haberman, K. L. Hacecky, and T. Newberger. 1992. Palmer LTER: Biomass and community composition of euphausids within the peninsula grid, November 1991 cruise. *Antarctic Journal of the U.S.*, this issue.
Smith, R. C., C. R. Booth, and J. L. Star. 1984. Oceanographic bio-optical profiling system. *Applied Optics*, 23:2,791-2,797.
Smith, R. C., R. R. Bidigare, B. B. Prezelin, K. S. Baker, and J. M. Brooks. 1987. Optical characterization of primary productivity across a coastal front. *Marine Biology*, 96:575-591.
Smith, R. C., B. B. Prezelin, R. R. Bidigare, and K. S. Baker. 1989. Bio-optical modeling of photosynthetic production in coastal waters. *Limnology Oceanography*, 34(8):1,524-1,544.
Smith, R. C., K. J. Waters, D. Menzies, K. S. Baker, and C. R. Booth. Oceanographic bio-optical profiling system II. In preparation.
Waters, K. J. and R. C. Smith. 1991. Palmer LTER: A sampling grid for the Palmer LTER program. *Antarctic Journal of the U.S.*, this issue.

Palmer LTER program: Hydrography and optics within the peninsula grid, zodiac sampling grid during the 1991-1992 field season

Raymond C. Smith, Karen S. Baker,
Phil Handley, and Tim Newberger

Center for Remote Sensing and Environmental Optics

and

Department of Geography
University of California at Santa Barbara
Santa Barbara, California 93106

The linkages between different trophic levels is a key focus of the Palmer long-term ecological research program (LTER). We selected seabirds, Adélie penguins and south polar skuas (Fraser et al. 1991) to represent upper-tropic level predators, and our study site included the breeding areas of these birds near Palmer Station. We established a fixed set of sampling stations (Palmer grid), within the small boat range of Palmer Station, in order to provide high-resolution time-series data in the immediate area of the LTER predator field and sampling linkage with cruise observations on the larger-scale PalLTER peninsula grid (see figure Waters and Smith 1991). Our objective was to obtain higher resolution physical, optical, chemical, and biological observations, comparable with ship observations, on the Palmer grid.

A Mark V zodiac was outfitted with a platform, two davits with blocks, hand winch, gas powered generator, and consoles for electronics (figure 1). We called this zodiac, when so outfitted, the regional optical zodiac experiment (ROZE) and used it to deploy

- a SeaBird conductivity-temperature-depth recorder (CTD) with SeaTech transmissometer and fluorometer to determine temperature, conductivity, depth, beam transmittance (660 nanometers), and stimulated fluorescence (chlorophyll a);
- an optical free-fall instrument (OFFI) to determine downwelling spectral irradiance and upwelling spectral radiance (Waters et al. 1990); and
- a biosonics instrument to acoustically estimate krill school density.

We used a Trimble Pathfinder Global Positioning System (GPS) and hand-held compass for navigation, a fishfinder for depth information, and an above-water spectral irradiance sensor to complement the in-water component of the OFFI. Here we present a few preliminary hydrographic and optical results that complement the Palmer grid pigment and nutrient observations.

Sigma-t, as a function of depth and time, are shown for the Palmer stations A through E (figures 2 and 3; see map: figure 2 Waters and Smith 1991 or figure 2 Prezelin et al. 1991a). Snow-covered pack ice covered most of Arthur Harbor (and station A) until mid-December 1991. During early December stations B through E shifted between open pack ice (0.4 to 0.6 ice cover) and open water (less than 0.1 ice cover) with several large icebergs in the area. By the end of December open water conditions (with occasional icebergs) prevailed. Pack ice covered the area surrounding stations A (95 percent), B (95 percent), and C (40 percent) for a few days in late January (20 January). In spite of the nearshore environment, these stations show a high degree of coherence with fresher water stabilizing the upper layer as the season progresses. Preliminary analysis suggests that stations D and E are reasonably representative of Palmer basin, but further work is necessary to test this hypothesis.

Figure 3 shows a comparison of beam transmittance (a measure of both organic and inorganic particulate material) and stimulated fluorescence (a measure of chl-*a*) as a function of depth and time at station A. The fluorescence data are consistent with high-pressure liquid chromatography chl-*a* observations (Prezelin et al. 1991b). Beam transmittance and fluorescence show space/time coherence until late January. At that time a heavy rain, accompanied by island and glacier runoff, decreased pigment biomass and increased the non-phytoplankton component of attenuation. Energy available for photosynthesis (data not shown) was redirected to nonviable particulate material. This same event reduced surface stratification (figure 3, sigmat) and mixed particles to greater depth, further reducing energy available for photosynthesis. This is a particularly dramatic illustration of physical and bio-optical coupling.

We are further analyzing these data with respect to the coupling between physical forcing, optical properties, nutrient distribution, and biological variability. Our goal is to define and model this coupling, using full spectral bio-optical models (Smith et al. 1987; Smith et al. 1989, Bidigare et al. 1992).

This work was supported by National Science Foundation grant DPP 90-11927 (RCS) and is Palmer LTER Publication No. 11.

Figure 1. Photograph of the ROZE (Mark V zodiac outfitted for the remote optical zodiac experiment) which was used to deploy a CTD (with fluorometer and transmissometer), an OFFI, and a biosonics instrument. CTD is being deployed, OFFI stored on the starboard side, biosonics fish on the port side. See text for details.

References

Bidigare, R. R., B. B. Prezelin, and R. C. Smith. 1992. Bio-optical models and the problems in scaling. In P. G. Falkowski (Ed.), *Primary Productivity and Biogeochemical Cycles in the Sea.* New York: Plenum Press, in press.

Fraser, W. R., W. Z. Trivelpiece, B. R. Houston, and D.R. Patterson. 1991. Palmer LTER: Seabird research undertaken during 1991-1992 at Palmer Station, Antarctic Peninsula. *Antarctic Journal of the U.S.,* this issue.

Prezelin, B. B., M. Moline, K. Seydel, and K. Scheppe. 1991a. Palmer LTER: Temporal variability in HPLC pigmentation and inorganic nutrient distribution in surface waters adjacent to Palmer Station, December 1991 - February 1992. *Antarctic Journal of the U.S.,* this issue.

Prezelin, B. B., N. P. Boucher, M. Moline, E. Stephens, K. Seydel, and K. Scheppe. 1991b. Palmer LTER: Spatial variability in phytoplankton distribution and surface photosynthetic potential with the peninsula grid, November 1991. *Antarctic Journal of the U.S.,* this issue.

Smith, R. C., R. R. Bidigare, B. B. Prezelin, K. S. Baker, and J. M. Brooks. 1987. Optical characterization of primary productivity across a coastal front. *Marine Biology,* 96:575-591.

Smith, R. C., B. B. Prezelin, R. R. Bidigare, and K. S. Baker. 1989. Bio-optical modeling of photosynthetic production in coastal waters. *Limnology Oceanography,* 34(8):1,524-1,544.

Smith, R. C., K. S. Baker, K. K. Hwang, D. Menzies, and K. J. Waters. 1991. Palmer LTER: Hydrography and optics within the Peninsula grid, November 1991 cruise. *Antarctic Journal of the U.S.,* this issue.

Waters, K. J. and R. C. Smith. 1991. Palmer LTER: A sampling grid for the Palmer LTER program, *Antarctic Journal of the U.S.,* this issue.

Waters, K. J., R. C. Smith, and M. R. Lewis. 1990. Avoiding ship-induced light-field perturbation in the determination of oceanic optical properties. *Oceanography,* 3(2):18-21.

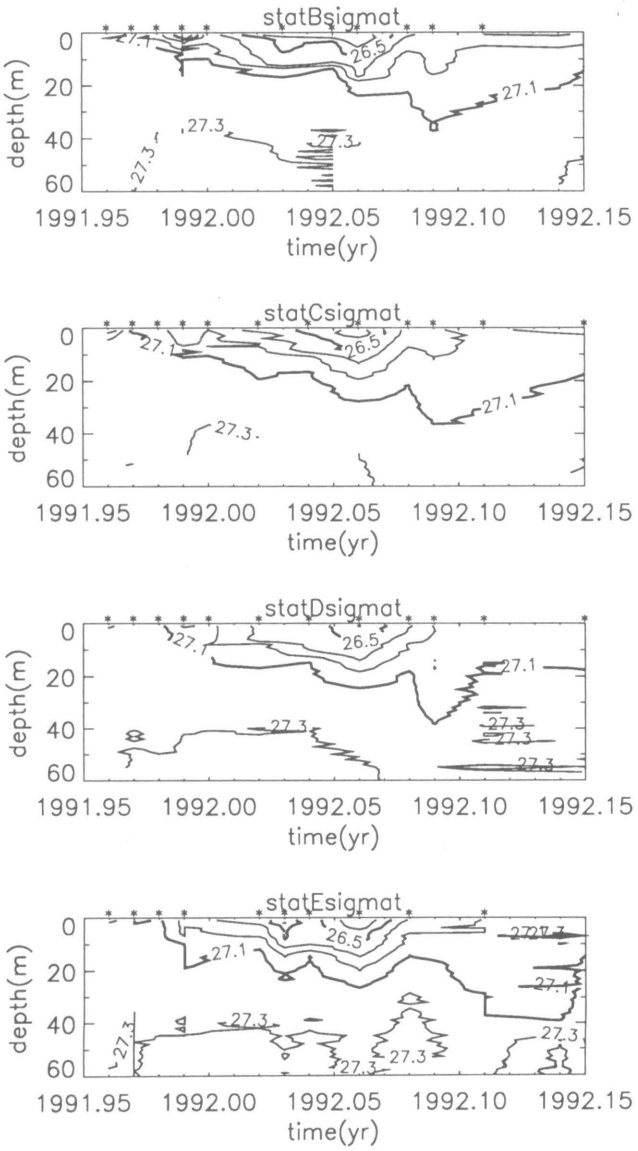

Figure 2. Sigma-t (kilograms per cubic meter) vs. depth (meters) and time for Palmer stations B through E. (top to bottom panel)

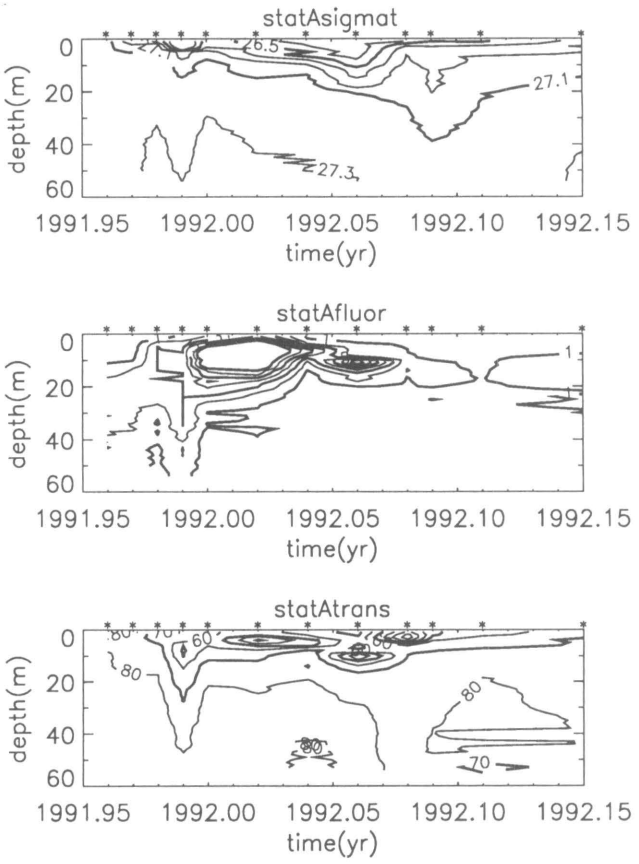

Figure 3. Sigma-t (as in figure 2), beam transmittance (percent per meter), and stimulated fluorescence (relative) as a function of time for station A.

Temporal variation of specific growth rates for phytoplankton in Lake Bonney, Antarctica

THOMAS R. SHARP AND JOHN C. PRISCU

Department of Biology
Montana State University
Bozeman, Montana 59715

Lake Bonney is one of several lakes located in the dry valleys region adjacent to McMurdo Sound. These lakes experience a strong seasonal variation in irradiance and day length; have permanent ice caps; strong vertical nutrient, oxygen, and conductivity gradients; and a virtual absence of planktonic grazers (Parker et al. 1982). The permanent 4-meter-thick ice cap of Lake Bonney reduces under-ice irradiance to less than 5 percent of incident and protects the lake from wind-induced turbulence. The ice cover, together with the strong salinity gradient (Spigel et al. 1990) and low advective stream inflow, creates a hydrodynamically stable water column in which the phytoplankton live, an uncommon situation for pelagic ecosystems. The nonturbulent environment allows for the phytoplankton genera present to become segregated along resource gradients (e.g., light, nutrients, and temperature) into distinct strata.

Three distinct phytoplankton assemblages exist within the trophogenic zone (Priscu et al. 1990; Sharp this issue; Lizotte and Priscu this issue). The assemblages consist of: (i) Cryptophyceae and Chlorohyceae from just under the ice to 8 meters; (ii) flagellated Chrylsophyceae and a small (less than 4 micrometers in diameter) unidentified coccoid from 8 to 16 meters; and (iii) flagellated Chlorophyceae and Chrysophyceae from 16 to 20 meters. These phytoplankton assemblages have been shown to have different photosynthesis-irradiance parameters (Lizotte and Priscu this issue). While earlier studies examined environmental factors that influence photosynthesis in the dry valley lakes (Vincent 1981; Parker et al. 1982; Vincent and Vincent 1982; Priscu et al. 1987), none of them focussed on temporal changes in photosynthetic or growth rates. Vincent (1981) suggested that phytoplankton growth rates are greatest during the austral winter-spring transition when nutrient concentrations should be maximal and irradience rises above the compensation point for photosynthesis. To test this hypothesis, we measured phytoplankton biomass (chlorophyll *a*) nominally every 5 to 7 days during our 1990-1991 (October 1990 to January 1991) and 1991-1992 (September to December 1991) sampling seasons to estimate specific growth rates of phytoplankton biomass from each of the discrete phytoplankton assemblages in Lake Bonney. Net specific growth rates for each phytoplankton assemblage were determined as the change in integrated chlorophyll over the period. Depth integration limits were 4 to 8 meters, 8 to 16 meters, and 16 to 20 meters for each of the respective assemblages.

The figure shows temporal distribution of net specific growth rates for each of the phytoplankton assemblages. Net specific growth rates in the surface phytoplankton layer showed no clear seasonal trend and tended to fluctuate around zero. Net growth rates in the 8- to 16-meter assemblage were positive during the winter-spring transition (September to mid-October) and decreased again in early November (day 300). The rate increased again in late November (day 320), remained near zero during December, and increased in January (day 1). The net growth rates of the 16- to 20-meter phytoplankton layer showed the most dynamic seasonal variation with negative values until mid-October (day 290), followed by a rapid increase and decrease by early December (day 330); the rates fluctuated around zero after day

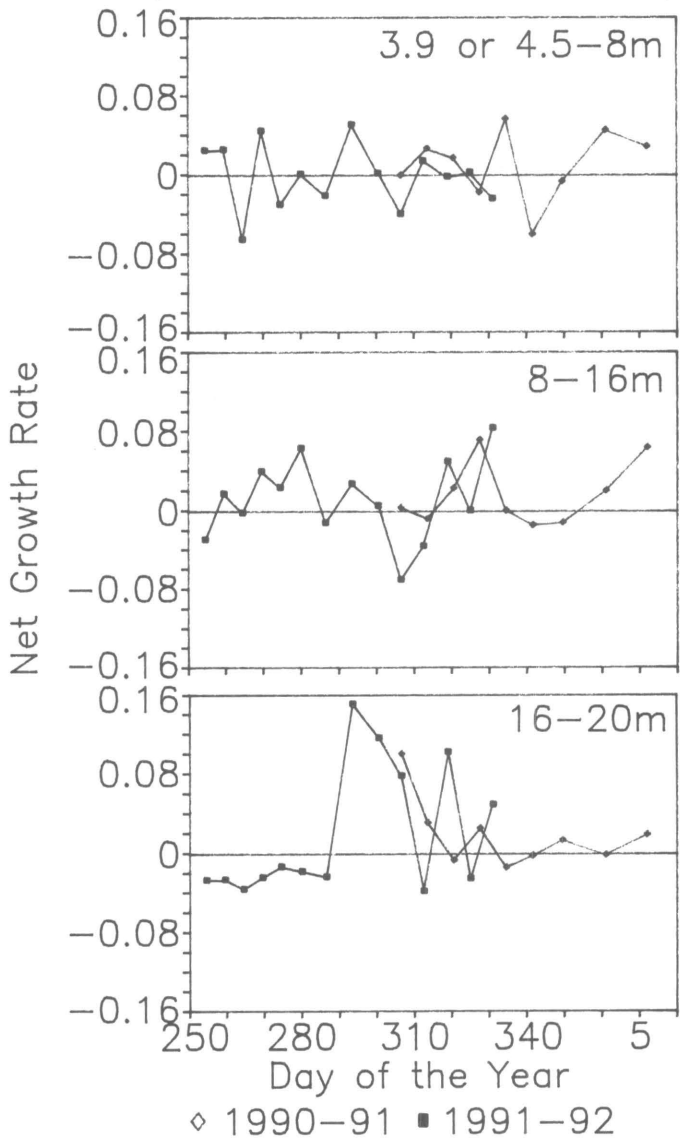

Temporal variation in net specific growth rates (per day) for the surface (4- to 8-meter), middle (8- to 16-meter), and deep (16- to 20-meter) phytoplankton assemblages during the 1990-1991 and 1991-1992 sampling seasons in Lake Bonney.

Average net specific growth rates (per day) for each phytoplankton assemblage.

Phytoplankton Assemblage	Specific growth rate
Surface	
1990-1991	
Day 303-11	0.0126
1991-1992	
Day 252-290	-0.0042
Day 290-334	0.0024
Middle	
1990-1991	
Day 303-11	0.0162
1991-1992	
Day 252-290	0.0142
Day 290-334	0.0095
Deep	
1990-1991	
Day 303-11	0.0157
1991-1992	
Day 252-290	-0.0241
Day 290-334	0.0623

330. Net growth rates were averaged (time weighted) over 1990-1991 (day 303-day 11). The rates from 1991-1992 were averaged over two periods; from day 252 to day 290 when there was a light: dark period and from day 290 to day 334 when the sun was continually above the horizon. The surface (4- to 8-meters) layer had the lowest rates averaged over 1990-1991 and the latter part of 1991-1992. Rates were similar in all three assemblages during 1990-1991. The surface layer had the highest average rate in 1990-1991. The average rate in the surface (4- to 8-meter) layer was negative from day 252 to day 290 in 1991-1992 (table), indicating that biomass declined. The middle (8- to 16-meter) layer had the highest average specific growth rate from day 252 to day 290 in 1991-1992. This high rate may have been influenced by settling of biomass from the surface layer rather than from production within the middle layer. The lowest and highest average rates were in deep (16- to 20-meter) layer from day 252 to day 290 and from day 290 to day 334, respectively, in 1991-1992.

The increasing growth rate with depth could have resulted from increased growth efficiency despite lower light because of the compensating effect of higher temperature and nutrient concentrations with depth. Also, because the highest rates occurred within the two deeper layers, they may be illusory, resulting not from primary production but from the settling of biomass from above. The average net specific growth rates for Lake Bonney phytoplankton are about four-fold lower than those previously reported for lake phytoplankton (Forsberg 1985). The rates are also lower than those for phytoplankton in antarctic lakes Fryxell and Vanda (mean growth rates of 0.072 and 2.16 per day were estimated from the data of Priscu et al. 1987. However, the rates reported by Priscu et al. (1987) are based on carbon incorporation into protein, and hence, do not include losses.

In summary, the period of maximal growth in the phytoplankton assemblages in Lake Bonney occurs after the onset of continuous day light (around 17 October), similar to what Tilzer and Dubinsky (1987) hypothesized for phytoplankton in the southern oceans. Our data imply that the hypothesis of Vincent (1981) must be revised if it is to apply to all antarctic lakes.

We thank Mike Lizotte, Ben Hatcher, Ron Nuggent, Joe Rudek, and Barb Kelley. This work was supported in part by National Science Foundation grant DPP 88-20591.

References

Forsberg, B. R. 1985. The fate of planktonic primary production. *Limnology and Oceanography*, 30:807-819.

Lizotte, M. P. and J. C. Priscu. 1992. Photosynthesis-irradiance relationships in phytoplankton from the physically stable water column of a perennially ice-covered lake (Lake Bonney, Antarctica). *Journal of Phycology*, 28:179-185.

Lizotte, M. P. and J. C. Priscu. 1992. Algal pigments as markers for stratified phytoplankton populations in Lake Bonney (dry valleys). *Antarctic Journal of the U.S.*, this issue.

Parker, B. C., G. M. Simmons Jr., K. G. Seaburg, D. D. Cathey, and F. C. T. Allnutt. 1982. Comparative ecology of plankton communities in seven antarctic oasis lakes. *Journal of Plankton Research*, 4:271-285.

Priscu, J. C., L. R. Priscu, W. F. Vincent, and C. Howard-Williams. 1987. Photosynthate distribution by microplankton in permanently ice-covered antarctic desert lakes. *Limnology and Oceanography*, 32:260-270.

Priscu, J. C., T. R. Sharp, M. P. Lizotte, and P. J. Neale. 1990. Photoadaptation by phytoplankton in permanently ice-covered antarctic lakes: Response to a non-turbulent environment. *Antarctic Journal of the U.S.*, 25:221-222.

Sharp, T. R. 1992. Phytoplankton ecology in Lake Bonney, Antarctica: Emphasizing temporal variation of growth and loss rates. Master of Science Thesis, Montana State University.

Spigel, R. H., I. V. Shepard, and J. C. Priscu. 1990. Temperature and conductivity finestructure from Lake Bonney. *Antarctic Journal of the U.S.*, 25:228.

Tilzer, M. M. and Z. Dubinsky. 1987. Effects of temperature and day length on the mass balance of antarctic phytoplankton. *Polar Biology*, 7:35-47.

Vincent, W. F. 1981. Production strategies in antarctic inland waters: Phytoplankton eco-physiology in a permanently ice-covered lake. *Ecology*, 62:1,215-1,224.

Vincent, W. F. and C. L. Vincent. 1982. Factors controlling phytoplankton production in Lake Vanda (77° S). *Canadian Journal of Fisheries and Aquatic Science*, 39:1,602-1,609.

Algal pigments as markers for stratified phytoplankton populations in Lake Bonney (dry valleys)

MICHAEL P. LIZOTTE AND JOHN C. PRISCU

Department of Biological Sciences
Montana State University
Bozeman, Montana 59717

Lake Bonney and other perennially ice-covered lakes located in the dry valleys near McMurdo Sound are among the most hydrodynamically stable systems known. The plankton of these lakes are entirely microbial, primarily algae and bacteria. Phytoplankton populations are highly stratified in vertical space and are typically dominated by flagellates. These phytoplankton show extreme physiological acclimation to their low irradiance environment (Lizotte and Priscu 1991, 1992; Neale and Priscu 1991).

Pigment signatures can be used to chemotaxonomically determine the relative biomass associated with major groups of phytoplankton based on the abundance of specific accessory pigments. Past studies of taxonomic composition in the dry valley lakes have been based on microscopic examination, but results have not always been quantitative, and different results have been reported from studies on fresh-filtered samples (Koob and Leister 1972) and preserved water samples (e.g., Parker et al. 1982). Furthermore, comparisons between pigment analyses and microscopic enumeration (from preserved samples) have shown that some phytoplankton groups can be greatly underestimated by the latter method (Gieskes and Kraay 1983). Over three field seasons, we collected samples for both the analyses of pigment composition by high-performance liquid chromatography (HPLC) and microscopic enumeration from preserved water samples. Our objective was to determine the vertical distribution of phytoplankton in the stratified waters of the dry valley lakes. If a single species dominates a particular depth strata, we may then be able to use pigment ratios or cellular concentrations to give more detail to our concurrent studies on the photophysiology of these unique phytoplankton populations (Lizotte and Priscu 1991, 1992; Neale and Priscu 1991; Sharp and Priscu; Priscu).

In this report, we will discuss pigment profiles from Lake Bonney (east lobe) collected during the 1990-1991 field season. Water from piezometric depths of 4 to 20 meters was sampled through holes (0.25 to 1 meter in diameter) in the ice cover. Particulates were collected on glass-fiber filters (Whatman GF/C) and placed immediately into liquid nitrogen. Pigments were extracted from filtered samples with acetone. Extracts were injected into Waters HPLC system consisting of a C-8 reverse-phase column, two pumps, a photodiode array detector, and fluorimeter. Pigments were separated with a linear gradient from 60 percent acetone/40 percent aqueous ion-pairing solution to 100-percent acetone over 20 minutes. Phytoplankton subsamples were preserved with 1 percent Lugol's solution, settled, and counted with an inverted microscope.

Profiles of chlorophyll *a* (a pigment common to all algae) and the major diagnostic accessory pigments in Lake Bonney show three distinct maxima (figure). Immediately below the ice, alloxanthin coincides with chlorophyll *a*, implying that algae of the *Cryptophyceae* are dominant. This corresponds with the presence of cryptophyte-type flagellates previously identified as *Chroomonas lacustris* (e.g., Parker et al. 1982). At intermediate depths, the fucoxanthin peak corresponds with the presence of flagellates identified as *Ochromonas sp.*, suggesting algae of the *Chrysophyceae* are dominant. The deepest peak in chlorophyll *a* (18 meters) followed an increase in chlorophyll *b*, suggesting the dominance of algae of the *Chlorophyceae*. The chlorophyll *b* peak coincides with the presence of flagellates previously identified as *Chlamydomonas subcaudata* (e.g. Koob and Leister 1972; Parker et al. 1982).

Seasonal trends in pigments show that the under-ice cryptophyte community peaked during the austral spring while deeper populations of chrysophytes and chlorophytes continued to grow into the summer. The profiles for fucoxanthin indicate that flagellated chrysophytes may have moved up the water column before forming a distinct peak at 12 meters. The strong gradients in salinity and temperature above 12 meters (e.g., Spigel et al. 1991) may present a limit to further upward migration.

Comparisons made between pigment profiles and phytoplankton cell counts in the ocean have shown that cryptophyte algae may be underestimated by the latter method (Gieskes and Kraay 1983). Our cell counts imply that the biovolume of cryptophytes was no higher than that of chlorophytes (*Chlamydomonas*) immediately below the ice (Sharp unpublished data), whereas pigment analysis showed a clear cryptophyte signature and little or no chlorophyte indicator pigments (chlorophyll *b* in figure). The upper water columns of Lake Hoare and Lake Fryxell (in the same valley as Lake Bonney) also had pigment signatures indicative of cryptophytes (Lizotte unpublished data). Because of the potential errors associated with cell preservation, pigment analysis gives us the first clear, quantitative picture of the relative abundance of phytoplankton in the dry valley lakes.

We thank Tom Sharp, Patrick Neale, Robert Spigel, and Ian Forne for their assistance in the field. This work was supported by National Science Foundation grant DPP 88-20591.

References

Gieskes, W. W. C. and G. W. Kraay. 1983. Dominance of Cryptophyceae during the phytoplankton spring bloom in the central North Sea detected by HPLC analysis of pigments. *Marine Biology*, 75:179-185.

Koob, D. D. and G. L. Leister. 1972. Primary productivity and associated physical, chemical, and biological characteristics of Lake Bonney: A

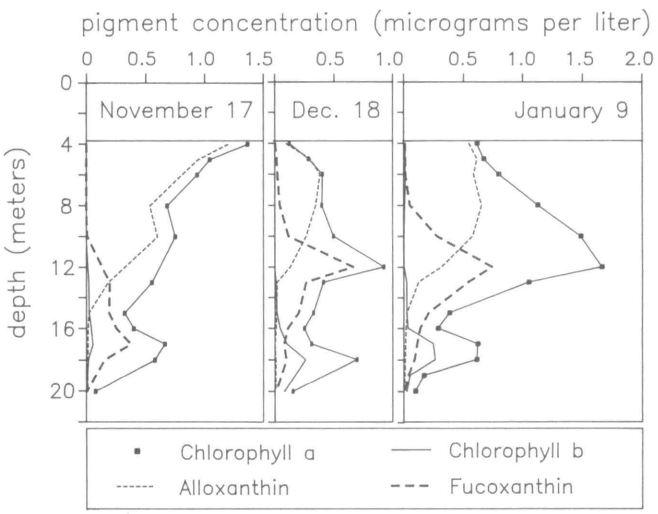

Profiles of algal pigment concentrations.

perennially ice-covered lake in Antarctica. (Antarctic Research Series) Washington, D.C.: American Geophysical Union. 20:51-68.
Lizotte, M. P. and J. C. Priscu. 1992. Photosynthesis-irradiance relationships in phytoplankton from the physically stable water column of a perennially ice-covered lake (Lake Bonney, Antarctica). *Journal of Phycology*, 28:179-185.
Lizotte, M. P. and J. C. Priscu. 1991. Natural fluorescence and photosynthetic quantum yields in vertically stable phytoplankton from perennially ice-covered lakes (dry valleys). *Antarctic Journal of the U.S.*, in press.
Neale, P. J. and J. C. Priscu. 1991. Variation of the fluorescence quantum yield in relation to photosynthesis by phytoplankton from perennially ice-covered Lake Bonney. *Antarctic Journal of the U.S.*, 26(5):228-230.
Parker, B. C., G. M. Simmons Jr., K. G. Seaburg, D. D. Cathey, and F. T. C. Allnut. 1982. Comparative ecology of plankton communities in seven antarctic oasis lakes. *Journal of Plankton Research*, 4:271-286.
Priscu, J. C. 1992. Particulate organic matter decomposition in the water column of Lake Bonney, Taylor Valley. *Antarctic Journal of the U.S.*, this issue.
Sharp, T. R. and J. C. Priscu. 1992. Temporal variations of phytoplankton-specific growth and loss rates in Lake Bonney, Antarctica. *Antarctic Journal of the U.S.*, this issue.
Spigel, R. H., I. Forne, I. Sheppard, and J. C. Priscu. 1992. Difference in temperature and conductivity between east and west lobes of Lake Bonney: Evidence for circulation within and between lobes. *Antarctic Journal of the U.S.*, 26(5):221-222.

Particulate organic matter decomposition in the water column of Lake Bonney, Taylor Valley, Antarctica

JOHN C. PRISCU

Department of Biological Sciences
Montana State University
Bozeman, Montana 59717

Phytoplankton biomass within the dry valley lakes adjacent to McMurdo Sound is surprisingly high despite photosynthetic rates that are light-limited (Priscu et al. 1987; Priscu 1989; Lizotte and Priscu 1992). Presumably, the accumulation of phytoplankton biomass in these systems is the result of low loss rates. Losses to grazing are minimal owing to the virtual lack of crustaceous zooplankton and phytoplankton sinking is also assumed to be low because most of the species in the lakes are flagellated and thus capable of maintaining themselves at specific depths (Priscu et al. 1990b; Lizotte and Priscu 1992a,b). Because grazing and sinking losses are potentially low in these systems, I conducted experiments to determine if bacterial decomposition of phytoplankton may be a significant sink for phytoplankton organic matter.

Potential decomposition rates of phytoplankton in the east lobe of Lake Bonney were determined by measuring the rate of $^{14}C0_2$ released from phytoplankton labeled with carbon-14. Equilibrium labeling was obtained by incubating phytoplankton collected immediately under the ice cap with saturating light (approximately 100 micromoles of quanta per meter squared per second) for up to 4 days with $NaH^{14}CO_3$. Equillibrium labeling of the major photosynthetic end-products has been shown to occur within 24 hours (Priscu et al. 1987). A known amount (in terms of activity and biomass) of labeled phytoplankton was concentrated onto Whatman GF/C glass-fiber filters, which were air-dried then suspended in gas-tight vials containing 10 milliliters of lake water from selected depths. $^{14}CO_2$ released via decomposition of phytoplankton was trapped on an ethanolamine-saturated glass-fiber filter placed within each vial. Parallel samples treated with 5 percent formalin (final concentration) were used to correct for $^{14}CO_2$ release unrelated to decomposition.

Results from decomposition experiments conducted in 1990 and 1991, along with corresponding phytoplankton primary productivity and chlorophyll *a* profiles, are presented in figure 1. Decomposition rates were always highest just beneath the permanent ice cap and declined with depth in the trophogenic zone (zone where primary productivity occurs; just beneath the ice to about 20 meters). Average decomposition rates within the

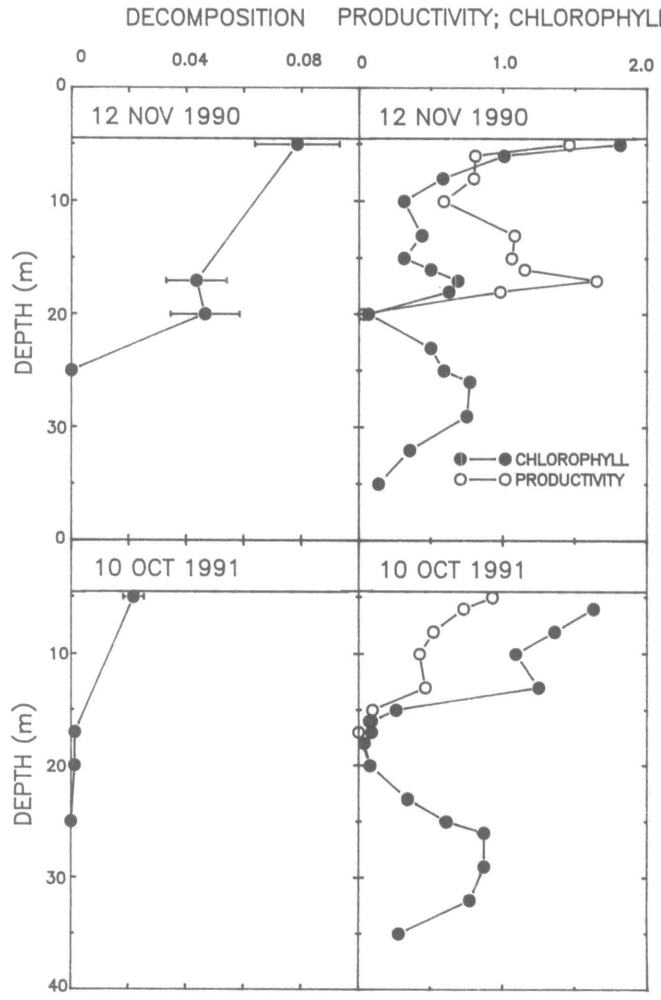

Figure 1. Profiles of decomposition rates (percent per day), primary productivity (micrograms carbon per liter per day), and chlorophyll (micrograms per liter) on 12 November 1990 and 10 October 1991 in the east lobe of Lake Bonney. The horizontal lines below the date denote the bottom of the ice.

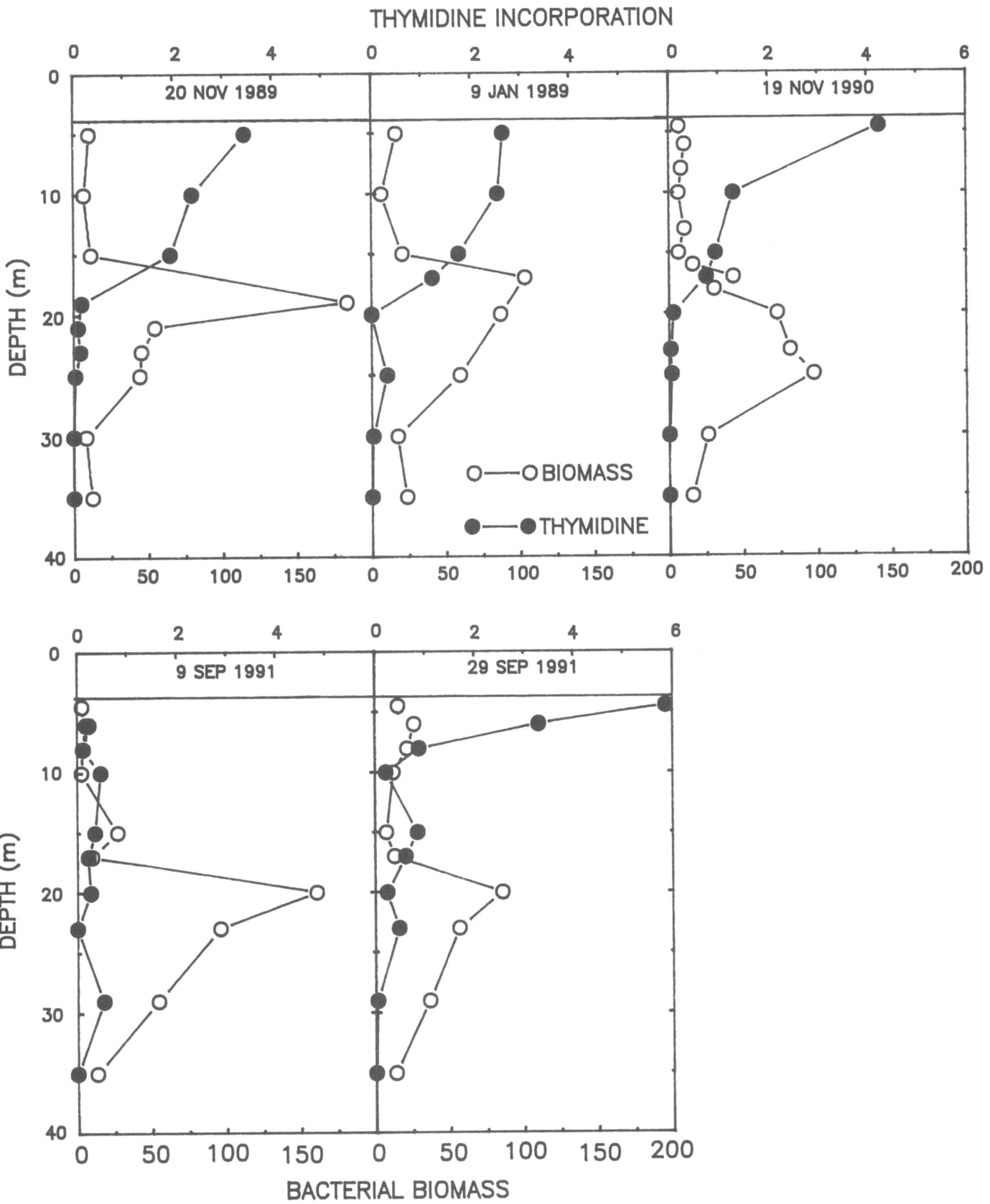

Figure 2. Profiles of bacterial activity (0.0001 nanomolar thymidine incorporation per hour) and bacterial biomass (micrograms carbon per liter) in the east lobe of Lake Bonney. The horizontal lines below the dates denote the bottom of the ice.

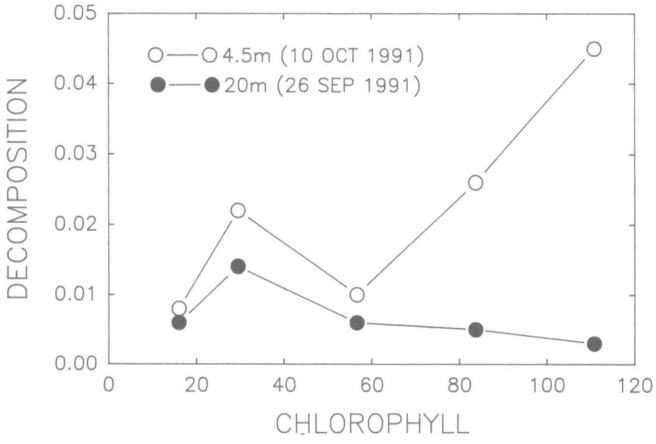

Figure 3. Decomposition rate (percent per day) as a function of chlorophyll *a* concentration (micrograms per liter) for water samples from the east lobe of Lake Bonney.

trophogenic zone were 0.056 and 0.008 percent per day for the 1990 and 1991 experimental dates, respectively (average 0.032). Data from phytoplankton photosynthesis measured over the spring and summer at Lake Bonney revealed an average increase in phytoplankton carbon of about three percent per day (J. C. Priscu, unpublished data). Hence, potential losses of phytoplankton from bacterial decomposition are several orders of magnitude lower than phytoplankton growth, a result confirmed using models for phytoplankton growth and loss (Sharp and Priscu 1992; Sharp 1992).

Decomposition was never measurable below the trophogenic zone (25 meters), which corresponds with a low or undetectable level of heterotrophic bacterial activity (tritium-thymidine incorporation) at 25 meters (figure 2). Interestingly, bacterial biomass was relatively high at 25 meters despite low thymidine incorporation. Collectively these results imply that bacteria below the trophogenic zone are inactive with respect to particulate organic matter decomposition and thymidine incorporation. Various inorganic nitrogen signatures below the trophogenic zone (Sharp and Priscu 1990; J. C. Priscu unpublished data) suggest that high bacterial biomass in this region may be due to chemoautotrophic nitrifying bacteria, which do not incorporate thymidine or oxidize organic carbon (Priscu et al. 1990a). The lack of phytoplankton decomposition below the trophogenic zone may explain the persistence of a chlorophyll peak in these aphotic waters (figure 1).

To assess the kinetic response of decomposition in the upper and lower trophogenic zone, decomposition rates were measured over a range of phytoplankton concentrations (figure 3). These experiments showed that bacterial decomposition activity at 4.5 meters generally increased with increasing phytoplankton biomass, whereas bacterial decomposition activity at 20 meters did not respond to additional phytoplankton biomass. Perhaps the exoenzymes required to hydrolyze particulate organic matter could not be induced in bacteria at 20 meters or perhaps deep-water bacteria in Lake Bonney are acclimated to using the large pool of dissolved organic carbon that exists at and below 20 meters (J. C. Priscu unpublished data). Bacterial enzymes may have also been saturated below the lowest level of phytoplankton used in the experiment.

Despite lack of clear biochemical explanations at this time, data obtained thus far support the following conclusions:

- Phytoplankton decomposition rates (and loss rates in general) are extremely low relative to phytoplankton production rates.
- Heterotrophic bacterial activity below the trophic zone is extremely low (and may be absent).
- Bacteria below the chemocline may be dominated by chemoautotophs (e.g., nitrifying bacteria).

I thank Tom Sharp, Michael Lizotte, Joseph Rudek, and Patrick Neale for their assistance in the field. This work was supported in part by National Science Foundation grant DPP 88-20591.

References

Lizotte, M. P. and J. C. Priscu. 1992a. Photosynthesis-irradiance relationships in phytoplankton from the physically stable water column of a perennially ice-covered lake. *Journal of Phycology*, 28:179-185.

Lizotte, M. P. and J. C. Priscu. 1992b. Algal pigments as markers for stratified phytoplankton populations in Lake Bonney (dry valleys). *Antarctic Journal of the U.S.*, this issue.

Priscu, J. C., L. R. Priscu, V. F. Warwick, and C. Howard-Williams. 1987. A photosynthate distribution by microphytoplankton in permanently ice-covered antarctic desert lakes. *Limnology and Oceanography*, 23(1):260-270.

Priscu, J. C. 1989. Photon dependence of inorganic nitrogen transport by phytoplankton in antarctic lakes. In W. F. Vincent and E. Ellis-Evans (Eds.), High Latitude Limnology. *Hydrobiologia*, 172. Klewer Press. 173-182.

Priscu, J. C., M. T. Downes, L. R. Priscu, A. C. Palmisano, and C. W. Sullivan. 1990a. Dynamics of ammonium oxidizer activity and nitrous oxide (N_2O) within and beneath antarctic sea ice. *Marine Ecology Progress Series*, 62:37-46.

Priscu, J. C., T. R. Sharp, M. P. Lizotte, and P. J. Neale. 1990b. Photoadaptation by phytoplankton in permanently ice-covered antarctic lakes: Response to a nonturbulent environment. *Antarctic Journal of the U.S.*, 25:221-222.

Sharp, T. R. and J. C. Priscu. 1991. Ambient nutrient levels and the effects of nutrient enrichment on primary productivity in Lake Bonney. *Antarctic Journal of the U.S.*, 25(5):226-227.

Sharp, T. R. 1992. Phytoplankton ecology in Lake Bonney, Antarctica: Emphasizing temporal variation of growth and loss rates. M.S. Thesis, Montana State University.

Sharp, T. R. and J. C. Priscu. 1991. Rates of production and growth for phytoplankton in Lake Bonney. *Antarctic Journal of the U.S.*, 26(5):225.

Sharp, T. R. and J. C. Priscu. 1992. Temporal variation of phytoplankton-specific growth and loss rates in Lake Bonney, Antarctica. *Antarctic Journal of the U.S.*, this issue.

Carbon cycling in a redox-stratified antarctic lake, Lake Fryxell

BRIAN L. HOWES, DAVID R. SCHLEZINGER,
DALE D. GOEHRINGER, AND SUSAN BROWN-LEGER

Biology Department
Woods Hole Oceanographic Institution
Woods Hole, Massachusetts 02543

The ice-free valleys of southern Victoria Land contain a variety of perennially ice-covered lakes. Lake Fryxell (75°35' S 163°35' E) is a closed basin lake (no outflow) in the lower Taylor Valley with a surface area of 7 square kilometers (Lawrence and Hendy 1985), a maximum basin depth of 18.7 meters, and a center-ice thickness of 4.5 meters. While light is greatly attenuated by the ice, enough penetrates to the water column to support active photosynthetic communities (Vincent 1981; Priscu et al. 1987; Priscu 1989; Seaburg et al. 1983). The central basin of Lake Fryxell supports some of the highest rates of carbon fixation for McMurdo Dry Valley lakes (Vincent 1981), which, coupled with the virtual absence of plant production in the watershed—hence limited input of allochthonous organic matter (Matsumoto et al. 1989; Aiken et al. 1991; McKnight et al. 1991)—results in an active carbon cycle dominated by internal cycling. The lake ice cover also affects carbon cycling within the lake by preventing wind-driven mixing. In the central basin of Lake Fryxell, the water column appears to be density stratified and amictic below a depth of 6 to 7 meters (figure 1 Lawrence and Hendy 1985), with dissolved constituents moving via diffusion.

The end-product of the phytoplankton production and the amictic water column is an aerobic euphotic zone (5-9.5 meters) and anoxic bottom waters resulting from the vertical transport and subsequent decay of particulate organic matter. The anoxic basin covers about 2.2 square kilometers or about one-third of the lake area. Unlike a well oxygenated water column, the redox stratified waters of Lake Fryxell allow for carbon mineralization through a diversity of terminal electron acceptor pathways (figure 2).

Despite many studies of the rates and controls of photosynthesis in these lake ecosystems (Vincent 1981; Priscu 1989; Koob and Leister 1972), almost none have addressed the rates and pathways of mineralization of the organic matter produced. The primary focus has been on nutrient transformations using *in situ* incubations (Vincent et al. 1981) or geochemical modeling (Canfield and Green 1985).

We are developing a carbon balance for Lake Fryxell based upon both *in situ* and modelled rates of organic matter turnover. Aerobic respiration of the water column was determined using bottle incubations: *in situ* with pulsed oxygen electrodes (Endeco, Inc.) and in laboratory (with poisoned controls) at *in situ* temperatures using electrodes (Orbisphere) and Winkler titrations. Denitrification has yet to be measured directly, but appears low because of the low concentration of dissolved nitrate (figure 2) consistent with the lack of a N_2 or nitrous-oxide signal in dissolved gas profiles and undetectable nitrous-oxide evolution in the presence of C_2H_2 (data not shown). Sulfate reduction in the water column was determined using a chromium reduction method (Howes et al. 1984) to recover microbially transformed $^{35}SO_4$ from reduced pools and measured SO_4 pools. Methane production modelled from methane profiles was determined by head space stripping of lake water and determination by gas chromatography (FID).

Aerobic respiration is the dominant respiratory pathway in the central basin of Lake Fryxell. Rates varied with depth in each year, with a broad maximum extending throughout most of the euphotic zone (figure 3a), yielding an annual integrated rate of 2,900 mmol $m^{-2}yr^{-1}$. Although this rate may be an over estimate, the *in situ* and laboratory methods yielded similar values in both years.

Combining rates of sulfate reduction in the water column (figure 3a) and sediments (Howes and Smith 1990), the annual areal rate ($2C = 1SO_4$) is 150 mmol C $m^{-2}yr^{-1}$. While calculations based on $S^=$ diffusion did not predict a significant watercolumn $S^=$ source (Howes and Smith 1990), the modelled rates are low because they do not include the high rates of $SO_4^=$ reduction and $S^=$ oxidation associated with carbon fixation measured below the interface.

Unlike less biogeochemically active elements (e.g., sodium, chlorine, magnesium, calcium, etc.) (Green et al. 1988; Lawrence and Hendy 1985), which have potential lifetimes in the water column of thousands of years, the major S pools are cycling much more rapidly, with the dissolved $S^=$ and $SO_4^=$ pools turning over about once every hundred years (9.5-18.5 meters) at constant reduction rates.

Vertical distribution of sulfate reduction in Lake Fryxell is similar to the Black Sea (Albert et al. in press), however, because of high ($SO_4^=$) and rates of delivery of organic matter to the sediments, water column and sediment rates are about equal on an areal basis. In contrast, Lake Fryxell sediments account for only about 5 percent of the total in spite of the much shallower

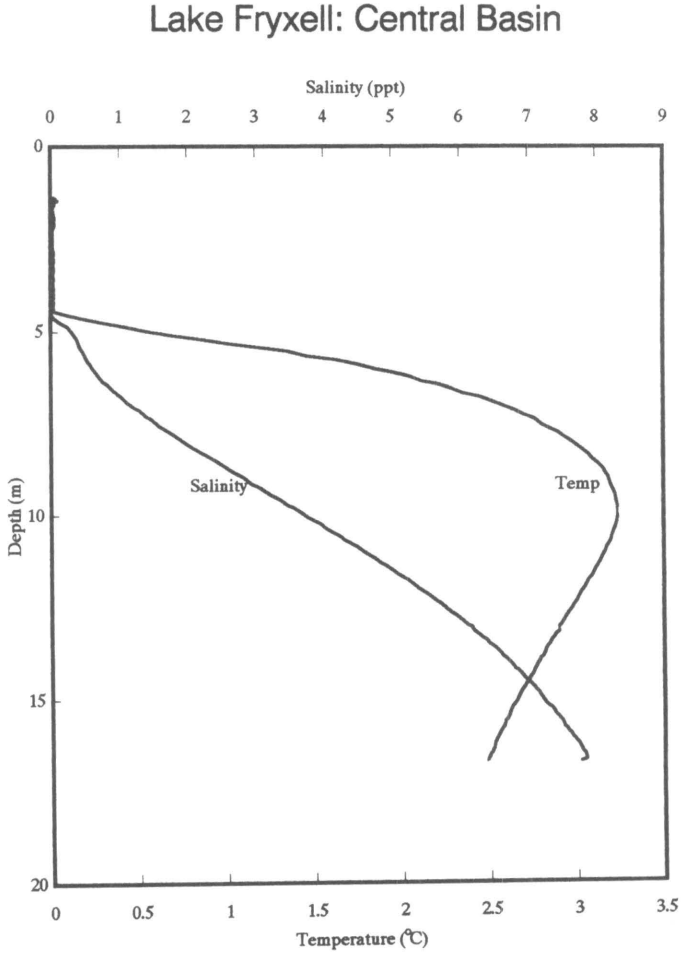

Figure 1. Depth profiles of temperature and salinity, December 1991.

water depth (18 vs. 2100 meters). This difference is most likely because of the influx of organic matter, and secondarily because of the limitation of sulfate, since the energy flow through sediment-sulfate reduction plus methanogenesis is still a small percentage of the water column sulfate- reduction rate.

Because of the amictic and low sulfate bottom waters (figure 2), rates of methanogenesis can be accurately measured by diffusion modelling. The flux from the sediments is 22 mmol C $m^{-2}yr^{-1}$; enrichment studies suggest this is about 80 vs. 20 percent through carbon-dioxide reduction vs. acetate fermentation (Smith et al. submitted). Methane represents a small proportion of the total carbon cycle (less than 0.5 percent), but is a mechanism (like $S^{=}$) for recycling energy to the upper water column to support anaerobic and aerobic microbial processes. Methane consumption in Lake Fryxell appears to be primarily anoxic, possibly linked to sulfate reduction with little reaching the oxic zone (figure 3a Reeburgh 1980, Iversen and Jorgensen 1985).

An unexpected finding was the apparent "gap" in carbon mineralization from 9.5-10.5 meters (figure 3a) where bacterial numbers, turbidity, and energy-charge ratios suggest the highest concentration of microbial activity (Smith and Howes 1990). As this interval coincides with the dissolved iron (figure 3b) and manganese maxima (Harnish et al. 1991), we predict an active metal cycle associated with microbial iron (and possibly Mn) reductions at these depths. Significant rates of iron reduction have been reported in seasonally ice-covered antarctic lakes (Ellis-Evans and Lemon 1989).

Overall, the total rates of organic matter mineralization are similar to organic matter input through photosynthesis (Vincent 1981); however, given the limited temporal coverage of extant productivity data, an exact comparison is not possible at present. There was a gradient of decreasing carbon mineralization with increasing distance from the euphotic zone. The finding that over 90 percent of the organic matter entering the water column is degraded aerobically is consistent with the density stratified water column and the apparent absence of pellet-forming grazers. Both features tend to maintain decomposing phytoplankton particles within the water column and decrease the role of the sediments in organic-matter cycling.

This research was supported by National Science Foundation grant DPP 89-18782. The authors are grateful to C. D. Taylor, R.A. Harnish, and R.L. Smith for discussions, and to B. Budka, M. Bryson, J. Weber, VXE-6, and Antarctic Support Associates for their tireless assistance in the conduct of this work.

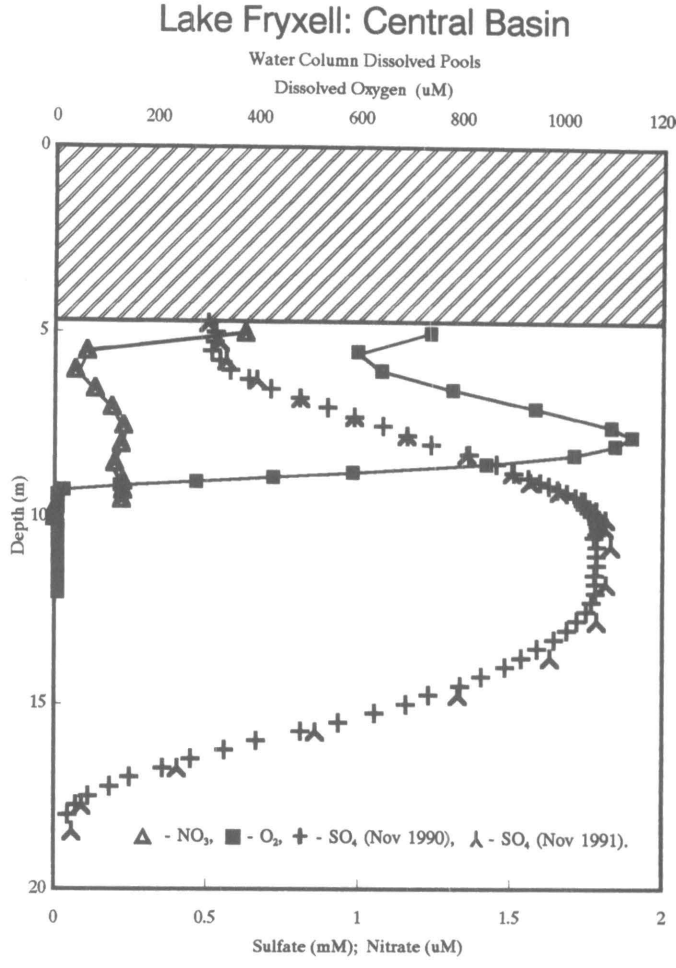

Figure 2. Depth profiles of water column oxygen, sulfate, and nitrate concentrations. Depths adjusted relative to 1990 water level.

References

Aiken, G. R., D. M. McKnight, R. L. Wershaw, and L. Miller. 1991. Evidence for the diffusion of aquatic fulvic acid from the sediments of Lake Fryxell, Antarctica. In R.A. Baker (Ed.), *Organic substances and sediments in water*. Lewis, in press.

Albert, D. C., C. D. Taylor, and C.S. Martens. In Press. Sulfate reduction rates and low molecular weight fatty acid concentrations in the water column and surficial sediments of the Black Sea. *Deep Sea Research*.

Canfield, D. E. and W. J. Green. 1985. The cycling of nutrients in a closed-basin antarctic lake, Lake Vanda. *Biogeochemistry*, 1:233-256.

Ellis-Evans, J. C. and E. C. G. Lemon. 1989. Some aspects of iron cycling in maritime antarctic lakes. *Hydrobiologia*, 172:149-164.

Green, W. J., M. P. Angle, and K. E. Chave. 1988. The geochemistry of antarctic streams and their role in the evolution of four lakes of the McMurdo dry valleys. *Geochimica et Cosmochimica Acta*, 52:1,265-1,274.

Harnish, R. A., J. F. Ranville, D. M. McKnight, and S. A. Spaulding. 1991. Redox mediated cycling of iron and manganese in Lake Fryxell: Associations with particulate, colloidal, and dissolved forms. *Antarctic Journal of the U.S.*, 26(5):230-232.

Howes, B. L., J. W. H. Dacey, and G. M. King. 1984. Carbon flow through oxygen and sulfate reduction pathways in salt marsh sediments. *Limnology and Oceanography*, 29:1,037-1,051.

Howes, B. L. and R. L. Smith. 1990. Sulfur cycling in a permanently ice-covered amictic antarctic lake, Lake Fryxell. *Antarctic Journal of the U.S.*, 25(5):230-233.

Iversen, N. and B. B. Jorgensen. 1985. Anaerobic methane oxidation rates at the sulfate-methane transition in marine sediments from Kattegat and Skagerrak (Denmark). *Limnology and Oceanography*, 30:944-955.

Koob, D. D. and G. L. Leister. 1972. Primary productivity and associated physical, chemical and biological characteristics of Lake Bonney: a perennially ice-covered lake in Antarctica. (Antarctic Research Series) Washington, D.C.: American Geophysical Union. 20:51-68.

Lawrence, M. J. F. and C. H. Hendy. 1985. Water column and sediment characteristics of Lake Fryxell, Taylor Valley, Antarctica. *New Zealand Journal of Geology and Geophysics*, 28:543-552.

Matsumoto, G. I., K. Watanuki, and T. Torrii. 1989. Vertical distribution of organic constituents in an antarctic lake: Lake Fryxell. *Hydrobiologia*, 172: 291-303.

McKnight, D. M., G. R. Aiken, and R. L. Smith. 1991. Aquatic fulvic acids in microbially-based ecosystems: Results from two antarctic desert lakes. *Limnology and Oceanography*, 36:998-1,006.

Priscu, J. C. 1989. Photon dependence of inorganic nitrogen transport by phytoplankton in perennially ice-covered antarctic lakes. *Hydrobiologia*, 172:173-182.

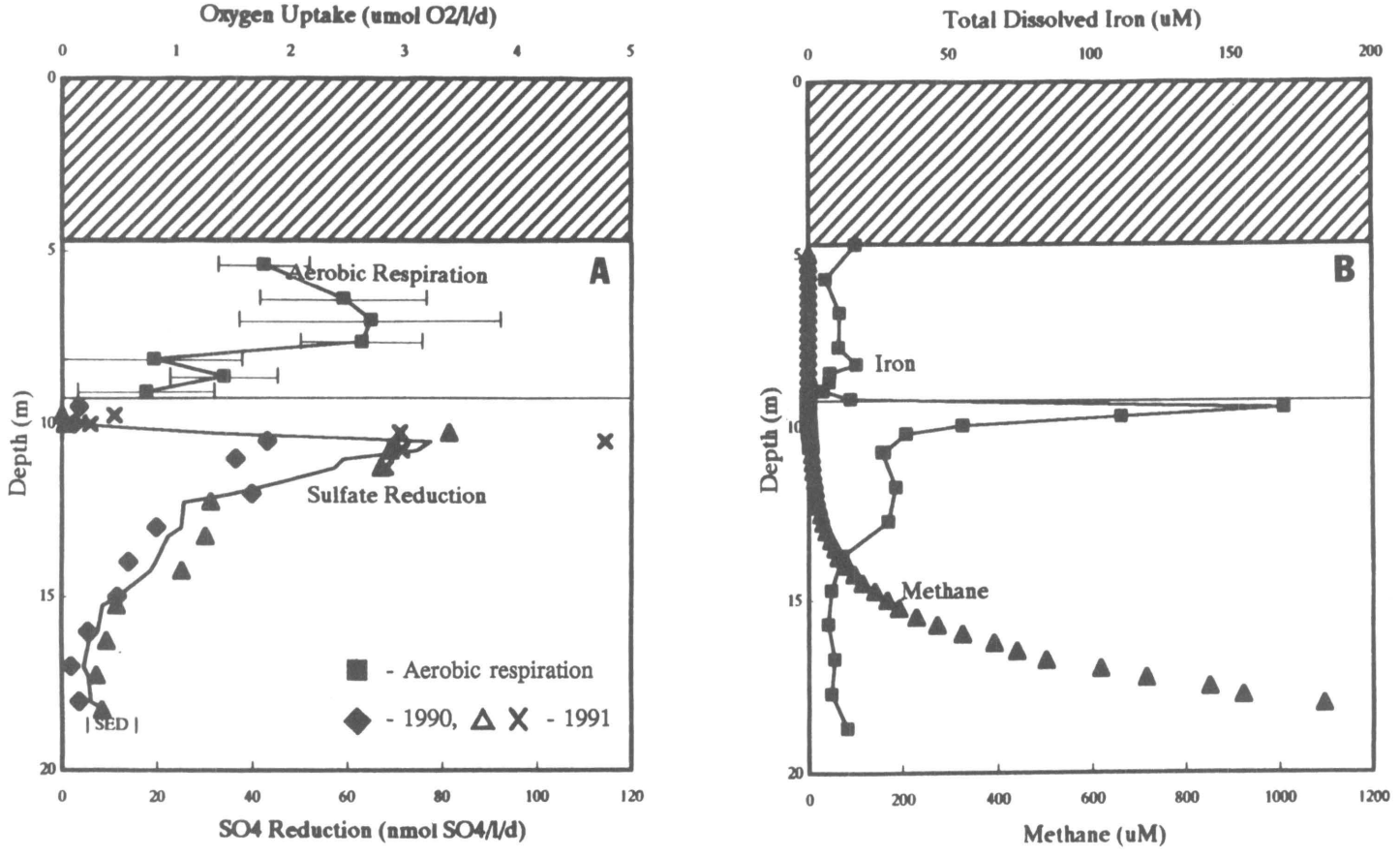

Figure 3(*A*). Depth profiles of water column oxygen uptake and sulfate reduction. Aerobic respiration is mean of 1990 and 1991 measurements ± S.E. Line represents the running mean of three separate studies of water column sulfate reduction. SED is mean of sulfate reduction in sediments collected in 1988 (Howes and Smith 1990). Line represents running mean based on all points of three. (*B*) Depth profiles of water column methane and dissolved iron concentrations. Horizontal line represents aerobic/anaerobic interface.

Priscu, J. C., L. R. Priscu, W. F. Vincent, and C. Howard-Williams. 1987. Photosynthate distribution by microplankton in permanently ice-covered antarctic desert lakes. *Limnology and Oceanography*, 32:260-270.

Reeburgh, W. S. 1980. Anaerobic methane oxidation: Rate depth distributions in Skan Bay sediments. *Earth Planetary Science Letters*, 47:345-352.

Seaburg, K.G., M. Kaspar, and B.C. Parker. 1983. Photosynthetic quantum efficiencies of phytoplankton from perennially ice-covered antarctic lakes. *Journal of Phycology*, 19:446-452.

Smith, R. L. and B. L. Howes. 1990. Bacterial biomass and heterotrophic activity in the water column of an amictic antarctic lake. *Antarctic Journal of the U.S.*, 25(5):233-235.

Smith, R. L., L. G. Miller, and B.L. Howes. In press. The geochemistry of methane in Lake Fryxell, an amictic, permanently ice-covered antarctic lake. *Biogeochemistry*.

Vincent, W. F. 1981. Production strategies in antarctic inland waters: Phytoplankton eco-physiology in a permanently ice-covered lake. *Ecology*, 62:1,215-1,224.

Trace gases over Antarctica: Bromine, chlorine, and organic compounds involved in global change

M. A. K. Khalil and R. A. Rasmussen

Global Change Research Center
Department of Environmental Science and Engineering
Oregon Graduate Institute
Beaverton, Oregon 97006

Many trace gases are increasing in the earth's atmosphere because of increasing population and global per capita consumption. The stable gases believed to be the most significant in causing future global warming or ozone depletion are carbon dioxide, methane, nitrous oxide, trichlorofluoromethane, and trichlorodifluoromethane (CO_2, CH_4,N_2O, CCl_3F, and CCl_3F_2). In addition, there are many more gases that have similar effects. While each of these minor gases may not effect the environment significantly, a large number of such gases together may be quite significant and rival or exceed the environmental effects from the main gases mentioned above. Of particular interest at present are chlorine- and bromine-containing gases that can deplete the ozone layer more effectively than most other gases.

To understand the global balance of environmentally significant trace gases we have been taking samples at carefully chosen locations all over the world. These locations consist of sites in the polar regions (Barrow, Alaska, and the South Pole), middle latitudes (Cape Meares, Oregon, and Cape Grim, Tasmania), and tropical regions (Hawaii and Samoa) of each hemisphere.

Systematic flask sampling at the South Pole poses logistical and scientific problems that greatly reduce the accuracy and precision of measurements of many trace gases and make it practically impossible to obtain accurate measurements of some trace gases, such as carbon tetrachloride and methyl chloroform (CCl_4 and CH_3CCl_3). In 1988 we began work to see whether Palmer Station (64° 46' S 64° 05' W) would be representative of the southern polar regions, as South Pole has been for the past. At Palmer it is much easier to obtain year-round samples and even to set up instruments for direct measurements. During the three and a half years since 1988 we have obtained weekly flask samples from Palmer Station and the South Pole. This paper is about the results of the Palmer experiment.

Average concentrations of chlorine and bromine gases in Antarctica: In table 1 we show the seasonally averaged concentrations of 13 trace gases at Palmer Station and the South Pole. These gases are nitrous oxide (N_2O) dichlorodifluormethane ($CC1_2F_2$, F-12), trichlorotrifluoroethane ($CC1_3F$, F-11), trichloroethane ($C_2C1_3F_3$, F-113), trichloromethane ($C_2H_3C1_3$) dichlorofluoromethane ($CHC1_2F$, F-22), Chloromethane or methylchloride (CH_3Cl), bromotrifluoromethane ($CBrF_3$, a halon fire extinguishing compound), bromochlorodifluoromethane ($CBrClF_2$, also a fire extinguishing compound), bromomethane or methylbromide (CH_3Br), dibromomethane (CH_2Br_2), methane (CH_4), carbon monoxide (CO), and hydrogen (H_2). Carbon monoxide, hydrogen, nitrous oxide, and chloromethane (CO, H_2, N_2O, and CH_3Cl) have both natural and anthropogenic sources while the rest of the chlorine- and bromine- containing gases are entirely man-made. Although we based all the calculations on monthly averages to save space, we have reported only seasonally averaged concentrations in table 1.

Differences between South Pole and Palmer: We calculated the average differences of the trace gas concentrations at the South Pole and Palmer by two methods. We took the difference and percent difference of concentrations at the two sites for each month as follows:

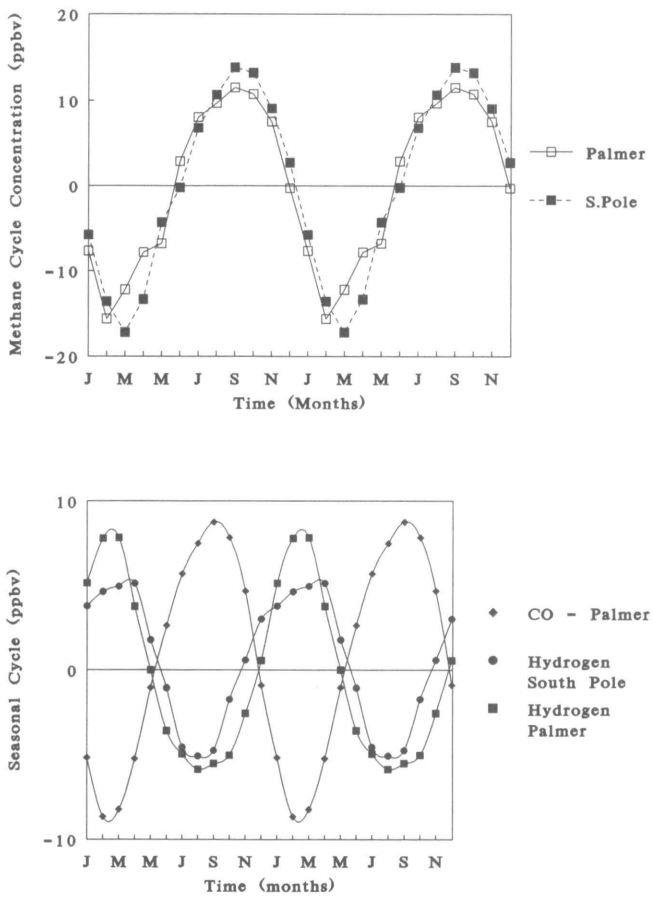

(*A*) The seasonal variations (top) of methane at the South Pole (90° S) and Palmer (64.5° S). (*B*) The seasonal cycles (bottom) of carbon monoxide (CO) and hydrogen (H_2). The opposite phase of carbon monoxide (CO) and hydrogen (H_2) is apparent. Cycles for carbon monoxide (CO) and hydrogen (H_2) are smoothed by taking six-point weighted running averages (weights = 0.222 for points 1 and 6, 0.333 for points 2 and 4, and 0.444 for point 3). This weighting scheme preserves the original shape while sharpening the image of the cycle. For clarity, in both figures the cycle is repeated twice.

Table 1: Seasonal averages of concentrations at Palmer Station and the South Pole.

		N_2O	F-12	F-11	F-113	CH_3CCl_3	H_2	F-22	I CH_3Cl	CH_4	CO
						Palmer Station					
F	1988	308.3	425.9	245.7	39.0	130.0	520.6	104.1	609.9	1664.0	61.6
W	1989	308.2	428.6	246.6	39.8	127.6	522.7	105.5	580.3	1651.0	39.9
Sp	1989	309.5	432.2	248.4	41.4	131.1	524.0	105.2	611.2	1653.5	38.9
Su	1989	308.5	444.3	254.9	43.6	135.5	507.0	109.3	600.1	1674.3	48.8
F	1989	309.1	446.1	254.0	43.5	133.6	507.0	111.2	594.1	1675.2	45.4
W	1990	308.8	449.3	256.1	44.1	132.5	516.5	114.2	567.3	1656.3	29.9
Sp	1990	308.8	454.8	259.2	45.5	135.0	515.9	115.7	616.0	1658.3	36.0
Su	1990	309.3	460.8	260.6	46.8	138.7	507.6	116.8	622.8	1678.1	46.0
F	1990	308.5	462.4	262.4	47.7	138.9	505.9	120.4	626.5	1686.7	43.4
W	1991	309.6	465.0	262.9	48.3	136.4	509.4	122.7	622.2	1670.5	32.7
Sp	1991	310.4	471.1	264.7	49.5	139.3	512.7	122.8	588.8	1673.3	32.9
Su	1991	310.6	478.8	266.8	51.1	141.9	506.6	126.8	590.2	1689.4	45.8
F	1991	311.2	486.7	271.3	52.3	145.0	508.1	130.9	569.3	1699.8	54.2
W	1992	310.9	489.9	272.5	51.9	148.6	517.4	134.2	564.7	1691.0	44.1
						South Pole					
F	1988	308.6	424.5	244.1	38.1	127.1	509.9	102.6	603.5	1667.2	66.4
W	1989	308.7	427.4	247.8	39.6	130.9	524.1	104.1	560.9	1651.7	30.1
Sp	1989	310.2	440.2	250.3	40.6	--	521.0	106.7	542.2	1647.7	25.2
Su	1989	310.7	443.1	252.3	42.5	142.8	512.6	108.8	559.5	1670.0	37.0
F	1989	310.7	448.1	255.5	43.6	138.3	514.6	112.7	580.4	1677.7	31.4
W	1990	310.2	453.6	258.3	44.8	139.8	516.0	114.7	560.3	1659.4	32.7
Sp	1990	310.2	455.2	258.6	45.2	132.4	515.0	114.7	524.5	1657.6	29.6
Su	1990	310.4	460.2	260.8	45.2	125.6	502.8	119.5	566.7	1678.6	27.9
F	1990	310.7	464.9	261.8	47.0	134.8	505.0	120.9	573.2	1684.2	42.1
W	1991	310.8	470.3	265.3	49.1	138.9	517.5	122.8	576.0	1669.4	34.6
Sp	1991	311.2	473.3	263.0	48.5	150.4	517.7	124.7	515.3	1668.1	30.5
Su	1991	311.3	480.1	265.8	49.6	147.2	506.7	127.3	562.4	1685.1	33.5
F	1991	312.3	483.7	268.1	51.7	143.8	504.9	129.5	575.5	1699.0	45.9
W	1992	312.2	482.6	269.6	52.5	143.3	514.0	131.5	565.2	1691.5	37.7

(1) $$\Delta Ci(t) = [Ci^{SP}(t) - Ci^{P}(t)]$$

(2) $$\%Ci\Delta(t) = \{[Ci^{SP}(t)/Ci^{P}(t) - 1\}\ 100\%$$

In these equations Ci(t) is the monthly averaged concentration of gas i during the month t where t = 1 to N spanning our data. For most gases there were (N =) 41 months of data. The superscript "P" is for concentrations at Palmer and "SP" for the South Pole. From these monthly estimates of the differences between concentrations we calculated the average differences over the length of the experiment. These differences and 90 percent confidence limits are reported in table 2 (Snedecor and Cochran 1980).

For the halocarbons the differences are very small and of no practical consequence even when statistically significant. The differences of carbon monoxide, hydrogen, and chloromethane (CO, H_2, and CH_3Cl) concentrations at the two sites are larger than for other gases. The causes of these differences are not known and may be related to sampling artifacts at the South Pole.

Cycles: Among the gases reported here, carbon monoxide, methane, hydrogen, and methyl chloroform (CO, CH_4, H_2, CH_3CC1_3) have substantial seasonal variations at the antarctic sites (and elsewhere). We compared the seasonal variations at the two sites to see if there were any differences. The average seasonal cycles are calculated based on the following model:

(3) $$C(t) = a + bt + \delta(t) + \varepsilon(t)$$

Here C(t) is the time series of concentrations, a +bt represents the linear trend, $\partial(t)$ are the seasonal cycles that repeat every 12 months, and E(t) are random fluctuations. The methods for calculating the seasonal cycles in equation (3) are described by Khalil and Rasmussen (1990).

In figure 1a we show the average seasonal cycle of methane at the two sites. The similarities are remarkable. The seasonal cycles of carbon monoxide and hydrogen (CO and H_2) are shown in figure 1b. At the South Pole the data were not precise enough to calculate the seasonal cycles of carbon monoxide (CO) over the period of this experiment. The cycles of hydrogen (H_2) are very similar at the two sites. It is also apparent that the seasonal variations of carbon monoxide (CO) and hydrogen (H_2) are opposite (when carbon monoxide (CO) is high, hydrogen (H_2) is low and vice versa.) This effect results from the unusual nature of the hydrogen cycle, as we reported earlier (Khalil and Rasmussen 1990.) The cycle of carbon monoxide (CO) is in phase with the cycles of methane (CH_4) and methyl chloroform (CH_3CC1_3).

Trends: The atmospheric trends of the gases at both the South Pole and Palmer were calculated using a linear model where the concentrations $C = a + bt + \varepsilon(t)$ (a and b are constants and t is time). The results are given in table 2. For gases that have seasonal cycles, we first subtracted the cycles before calculating the trends. The trends for all gases appear to be the same at the two sites.

We also calculated the trends of the differences of concentrations at the two sites by the following equation:

(4) $$\Delta C_i(t) = \alpha + \beta t$$

where Ci(t) is as in equation 1. If the trend of a gas is different at the two sites, then beta will not be zero. The results are shown

Table 2: Trends and concentrations of trace gases at the South Pole and Palmer Station (9/1988-1/1992)

	Differences				Trends: Palmer			Trends: S.P.			Difference	
	ΔC	δΔ	%ΔC	δ%D	a	b	δb	a	b	δb	b	δb
N_2O	1.1	0.2	0.4	0.1	307	0.8	0.2	308	0.9	0.2	-0.1	0.2
F-12	-0.2	1.1	0.0	0.2	409	19.5	0.9	412	18.7	0.9	0.8	1.2
F-11	-0.8	0.6	-0.3	0.2	239	8.1	0.4	241	7.4	0.4	0.6	0.6
F-113	0.8	0.3	-1.7	0.6	36	4.2	0.4	35	4.2	0.2	-0.1	0.3
CH_3CCl_3	1.4	2.0	-0.3	0.2	125	4.7	0.39	126	4.9	1.8	0.3	2
F-22	-0.4	0.5	-0.3	0.4	95	9.0	0.4	95	9.1	0.4	-0.1	0.5
CH_3Cl	-36	11	-6	2	611	-5	6	570	-4	4	-1.0	10
$CBrF_3$	- -	- -	- -	- -	2.3	0.4	0.2	- -	- -	- -	- -	- -
$CBrClF_2$	- -	- -	- -	- -	2.1	0.5	0.3	- -	- -	- -	- -	- -
CH_3Br	- -	- -	- -	- -	8.8	0.0	0.8	- -	- -	- -	- -	- -
CH_2Br_2	- -	- -	- -	- -	2.3	- -	- -	- -	- -	- -	- -	- -
CH_4	-2.2	1.8	-0.1	0.1	1645	11.0	0.9	1646	10.2	0.7	0.7	1.1
CO	-7.2	2.5	-15	6	46	- -	- -	37	- -	- -	-0.1	2
H_2	-8.9	2.5	-20	6	55	- -	- -	45	- -	- -	0.3	2

Units: Concentrations and differences of trace gas concentrations are in parts per billion (ppbv) for N_20, CO, H_2, and CH_4, and in parts per trillion (pptv) for the other gases. Trends are in ppbv/yr or pptv/yr as appropriate. **Uncertainties:** All ± values are 90% confidence limits, expressed as Δx where x = Δ, %Δ or b.
Parameters: ΔC is concentration at Palmer minus the concentration at the South Pole. The difference in concentrations during each month is averaged to calculate ΔC. %Δ is the percent difference of concentrations relative to Palmer measurements. The trends are calculated by the linear model C = a + bt. Here "a" represents the concentration at the base time (1/1988) and b represents the rate of increase in ppbv/yr or pptv/yr as appropriate. The column under "difference" represents the trend of the difference of concentrations between Palmer Station and the South Pole. When it is not statistically greater than zero, it means that the trends at the two locations are the same. - - represent cases when there are insufficient data to estimate the parameter.

in the last two columns of table 2. Beta is not significantly different from zero.

We conclude that, based on the comparisons, for all practical purposes the concentrations of long-lived trace gases are the same at Palmer Station as at the South Pole.

Major funding for this project was provided by National Science Foundation grant DPP 87-17023. We thank R. Dalluge and R. Gunawardena for their contributions. Additional support was provided by the Biospherics Research Corporation and the Andarz Company.

References

Khalil, M. A. K. and R. A. Rasmussen. 1990. Seasonal cycles of hydrogen and carbon monoxide in the polar regions: Opposite phase relationships. *Antarctic Journal of the U.S.*, 24(5):238-239.

Snedecor, G. W. and W. G. Cochran. 1980. *Statistical methods.* Ames: Iowa State University Press.

Decline in the accumulation rates of atmospheric chlorofluorocarbons 11 and 12 at the South Pole

T. H. Swanson*, J. W. Elkins, T. M. Thompson, S. O. Cummings*, J. H. Butler, and B. D. Hall†

National Oceanic and Atmospheric Administration
Climate Monitoring and Diagnostics Laboratory
Boulder, Colorado 80303

*Also with: *Cooperative Institute for Research in Environmental Sciences, University of Colorado, Boulder, Colorado 80309*

†Current address: *Washington State University, Department of Chemical Engineering, Pullman, Washington 99164*

Chlorofluorocarbons (CFCs) 11 and 12 represent in combination about 50 percent of the total abundance of organic chlorine in the atmosphere (Prather and Watson 1990). After their useful function in refrigeration, air conditioning, and the production of aerosols and foams (Gamlen et al. 1986), the CFCs are released into the troposphere where they are relatively stable. The CFCs are subsequently transported into the stratosphere where ultraviolet radiation from the sun breaks the CFC molecules down and the released chlorine catalytically destroyes stratosphere ozone (Molina and Rowland 1974). The discovery of the antarctic ozone hole by Farman et al. (1985) led to increased international efforts to reduce CFC emissions, including the Montreal Protocol to Reduce Substances that Deplete the Ozone Layer (United Nations Environment Programme 1987). It is useful therefore to monitor the accumulation rates of the CFCs at the South Pole, because it is the ground base station farthest removed from industrial countries of the northern hemisphere where 95 percent are the CFCs are released (Gamlen et al. 1986).

Scientists from the Climate Monitoring and Diagnostics Laboratory (CMDL) within the National Oceanic and Atmospheric Administration (NOAA) have been measuring the atmospheric

mixing ratios for the CFCs and nitrous oxide at the Clean-Air Facility (CAF) at Amundsen-Scott South Pole Station since 1977. The most significant trend observed in data from the South Pole station and other remote sites throughout the world has been the growth of the mixing ratios of CFCs in the troposphere. However, recent data from the monitoring station at the South Pole and from other sites have shown a significant decrease of the accumulation rates of CFC-11 and CFC-12 during the last 2 years.

From 1977 to the present, NOAA scientists collected a pair of flask samples of air once a week at the surface at the South Pole during the austral summer field season from November to mid-February (Elkins et al. 1988, Hall et al. 1990, Elkins et al. 1992). Prior to 1982 flask samples were also collected once a month during the rest of the year. In 1992, the program was expanded again to have NOAA personnel collect flask samples during the winter season, when the station is closed to air travel. The flasks are sent back to the Boulder laboratories for analysis by electron capture-gas chromatography (EC-GC). The experimental details and data selection methods for flask sampling were described by Thompson et al. (1985). The monthly means of the mixing ratios for CFC-11 and -12 measured from flasks are shown in figure 1. The mean standard deviation (s.d.) of the flask monthly means was ±1.8 parts per trillion (ppt) for CFC-11 and ±1.9 ppt for CFC-12.

During the 1983 summer field season, a manually operated gas chromatograph (GC) was installed at the CAF to complement the flask program (Elkins et al. 1988). This GC operated on a weekly basis and provided measurements of CFC-11 and CFC-12 (see figure 1). For the manually operated GC, the mean standard deviation of the monthly means was ±2.4 ppt for CFC-11 and ±3.4 ppt for CFC-12. In 1988, to improve the quality of the data, computer-controlled switching valves were installed to allow for the continuous automated operation of the *in situ* gas chromatograph (GC) and to make the South Pole GC to be almost identical to our *in situ* GCs installed at other sites under the Radiatively Important Trace Species (RITS) program of NOAA (Hall et al. 1990). Cycling the GC every half hour, allowing a measurement of ambient air every hour, also improved precision. This procedure yielded analytical precisions for daily means of ±1.2 ppt (1 standard deviation, 1 *SD*) for CFC-11 and ±1.4 ppt for CFC-12.

Calibration of the *in situ* GC system involves using two working standards filled with air collected from Niwot Ridge, Colorado. One is diluted with zero air to values below 10 percent of ambient air at the South Pole. All working standards are certified against gravimetric standards prepared by our laboratory to within ±2 percent (95 percent c.i.) or better accuracy at the ppt level.

The mixing ratios of CFC-11 and CFC-12 for air sampled at the South Pole indicate definite increasing trends in both flask and *in situ* gas chromatographic data, which have also been reported elsewhere (Rasmussen and Khalil 1986; Cunnold et al. 1986; Elkins et al. 1988; Hall et al. 1990). The long-term trends of increasing mixing ratios of the CFCs are apparent in figure 1. Recent observations, however, seem to indicate that the growth rates of CFCs have decreased since 1989.

To illustrate this change, we divide the data set into separate data sets, before and after 1988, because the precision and sampling frequency of the data set before 1988 were both less than after 1988. A locally weighted least squares or loess fit (Cleveland 1979) was applied to each set. A loess fraction (f) of 0.45, a rigid fit, was used for data prior to 1988. An f value of 0.23 was used for data after 1988 (figure 1). Estimates of the growth rates for CFC-11 and CFC-12 were calculated by differentiating the loess fits versus time (figure 2). Prior to 1988, the mean growth rates of the CFCs in the troposphere at the South Pole station were

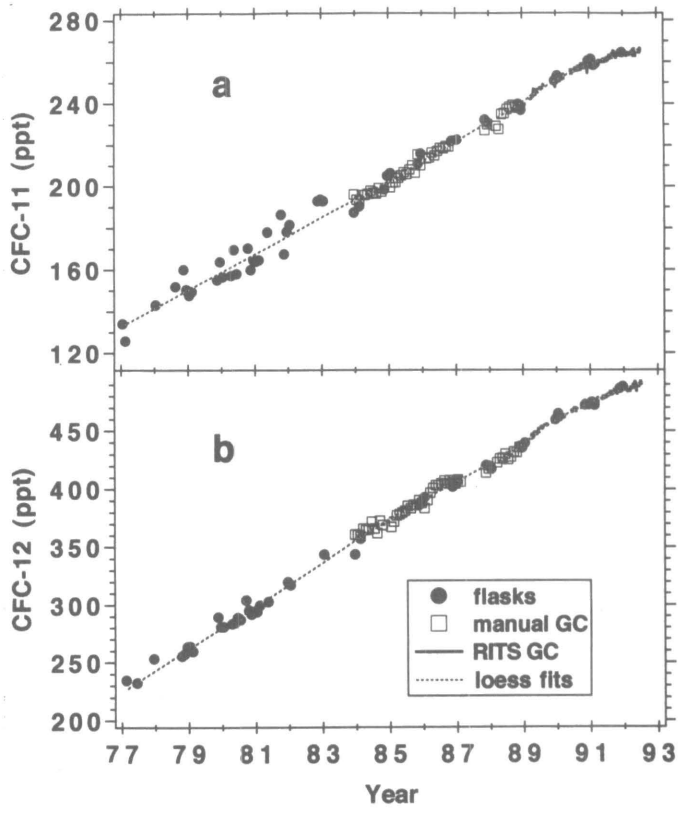

Figure 1. The mixing ratios in parts per trillion (ppt) of (*A*) CFC-11 and (*B*) CFC-12, for air sampled at the South Pole Clean-Air Facility. Monthly means are shown for the manually operated gas chromatograph (GC,□) and the flask samples (•), while daily means are shown for the *in situ*, Radiatively Important Trace Species (RITS) automated GC (—). The *dashed line* is a calculated fit using the statistical smoothing of a locally weighted least squares (loess) regression (Cleveland 1979) from the Dataplot graphics and statistical software (Filliben 1981) (see text).

relatively constant at about 9.1±0.5 (1 *SD*; number of points, n=64) ppt per year for CFC-11 and 17.5±1.4 (1 *SD*; n=63) ppt per year for CFC-12. Between 1988 and 1990, there was a slight increase in the mean growth rates of 10.0±0.5 (1 *SD*; n=19) ppt per year for CFC-11 and 19.7±2.0 (1 *SD*; n=21) ppt per year for CFC-12. resulting from increased production reported by the CFC producers (AFEAS, 1991). From 1990 to mid-1992, the growth rates of CFCs dropped to mean values of 5.8±1.8 (1*SD*; n=30) ppt per year for CFC-11 and 12.9±2.0 (1*SD*; n=28) ppt per year for CFC-12.

It has been proposed by Elkins et al. (1993) that the decline in the growth rates observed by NOAA/CMDL are directly related to the international efforts, both mandated and voluntary, to reduce CFC emissions. During the upcoming 1993 and 1994 field seasons, our laboratory plans further changes in the South Pole system to improve the precision, reliability, and the quality of the data, and to monitor more CFC molecules to document further the decline and to extend our understanding of the transport of these compounds to the atmosphere over Antarctica.

We gratefully acknowledge the contributions of all NOAA personnel involved in collecting flask samples and maintaining the EC-GC at the South Pole. Special thanks are given to the staff and contractors of the U.S. National Science Foundation for their operational and logistical support. We also appreciate the assistance given by R. A. Rasmussen, W. D. Komhyr, E. G. Dutton, K.B.

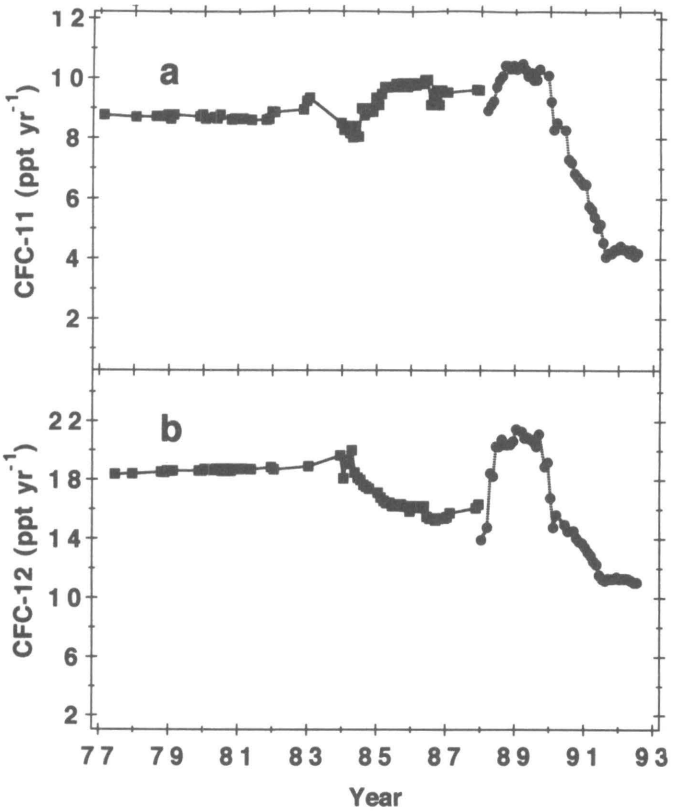

Figure 2. The change in growth rates in parts per trillion (ppt) per year (ppt yr^{-1}) for (a) CFC-11 and (b) CFC-12, for air sampled at the South Pole Clean-Air Facility. These estimates of the growth rates for CFC-11 and CFC-12 were calculated by differentiating the loess fit of the mixing ratio data sets in figure 1. The rate of changes for both CFCs were calculated using a loess fraction (f) of 0.45 to smooth data between 1977 and 1988 (■) and an f value of 0.23 to smooth data from January 1988 to June 1992 (•) (Cleveland 1979).

Egan, C. M. Brunson, R. C. Myers, and B. G. Mendonca. This work was supported in part by the Atmospheric Chemistry Project of NOAA's Global Climate Change Program.

References

AFEAS 1991. *Chlorofluorocarbons (CFC's) 11 and 12*, Washington, D.C.: Alternative Fluorocarbons Environmental Acceptability Study.

Cleveland, W. S. 1979. Robust locally-weighted regression and smoothing scatterplots. *Journal of the American Statistical Association*, 74:829-836.

Cunnold, D. M., R. G. Prinn, R. A. Rasmussen, P. G. Simmonds, F. N. Alyea, C. A. Cardelino, A. J. Crawford, P. J. Fraser, and R. D. Rosen. 1986. Atmospheric lifetime and annual release estimates for $CFC1_3$ and CF_2C1_2 from 5 years of ALE data. *Journal of Geophysical Research*, 91(D10):10,797-10,817.

Elkins, J. W., T. M. Thompson, B. D. Hall, K. B. Egan, and J. H. Butler. 1988. NOAA/GMCC halocarbons and nitrous oxide measurements at the South Pole. *Antarctic Journal of the U.S.*, 23:76-77.

Elkins, J. W., T. M. Thompson, T. H. Swanson, J. H. Butler, B. D. Hall, S. O. Cummings, D. A. Fisher, A. G. Raffo. 1993. Slowdown in the growth rates of atmospheric chlorofluorocarbons 11 and 12. *Nature*, submitted.

Farman, J. C., B. G. Gardiner, and J. D. Shanklin. 1985. Large losses of total ozone in Antarctica reveal seasonal ClO_x/NO_x interaction. *Nature*, 315:207-210.

Filliben, J. J. 1981. Dataplot—An interactive high-level language for graphics, non-linear fitting, data analysis, and mathematics. *Computer Graphics*, 15(3):199-213.

Gamlen, P. H., B. C. Lane, P. M. Midgley, and J. M. Steed. 1986. The production and release to the atmosphere of CCl_3F and CCl_2F_2 (chlorofluorocarbons CFC-11 and CFC-12). *Atmospheric Environment*, 20(6):1,077-1,085.

Hall, B. D., J. W. Elkins, J. H. Butler, T. M. Thompson, and C. M. Brunson. 1990. Improvements in nitrous oxide and halocarbon measurements at the South Pole. *Antarctic Journal of the U.S.*, 25(5):252-253.

Molina, M. J. and F. S. Rowland. 1974. Stratospheric sink for chlorofluoromethanes: Chlorine atom catalyzed destruction of ozone. *Nature*, 249:810-814.

Prather, M. J. and R. T. Watson. 1990. Stratospheric ozone depletion and future levels of atmospheric chlorine and bromine. *Nature*, 344:729-734.

Rasmussen, R. A. and M. A. K. Khalil. 1986. Atmospheric trace gases: Trends and distributions over the last decade. *Science*, 232:1,623-1,624.

Thompson, T. M., W. D. Komhyr, and E. G. Dutton. 1985. Chlorofluorocarbon-11, -12, and nitrous oxide measurements at the NOAA/GMCC baseline stations (16 September 1973 to 31 December 1979). *NOAA Technical Report ERL 428-ARL 8*. Boulder, Colorado: NOAA Environmental Research Laboratories.

United Nations Environment Programme. 1987. *Montreal Protocol to Reduce Substances that Deplete the Ozone Layer Report. Final Report*. New York: United Nations Environment Programme.

Halogen and sulfur content of volcanic emissions from Mount Erebus, Ross Island, Antarctica

Grazyna Zreda-Gostynska and Philip R. Kyle

Department of Geoscience
New Mexico Institute of Mining and Technology
Socorro, New Mexico 87801

Mount Erebus, a stratovolcano composed of anorthoclase phonolite lavas, is at present the most active volcano on the antarctic continent. The unusual, highly alkaline composition of Erebus magma presents a rare opportunity to study gases exsolving from such a melt. The purpose of our work was the characterization of the composition of volcanic gases emitted from Mount Erebus. We examined three components (sulfur, chlorine, and fluorine) in the gas. These components are also the most abundant species in the samples we collected. Moreover, as already documented in literature (Noguchi and Kamiya 1963; Murata et al. 1964; Stoiber and Rose 1970; Menyailov 1975; Naughton et al. 1975; Giggenbach 1975; Hirabayashi et al. 1982 and 1986; Miller et al. 1990; and many others), the relative abundances of sulfur, chlorine, and fluorine in the volcanic gas plumes are useful in the forecasting of eruptive activity and helpful in the analysis of magma movement in the conduit. Finally, volcanic gases act as transporting agents for various metals, many of which form volatile compounds with either sulfur, chlorine, or fluorine.

During the antarctic summers of December 1986 through January 1991 we collected samples of Erebus gases, using filter packs composed of one particulate filter and two base impregnated filters called treated filters (Finnegan et al. 1989). In 1986 and 1988 we impregnated filters with 1 M ^{7}LiOH, whereas in 1989 and 1991 we used 3 M ^{7}LiOH and tetrabutyl ammonium hydroxide. The particulate filter captures large particles (ash and various sublimates) and droplets present in the plume while treated filters collect acid gases. We collected samples in the plume passing over the northwestern rim of the Erebus crater. In addition, we also remotely measured the output of sulfur dioxide by correlation spectrometer (COSPEC) (Stoiber et al. 1983; Kyle et al. in prep.).

The collected filters were analyzed by instrumental neutron activation analysis for chlorine and fluorine and by ion chromatography for sulfur. All concentrations are expressed in micrograms of element per cubic meter of air sampled (table 1) and calculated as element-to-sulfur weight ratios. Since the emission rate of sulfur (as sulfur dioxide) can be measured independently by COSPEC, knowing the element to sulfur ratio allows us to calculate the emission rates of other elements.

Between 1986 and 1991 the emission rates of hydrogen chloride and hydrogen fluoride from Mount Erebus increased from 4.3 to 12.4 gigagrams per year and from 2.4 to 4.7 gigagrams per year, respectively (table 2). COSPEC measurements showed sulfur dioxide output increasing from 7.7 to 25.9 gigagrams per year during the same period. We also observed a small but statistically significant change in the gas composition from year to year as exemplified by the relative proportions of sulfur, chlorine, and fluorine. The samples collected in 1986 and 1989 are characterized by higher proportion of fluorine and lower sulfur than samples from 1988 and 1991. Although it is tempting to interpret this variation as cyclical, there are not enough data to confirm a real cyclic pattern. Future investigations will help to characterize this pattern better. These observations suggest a temporal and possibly also spatial variability of the volatile content of Erebus magma. Although there is a large number of possible explanations of this variability, we favor a model in which a change in the amount of exsolved sulfur and halogens results from the heterogeneous volatile content of the melt. The heterogeneity is attained by a presence of the extraneous volatile (most likely carbon dioxide) that may be injected into the base of the magma chamber from the deeper part of the magmatic system. The carbon dioxide aids in the vesiculation process and in the removal of other volatiles from the melt. However, the lack of experimental data on solubility of sulfur and halogens in the alkaline melts in the presence of carbon dioxide currently prevents us from further testing our model.

We also observe another, smaller scale variability displayed by changes of sulfur to chlorine and fluorine to chlorine weight ratios in the gas. The changes in sulfur to chlorine and fluorine to chlorine ratios are well correlated with each other. In our interpretation these changes are related to the convective movement of magma in the conduit at shallow depths where the gases exsolve from magma. The bubbles formed at greater depths have high chlorine, but low fluorine and sulfur content while these formed closer to the surface are characterized by the opposite trend. Although we suspect these changes occur periodically, at present the time resolution of filter samples does not allow for any definite conclusions.

It has been informally suggested earlier that Erebus emissions because of their high output of chlorine may be contributing to the development of the antarctic ozone hole. Although there are

Table 1. Chlorine, sulfur, and fluorine concentrations (in micrograms per cubic meter) and fluorine to chlorine and sulfur to chlorine weight ratios on treated filters samples collected at Mount Erebus.

Year	Date	Cl ($\mu g\ m^{-3}$)	F ($\mu g/m^{-3}$)	S ($\mu g/m^{-3}$)	F/Cl	S/Cl
1986[a]	Dec.19	371	183	543	0.49	1.46
	Dec.19	291	166	276	0.57	0.95
	Dec.20	1665	806	609	0.48	0.37
	Dec.20	1445	649	937	0.45	0.65
	Dec.21	1641	658	n.a.	0.40	—
	Dec.22	631	228	478	0.36	0.76
	Dec.23	650	936	1044	1.44	1.61
	Dec.24	386	455	2147	1.18	5.56
	Dec.24	412	258	858	0.63	2.08
	[a]Mean F/Cl and S/Cl ratios for 1986				0.67	1.68
				std	0.38	1.67
1988	Dec.13	191	54	338	0.28	1.77
	Dec.16	320	138	266	0.43	0.83
	Dec.16	114	67	90	0.58	0.79
	Dec.16	226	100	223	0.44	1.03
	Dec.16	240	98	183	0.41	0.77
	Dec.16	319	128	387	0.40	1.21
	Dec.16	344	158	253	0.46	0.74
	Dec.16	412	136	445	0.33	1.08
	Dec.17	251	75	813	0.30	3.24
	Dec.20	148	87	228	0.59	1.55
	Dec.20	86	33	89	0.38	1.04
	Dec.21	215	71	156	0.33	0.72
	Mean F/Cl and S/Cl ratios for 1988				0.41	1.23
				std	0.10	0.71
1989	Nov.24	284	128	364	0.45	1.28
	Dec.02	334	192	150	0.57	0.45
	Dec.04	258	243	567	0.94	2.20
	Dec.07	118	101	110	0.85	0.54
	Dec.08	26	41	128	1.59	5.01
	Dec.08	69	99	73	1.43	1.06
	Dec.09	68	42	56	0.62	0.82
	Dec.10	192	88	77	0.46	0.40
	Dec.10	49	37	102	0.76	2.08
	Dec.11	45	24	82	0.55	1.83
	Dec.11	153	72	132	0.47	0.86
	Dec.12	51	51	87	1.01	1.72
	Dec.14	82	67	123	0.81	1.51
	Dec.16	269	158	187	0.59	0.70
	Dec.17	140	49	84	0.35	0.60
	Dec.18	677	285	267	0.42	0.39
	Mean F/Cl and S/Cl ratios for 1989				0.74	1.37
				std	0.36	1.14
1991	Jan.13	189	60	130	0.32	0.69
	Jan.14	153	46	164	0.30	1.08
	Jan.14	87	19	94	0.22	1.08
	Jan.15	365	90	349	0.25	0.96
	Jan.16	22	14	45	0.62	2.05
	Jan.16	210	59	258	0.28	1.23
	Jan.18	51	51	174	1.01	3.43
	Jan.19	143	76	253	0.53	1.77
	Jan.19	58	28	99	0.48	1.71
	Jan.20	46	29	79	0.63	1.72
	Jan.20	31	23	67	0.74	2.14
	Jan.21	51	18	52	0.35	1.02
	Jan.21	165	63	207	0.38	1.25
	Jan.22	240	95	301	0.40	1.25
	Jan.22	284	114	233	0.40	0.82
	Jan.23	146	63	64	0.43	0.44
	Mean F/Cl and S/Cl ratios for 1991				0.44	1.37
				std	0.21	0.72
	Mean F/Cl and S/Cl ratios for all years				0.56	1.38
				std	0.31	1.02

[a] Cl and F results for 1986 from Meeker (1988).
Chlorine and fluorine determined by instrumental neutron activation analysis, sulfur by ion chromatography. Approximate analytical errors 5-10 percent.
n.a. = not analyzed

Table 2. Measured sulfur dioxide output[a] and calculated emission rates of hydrogen chloride and hydrogen fluoride (in gigagrams per year) from Mount Erebus.

	SO_2	Cl/S	F/S	HCl	HF
Dec. 1986	7.7	1.08	0.61	4.3	2.4
Dec. 1988	9.8	0.98	0.41	5.0	2.0
Dec. 1989	19.0	1.15	0.71	11.2	6.8
Jan. 1991	25.9	0.93	0.36	12.4	4.7

[a] SO_2 emission rates from Kyle et al. (in prep.)

several arguments supporting this idea, such as the circulation pattern around Antarctica leading to the isolation of Erebus influences to smaller area, high altitude of emissions (Erebus elevation is 3,794 meters; plume height can reach 100-200 meters), and disappearance of tropopause in the winter, it is still unclear whether the emitted chlorine can enter the stratosphere before its removal from the plume, and what its concentration is.

Recently (Zreda-Gostynska et al. 1992) we noted another environmental effect of high chlorine concentrations in Erebus emissions. We suggested that Erebus may be a source of the "excess" inorganic chlorine found in the snow on the antarctic plateau (Delmas et al. 1982; Legrand and Delmas 1988). From the experimental work of Mroz et al. (1989) we know there is a rapid poleward transport of tropospheric air masses during the antarctic summer months. The chlorine in the Erebus plume could thus be transported inland and deposited in the snow. Our calculations (Zreda-Gostynska et al. 1992) demonstrate that this process is quite feasible.

This work was supported in part by National Science Foundation grant DPP 87-16319. We would also like to thank Bob Andres, David Caldwell, Nelia Dunbar, Bill McIntosh, Kim Meeker, Kurt Panter, Franco Pratti, Ken Sims, and Lauri Sybeldon for the field assistance. The VXE-6 helicopter squadron has provided wonderful support over the years. We are very grateful to David Finnegan of the Los Alamos National Laboratory and Mike Glascock and Jeff Denison from University of Missouri Research Reactor in Columbia, Missouri, for help with instrumental neutron activation analysis of samples, and to Lynn Brandvold and Jeanne Verploegh from the New Mexico Bureau of Mines and Natural Resources for help with the ion chromatography work.

References

Delmas, R., M. Briat, and M. Legrand. 1982. Chemistry of south polar snow. *Journal of Geophysic Research,* 87:4,314-4,318.

Delmas, R. J., M. Legrand, A. J. Aristarain, and F. Zanolini. 1985. Volcanic deposits in antarctic snow and ice. *Journal of Geophysical Research,* 90:12,901-12,920.

Finnegan, D., J. P. Kotra, D. M. Herman, and W. H. Zoller. 1989. The use of ^{7}1iOH-impregnated filters for the collection of acidic gases and analysis by instrumental neutron activation analysis. *Bulletin of Volcanology,* 51:83-87.

Giggenbach, W. F. 1975. Variations in the carbon, sulfur and chlorine content of volcanic gas discharges from White Island, New Zealand. *Bulletin Volcanologique,* 39:15-27.

Hirabayashi, J., J. Ossaka, and T. Ozawa. 1982. Relationship between volcanic activity and chemical composition of volcanic gases—A case study on the Sakurajima Volcano. *Geochemical Journal,* 16:11-21.

Hirabayashi, J., J. Ossaka, and T. Ozawa. 1986. Geochemical study on volcanic gases at Sakurajima Volcano, Japan. *Journal of Geophysical Research,* 91:12,167-12,176.

Kyle, P. R., K. Meeker, and D. L. Finnegan. 1990. Sulfur dioxide and HCl emissions from Mount Erebus, Antarctica. *Geophysical Research Letters,* 17:2,125-2,128.

Kyle, P. R., L. M. Sybeldon, W. C. McIntosh, K. Meeker, and R. Symonds. 1991. Sulfur dioxide emission rates from Mount Erebus, Antarctica. In P. R. Kyle (Ed.), *Volcanological Studies of Mount Erebus, Antarctica.* Antarctic Research Series. Washington, D.C.: American Geophysical Union, in press.

Legrand, M. R. and R. J. Delmas. 1988. Formation of HCl in the antarctic atmosphere. *Journal of Geophysical Research,* 93:7,153-7,168.

Meeker, K. 1988. The emission of gases and aerosols from Mount Erebus volcano, Antarctica, Master of Science Thesis. Socorro, New Mexico: New Mexico Institute of Mining and Technology.

Menyailov, I. A. 1975. Prediction of eruptions using changes in composition of volcanic gases. *Bulletin Volcanologique,* 39:112-125.

Miller, T. L., W. H. Zoller, B. M. Crowe, and D. L. Finnegan. 1990. Variations in trace metal and halogen ratios in magmatic gases through an eruptive cycle of the Pu'u O'o vent, Kilauea, Hawaii: July-August, 1985. *Journal of Geophysical Research,* 95:12,607-12,615.

Mroz, E. J., M. Alei, J. H. Cappis, P. R. Guthals, A. S. Mason, and D. J. Rokop. 1989. Antarctic atmospheric tracer experiments. *Journal of Geophysical Research,* 94:8,577-8,583.

Murata, K. J., W. U. Ault, and D. E. White. 1964. Halogen acids in fumarolic gases of Kilauea Volcano. *Bulletin Volcanologique,* 27:367-368.

Naboko, S. I. 1959. Volcanic exhalations and products of their reactions as exemplified by Kamchatka-Kuriles Volcanoes. *Bulletin Volcanologique,* 20:121-136.

Naughton, J. J., V. Lewis, D. Thomas, J. B. Finlayson. 1975. Fume composition found at various stages of activity at Kilauea Volcano, Hawaii. *Journal of Geophysical Research,* 80:2,963-2,966.

Noguchi, K. and H. Kamiya. 1963. Prediction of volcanic eruption by measuring the chemical composition and amounts of gases. *Bulletin Volcanologique,* 26:367-378.

Stoiber, R. E. and W. I. Rose. 1970. The geochemistry of Central American volcanic gas condensates. *Geological Society of America Bulletin,* 81:2,891-2,912.

Stoiber, R. E., L. L. Malinconico, and S. N. Williams. 1983. Use of the correlation spectrometer at volcanoes. In H. Tazief and J. C. Sabroux (Eds.), *Forecasting volcanic events.* Amsterdam: Elsevier, 425-444.

Zreda-Gostynska, G., P. R. Kyle, and D. Finnegan. 1992. Mount Erebus as a source of excess Cl in the antarctic snow and ice. (Abstract), American Geophysical Union Chapman Conference on Climate, Volcanism and Global Change.

Volcanic aerosol and ozone depletion within the antarctic polar vortex during the austral spring of 1991

TERRY DESHLER

Department of Atmospheric Science
University of Wyoming
Laramie, Wyoming 82071

ALBERTO ADRIANI

Istituto di Fisica dell' Atmosfera
CNR, Frascati, Italy

Soon after the initial reports of ozone depletion over Antarctica and the implication of polar stratospheric clouds as crucial to the ozone destruction process, vertical profiles of ozone and aerosol have been measured during the austral spring from McMurdo Station, Antarctica (78° S) (e.g., Deshler et al. 1991; Johnson et al. 1992). In 1990 and 1991 these studies were additionally supported with lidar measurements (Gobbi et al. 1991). The period, 1986-1990, was volcanically quiescent; and the 1991 polar stratosphere was not expected to be different since the eruptions of Pinatubo (15° N, 13-15 June) and Cerro Hudson (46° S, 12-15 August) had both occurred after the 1991 polar vortex had formed.

The 1991 balloon-borne observations of aerosol and ozone began 23 August and continued until 1 November; and the lidar measurements, from 26 August until 10 October. The lidar measurements during the period 11 September to 10 October are shown in figure 1 as profiles of scattering ratio, the ratio of back scattering resulting from aerosol and molecules to that produced only by molecules. Above 15 kilometers the stratosphere was very clean, and we observed only background stratospheric aerosols; however, on 11 and 12 September, we observed thin particle layers between 8 and 13 kilometers. These layers were inhomogeneous in both the vertical and horizontal. Lidar and aerosol profiles on 13 September indicated a very clean stratosphere both above and below 15 kilometers, with the exception of two thin layers at 10 and 12 kilometers. We obtained additional evidence of this early September appearance of volcanic aerosols with condensation nuclei profiles which showed a region of very high aerosol concentration between 9 and 13 kilometers on 8 September and every flight thereafter, indicating homogeneous nucleation of new aerosols.

Fresh volcanic layers are the primary source for such high concentrations of new aerosols, but these high concentrations last only a short time because of coagulation. For the volcanic aerosols in Antarctica these observations of homogeneous nucleation, along with the altitude of the observations, help identify the source of the volcanic aerosols as Cerro Hudson (45° S 73° W), which erupted 12-15 August.

We completed optical particle counter flights on 27 September and 8 October. The vertical profile of aerosols, compared with lidar and temperature measurements, on 27 September is shown in figure 2. The combination of the persistent scattering ratios, low depolarization, and high aerosol concentration points to the fact that a great deal of volcanic aerosols were entrained into the vortex between 13 and 20 September and remained there rela-

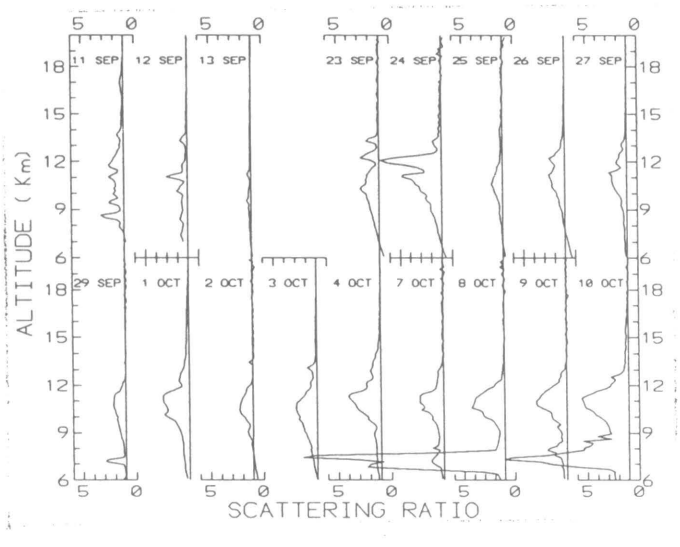

Figure 1. Lidar profiles of scattering ratio from 11 September 1991 to 10 October 1991 at McMurdo Station, Antarctica. Profiles from 29 August to 7 September (not shown) indicated only the stratospheric background aerosols.

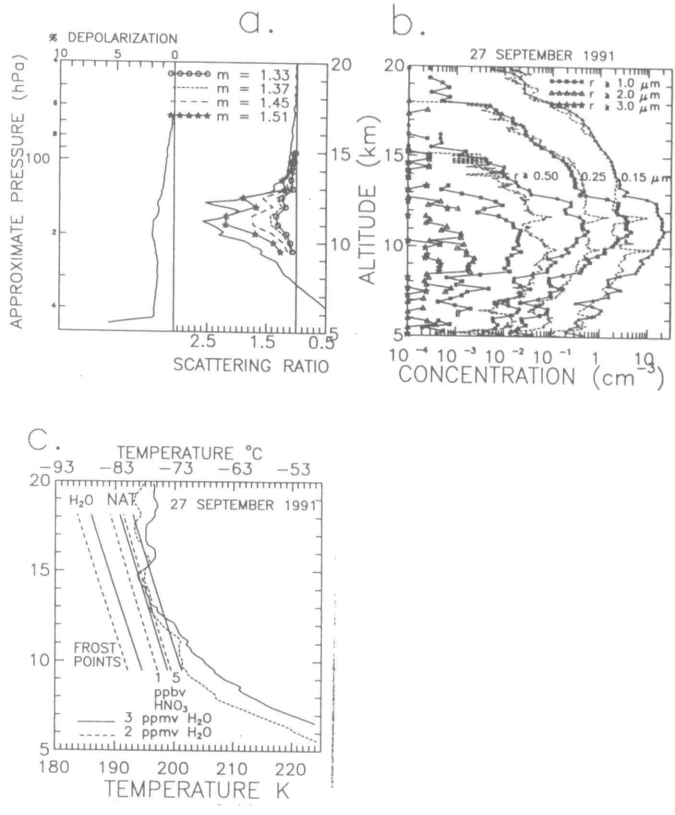

Figure 2(*A*), Lidar; (*B*), aerosol; and (*C*) temperature profiles on 27 September. The calculated scattering ratios, assuming different indices of refraction, are shown compared with the lidar measurements. The *dashed lines* on the aerosol and temperature profiles represent the background stratospheric conditions as measured on 13 September 1991. Note the thin volcanic layers observed at this time. The *straight lines* on the temperature profile represent existence temperatures for polar stratospheric clouds containing nitric acid trihydrate (Hanson and Mauersberger 1988) and water ide, assuming the vapor concentrations indicated.

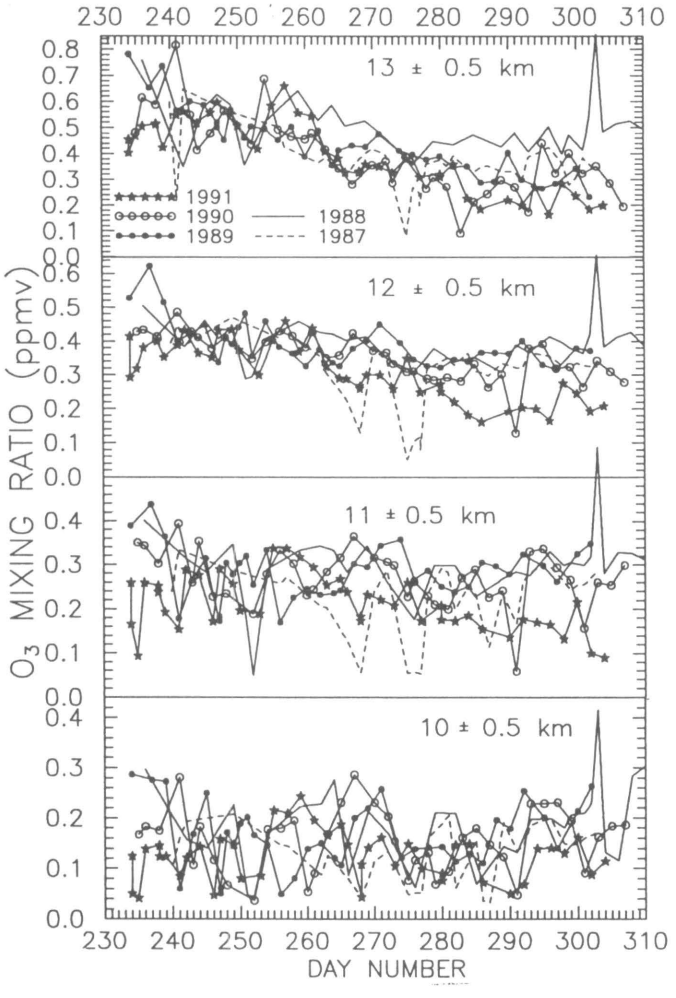

Figure 3. Temporal history of 0.5-kilometer averages of the 1991 ozone mixing ratio, 10-13 kilometers, compared with ozone measurements collected 1987 to 1990.

tively undisturbed through the end of the measurements in October.

During each antarctic spring since 1986 approximately 40 ozone profiles have been measured at McMurdo (Johnson et al. 1992). The results of these measurements have been quite consistent, indicating that during years of severe ozone depletion—1987, 1989, 1990, 1991—approximately half the total column of ozone is lost with more than 80 percent of the loss occurring between 12 and 20 kilometers. While above 20 kilometers ozone is quite variable because of polar vortex movements, the ozone at 12 kilometers and below has been very constant, except for occasional soundings with a higher than normal tropopause. The stability of this low altitude ozone changed in 1991. Figure 3 shows that ozone between 11 and 13 kilometers in 1991 is clearly lower than the previous four-year record. This change began when the volcanic aerosols first appeared and after one month ozone at these altitudes was reduced by 50 percent, compared with the previous four years. The half-life for ozone decay in this region was 30-40 days, one-half to two-thirds the rate observed for the decay of ozone at 18 kilometers resulting from chlorine processing by polar stratospheric clouds. Hofmann and Solomon (1989) have suggested that the presence of volcanic aerosols can lead to ozone depletion because of heterogeneous reactions on the volcanic aerosol surface. To our knowledge the measurements presented here, and more completely in Deshler et al. (1992), are the first direct *in situ* measurements confirming that volcanic aerosols can play a part in ozone destruction.

Gratitude is extended to G. Di DonFrancesco, B. Johnson, L. Womack, and R. Thompson for help with the measurements in Antarctica. This research was supported by the National Science Foundation grant DPP 90-17805 and the Italian National Program for Antarctic Research under the FAADR grant.

References

Deshler, T., A. Adriani, D. J. Hofmann, and G. P. Gobbi. 1991. Evidence for denitrification in the 1990 antarctic spring stratosphere: II Lidar and aerosol measurements. *Geophysical Research Letters,* 18:1,999-2,002.

Deshler, T., A. Adriani, G. P. Gobbi, D. J. Hofmann, G. Di Donfrancesco, and B. J. Johnson. 1992. Volcanic aerosol and ozone depletion within the antarctic polar vortex during the austral spring of 1991. *Geophysical Research Letters,* 19:1,819-1,822.

Gobbi, G. P., T. Deshler, A. Adriani, and D. J. Hofmann. 1991. Evidence for denitrification in the 1990 antarctic spring stratosphere: I Lidar and temperature measurements. *Geophysical Research Letters,* 18:1,995-1,998.

Hanson, D. R. and K. Mauersberger. 1988. Laboratory studies of the nitric acid trihydrate: Implications for the south polar stratosphere. *Geophysical Research Letters,* 15:855-858.

Hofmann, D. J. and S. Solomon. 1989. Ozone destruction through heterogeneous chemistry following the eruption of El Chichon. *Journal of Geophysical Research,* 94:5,029-5,041.

Johnson, B. J., T. Deshler, R. L. Thompson. 1992. Vertical profiles of ozone at McMurdo Station, Antarctica; spring 1991. *Geophysical Research Letters,* 19:1,105-1,108.

Fourier Transform Infrared spectroradiometer measurements of atmospheric longwave emission over Palmer Station, spring 1991

DAN LUBIN

California Space Institute
University of California, San Diego
La Jolla, California 92093-0221

CATHERINE GAUTIER

Earth Space Research Group
University of California, Santa Barbara
Santa Barbara, California 93111

To better understand the atmospheric radiation budget over the Antarctic Peninsula and southern ocean,s we deployed a Fourier Transform Infrared (FTIR) spectroradiometer at Palmer Station during austral spring, 1991. This instrument, based on the Bomem (Inc.) MB-100 Michelson interferometer, measured spectral emission from the zenith sky with 1 inverse centimeter wavenumber resolution throughout the mid-infrared (500-2,000 inverse centimeters). Radiometric calibration was established using a blackbody radiation source traceable to the National Institute for Standards and Technology, operating at several temperatures between 250 and 300 Kelvin (after Revercomb et al. 1988). We had excellent field support for this experiment, including construction of a shelter for the instrument, and an uninterrupted supply of liquid nitrogen. We were therefore able to operate the spectroradiometer without interruption from 25 August to 17 November 1991, and measurements were made four to five times daily. We thus have a data set that defines the longwave radiation environment of the region, in much the same way as the National Science Foundation ultraviolet (UV) monitor at Palmer Station defines the UV and visible radiation environment (Lubin et al. 1992). Ancillary measurements included all-sky video and still photography, measurements of ozone and cloud transmittance from the UV-monitor, Advanced Very High Resolution Radiometer satellite data tracked and archived by the Scripps Antarctic Research Center (ARC) Terascan facility at Palmer Station, and standard meteorological data recorded daily.

Examples of emission spectra. Figure 1 shows mid-infrared (IR) emission measured by the spectroradiometer at Palmer Station on 9 September 1991, at local noon. During this measurement the sky was clear, and the spectrum shows the major emission features of carbon dioxide (500-750 centimeters^{-1}), ozone (1,000-1,070 centimeters^{-1}), and water vapor (1,250-2,000 centimeters^{-1}). Emission features from other "greenhouse" trace gases can be found in the "window" region between 760 and 1,250 centimeters^{-1} (Goody and Yung 1989).

Also plotted in figure 1 are two theotetical emission spectra generated by the widely-used LOWTRAN 7 radiative transfer model. These model calculations utilized sub-arctic winter and sub-arctic summer model atmospheres (U.S. Standard Atmosphere 1976), having surface temperatures of 257 K and 288 K, respectively. On 9 September the surface temperature at Palmer Station was 273 K, and the emission spectrum generally lies evenly spaced between the two LOWTRAN results. One exception is the ozone emission feature, the measurement of which lies much closer to the sub-arctic winter LOWTRAN result. The column ozone abundance over Palmer Station was 195 Dobson units (well into the ozone-hole season), whereas the LOWTRAN calculations were done with an unperturbed ozone layer.

Figure 2 shows emission spectra under three different overcast sky conditions at Palmer Station. The upper spectrum (C) was recorded during snowfall, and it is essentially a blackbody spectrum throughout the mid-IR. The middle curve (B) was measured under a low stratus layer (base altitude approximately 450 meters). This curve appears to be a superposition of two blackbody spectra, a warmer one in the opaque carbon dioxide (CO_2) and water vapor emission regions (with many individual carbon dioxide and water vapor emission features still visible), and a colder one in the mid-IR window. The lower curve (A) was measured under an altostratus layer (base altitude approximately 1.5 kilometers), and examination of this spectrum around 1,050 centimeters^{-1} shows that this type of cloud is thin and/or cold enough that the ozone emission feature can still be seen. Radiative transfer calculations are needed to determine whether this feature is due to stratospheric ozone seen through the cloud, or tropospheric ozone below the cloud.

Discussion. Overcast is the most common sky condition at Palmer Station (Warren et al. 1986). Of all overcast layers sampled by the spectroradiometer, high overcast layers (altostratus, having spectral signatures similar to figure 2, curve A) occurred approximately 27 percent of the time. The remainder were lower overcast layers having spectral signatures closer to figure 2, curve B. While most of the clouds appear to behave nearly like blackbodies, we need to estimate their emissivity. If we plot the cloud brightness temperatures in the 760-1,250 centimeters^{-1} window versus estimates of the cloud-base temperature (obtained from model atmospheres based on 1988 NASA/Wallops Flight Facility ozonesonde data, G. Brothers, personal communication), as in figure 3, we see that the vast majority of the clouds at all levels appear to be radiating at temperatures colder than their base. This is most evident for altostratus layers, and figure 3 suggests

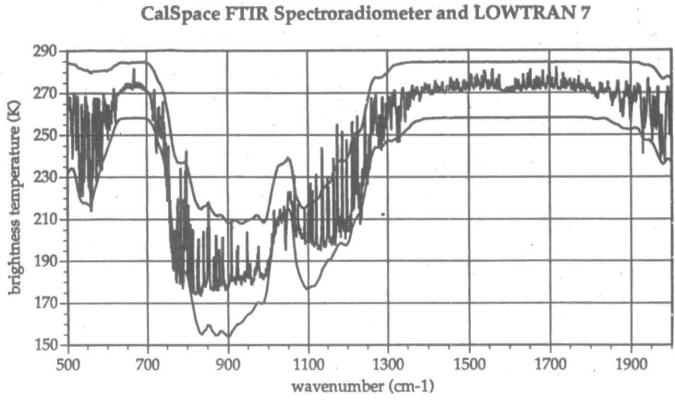

Figure 1. Emission spectrum measured by the California Space Institute FTIR Spectroradiometer under clear skies at Palmer Station, on 9 September 1991, at local noon. The smoother curves above and below the measurement refer to emission spectra calculated by the LOWTRAN 7 radiative transfer model using sub-arctic summer and sub-arctic winter, respectively. The measurement was made at 1 centimeter^{-1} resolution while the LOWTRAN calculations were performed at 20 centimeters^{-1} resolution.

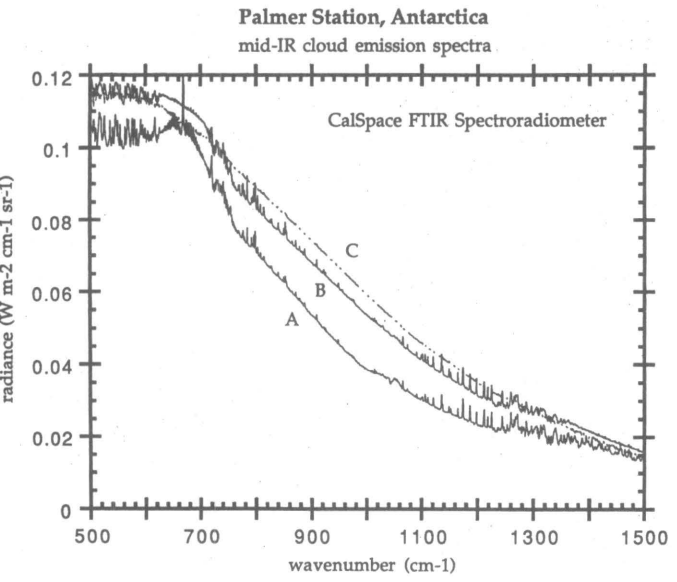

Figure 2. Emission spectra measured by the CalSpace FTIR Spectroradiometer under overcast sky conditions at Palmer Station. Spectrum A was recorded at local noon on 6 September 1991, under an altostratus layer. Spectrum B was recorded at local noon on 10 September 1991, under a low stratus deck. Spectrum C was recorded at local noon on 24 September 1991, under a snowfall.

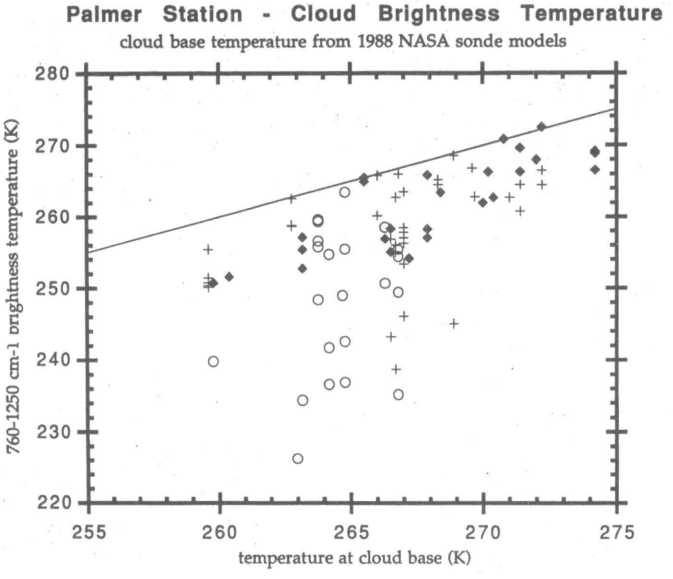

Figure 3. Cloud brightness temperature in the mid-IR window, as measured by the CalSpace FTIR Spectroradiometer, plotted against estimated cloud-base temperature. Cloud-base temperature is estimated using model atmospheres derived from ozonesonde data recorded at Palmer Station during spring 1988. The ozonesonde data was used to parameterize lapse rate as a function of surface temperature, the latter being recorded during each FTIR measurement. Diamonds refer to low stratus layers, crosses refer to mid-level stratus layers, and circles refer to altostratus layers.

that most clouds over the Antarctic Peninsula have emissivities less than unity. The average cloud-base temperatures for low overcast (0-0.6 kilometers), middle overcast (0.6-1.2 kilometers) and high overcast (altostratus, 1.2 kilometers and higher) are 268 K, 267 K, and 265 K, respectively. In contrast the average brightness temperatures in the mid-IR window, as measured by the FTIR spectroradiometer, are 262 K, 258 K, and 248 K, respectively, for low, middle, and high overcast layers.

This suggests average grey emissivities of 0.87, 0.80, and 0.64 for low, middle, and high overcast layers. Emissivities less than unity have also been observed in Arctic Stratus clouds (Curry and Herman 1985).

If we define the longwave *cloud forcing* at the earth's surface as the difference between flux under cloudy skies and flux under clear skies (Slingo and Slingo 1988, Ramanathan et al. 1989), then the average cloud forcing in the mid-IR window is 65 watts per square meter for low overcast, 59 watts per square meter for mid-level overcast, and 45 watts per square meter for altostratus. The longwave cloud forcing at the top of the atmosphere (sum of atmosphere and surface effects) estimated from the Earth Radiation Budget Experiment is small (less than 20 watts per sqaure meter at high latitudes, Li and Leighton 1991), suggesting the importance of surface effects. Sea-ice models are sensitive to parameterizations of longwave radiation (Shine and Henderson-Sellers 1985), and modern general circulation models (e.g. Slingo and Slingo 1991) require accurate representations of longwave cloud emissivity. We hope that this FTIR data set from the Antarctic Peninsula will complement the FTIR experiments that have been carried out at the South Pole (Goldman et al. 1988), and will contribute to a better understanding of the atmospheric radiation budget at high latitudes.

This work was supported by the California Space Institute under grant CS-11-90, by the Department of Energy Atmospheric Radiation Monitoring (ARM) Program under grant DOE 90ER61062, and by National Science Foundation grant DPP 90-18207.

References

Curry, J. A., and G. F. Herman. 1985. Infrared radiative properties of summertime arctic stratus clouds. *Journal of Climate and Applied Meteorology*, 24:525-538.

Goody, R. M., and Y. L. Yung. 1989. *Atmospheric Radiation: Theoretical Basis.* New York: Oxford University Press, 519.

Goldman, A., F. J. Murcray, and D. G. Murcray. 1988. Measurements of several atmospheric gases above the South Pole in December, 1986 from high resolution 3- to 4-micron solar spectra. *Journal of Geophysical Research*, 93(D6):7,069-7,074.

Li, Z. and H. G. Leighton. 1991. Scene identification and its effect on cloud radiative forcing in the Arctic. *Journal of Geophysical Research*, 96(D5): 9,175-9,188.

Lubin, D., B. G. Mitchell, J. E. Frederick, A. D. Alberts, C. R. Booth, T. Lucas, and D. Neuschuler. 1992. A contribution toward understanding the biospherical significance of antarctic ozone depletion. *Journal of Geophysical Research*, 97(D8):7,817-7,828.

Ramanathan, V., R. D. Cess, E. F. Harrison, P. Minnis, B. R. Barkstrom, E. Ahmad, and D. Hartmann. 1989. Cloud-radiative forcing and climate: Results from the Earth Radiation Budget Experiment. *Science*, 243:57-62.

Revercomb, H. E., H. Buijs, H. B. Howell, D. D. LaPorte, W. L. Smith, and L. A. Sromovsky. 1988. Radiometric calibration of IR Fourier transform spectrometers: Solution to a problem with the High-Resolution Interferometer Sounder. *Applied Optics*, 27:3,210-3,218.

Shine, K. P., and A. Henderson-Sellers. 1985. The sensitivity of a thermodynamic sea-ice model to changes in surface albedo parameterizations. *Journal of Geophysical Research*, 90(D1):2,243-2,250.

Slingo, A., and J. M. Slingo. 1988. The response of a general circulation model to cloud longwave radiative forcing. I: Introduction and initial experiments. *Quarterly Journal of the Royal Meteorological Society*, 114:1,027-1,062.

Slingo, A. and J. M. Slingo. 1991. Response of the National Center for Atmospheric Research Community Climate Model to improvements in the representation of clouds. *Journal of Geophysical Research*, 96(D8):15,341-15,357.

Warren, S. G., C. J. Hahn, J. London, R. M. Chervin, and R. L. Jenne. 1986. *Global distribution of total cloud cover and cloud type amounts over the ocean*. NCAR Technical Note NCAR/TN-317+STR, DOE/ER-0406, Boulder, Colorado: National Center for Atmospheric Research.

Extended observations of atmospheric infrared absorption and emission

FRANK J. MURCRAY AND RENATE HEUBERGER

Department of Physics
University of Denver
Denver, Colorado 80208

As the interest in the greenhouse effect is growing and the problem of the depletion of the ozone layer becomes more severe, the measurement of atmospheric composition and of radiative transfer becomes more important. To detect changes and to understand the processes that cause these problems, it is necessary to take measurements over an extended period of time. The atmospheric research group of the University of Denver (DU) has measured atmospheric composition with infrared techniques for several years.

During the previous season (1990-1991), a Fourier Transform Infrared (FTIR) spectrometer was installed in the New Zealand Arrival Heights building. After installation, the instrument was turned over to the New Zealand science technician for operation. During the austral fall and spring, solar absorption spectra were collected to measure column abundances of nitric acid using its absorption near 12 microns (880 wavenumbers) (Keys et al. 1992). This effort was conducted in collaboration with the New Zealand Department of Scientific and Industrial Research (DSIR).

In January 1992, Renate Heuberger of DU installed a small FTIR system on the roof of Skylab at the South Pole. The spectrometer was set up during the austral winter to collect atmospheric emission data by measuring column abundances of water vapor, carbon dioxide, ozone, fluorocarbon 11, fluorocarbon 12, and nitric acid, as well as absolute total radiance in the region of 7-20 microns (500-1,500 wavenumbers). The change of nitric acid during the long absence of sunlight is of special interest.

This project is a continuation of an experiment that started in 1989, when the spectrometer was taking data for over a year (Murcray et al. 1990 and 1991). The experience of the previous year showed that the signal-to-noise ratio needed to be improved for the measurement of accurate column abundances of nitric acid during the winter, when the signals are extremely low. The instrument was taken back to DU, where several changes were made. During the first year that the spectrometer was running at the South Pole, a heater failed on the warm blackbody; and only the blackbody at ambient temperature was available for calibration. The heater was repaired, and a more accurate calibration with two blackbodies will be possible for this year. In addition,

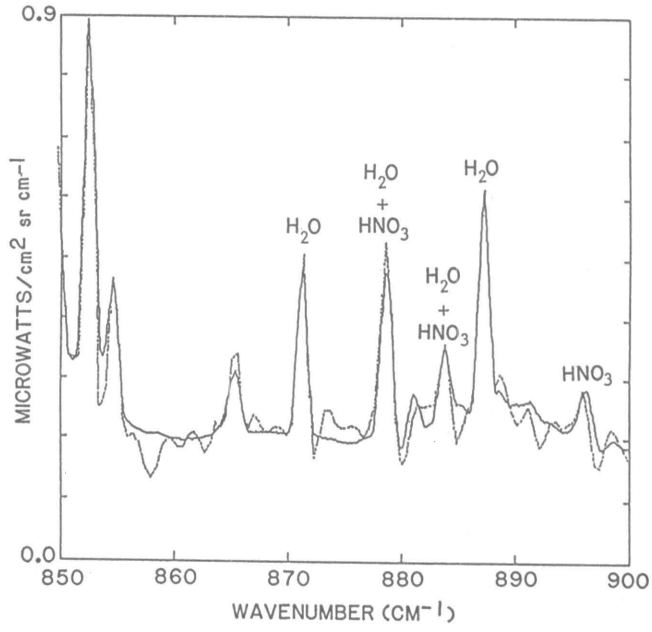

Calculated and experimental spectra for water and nitric acid (HNO_3). The fit for the nitric acid line at 896 centimeters^{-1} is not very good, since the line parameters for this line are not well known. On the left, part of the fluorocarbon-11 feature can be seen.
Vertical column amounts: H_2O 3.8 * 10^{21} molec./cm^{-2}; HNO_3 2.0 * 10^{16} molec./cm^{-2}; *solid line:* calculated data; *broken line:* experimental data. (Note: The spectrum was taken at the South Pole on 6 December 1989.)

a third blackbody of adjustable temperature is being used once a month for reference to show any degradation of the other two blackbodies exposed to wind and snow. For the calculation of absolute total radiance, an exact calibration is necessary. Steve Warren of the University of Washington wintered at the South Pole during 1992 and conducted these calibrations. He also observed the sky conditions at the time of each measurement and

Water vapor values for South Pole, 1989-1990

Date	Vertical column (molecules/cm^2)	Precipitable water content (mm)
12/06/89	3.8 * 10^{21}	1.1
12/09/89	5.0 * 10^{21}	1.5
12/12/89	5.5 * 10^{21}	1.6
04/10/90	3.8 * 10^{21}	1.1
09/07/90	0.7 * 10^{21}	0.2

phenomena, for example, blowing snow and diamond dust, which have a strong influence on emission measurements taken from the ground. To achieve better signal-to-noise ratio, the scheduling program that usually takes data every 12 hours needs to be changed to more frequent measurements during clear-sky conditions. The data collection is fully automated needing a minimum of attention.

The table shows values for water vapor in vertical column amounts and precipitable water contents for the South Pole for 1989-1990. The figure shows the water and nitric acid lines both measured and calculated for five dates from 6 December 1989 through 7 September 1990. The value of $2.0 * 10^{16}$ molecules per centimeter^2 for nitric acid is typical for the South Pole during the austral summer (Jones 1992).

Both projects were supported by National Science Foundation grant DPP 89-17643 and by the National Aeronautics and Space Administration. The first project was also supported by the DSIR and the New Zealand Antarctic Program.

References

Jones, N. B. 1992. Application of improved HNO_3 band model parameters to South Pole atmospheric emission measurements. Ph.D. diss., University of Denver.

Keys, J. G., P. V. Johnston, R. D. Blatherwick, and F.J. Murcray. 1992. New evidence of heterogeneous reactions involving nitrogen compounds in the antarctic stratosphere. *Nature*, in press.

Murcray, F. J. and R. Heuberger. 1990. Infrared atmospheric absorption and emission measurements. *Antarctic Journal of the U.S.*, 25(5):244-6.

Murcray, F. J. and R. Heuberger. 1992. Year-round measurement of atmospheric infrared emission at the South Pole. *Antarctic Journal of the U.S.*, 26(5)278-281.

Simultaneous ozone and polar stratospheric cloud observations at Amundsen-Scott South Pole Station during winter and spring 1991

James M. Rosen and Norman T. Kjome

Department of Physics and Astronomy
University of Wyoming
Laramie, Wyoming 82071

S.J. Oltamans

National Ocean and Atmospheric Administration
Climate Monitoring and Diagnostic Laboratory
Boulder, Colorado 80303

The critical role that polar stratospheric clouds (PSCs) play in heterogeneous chemical ozone depletion schemes is well recognized. The South Pole is one of the most productive sites to study this interaction because temperatures low enough for extensive PSC formation occur every year. In addition, PSC activity continues through stratospheric sunrise over Antarctica; thus providing an unusual opportunity to directly observe possible correlation between ozone and PSCs during the initial stages of "ozone hole" formation.

In this work, we conducted a series of simultaneous PSC and ozone observations from balloon-borne sensors launched at the South Pole starting before the beginning of PSC activity and continuing until the initial formation of the ozone hole. These observations were augmented with frost-point soundings and additional ozone soundings.

PSC observations were made with a balloon-borne backscattersonde operating at wavelengths of 490 and 940 nanometers. This device, described by Rosen and Kjome (1991), is used for research in the north polar vortex as well as for monitoring aerosols at mid-latitudes. Briefly, the instrument measures the amount of locally backscattered light at two wavelengths from a flash-lamp beam. The final data product is essentially the same as that of lidar systems, but with comparatively high resolution (about 30 meters). All instruments are calibrated before flight against a standard which has a known response in aerosol-free air. The signal in the two color regions provides limited but useful particle-size information.

Ozone measurements were made with a commercial sensor (ECC ozonesonde) modified to be part of the same instrument and telemetry package as the backscattersonde. Truly simultaneous measurements of both ozone and PSCs were obtained. In addition, simultaneous air temperature and pressure measurements were acquired with the backscattersonde.

Balloon-borne frost-point measurements were made with an instrument described by Oltmans (1985). Previous measurements using this instrument in Antarctica have been reported by Rosen et al. (1991).

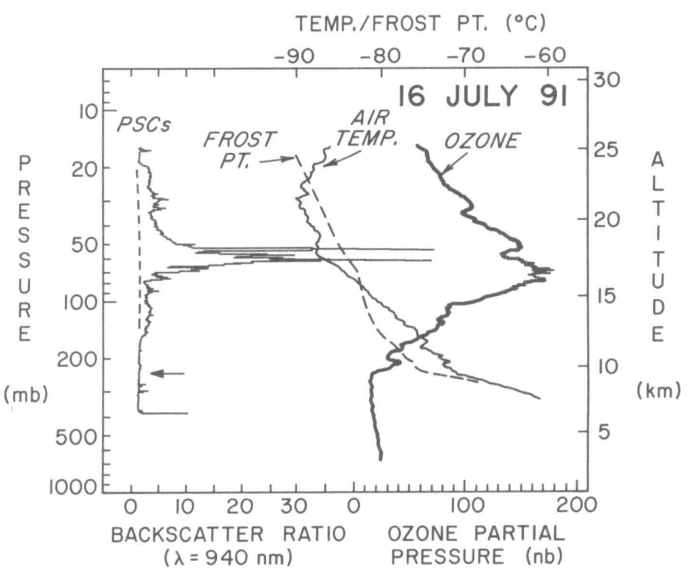

An example of the vertical profiles obtained during this research project. See text for explanation and interpretation.

One of the goals of this work was to characterize the PSCs and their environment at the onset of formation. However, due to several launch mishaps, the initial period was missed. The last sounding before the occurrence of PSCs was on 17 May when the minimum stratospheric temperature was about -79 °C -1 °C warmer than the expected temperature of initial formation. The next successful sounding was made on 12 June after the minimum stratospheric temperatures dropped will below -80 °C and extensive PSC formation had already begun.

The figure shows the results of a sounding made more than one month after the beginning of extensive PSC activity. The frost-point profile illustrated in this figure was obtained on 12 January 1991, and represents initial conditions in the vortex. According to the figure, by 16 July the stratospheric air temperature had cooled well below the initial frost-point and a large fraction of the water vapor would have already condensed. However, in the altitude range of 20 to 45 millibars the backscatter signal is relatively small and does not indicate the presence of significant condensed material. This suggests that the particles have already fallen out, resulting in dehydration of the stratosphere. The magnitude of the backscatter layer at 60 millibars can only be explained by condensed water vapor. The inverse correlation of this dense PSC layer with the structure in the ozone suggests recent transport from outer regions of the vortex. It is too early in the season for the usual ozone hose to have started development. Because the dense PSC layer is recent, the particles would not have had time to fall out of the stratosphere, as did the particles that must have formed earlier in the 20 to 45 millibar range.

Mike O'Neil and John Lowell were responsible for preparing instruments and launching the balloons. They were often required to work outside for extended periods at temperatures below -60 °C, so their efforts are greatly appreciated.

This work was supported by National Science Foundation grant DPP 88-16563.

References

Oltmans, S. J. Measurements of water vapor in the stratosphere with a frost-point hygrometer. *Proceedings of Moisture and Humidity*, Washington, D.C. 15-18 April, 1985. 252-8.

Rosen, J. M., N. T. Kjome, S. J. Oltmans. 1991. Balloon-borne observations of backscatter, frost point and ozone in polar stratospheric clouds at the South Pole. *Geophysical Research Letters*, 18:171-174.

Rosen, J. M. and N. T. Kjome. 1991. Backscattersonde: a new instrument for atmospheric aerosol research. *Applied Optics*, 30:1,552-1,561.

Antarctic automatic weather stations: Austral summer 1991-1992

Charles R. Stearns and George A. Weidner

Department of Atmospheric and Oceanic Sciences
University of Wisconsin
Madison, Wisconsin 53706

The United States Antarctic Program (USAP) of the National Science Foundation Office of Polar Programs (OPP) places automatic weather stations (AWS) units in remote areas of Antarctica in support of meteorological research and operations. The AWS data are collected by the ARGOS data collection system on board the National Oceanic and Atmospheric Administration (NOAA) series of polar orbiting satellites.

In the AWS system the basic AWS units measure air temperature, wind speed, and wind direction at a nominal height of 3 meters above the surface and air pressure at the electronics enclosure. Some AWS units may measure relative humidity at 3 meters, air temperature difference between 3 meters and 0.5 meters above the surface. The AWS unit at Pegasus South (table 1) measures millivolt signals using a differential amplifier with a gain of 480 to amplify the thermocouple voltage to the 0 to 1 vdc range of the analog to digital converter and a differential multiplexer to select the channels. The system is used to measure the temperature profile in the ice to a depth of 1.60 meters. AWS units equipped with the vertical air temperature difference and relative humidity are used to estimate the sensible and latent heat fluxes. Some results of the estimates are presented by Stearns (1992) and show that there is a net removal of water (ice) from the surface in Antarctica and the removal is largest during the summer months, amounting to as much as 80 percent of the net annual accumulation at Lettau site on the Ross Ice Shelf.

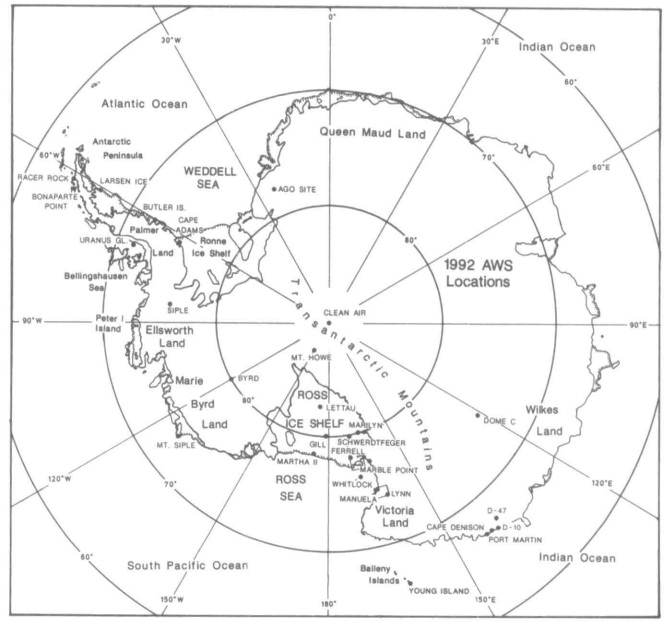

Figure 1. Map of Antarctica showing the locations of the AWS units for 1992. The units in the *rectangle* about Manuela site are shown in figure 2.

The table gives the unit's latitude, longitude, and the start date for USAP AWS units in 1992. The AWS units are grouped together based on the area and usually are related to a single meteorological experiment in the area. Stearns and Weidner (1991) describe the AWS activities during the previous austral summer.

The AWS units are located in arrays for meteorological experiments and at other sites for operational purposes. Any one AWS

AWS Locations for 1992, including the ARGOS ID and WMO Number. D-80 is not received.

Site	ARGO ID	Lat. (deg)	Long. (deg)	Alt. (m)	Date Start	Stop	WMO#
			Adelie Coast				
D-10	8914	66.70° S	139.80° E	240	Feb 80		89832
D-47	8916	67.38° S	138.72° E	1560	Jan 83		89834
D-80	8919	70.02° S	134.72° E	2500	Nov 84		89836
Dome C	8904	74.50° S	123.00° E	3280	Feb 80		89828
Port Martin	8934	66.82° S	141.39° E	39	Jan 90		
Cape Denison	8933	67.02° S	142.68° E	31	Jan 90		
West Antarctica							
Byrd Station	8903	80.00° S	120.00° W	1530	Feb 80		89324
Siple St.	8910	75.90° S	83.92° W	1054	Jan 82		89284
Mount Siple*	8981	73.20° S	127.05° W	30	Feb 92		
			Ross Island Region				
Marble Point	8906	77.43° S	163.75° E	120	Feb 80		89866
Ferrell	8907	78.02° S	170.80° E	45	Dec 80		89872
Jimmy		77.87° S	166.81° E	202	Dec 81		
Pegasus N.	8927	77.95° S	166.51° E	10	Jan 90		89667
Pegasus S.	8937	78.03° S	166.60° E	10	Jan 91		
Minna Bluff	8915	78.50° S	166.51° E	900	Jan 91		
Linda	8921	78.50° S	168.35° E	50	Jan 91		
Willie Field*	8901	77.11° S	167.00° E	20	Jan 92		
Ocean Islands							
Whitlock	8913	76.24° S	168.70° E	275	Jan 82		89865
Young Island	8980	66.28° S	162.33° E	30	Dec 90		89660
Ross Ice Shelf							
Marilyn	8931	79.98° S	165.03° E	75	Jan 84		89869
Schwerdt	8924	79.94° S	169.83° E	60	Jan 85		89868
Gill	8924	80.03° S	178.63° W	55	Jan 85		89863
Lettau	8908	82.59° S	174.27° W	55	Jan 86		89377
Martha II	8900	78.38° S	173.42° W	18	Feb 87	Feb92	89374
			Reeves Glacier				
Manuela	8905	74.92° S	163.60° E	80	Feb 84		89864
Shristi	8909	74.92° S	161.58° E	1200	Dec 87		89862
Sandra	8923	74.48° S	160.48° E	1525	Jan 88		89861
Lynn	8935	74.21° S	160.39° E	1772	Jan 88		89860
			Antarctic Peninsula				
Larsen Ice	8926	66.97° S	60.55° W	17	Oct 85		89262
Butler Is.	8902	72.20° S	60.34° W	91	Mar 86		89266
Uranus	8920	71.43° S	68.93° W	780	Mar 86		89266
Cape Adams	8917	75.01° S	62.53° W	25	Jan 89		89268
Racer Rock	8930	64.16° S	61.54° W	17	Nov 89		89261
BAS-AGO	8932	77.52° S	23.74° W	1545	Jan 91		89024
Bonaparte Pt.*	8912	64.78° S	63.06° W	8	Nov 91		
			High Polar Plateau				
Clean Air	8918	90.00° S		2835	Jan 86		89208
Mount Howe*	8982	87.32° S	149.55° W	2400	Jan 92		

* New sites during 1991-1992 field season.

unit may contribute to several experiments, and all contribute to operational purposes especially for preparation of weather forecasts for aircraft flights to and from New Zealand and within Antarctica.

The polar AWS units support the following research and operational areas:

- barrier wind flow along the Antarctic Peninsula and the Transantarctic Mountains;
- katabatic wind flow down the slope to the Adelie Coast, Reeves Glacier, Beardmore Glacier, and West Antarctica;
- mesoscale circulation and the sensible and latent heat fluxes on the Ross Ice Shelf;
- climatology of Byrd, Siple, and Dome C Stations;
- research in antarctic coastal ecosystem rates along the Antarctic Peninsula;
- meteorological support for air operations at McMurdo Station, Antarctica;
- monitoring for possible station locations aircraft landing sites;
- long-term ecological research along the Antarctic Peninsula.

The 1991-1992 field season started when Tony Amos replaced the electronics at the Racer Rock AWS site during November 1991. The pressure system became erratic shortly after installa-

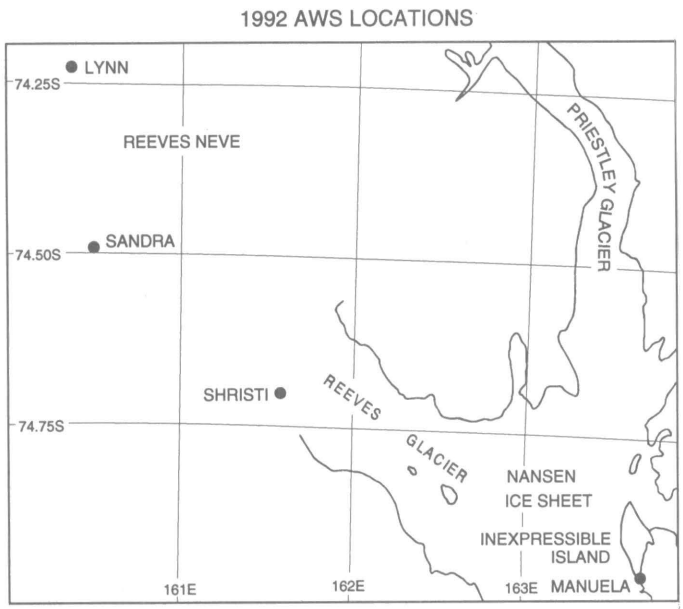

Figure 2. Map of the 1992 locations of the AWS units in the Reeves Glacier area of Antarctica, including Manuela site.

tion in 1990. The *Polar Duke* provided transportation to the site. In January 1992 Amos installed an AWS unit on Bonaparte Point in support of long-term ecological research.

On the *Polar Sea* cruise from Portland, Australia, to McMurdo, Antarctica, Stearns replaced the broken aerovane at Manuela site. Equipment and weather conditions were unfavorable for the installation of dog-house AWS units on Scott and Possession Islands. Stearns arrived at McMurdo on 4 January 1992; Weidner, R. Holmes, and R. Doornbos arrived at McMurdo Station on 6 January 1992.

Upon our arrival at McMurdo, a clamor arose requesting an AWS unit on the blue-ice area north of Mount Howe. The blue ice is being investigated as a potential blue-ice runway. We made a trip to the South Pole and then to the blue ice at Mount Howe on 11 January 1992. With the help of Bill Barber and the crew of the Twin Otter, we installed the AWS unit near the outhouse on the blue ice.

Weidner, Holmes, and Doornbos replaced the faulty aerovane and electronics at Linda site on 15 January 1992. Stearns, Doornbos, and Holmes replaced the aerovane, electronics, and antenna at Minna Bluff on 16 January 1993. We visited Pegasus North and Pegasus South sites on 22 January and found them to be in good condition. The anchors had not melted out of the ice.

We raised the tower 5 feet and replaced the aerovane and electronics at Lynn site on 23 January 1992. On the return flight to McMurdo we removed the AWS unit at Sushila site.

We installed an AWS unit at the west end of Williams Field to provide meteorological information throughout the year in anticipation of possible year-round operations and for comparison with the Pegasus sites.

We installed a Geoteck WS-201 wind system at Jimmy site to see if the system would withstand the annual season at a relatively peaceful site. The aerovanes currently used to measure wind speed and direction are not always functioning throughout the year. If an aerovane lasts an average of 5 years, then 7 aerovanes need replacement and repair each year.

Members of the British Antarctic Survey raised the Siple Station AWS unit one 5-foot tower section, reinstalled the Uranus Glacier AWS, and replaced the Butler Island and Larsen Ice Shelf aerovanes.

Expedition Polaris Francaises replaced the aerovane at Port Martin, and the electronics at D-47 and at D-10.

The marine science technicians of the U.S. Coast Guard icebreaker *Polar Sea* removed the AWS unit at Martha 2, because the unit was nearly buried with snow. The *Polar Sea* helicopter crew installed a dog-house AWS unit at Mount Siple.

The AWS program is currently supported by National Science Foundation grants DPP 88-21894 and DPP 90-15586. The British Antarctic Survey installs and services the AWS units in the Antarctic Peninsula area. Expeditions Polaires Francaises installs and services the AWS units along and inland from the Adelie Coast.

References

Stearns, C. R. 1992. Sensible and latent heat fluxes on the Ross Ice Shelf, Antarctica. Accepted for the *Antarctic Research Series.*

Stearns, C. R. and G. A. Weidner. 1991. Antarctic automatic weather stations: Austral summer 1990-1991. *Antarctic Journal of the U.S.*, 26(5):247-250.

Maximum and minimum temperature trends at McMurdo Sound Station

David A. Braaten and Gisela A. M. Dreschhoff

Department of Physics and Astronomy
University of Kansas
Lawrence, Kansas 66045

We have obtained copies of daily surface weather observation sheets for McMurdo Sound Station, Antarctica from the National Climatic Data Center. These data span a 35-year period from March 1956 through October 1990. The data obtained lack 16 months during the last 3 years (1988-1990). These data sheets contain weather observations generally taken at 3-hour intervals and include sky condition, temperature, humidity, wind, pressure, and precipitation, as well as daily summaries of maximum and minimum temperature, precipitation, and peak wind. For this investigation, we took the daily maximum and minimum temperatures manually from either paper or microfiche and entered them into a desktop computer for analysis. We conducted extensive error checks on the digitized data before analysis; this included checks for consistency and outliers.

The monthly mean of the daily maximum and minimum temperatures at McMurdo Station between 1956 and 1990 are shown in figures 1 and 2, respectively. The greatest maximum and minimum temperatures occur in January, and the lowest maximum and minimum temperatures occur in August. Both the maximum and minimum temperatures vary more during the months without sunlight than during periods with sunlight; this

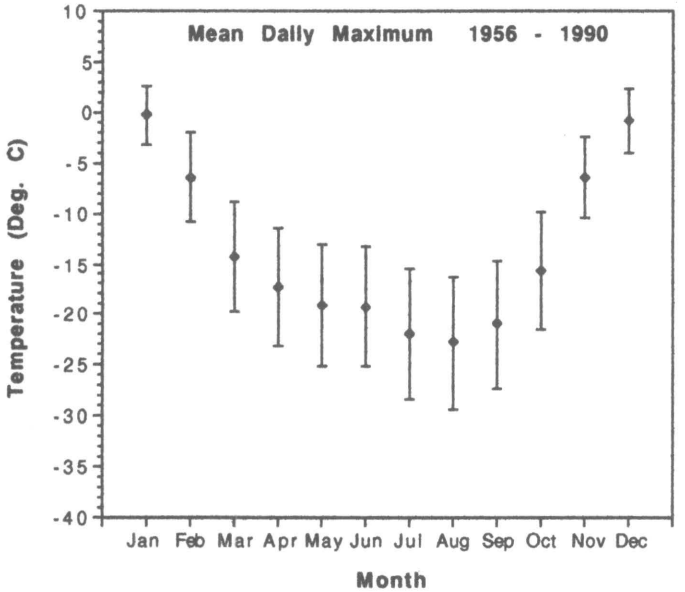

Figure 1. Mean daily maximum temperature by month between 1956 and 1990. *Error bars* indicate the standard deviation.

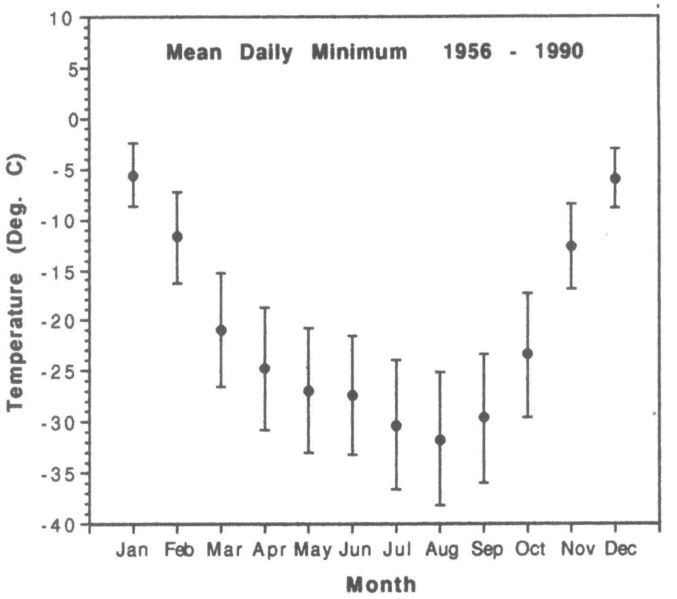

Figure 2. Mean daily minimum temperature by month between 1956 and 1990. *Error bars* indicate standard deviation.

finding is similar to that of Hanson (1990) for hourly and/or 3-hourly temperatures at the South Pole.

We examined long-term changes in maximum and minimum temperature at McMurdo for evidence of global warming. The time interval used in this analysis is from 1957 to 1987, the years for which we obtained complete temperature records. For each data set, we first averaged the temperatures for each year and then transformed them to temperature anomalies by subtracting the long-term average temperature from the period 1957-1980. Figure 3 is a plot of the maximum and minimum temperature anomalies for the 31-year period. These temperatures are positively correlated with a correlation coefficient of 0.81. Also shown on figure 3 are linear least squares regressions to the two data sets. The slope of these regression lines indicates the temperature trend over the period investigated. The trend of temperature minima is nearly zero with a temperature increase over this period of only 0.01 °C. The trend of temperature maxima has a strong positive slope with a temperature increase over this period of 1.51 °C.

The maximum and minimum temperature trends observed at McMurdo Station are the exact opposite of those in regional, mid-latitudes studies of maximum and minimum temperature climatology between 1950 and 1990 conducted by Karl et al. (1991). Karl et al. found that maximum temperatures over the past 40 years have been nearly constant while minimum temperatures have been increasing. The differences in these trends have been attributed to the role of atmospheric aerosols, which reduce the temperature at the surface during the day by scattering direct solar radiation but which have no effect on surface temperature at night. Although the McMurdo data are confounded with periods without a diurnal cycle, the increasing maximum temperature trend observed at McMurdo is consistent with the conclusions of Karl et al. since Antarctica is a pristine environment with low concentrations of atmospheric aerosols in the troposphere. The minimum temperature trend at McMurdo cannot be reconciled, since this is also expected to increase.

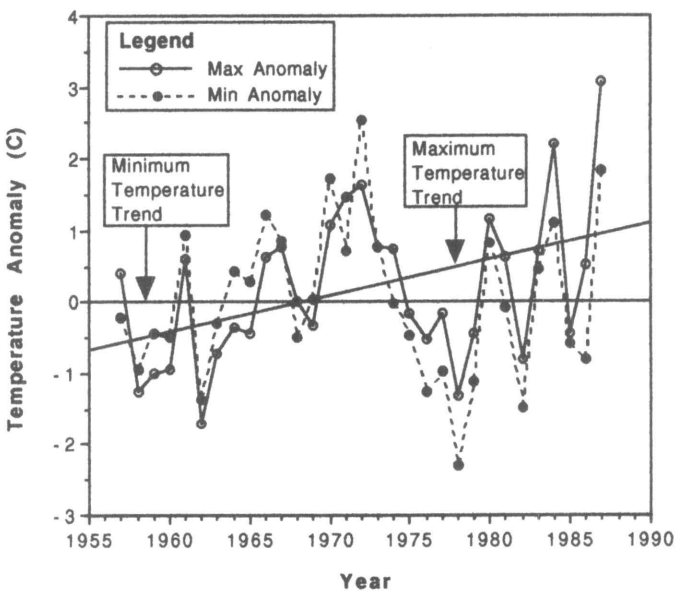

Figure 3. Annual average daily maximum and minimum temperature anomaly for McMurdo Sound Station, Antarctica, for 1957-1987. *Trend lines* are a linear regression to the respective data. All data were normalized to the average of 1957-1980.

We are grateful to Andy Ward for his careful work in exacting climatological data from copies of handwritten weather observation sheets and inputting the data to a computerized data base.

This project was supported in part by U.S. Air Force contract AFOSR-88-0065 and National Science Foundation grant DPP 89-19190.

References

Hanson, K. J. 1990. The South Pole Station temperature chronology and the global warming problem. *Antarctic Journal of the U.S.*, 25(5):247-249.

Karl, T. R., G. Kukla, V. N. Razuvayev, M. J. Changery, R. G. Quayle, R. R. Heim, D. R. Easterling, and C. B. Fu. 1991. Global warming: Evidence for asymmetric diurnal temperature change. *Geophysical Research Letters*, 18(12):2,253-2,256.

On the half-yearly pressure oscillation in eastern Antarctica

GERD WENDLER

Geophysical Institute
University of Alaska
Fairbanks, Alaska 99775

MICHAEL POOK

Institute of Antarctic and Southern Ocean Studies
(IASOS)
University of Tasmania
Hobart, Australia

In 1980, automatic weather stations (AWS), reporting via satellite, were placed in eastern Antarctica (e.g., Stearns and Wendler 1988). Surface climatological data have been obtained from these stations for about a decade. This year, instead of giving a general review of our activities, we will present a detailed discussion of one specific climatic element-atmospheric pressure.

One AWS, D10, is located 5 kilometers from the coast, and about 10 kilometers from Dumont d'Urville, the main French Antarctic station, which is situated on an island. The slope is relatively steep (1:20) and snow-covered all year.

The atmospheric pressure displays a semi-annual variation with a main maximum in summer (January and December) and a secondary maximum in mid-winter (June). As can be seen from figure 1, the minima occur in the intermediate seasons, the spring one (September) being more pronounced than that in autumn. This semi-annual variation in atmospheric pressure has been described previously (e.g., Schwerdtfeger and Prohaska 1956; van Loon 1966, 1967). Van Loon (1966) described the annual pressure variation at sea level, zonally averaged for 65° S, using the first and second harmonics, by the following expression: Y=986.4hPa+0.6hPasin(x+35°)+2.8hPasin(2x+110°) with Y=actual sea level pressure, and x=time of the year (for 1 January x=0).

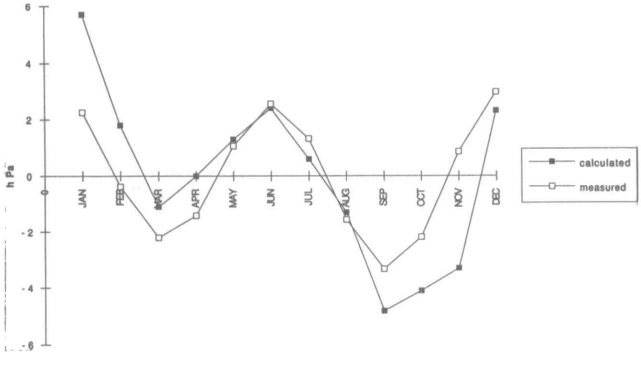

Figure 1. Normalized annual course of surface pressure as observed at D10 (66.7° S 139.8° E) compared with van Loon's expression for the zonally averaged surface pressure at 65° S.

A comparison of this relationship and the observed pressure at D10 shows good agreement (figure 1). Perfect agreement cannot be expected because van Loon's equation was derived from 6 years of data and is valid for the zonally averaged latitude of 65° S. D10 is located at 66.7° S 139.8° E, at an elevation of 240 meters. Since the mean pressure was 33.7 hecta Pascal less than van Loon's value, which is valid for sea level, we have normalized the comparison in figure 1. It can be seen that the annual courses of the sea-level pressures follow each other fairly closely, and the two maxima and minima are observed for identical months. Furthermore, the minimum is less pronounced in both cases in autumn (March) than in spring (September).

We now make the following assumptions:

- The north-south gradient of the radiation drives the circulation: the stronger the gradient, the stronger the circulation.
- The depth of the circumpolar trough is an index of the strength of this circulation.

For simplicity, we use the extraterrestrial radiation (ET) be-

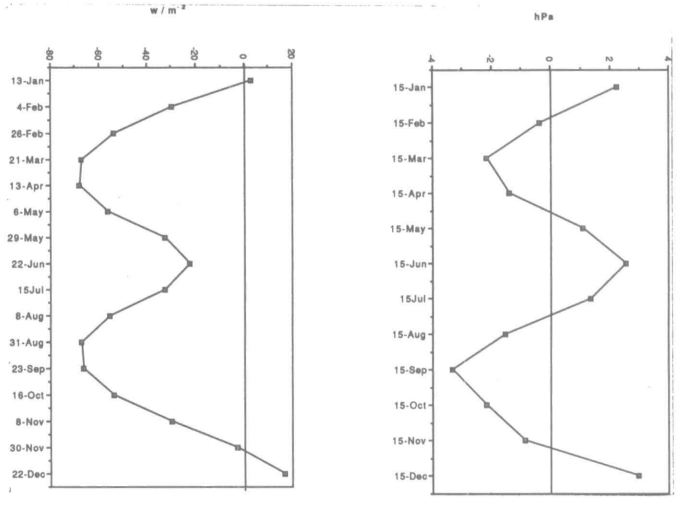

Figure 2. Normalized annual course of surface pressure as observed at D10 (66.7° S 139.8° E) (left), and (right), the gradient of the extra-terrestrial radiation at the top of the atmosphere between 70° S and 60° S.

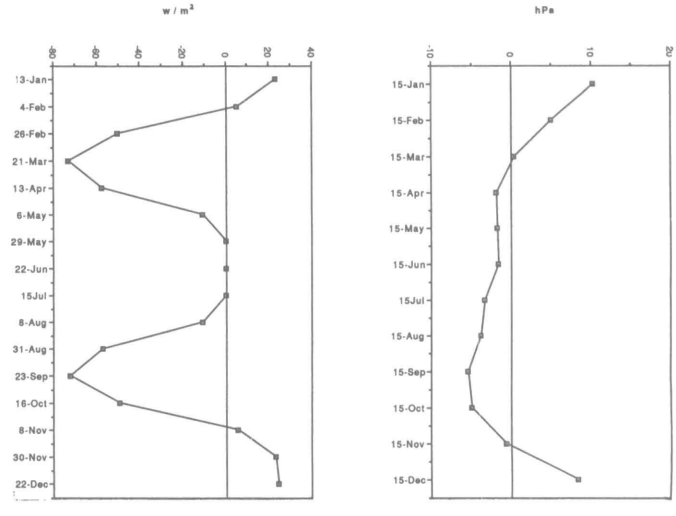

Figure 3. Normalized annual course of surface pressure as observed at Dome C (74.5° S 123.0° E) (left), and (right), the gradient of the extra-terrestrial radiation at the top of the atmosphere between 80° S and 70° S.

tween 70° S and 60° S as an indication of the radiative forcing. This radiative gradient and the observed surface pressure are presented in figure 2. The agreement between the two curves is astonishingly good. The only major discrepancy between the graphs occurs at the vernal equinox where the surface pressure displays a more pronounced minimum than in autumn. Of course, the radiative gradient at the top of the atmosphere shows no variation between the equinoxes. The intensification of the pressure trough in spring is related to the maximum sea-ice extent at this time of the year.

However, such a good agreement deteriorates with altitude. Dome C is our highest AWS station, located at 3,280 meters above sea level at 74.5° S and 123° E. Again, some 10 years of data are available. In figure 3, the surface pressure and the ET (this time the gradient between 80° S and 70° S) are given. While the radiative forcing still displays the strong half-yearly oscillation, which is zero in midwinter due to continuous darkness, the pressure displays only one large summer maximum. There might be a slight indication of a secondary maximum in winter, but it is very weak.

In summary, data from remotely located automatic weather stations in Antarctica have demonstrated that the semi-annual pressure variation is well established near sea level. However, with increasing altitude the variation becomes weaker and in the interior of Antarctica only a trace remains.

We would like to thank J. Sun who performed the data processing. This work was supported by National Science Foundation grant DPP 90-17969.

References

Schwerdtfeger, W. and F. Prohaska. 1956. Der Jahresgang des Luftdrucks auf der Erde und seine halbjährige Komponente. *Metetorologische Rundschau*, 9:33-43.

Stearns, C. R. and G. Wendler. 1988. Research results from antarctic automatic weather stations. *Reviews of Geophysics*, 26(1):45-61.

van Loon, H. 1966. Summary of a paper on the half-yearly oscillation of the sea-level pressure in middle and high southern latitudes. *WMO Technical Bulletin*, 419-427.

van Loon, H. 1967. The half-yearly oscillations in middle and high southern latitudes and the coreless winter. *Journal of the Atmospheric Sciences*, 24: 472-486.

Wind speed, wind direction, and air temperature at Pegasus North during 1991

Charles R. Stearns and
George A. Weidner

Department of Atmospheric and Oceanic Sciences
University of Wisconsin
Madison, Wisconsin 53706

Automatic weather station (AWS) units are installed at the north and south ends of Pegasus blue-ice runway on the Ross Ice Shelf near Ross Island, Antarctica, and at Minna Bluff and Linda sites in support of the meterology of the blue-ice runway (figure 1). The purpose of the AWS units is to determine the reason for the blue ice and to learn to forecast the extreme wind speeds observed in the area. Previous meterological results from the Pegasus runway are presented by Stearns and Weidner (1990, 1991). Stearns and Weidner (1992) present information related to other AWS units in Antarctica.

The basic AWS units measure air temperature, wind speed, and wind direction at a normal height of 3 meters above the surface and air pressure at the electronics enclosure. The AWS units at Pegasus North and Pegasus South sites measure relative humidity at 3 meters and the air temperature difference between 3 meters and 0.5 meters above the surface. The AWS unit at Pegasus South measures °1 millivolt signals using a differential amplifier with a gain of 480 to amplify the thermocouple voltage to the range of 0 to 1 volts direct current used by the analog-to-digital converter. The system is used to measure the temperature profile in the ice to a depth of 1.60 meters using thermocouples. Channels are selected by a differential multiplexer. The vertical air temperature difference and relative humidity are used to estimate the surface sensible and latent heat fluxes.

Meteorological data at three hourly intervals are used to prepare the results presented here.

The table presents the monthly means and extremes for temperature, wind, and the surface sensible and latent heat fluxes for Pegasus North site. Data are available only for the first 10 months of 1991 at the present time. Figure 2 shows the 10°-wide sector mean wind speed and wind direction frequency as a function of the sector wind direction for Pegasus North site. The pattern of 1989 and 1990 is repeated, with the most frequent sector wind direction being about 65° and the highest sector mean wind speed being from about 195° for the 10-month period. The maximum wind gust was in May 1991. Figure 3 shows the wind speed and wind direction at three hourly intervals for May 1991. The two gusts during May were from about 190° and persisted from 1 to 2 days. Unfortunately, the wind system at Minna Bluff was not operating in May 1991, so the two sites could not be compared. Graphs of three hourly wind speeds for Pegasus North in February 1991 showed two gusts that could be compared to the wind record for Minna Bluff. The Minna Bluff gusts occurred over a longer period of time, started earlier, and had a higher maximum speed than the gusts recorded at Pegasus North. The lead time at Minna Bluff compared to Pegasus North was approximately 24 hours.

The possible melting of the ice and snow around the Pegasus blue-ice runway may be associated with air temperatures above

Monthly mean air temperature (°C), wind speed (meters per second), resultant wind speed and direction (VV/DD), maximum wind speed and direction (VV/DD), sensible heat flux (Q_o), and latent heat flux (E_o) for Pegasus North from January through October 1991. VV is the wind speed in meters per second and DD is the wind directions in degrees clockwise from north. The units for Q_o and E_o are watts per square meter.

Month	Temp.	Speed	Resultant	Max. wind	Q_o	E_o
Jan	-4.0	3.2	2.3/66	12.7/171	-4.1	14.0
Feb	-8.0	4.5	2.6/127	23.4/195	-21.7	4.9
Mar	-22.3	4.9	3.2/92	25.7/195	-9.0	4.4
Apr	-24.7	3.8	2.2/89	22.6/164	-28.5	0.3
May	-29.7	5.1	2.3/146	33.3/188	-44.5	1.1
June	-24.2	4.9	2.7/121	31.8/194	-39.2	2.7
July	-31.6	4.2	2.0/104	31.8/192	-31.0	0.9
Aug	-32.8	3.1	2.1/92	19.6/189	-26.9	0.8
Sep	-24.3	6.4	3.3/143	29.5/198	-36.8	0.2
Oct	-20.7	4.1	1.8/123	25.1/187	-17.3	5.6

freezing occurring in the area during December and January. Figure 4 shows 35 occurrences of air temperatures above freezing at Pegasus North AWS site in January 1991. Figure 2 in Stearns and Weidner (1991) shows 87 occurrences of air temperatures above freezing in December 1990. The observations at are three hourly intervals. The temperatures above freezing for December 1990 and January 1991 are most frequently associated with wind directions from 300° through north to 80° and from 100° through 210°. People who work at Pegasus runway and then return to Williams Field frequently report that the air temperature is higher at Pegasus runway. During the 1991-1992 austral summer, an AWS unit was installed at the west end of Williams Field runway, so the two locations can be compared in the future.

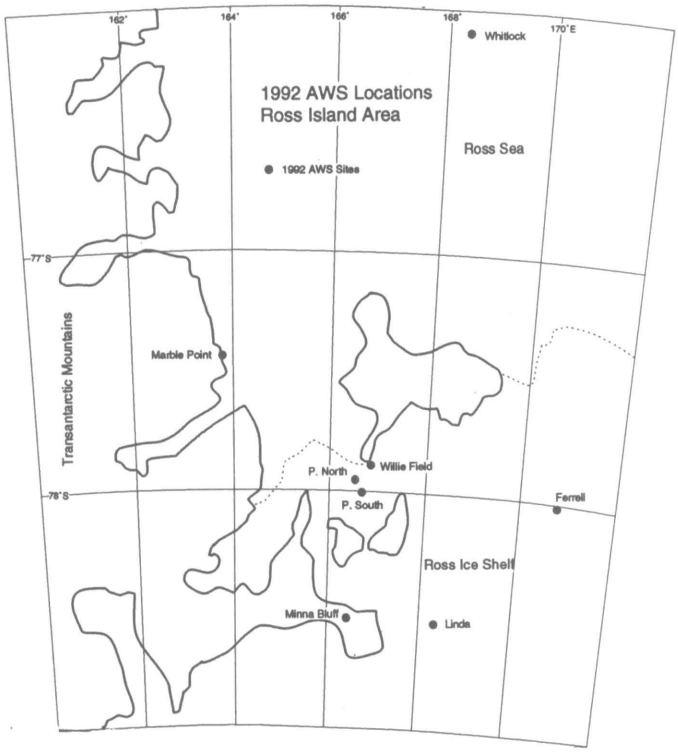

Figure 1. Map of the Ross Island area in Antarctica showing the locations of Pegasus North, Pegasus South, Ferrell, Linda, Minna Bluff, and Marble Point AWS units.

The table includes monthly means of the surface-sensible and latent flux. The pattern for monthly means of the surface-sensible and latent heat fluxes is similar to the pattern for 1990 (Stearns and Weidner 1991). During December and January, there is active melting of the snow around the Pegasus runway due to the advection of warm air. When warm air is advected into the area, the vertical air temperature difference can be between 1 to 2 °C with wind speeds above 5 meters per second, resulting in large sensible heat fluxes to the surface melting the snow. The latent heat flux remains positive, indicating that sublimation of ice is

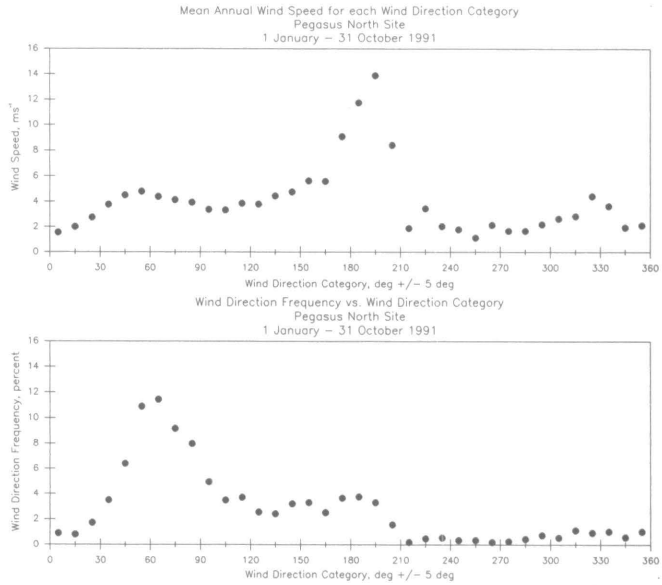

Figure 2. Mean annual wind speed and the frequency of the wind direction in a 10°-wide sector as a function of the direction of the sector at Pegasus North AWS site.

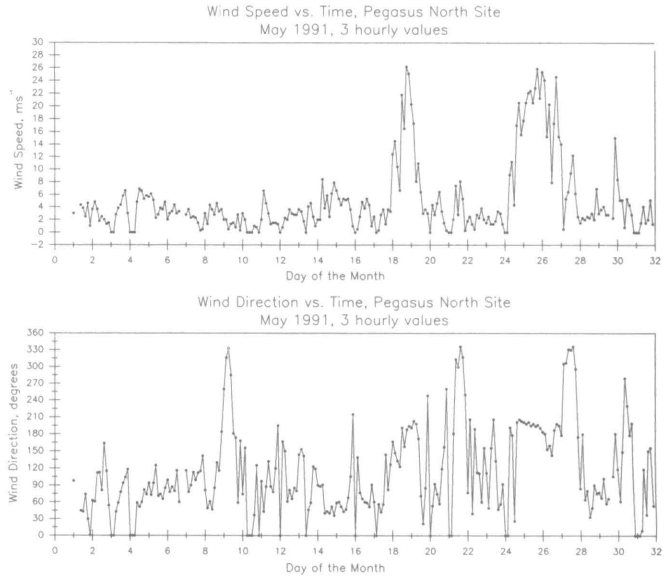

Figure 3. Wind speed and wind direction at three hourly intervals for Pegasus North AWS site during May 1991. May 1991 had the highest mean wind speed and the highest maximum wind speed from January through October 1991.

taking place as the temperature of the ice and snow remains at freezing or below. The sublimation at Pegasus North site exceeded 35 millimeters of water equivalent for the 10 months of 1991. The sublimation for 12 months in 1990 amounted to 100 millimeters of water equivalent.

References

Stearns, C. R. and G. A. Weidner. 1990. Wind speed events and wind direction at Pegasus site during 1989. *Antarctic Journal of the U.S.*, 25(5):258-262.

Stearns, C. R. and G. A. Weidner. 1991. Wind speed, wind direction, and air temperature at Pegasus North during 1990. *Antarctic Journal of the U.S.*, 26(5):251-253.

Stearns, C. R. and G. A. Weidner. 1992. Antarctic automatic weather stations: Austral summer 1991-1992. *Antarctic Journal of the U.S.*, this issue.

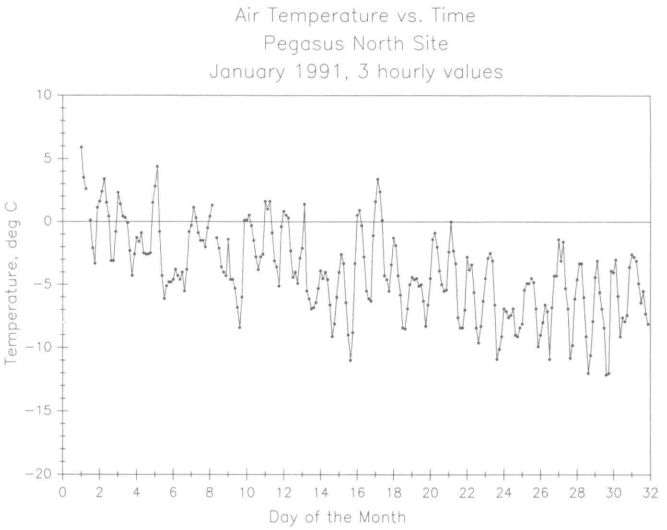

Figure 4. January 1991 air temperature for Pegasus North AWS site. The air temperature at three hourly intervals exceeded the freezing point 35 times.

Katabatic wind forcing of tropospheric circumpolar motions about Antarctica

THOMAS R. PARISH

Department of Atmospheric Science
University of Wyoming
Laramie, Wyoming 82071

Katabatic winds are commonplace features within the lowest few hundred meters of the antarctic troposphere. The radial drainage pattern off the elevated plateau and downslope increase in the magnitude of the katabatic wind imply that subsidence must occur over Antarctica. Thus, a secondary circulation extending throughout the troposphere becomes established in the high southern latitudes. The resulting convergence in the upper troposphere above Antarctica acts to generate cyclonic vorticity; a circumpolar vortex develops with time. A schematic illustration of this meridional circulation is shown in figure 1. A number of numerical simulations have depicted the sensitivity of the troposphere to the katabatic wind regime. Here the results of one such numerical experiment are presented. Additional discussion appears in Parish and Bromwich (1991) or Parish (1992).

The model used in the numerical experiments is a modified version of that described by Anthes and Warner (1978). Parish and Waight (1987) give a description of the model including the relevant equations. The model is written in sigma coordinates to allow for inclusion of irregular terrain. The model uses a total of 15 vertical levels (σ= .996, .99, .98, .97, .96, .94, .92, .90, .85, .775, .70, .60, .50, .30, .10); the pressure at the top of the model is 250 hectopascals. The high resolution in the lower levels of the atmosphere is necessary to depict the katabatic wind. The lowest sigma level corresponds to a height of approximately 20 meters above ground level.

The numerical experiment described is a 20-day model simulation starting from a rest state in which no horizontal pressure gradients are present. All motion is therefore derived from the radiative cooling of the sloping ice surface and subsequent evolution of the katabatic wind regime. The simulation represents polar night conditions where no solar radiation reaches the antarctic surface. I took an initial temperature field from the sounding shown in Schwerdtfeger (1984; see his figure 6.9); the thermal structure at the start of the model run is without a surface inversion and is assumed to be representative of tranquil conditions before strong katabatic wind events. I assumed the domain over the ocean to be covered by a solid ice shelf. The Coriolis parameter remains constant over the entire model domain and set to 0.00014.

The katabatic wind regime develops rapidly; the coastal katabatic wind speed reaches a maximum of nearly 14 meters per

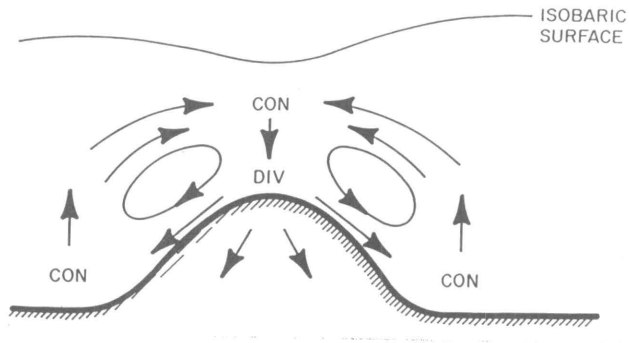

Figure 1. Conceptual depiction of the meridional mass circulation over Antarctica forced by the katabatic wind regime.

second after approximately eight hours. Figure 2a shows the initial 24-hour evolution of the downslope component of the wind and the potential temperature in the lowest kilometer of the atmosphere at the coastal grid point. This katabatic wind speed compares favorably with observations from katabatic-prone coastal stations. The modeled katabatic wind is shallow, contained within a depth of approximately 200 meters. After the downslope component reaches a maximum, values begin to decline. By 24-hours downslope components have been reduced to approximately 8.3 meters per second. Figure 2b illustrates the evolution of the coastal downslope and cross-slope wind components and potential temperature during the remainder of the 20-day integration period. An important aspect is the persistent decay of the katabatic wind intensity in the lower levels of the atmosphere. The downslope component of the wind at the coast decreases by nearly 65 percent from day 1 to day 20; the total katabatic wind speed at the coast has been reduced by nearly 50 percent from the 24-hour results to 5.6 meters per second by 20-days. The pattern of the model-produced downslope wind components at grid locations in the interior of the continent show comparable trends. This decay of the katabatic wind regime is a consequence of the developing adverse horizontal pressure gradient force in the upper atmosphere associated with the vortex development.

As discussed earlier, the low level katabatic wind circulation sets up a meridional circulation over Antarctica. The upper-level convergence above the continent generates cyclonic vorticity in the upper troposphere, thereby leading to the development of an upper-level vortex. Figure 3 depicts the cross-slope (zonal) components of motion in the middle and upper troposphere above the antarctic terrain at the end of the 20-day integration period. A vortex has developed with maximum zonal wind speeds in excess of 12 meters per second. As evidenced in figure 3, the strongest zonal winds are situated in a band above the coastal periphery. A noticeable southerly shift of the isotach pattern with height is apparent. This shift is most likely the result of the shape of the continent.

It is clear from such studies that the shallow antarctic katabatic wind regime is a potentially important factor in shaping the dynamics over nearly the entire troposphere in the high southern latitudes. It appears as if the persistent antarctic katabatic wind regime helps anchor the broad southern hemisphere circumpolar vortex over the continent.

This work was supported by National Science Foundation grants DPP 87-16127 and DPP 89-16998.

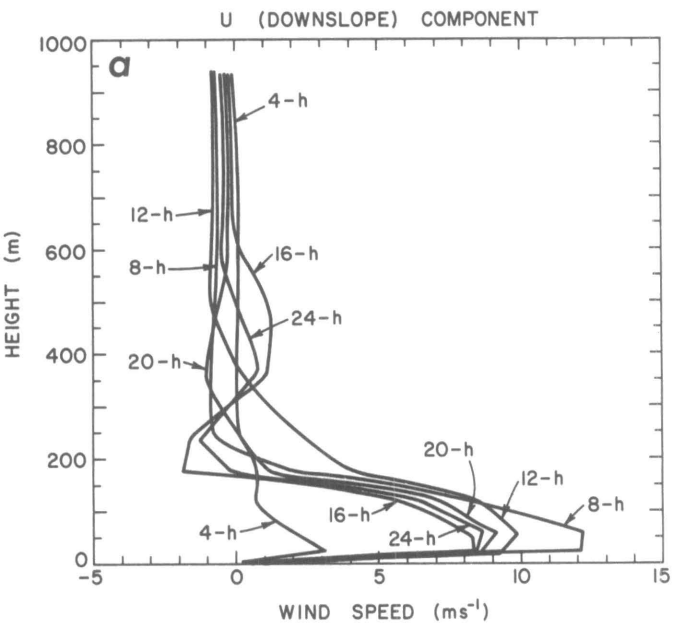

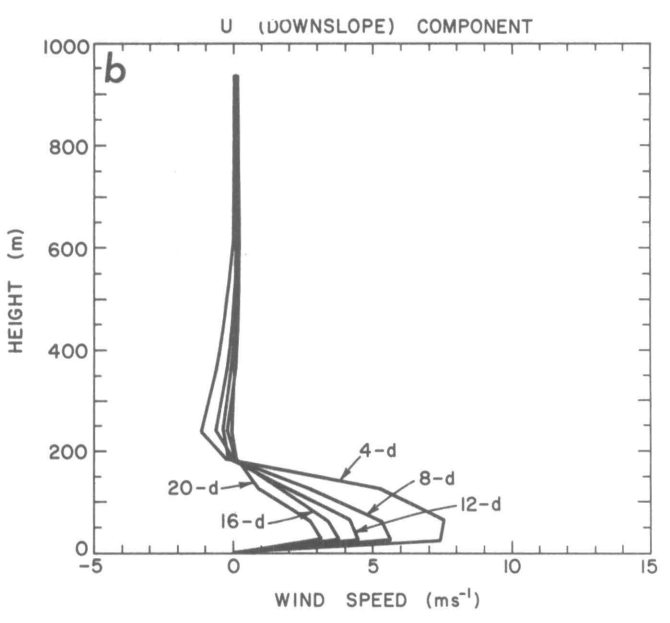

Figure 2. Evolution of the downslope wind components in the lowest 1,000 meters during (*A*) first 24-hours and (*B*) entire 20-day simulation.

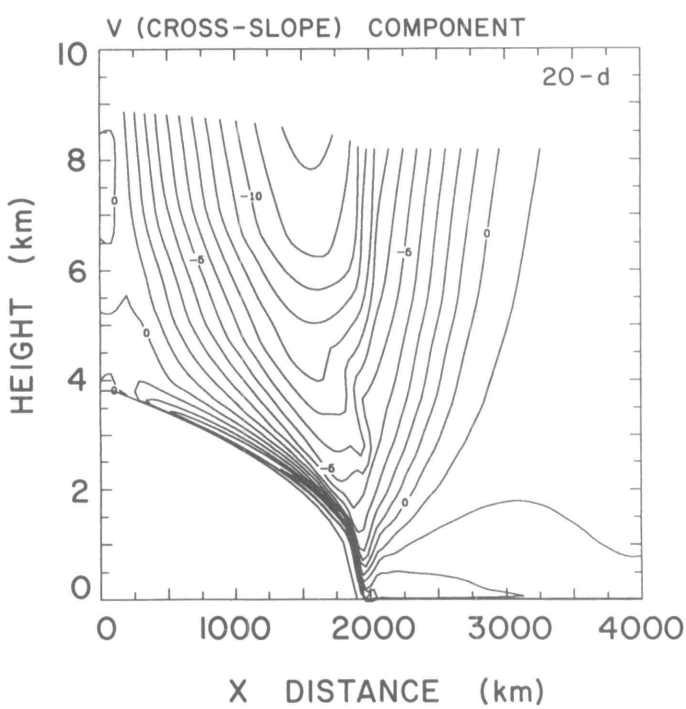

Figure 3. Cross section zonal wind component, 20-day simulation.

References

Anthes, R. A. and T. T. Warner. 1978. The development of hydrodynamical models suitable for air pollution and other mesometeorological studies. *Monthly Weather Review*, 106:1,045-1,078.

Parish, T. R. 1992. On the role of antarctic katabatic winds in forcing large scale tropospheric motions. *Journal of Atmospheric Sciences*, 15:1,374-1,385.

Parish, T. R. and D. H. Bromwich. 1991. Continental-scale simulation of the antarctic katabatic wind regime. *Journal of Climatology*, 4:135-146.

Parish, T. R. and K. T. Waight. 1987. The forcing of antarctic katabatic winds. *Monthly Weather Review*, 115:2,214-2,226.

Schwerdtfeger, W. 1984. Weather and Climate of the Antarctic. Amsterdam: Elsevier, 261 pp.[PB]

Mesoscale cyclogenesis over the southeastern Pacific Ocean

Jorge F. Carrasco* and David H. Bromwich

Byrd Polar Research Center
and
Atmospheric Science Program
The Ohio State University
Columbus, Ohio 43210

Recent observational studies (Carleton and Carpenter 1990; Fitch and Carleton 1992; Carleton and Fitch 1993; Turner and Thomas 1992) have shown that one of the areas of recurrent mesoscale cyclone formation is located over the southeastern Pacific Ocean. Lyons (1983) already had studied the characteristics of intense antarctic depressions in the vicinity of the Drake Passage, finding that they originated over the Bellingshausen Sea and moved toward the southern tip of South America. He concluded that intense baroclinic development, as a result of cold-air outbreaks from the antarctic continent behind cold fronts, was the most likely mechanism to be associated with these depressions. Recently, Turner and Thomas (1992) and Carleton and Fitch (1993) also found mesoscale cyclone formation was linked to cold-air advection into the Bellingshausen Sea area. The first pair of authors examined satellite images from a 6-month period (September 1983 to February 1984) to study mesoscale cyclones in the vicinity of the Antarctic Peninsula. A large number of mesoscale vortices occurred over the western Bellingshausen Sea, with secondary maxima north of the Antarctic Peninsula and off the coast of Marie Byrd Land. Most of the mesocyclones developed within cold-air outbreaks that usually take place behind the synoptic lows that decay over the southeastern Pacific Ocean. Carleton and Fitch (1993) studied the winter seasons of 1988 and 1989. They found that the occurrence of mesoscale cyclones over the Amundsen-Bellingshausen Sea region was associated with a negative departure of the 1000 to 500 hectopascal geopotential thickness (with respect to the 1988-1989 winter mean), which suggests a cold-air outbreak from the interior of West Antarctica onto the southeastern Pacific Ocean.

A survey of mesoscale cyclogenesis over the Amundsen and Bellingshausen seas was carried out using all available satellite images for August 1989 to February 1990 which were collected at Palmer Station (Van Woert et al. 1992). The satellite images were extracted in an infrared format at a spatial resolution of 3.3 kilometers centered over Palmer Station. This provided reasonably high-resolution images covering a large area surrounding the station for identification and tracking of mesoscale vortices. The satellite data were processed on a Sun 4/110 workstation using a TeraScan software package developed by SeaSpace. The capability of zooming and/or enhancing the satellite image displayed on a computer screen facilitate detection of mesoscale vortices. The identification of mesoscale cyclones was based upon the cyclonic appearance of the cloud signature, following the general techniques described in the literature dealing with satellite studies of mesoscale cyclones (e.g., Forbes and Lottes 1985; Businger and Reed 1989; Carleton and Carpenter 1990; Heinemann 1990). All cloud signatures with a cyclonic shape and a diameter of less than 1,000 kilometers were counted as a mesoscale cyclone and plotted on a chart. Also, when possible, they were tracked in order to estimate average trajectories of these mesoscale features.

Column 1 in the table gives the number of days for each month for which satellite data were not available. September, October, and November had large gaps of 21, 18, and 18 missing days, respectively. Column 2 listed the total number to mesoscale

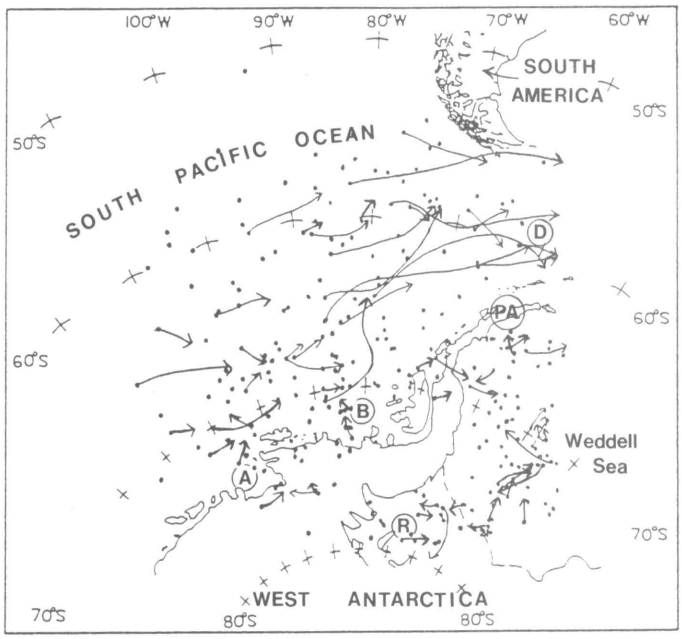

Figure 1. Spatial distributions of the initial location and trajectories of mesoscale cyclones for August 1989 to February 1990. Letters A, B, D, R, and PA respectively denote Amundsen Sea, Bellingshausen Sea, Drake Passage, Ronne Ice Shelf, and Antarctic Peninsula.

*Permanent Affiliation: *Direccion Meteorologica de Chile, Santiago, Chile.*

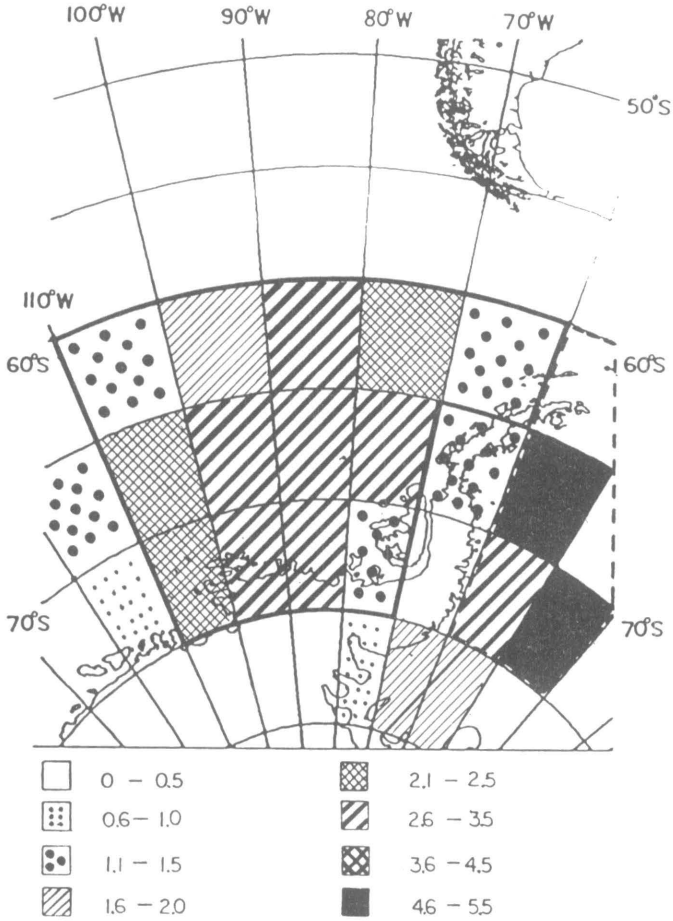

Figure 2. Spatial frequency distribution of initial mesoscale cyclone appearance observed per 5° latitude and 10° longitude per 30 days, during August 1989 to February 1990. *Heavy solid line* defines area 1, and *heavy dashed line* defines area 2.

cyclones observed to the west of the Antarctic Peninsula and poleward of 60° S, and column 3 gives the ratio between the number of mesoscale cyclones and the total days for which satellite images were available (analyzable days, hereafter) in that month. The ratio suggests a peak in the number of mesoscale cyclones (i.e., total cyclones per week of analyzable days) observed in this area. It shows that the maximum in December corresponds to 10.5 mesocyclones observed each week. The minimum was found in August, which showed 3.5 mesoscale cyclones each week.

Figure 1 shows that the initial location and the trajectories of the mesoscale vortices during the study period. Although the results indicate an almost homogeneous distribution of mesoscale cyclones over the southeastern Pacific Ocean, they tend to cluster close to the coast. Figure 1 also shows significant mesoscale activity over the Weddell Sea and Ronne Ice Shelf, as well as a few mesocyclones over the interior of West Antarctica. To study the special frequency distribution of initial mesoscale cyclone appearance, the monthly average frequency distribution was calculated from the number of vortices counted within a box of 5° latitude and 10° longitude for the entire study period, but is expressed in terms of per month analyzable days. Figure 2 shows the spatial frequency for August 1989 to February 1990. The map defines the area considered in this study. To the west of the peninsula, a frequency maximum is located over the

Mesoscale cyclones over the southeastern South Pacific Ocean for August 1989 to February 1990.

Month	Missing days	Number of cyclones	Normalized cyclone total*	Normalized weekly no. cyclones**
August	3	14	0.5	3.5
September	21	8	0.9	6.2
October	18	11	0.8	5.9
November	18	14	1.1	8.2
December	5	39	1.5	10.5
January	2	30	1.0	7.2
February	3	20	0.8	5.6

*Ratio between number of mesoscale cyclones and the total days for which satelite images were available (analyzable days) in that month.
**Number of cyclones per analyzable day times seven.

Bellingshausen Sea (2.6 to 3.5 mesocyclones per 5° latitude x 10° longitude per 30 days) and areas to the north. A secondary maximum (2.1 to 2.5 mesocyclones) can be observed over the Amundsen Sea. The highest frequency is located over the Weddell Sea (4.6 to 5.5 mesoscale vortices). This spatial distribution of the vortices on both sides of the peninsula is opposite to that shown by Turner and Thomas (1992). Their results placed the highest frequency over the Amundsen-Bellingshausen Sea area. Further studies are needed to investigate the causes of this interannual variability.

The satellite-observed trajectories of mesoscale vortices (figure 1) indicate that most of them were quasi-stationary features. Only about 23 percent of the vortices observed to the west of the Antarctic Peninsula (area 1 in figure 2) could be tracked. The vortices tend to acquire a northeastward trajectory from their initial satellite-observed location toward the Drake Passage, suggesting that these perturbations may originate to the south or southwest of their initial detection point. Over the Weddell Sea area (area 2 in figure 2), about 27 percent of the vortices could be tracked. Most of these moved toward the north. Over the Ronne Ice Shelf, no preferred direction was noted.

In summary, the spatial distribution and trajectories of mesoscale cyclones over the southeastern Pacific Ocean confirm the mesoscale cyclogenesis activity over this area and suggest a maximum in December. Individual case studies (not included: Carleton and Fitch 1993; Turner and Thomas 1992; Carrasco 1992) reveal that cold-air outbreaks into the warmer maritime environment of the Pacific Ocean, associated with synoptic-scale cyclones, appear to be the prevailing circulation that sets up conditions for mesoscale cyclogenesis. The near-surface antarctic katabatic wind simulation (Parish and Bromwich 1987) indicates a source of cold katabatic air in the Amundsen Sea. The secondary frequency maximum found by this investigation (and also by Turner and Thomas 1992) indicates that these features may be associated with katabatic wind outbreaks coming down from the interior of West Antarctica, as suggested by Parrish and Bromwich (1986). However, from the present study, no clear linkage can be inferred between katabatic airflow and mesoscale cyclone activity over the southeastern Pacific Ocean, as is clearly found over the Ross Sea-Ross Ice Shelf area (Bromwich 1989; Bromwich 1991; Carrasco 1992; Carrasco and Bromwich 1993).

This research was supported by National Science Foundation grant DPP 88-16792. The satellite imagery was recorded by U.S. Antarctic Program personnel at Palmer Station and obtained from Robert Whritner of the Antarctic Research Center at Scripps

Institution of Oceanography, University of California, La Jolla, California, National Science Foundation grant DPP 88-15818.

References

Bromwich, D. H. 1989. Subsynoptic-scale cyclone developments in the Ross Sea sector of the Antarctic. In P.F. Twitchell, E.A. Rasmussen, and K.L. Davidson (Eds.), *Polar and Arctic Lows*. Hampton, Virginia: Deepak Publishing, 331-354.

Bromwich, D. H. 1991. Mesoscale cyclogenesis over the southwestern Ross Sea linked to strong katabatic winds. *Monthly Weather Review*, 119:1,736-1,752.

Businger S. and R. J. Reed. 1989. Polar Lows. In P.F. Twitchell, E.A. Rasmussen, and K.L. Davidson (Eds.), *Polar and Arctic Lows*, Hampton, Virginia: A. Deepak Publishing, 3-45.

Carleton, A. M. and D. A. Carpenter. 1990. Satellite climatology of "polar lows" and broadscale climatic associations for the Southern Hemisphere. *International Journal of Climatology*, 10:219-246.

Carleton, A. M. and M. Fitch. 1993. Synoptic aspects of antarctic mesocyclones. *Journal of Geophysical Research*, in press.

Carrasco, J. F. 1992. A mesoscale cyclogenesis study adjacent to the Pacific coast of Antarctica. M.S. Thesis, Atmospheric Sciences Program, The Ohio State University.

Carrasco, J. F. and D. H. Bromwich. 1993. Mesoscale cyclogenesis dynamics over the southwestern Ross Sea, Antarctica. *Journal of Geophysical Research*, in press.

Forbes, G. S. and W. D. Lottes. 1985. Classification of mesoscale vortices in polar airstreams and the influence of the large scale environment on their evolution. *Tellus*, 37(A):132-155.

Fitch, M. and A. M. Carleton. 1992. Antarctic mesoscale regimes from satellite and conventional data. *Tellus*, 44(A):180-196.

Heinemann, G. 1990. Mesoscale vortices in the Weddell Sea region (Antarctica). *Monthly Weather Review*, 118:779-793.

Lyons, S. W. 1983. Characteristic of intense antarctic depressions. In *First International Conference on Southern Hemisphere Meteorology*. Boston, Massachusetts: American Meteorological Society, 238-240.

Parish, T. R. and D. H. Bromwich. 1987. The surface windfield over the antarctic ice sheets. *Nature*, 328:51-54.

Turner, J. and J. P. Thomas. 1992. Southern ocean weather systems in satellite imagery and operational numerical analyses. In *Proceedings of the Sixth Conference on Satellite Meteorology and Oceanography*. 6-10 January 1992, Atlanta, Georgia. Boston, Massachusetts: American Meteorological Society, 149-152.

Van Woert, M. L., R. H. Whritner, D. E. Waliser, D. H. Bromwich, and J. C. Comiso. 1992. ARC: A source of the multisensor satellite data for polar science. *Eos Transactions*, American Geophysical Union, 73(6):6,575-6,576.

Katabatic airflows over Siple Coast, West Antarctica

YANG DU AND DAVID H. BROMWICH

Byrd Polar Research Center and
Atmospheric Sciences Program
The Ohio State University
Columbus, Ohio 43210

Antarctic wind records show strong katabatic outflows at many points along the steep coast of the continent, such as at Cape Denison and Terra Nova Bay. The antarctic wind regime is shaped largely by the ice topography (Schwerdtfeger 1970). Ball (1960) pointed out that the magnitude of the terrain-induced pressure gradient force is directly proportional to both the steepness of the terrain and the strength of the temperature inversion in the lower atmosphere. Parish (1981) proposed that a large-scale convergence of cold air from the continental interior results in such strong and persistent coastal katabatic winds. Parish and Bromwich (1987) simulated the surface winds over Antarctica, and showed that the drainage pattern is highly irregular with areas of pronounced confluence and difluence near the coast. The Siple Coast area of West Antarctica, unlike most parts of Antarctica, has terrain slopes that are steeper in the interior than adjacent to the coast. The Siple Coast area was found to be one of the most significant confluence zones about the continental periphery (see figure 1). This paper analyzes the windfield over the Siple Coast area simulated by the three-dimensional primitive equation model

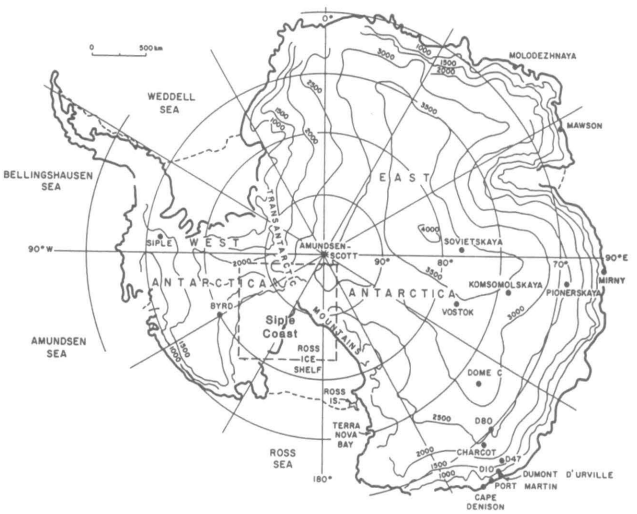

Figure 1. The antarctic continent with selected geographic features and scientific stations. Height contours in meters (after Parish and Bromwich, 1989). The *square* denotes the region shown in figure 2.

described in Parish and Waight (1987) and compares it with field observational data summarized by Bromwich (1986).

The model equations used are written in terrain-following σ (sigma) coordinates (10 levels) with highest vertical resolution in the lower portion of the atmosphere. The model domain consists of 160x160 grid points at a spatial resolution of 20 kilometers. The ice heights are taken from an accurate terrain map (Drewry 1983). Longwave radiation is explicitly included, following Cerni and

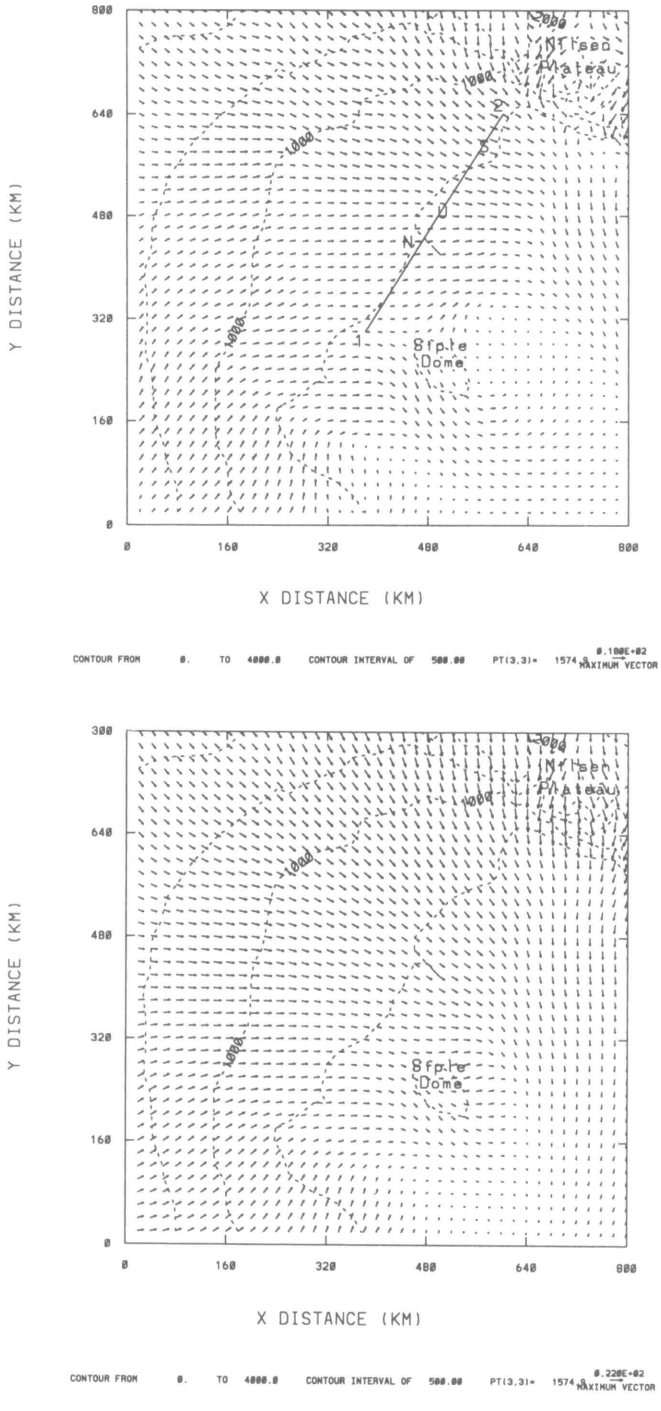

Figure 2. Wind vectors over the Siple Coast area and its vicinity after 24-hour simulation. *(Top)* with initial state of rest. N stands for North Camp, U for Upstream B, and S for South Camp. *Line* 1-2 is the cross section shown in figure 3. *(Bottom)* with initially prescribed pressure field.

Parish (1984). No allowance is made for effects of shortwave radiation and clouds. Thus, the results represent the antarctic winter wind regime for clear-sky conditons. Two 24-hour runs were performed. One started from a state of rest throughout the model domain, and the other started from a prescribed synoptic-scale pressure field associated with katabatic surges across the Ross Ice Shelf (Bromwich et al. 1992). Initially, the wind field is in geostrophic balance with the pressure field.

Figure 2 presents the simulated results of the surface-wind vectors over the Siple Coast and its vicinity, from the two model runs after 24-hour integration. Effects of synoptic disturbances on the windfield over Siple Coast are evident. The run with the specific initial synoptic pressure field (figure 2b) results in stronger winds and more downslope flows, though the confluence zone near Siple Coast is noticeable in both runs. The average simulated wind speed in the confluence zone increases from 8.6 to near 14 meters per second, and the wind direction becomes 20° to 30° more downslope. The stronger downslope winds suggest that the cold air is more efficiently transported from the interior to the coastal margin and potentially enhances the surface flow over the Ross Ice Shelf, where the slope is near zero. Bromwich et al. (1992) indicated that cyclones over southern Amundsen Sea are often associated with katabatic winds that cross Siple Coast and propagate far across the Ross Ice Shelf. The run with the initial state of rest (figure 2a) produces nearly stagnant flows downwind of isolated peaks near the coast, such as Siple Dome and the Nilsen Plateau area. The upstream flows are blocked by these obstacles and are forced to blow around them. With the inclusion of the synoptic pressure field, the airflows are able to blow over these obstructions (figure 2b). The flow becomes more uniform. The simulated surface winds show significant downslope outflows, especially over the Nilsen Plateau area. Studies (Bromwich et al. 1992) show that the Nilsen Plateau area is one location where prominent dark signatures are often found on wintertime thermal infrared satellite images during katabatic survey events.

Bromwich (1986) summarized simultaneous wind observations taken at three temporary camps around the Siple Coast area during the austral summers of 1984-1986. He noted that South Camp is most likely located in the confluence zone whose northern edge is close to, but south of, Upstream B. The simulated windfield supports this notion. The confluence zone is concentrated on the southern part of the Siple Coast. This is illustrated in figure 3, a vertical wind-speed cross section oriented along the three camps. From North Camp to Upstream B to South Camp, the wind speed increases in both runs. A significant increase appears between Upstream B and South Camp. In the run without synoptic pressure gradients, the maximum wind axis of about 15 meters per second is located south of South Camp, where the terrain slope is steeper. Its northern boundary is between Upstream B and South Camp. This is similar to the analysis by Bromwich and Du (1991). In the run with the specified pressure field, the zone of strong near-surface winds is wider and deeper (figure 3b). At levels higher than about 800 meters, the winds mostly are determined by the imposed pressure field. A shallower and weaker near-surface wind zone extends north of Upstream B. This strongly supports the notion (Bromwich 1986) that Upstream B sometimes is embedded within the confluence zone. The location of the strongest winds approximates that of the first run, but the speeds are nearly twice as strong. The height of the maximum speed increases from about 100 meters to more than 200 meters. This emphasizes the important role of vertical mixing in determining the wind regime in the surface boundary layer. The strong winds over the Siple Coast area due to the influence of synoptic cyclones lead to the enhancement of the vertical exchanges of momentum and sensible heat. As a result, the average simulated surface temperature increases by about 3 °C in response to the stronger vertical mixing of the near-surface air. The location of the strongest winds is barely affected by the synoptic-scale disturbances centered in the southern Amundsen Sea. Presumably, the shape of the ice terrain is the

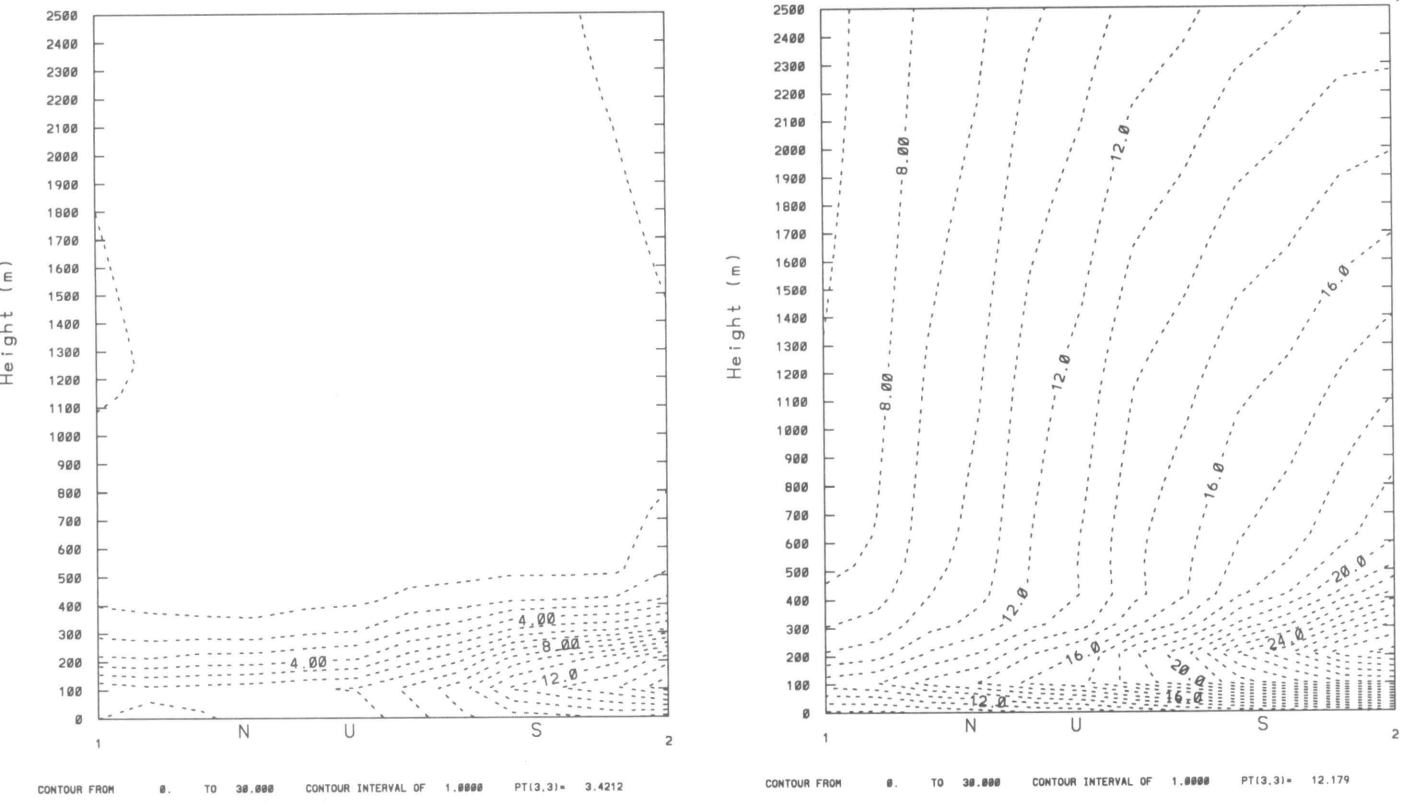

Figure 3. Vertical wind-speed cross sections along the three camps. *(Left)* For initial state of rest and *(right)* for initially prescribed pressure field.

main factor locating the strongest part of the confluence zone. This is important in understanding the highly irregular wind pattern over the antarctic continent. Qualitatively, the location of the simulated confluence zone is very consistent with the observed wind data.

This research was supported by National Science Foundation grant DPP 89-16921 to D. H. Bromwich. T. R. Parish provided valuable assistance with the modeling. The simulations were performed on the CRAY Y-MP of the Ohio Supercomputer Center, which is supported by the State of Ohio.

References

Ball, F. K. 1960. Winds on the ice slopes of Antarctica. *Antarctic Meteorology, Proceedings of the Symposium,* Melbourne, 1959. New York: Pergamon, 9-16.

Bromwich, D. H. 1986. Surface winds in West Antarctica. *Antarctic Journal of the U.S.,* 21(5):235-237.

Bromwich, D. H., J. F. Carrasco, and C. R. Stearns. 1992. Satellite observations of katabatic wind propagation for great distances across the Ross Ice Shelf. *Monthly Weather Review,* 120:1,940-1,949.

Bromwich, D. H. and Y. Du. 1991. Numerical simulation of the katabatic winds over West Antarctica. *Antarctic Journal of the U.S.,* 26(5):261-264.

Cerni, T. A. and T. R. Parish. 1984. A radiative model of the stable nocturnal boundary layer with application to the polar night. *Journal of Climate and Applied Meteorology,* 23:1,563-1,672.

Drewry, D. J. 1983. The surface of the antarctic ice sheet. In D. J. Drewry (Ed.), *Antarctica: Glaciological and Geophysical Folio, Sheet 2.* Cambridge, England: Scott Polar Research Institute.

Parish, T. R. 1981. The katabatic winds of Cape Denison and Port Martin. *Polar Record,* 20:525-532.

Parish, T. R. and D. H. Bromwich. 1987. The surface windfield over the antarctic ice sheets. *Nature,* 328:51-54.

Parish, T. R. and K. T. Waight. 1987. The forcing of antarctic katabatic winds. *Monthly Weather Review,* 115:2,214-2,226.

Schwerdtfeger, W. 1970. The climate of the Antarctic, Vol. 14. In S. Orvig, (Ed.) *World Survey of Climatology,* H. E. Landsberg, E., Elsevier, 253-355.

Photopolarimetry of halos and ice-crystal sizing

G. P. Können

Royal Netherlands Meteorological Institute
De Bilt, The Netherlands

During nearby displays I recorded the linear polarization and intensity distributions of halos and simultaneously made replicas of the halo-generating ice crystals. My purpose was to explore halopolarimetry as a tool of remote sensing for crystals and to relate the diffraction broadening of the halo polarization and intensity directly with the sizes of the collected crystals.

I obtained polarization and intensity distributions of halos by means of the portable, four-lens monochromatic polarimetric camera (Können and Tinbergen 1991) shown in figure 1. This

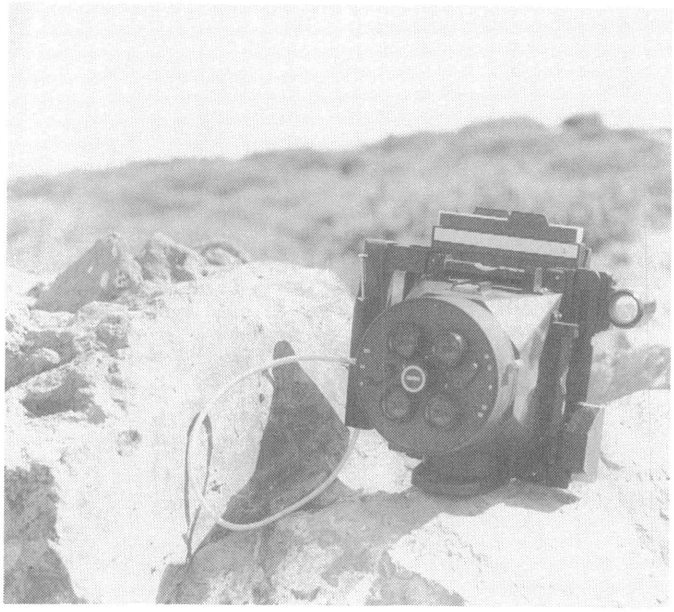

Figure 1. I used this four-lens polarimetric camera to measure polarization and intensity distribution of halos.

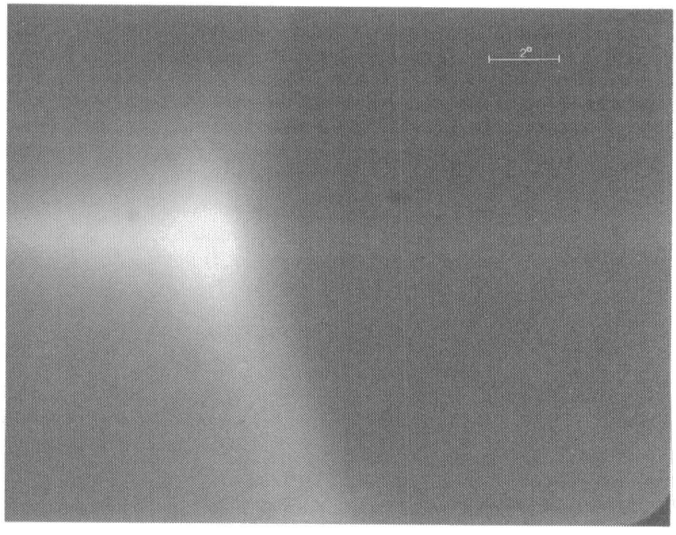

Figure 2. Diffraction-broadened parhelion, recorded on 1 January 1990 at 1403 Universal Time at Amundsen-Scott South Pole Station.

camera is a rebuilt commercial camera for passport photographs of 125-millimeter focal length. It takes four pictures simultaneously on one single Kodak Tri-X sheet film negative. Behind each lens is a polarizer, cut from the same sheet and with their orientations increasing in steps of 45°. The light then passes a filter with maximum transmission at 590-nanometer wavelength and 33-nanometer full width at half maximum. The negatives were digitized with a densitometer at a resolution of 50 x 50 micrometers. After conversion from density to intensity, the intensities in the pixels of the four images corresponding to the same area of sky were compared. The sum of the intensity of the pixels in two orthogonally polarized images provides the intensity I; its difference in the two pairs of orthogonally polarized images provides the second Stokes parameter Q and the third Stokes parameter U, respectively. The camera has a spirit level and a sun finder; if the sun is centered in that finder, the scattering angle in the images is known to within an accuracy of about 0.2°.

Figure 2 shows one of the four polarimetric images of a bright parhelion, taken on 1 January 1990 at 1403 Universal Time at Amundsen-Scott South Pole Station. The solar elevation was 23°. Figure 3 shows the intensity I and second Stokes parameter Q as a function of scattering angle, obtained from two of the four images on the digitized negative. Figure 3 passes straight through the intensity maximum of the parhelion. The plane of reference of the Stokes parameters is the horizontal, which closely coincides with the scattering plane. In the third Stokes parameter (not shown), the halo is not apparent so that the positive signal in Q indicates that the halo polarization is essentially horizontal. The degree of polarization equals Q/I. Note that the peak in Q occurs at a smaller scattering angle than does the halo intensity peak.

The parhelion polarization arises as follows (Können and Tinbergen 1991): After the entrance in the birefringent ice crystal, the light splits up into two polarized beams, each of them producing its own parhelion. Since the index of refraction is slightly different, the scattering angle domains of the two polarized parhelia are slightly shifted. In the region where the parhelion intensity changes rapidly with scattering angle, one of the polarized components predominates. The steepest part of the intensity distribution is near the geometrical parhelion scattering angle; hence, this is the region where strongest polarization is observed (see figure 3). Visually, the parhelion polarization manifested itself clearly as a 0.1° shift in halo position when viewed through a rotating polarizer.

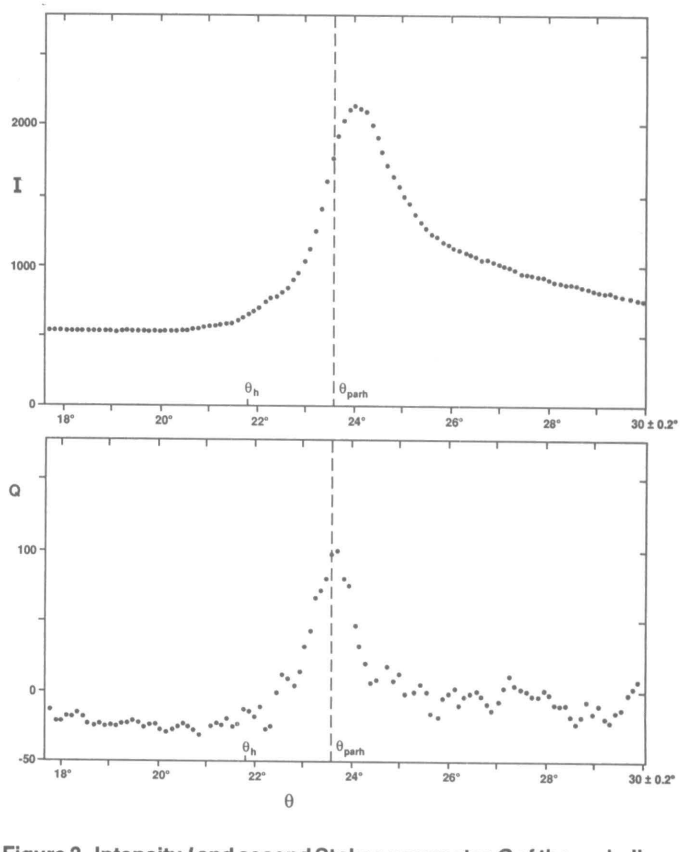

Figure 3. Intensity *I* and second Stokes parameter *Q* of the parhelion of figure 2 as a function of scattering angle θ. The 22° halo angle (random crystal orientation) and the parhelion scattering angle (preferential orientation) are denoted by θ_h and θ_{parh}, respectively. Q>0 indicates horizontal polarization; Q/I is degree of polarization.

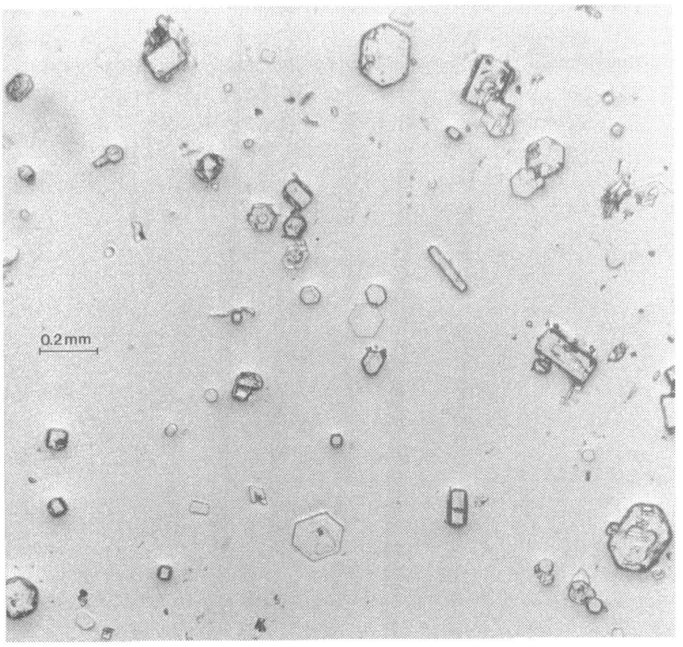

Figure 4. Some crystals that made the halo of figure 2.

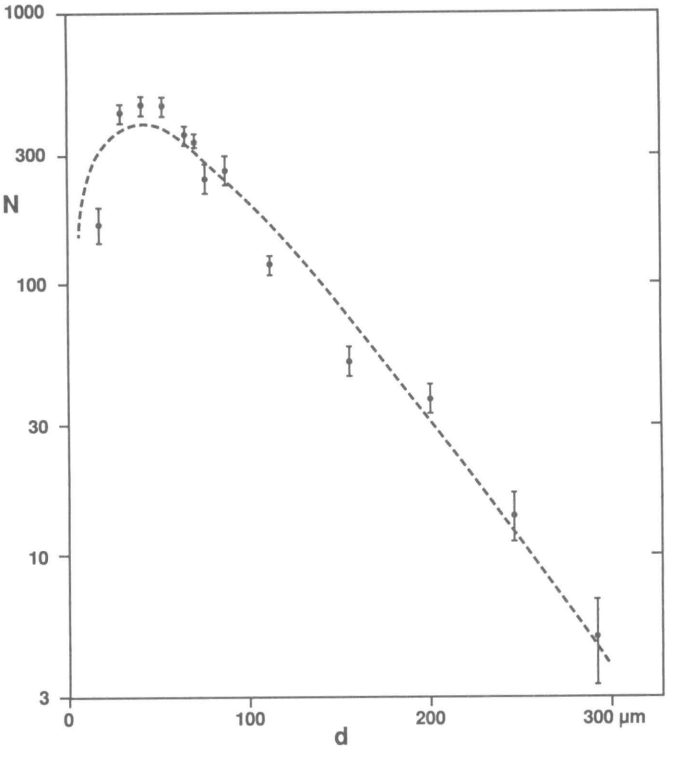

Figure 5. Size distribution of the ice crystals collected during the halo. The size *d* is the crystal hexagon diameter; *N* is the number of crystals per unit size interval. The *dashed line* is a gamma distribution with power one and the observed mean size of 80 micrometers as parameters.

The amount of polarization depends on the slope of the intensity distribution, which is in its turn dependent on the diffraction broadening of the parhelion, caused by the small slit-width of the crystals. Basically, the Q-peak represents a diffraction-broadened delta function. In figure 3, the angular distance $\theta_{1/2}$ between the maximum Q and its half value point is 0.49°.

During the halo display, I made replicas of the falling ice crystals in acrylic spray (see also Tape 1983). Figure 4 shows a picture of some of the replicated crystals in a crystal sample taken 5 minutes after the polarimetric parhelion picture. Since the parhelion remained apparent in front of a nearby black object, the sampled crystals can be considered as halo makers. Mostly they are thin plates lying flat on the spray-covered glass. Figure 5 shows the hexagon size distribution of the crystals, i.e., the number of crystals per unit size interval as a function of hexagon diameter. The observed size distribution resembles closely a gamma distribution with power one and mean size 80 micrometers. The mean thickness of the plates was 30 micrometers. The relation between aspect ratio (crystal length divided by hexagon diameter) and hexagon size could not be determined quantitatively, although it apparently decreased with size (see also Pruppacher and Klett 1978). Assuming the aspect ratio to be constant, a straightforward calculation of $\theta_{1/2}$ of the parhelion Q-peak from the integral of the standard diffraction function for a slit over the observed particle-size gamma distribution predicts $\theta_{1/2}$=0.21°; assuming the thickness to be constant, we get $\theta_{1/2}$=0.26°. Hence, both calculations lead to a $\theta_{1/2}$ of a factor two too small compared with the observed value of 0.49°.

The explanation for this discrepancy can be internal reflection in the crystal, causing a loss of parhelion-generating light in favor of the subparhelion. This loss of parhelion-contributing light becomes increasingly strong for big hexagons when the aspect ratio decreases with size. Hence, there is a predominant contribution of small crystals to the light of the parhelion, and therefore its diffraction broadening is larger than expected from the hexagon size distribution alone. Apparently it leads to an underestimation of a factor two when sizes of parhelion-making crystals are determined optically from the polarization or intensity distribution of this halo. This selection effect is characteristic of the parhelion; a circular 22° halo would not suffer from this.

It is not obvious that high-level crystals have the same size distribution as do low-level ones; the observed gamma distribution may represent just an early stage to be evolved to another distribution with larger sizes. Diffraction-broadened parhelia are indeed rare in the high-level displays of the mid-latitudes; mostly their appearance resembles more that of figure 16 in Können and Tinbergen 1991, with a sharp inner edge. Since, in general, the size distribution of halo-making crystals cannot be determined directly, it is important to know what the optically determined size means. A good parameter for this is the size that contributes most to the intensity. However, to get this figure from the present measurements, we have to multiply the optically determined size obtained with the earlier method (Können and Tinbergen 1991) by a factor of about 0.8. An advantage of this parameter is that it is not very sensitive to the size distribution, at least for gamma distributions with powers up to 5.

The present measurements support our view (Können and Tinbergen 1991) that halo polarimetry is a sensitive tool for detecting birefringent crystals in the terrestrial atmosphere or in the atmospheres of other planets. On the other hand, it turns out that for certain halos, including the parhelion, the optically determined crystal size bears no obvious relationship to the real crystal dimensions in the halo-generating cloud.

At South Pole and Vostok, the polarization of several other types of halo have been recorded. Some findings are as follows:

- A circumzenithal arc, observed simultaneously with the parhe-

lion depicted in figure 2, had an overall degree of polarization of about 20 percent, but near its inner edge the polarization was considerably less because of the birefringence effect. No change of sign of the polarization was observed in that region.

• The 120° parhelion is in horizontally polarized light about 0.2° higher over the horizon and 0.05° closer to the sun than in vertically polarized light (solar elevation 23°). These values are in agreement with those calculated from the internal reflection laws for birefringent substances for this solar elevation. The vertical shift of that halo in polarized light could be seen visually; the horizontal one not.

The fieldwork has been performed in cooperation with W. Tape. J. H. M. van Lieverloo, KIWA, assisted with the size determinations, and R. S. Le Poole provided assistance in using the Leiden University Astroscan densitometer. J. Tinbergen advised on the polarimetry; the camera was rebuilt by H. Deen, Kapteyn Observatory, Roden. This research was supported by National Science Foundation grant DPP 88-16515 and partly by the Netherlands Organization for Scientific Research.

References

Können, G. P. and J. Tinbergen. 1991. Polarimetry of a 22° halo. *Applied Optics*, 30:3,382-3,400.

Tape, W. 1983. Some ice crystals that made halos. *Journal of Optical Society of America*, 73:1,641-1,645.

Pruppacher, H. R. and J. D. Klett. 1978. *Microphysics of clouds and precipitation*. Dordrecht, Netherlands: Nijhoff.

Spectral reflectance of antarctic snow: "Ground truth" and spacecraft measurements

R. W. Carlson, T. Arakelian, and W. D. Smythe

Jet Propulsion Laboratory
California Institute of Technology
Pasadena, California 91109

The cold climate of Antarctica is a result of the high reflectance of snow and of the corresponding small amount of energy that is absorbed from the incident sunlight. The energy-absorption rate depends on such variables as grain size, impurities, and incidence angle, as well as on the wavelength of the incident light. In the visible region, ice is highly nonabsorbing, but becomes a strong absorber in the infrared because of molecular vibrational transitions. To understand energy-absorption rates, it is important to investigate the optical properties of antarctic snow over an extended wavelength range—from the ultraviolet to the infrared. Furthermore, for climatological purposes, it is important to understand these properties throughout the antarctic continent. This can only be accomplished by a program of aircraft or satellite remote sensing measurements in conjunction with locally established "ground truth."

In this article, we briefly describe field measurements of the spectral reflectance of snow at two sites, and compare the optically derived snow grain sizes with photographic measurements of the surface grains. These "ground-truth" data are then used to corroborate spacecraft remote-sensing measurements, thereby extending our localized measurements to continental scales.

The field measurements were obtained in December 1989 at the Amundsen-Scott South Pole Station and in December 1991 at the Vostok Station (78° S 107° E). The field instrumentation consists of a portable diffraction-grating spectrometer mounted on a 1-meter-long goniometric arm. This arm swings in a vertical plane, allowing spectral measurements to be obtained over nearly a 180-degree range of emission angles . We obtained complete spectra for nadir viewing with a variety of solar zenith angles. The goniometric measurements were obtained for a variety of individual wavelengths, both inside and outside of water absorption bands. Here we discuss only a few of the spectra and none of the goniometric measurements.

The experimental procedure was used to measure the spectral radiance for a chosen area of snow, which receives sunlight as well as diffuse radiation from the sky. We then block the sunlight and measure the radiance for only incident skylight. The procedure is repeated using calibrated diffuse reflectance standards such as Halon and sulfur surfaces. With this set of measurements, we obtain the bidirectional reflectance of the snow surface and the diffuse-directional reflectance appropriate to skylight. We also find the relative contribution of diffuse skylight to the total radiance, which is appreciable in the ultraviolet and blue regions of the spectrum.

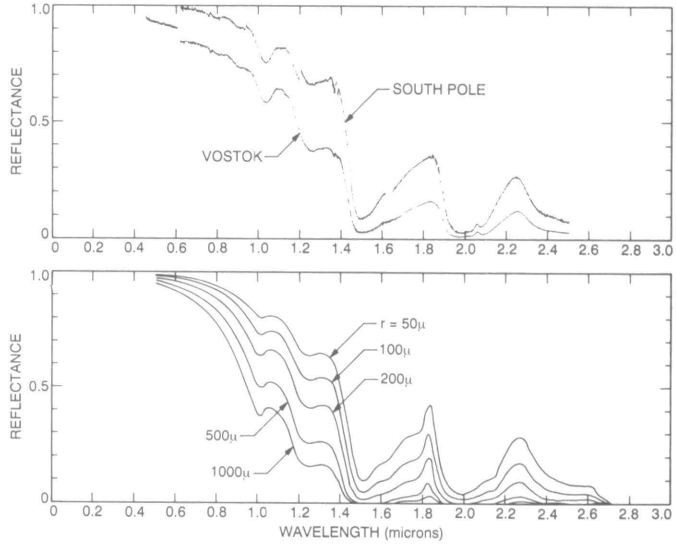

Figure 1. Spectral reflectance of snow. The upper panel is directional-directional reflectance spectra measured at the South Pole and Vostok stations. For both sites, the incidence angle was about 68 degrees and the emission angle was zero, relative to the vertical. The lower panel shows theoretical directional (60 degree) - hemispherical reflectances, computed for varying grain radii by Wiscombe and Warren (1981). A comparison indicates that snow particles at South Pole and Vostok are about 50 and 200 microns in radius, respectively.

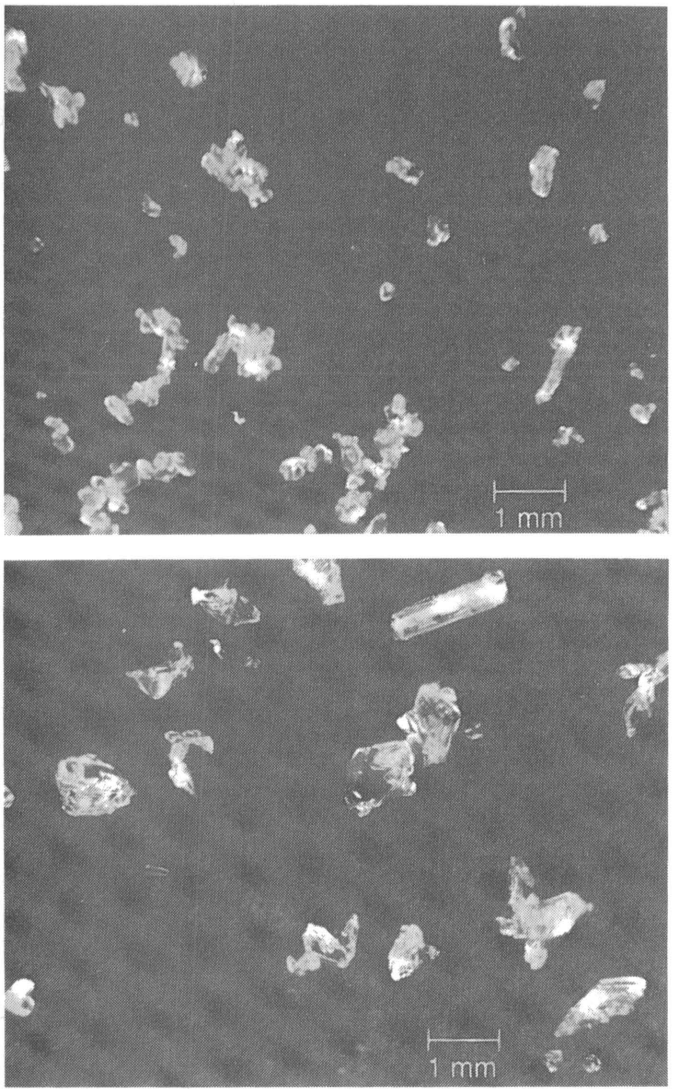

Figure 2. Photographs of surface snow grains. The upper panel shows a representative sample found at the South Pole December 1989, while the lower panel is for Vostok, December 1991. The Vostok grains are several times larger than those of the South Pole, in agreement with their spectra.

Spectra obtained at South Pole and Vostok are shown in figure 1. The well-known water-ice absorption features occurring at 0.81, 0.90, 1.04, 1.25, 1.50, 1.65, and 2.0 microns are quite evident. All of these absorption features are stronger in the Vostok spectrum than for South Pole. This can be explained as longer path lengths for light passing through the absorbing ice grains, i.e., the snow particles at Vostok are larger than those at South Pole.

We can quantify the differences in grain size by comparing the observed spectra with the theoretical reflectance spectra computed by Wiscombe and Warren (1981), which are shown in the bottom panel of figure 1. Comparing the observed and theoretical spectra, we estimate that the mean grain radius at South Pole is roughly 50 microns, while Vostok snow grains possess a mean radius of about 200 microns.

These spectroscopic radii are in good agreement with direct measurements. Representative photographs of surface snow grain samples are shown in figure 2. At the South Pole, a mean photographically derived radius of 75 microns is found and is somewhat larger than the above spectroscopic value of 50 microns. At Vostok, a 200-micron radius was found for both the photographic and spectral measurements.

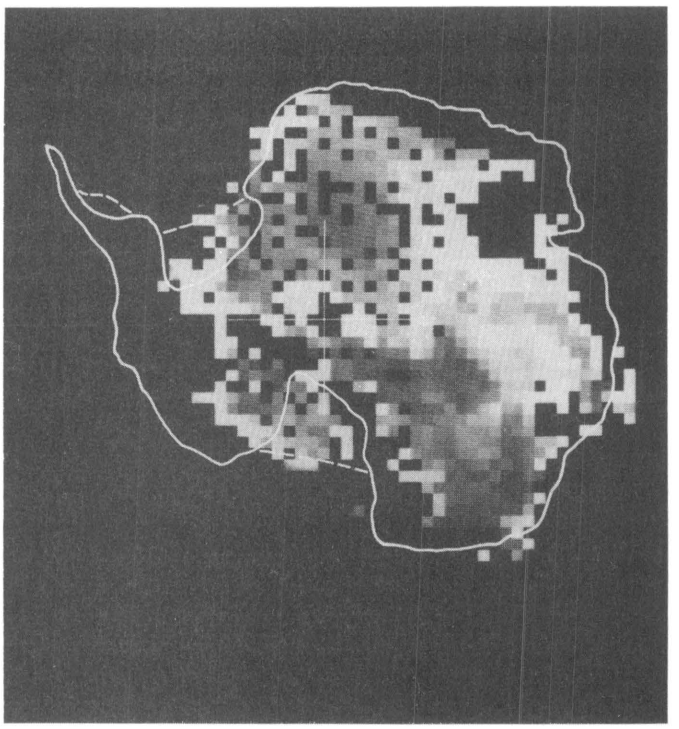

Figure 3. Snow grain-size distribution over Antarctica. The map was derived from Galileo spacecraft flyby data, using the ratio of intensities at 1.5 and 1.7 microns. Bright pixels correspond to approximately 50 micron radius particles, while dark gray pixels represent grains of about 200 micron radius.

Encouraged by the good agreement between the spectrally derived radii and the directly measured values, we examined spectra taken by the Near-Infrared Mapping Spectrometer (NIMS) experiment (Carlson et al. 1992). These data were obtained from the Galileo spacecraft during the 8 December 1990 flyby of the earth. Spatially resolved spectra were obtained in the 0.7 to 5.2 micron region and arise from reflected sunlight and thermal emission.

In this initial attempt to map the grain-size distribution across Antarctica, we focus on the region of characteristic water ice absorption features, in particular, the region extending from 1.5 microns to 2.5 microns (see figure 1). Both theoretical and observed spectra show that the ratios of reflectivity at peaks and valleys varies with grain size. For the map shown here, we use the ratio of signals at 1.5 and 1.7 microns. At these wavelengths, atmospheric gases such as H_20 vapor, are fairly transparent, particularly for the dry atmosphere over the polar plateau. It is also possible, in this wavelength range, to distinguish between thick clouds and snow, due to the high reflectivity of the cloud particles compared with snow. The presence of thin clouds, however, influences our results, so cloudy regions occuring near the coast and ice shelves must be regarded with special caution. Using the ratio of intensities provides a measure that is independent of sastrugi and other geometric effects, at least to a first approximation.

The results are shown in figure 3. Bright pixels represent high values of the ratios of 1.5 and 1.7 micron intensities, which correspond to small particles. It is gratifying that this map, albeit preliminary, is consistent with our South Pole and Vostok field data. Near the South Pole, the NIMS data indicate small particles of order 50 microns in radius, with grains at Vostok three to four times larger. This map shows similarity with a microwave gradi-

ent map derived by Fily and Benoist (1991), which is related to near-surface grain size (Surdyk and Fily 1991).

The mean grain size appears to vary across the continent, but the observed distribution shows no immediately obvious correlation with topographical or meteorological parameters. It is clear that there are large variations in grain sizes. Because the rate of solar-energy absorption depends upon grain size, this spatial variability must be considered in climatological estimates of the net albedo of Antarctica.

Continuing analyses of the field measurements will lead to refined algorithms with which to analyze the remote-sensing data. Additional spacecraft data will be obtained during the second, and last, Galileo earth flyby, occurring in December 1992.

This work was supported by National Science Foundation grant DPP 89-22832, and by the National Aeronautics and Space Administration's Galileo Project.

References

Carlson, R. W., P. R. Weissman, W. D. Smythe, J. C. Mahoney, and the NIMS Science and Engineering Teams. 1992. Near infrared mapping spectrometer on Galileo. *Space Science Review*, 60:457-502.

Fily, M. and J. P. Benoist. 1991. Large-scale study of the microwave signature of the antarctic ice sheet. *Proceedings of the 5th International Colloquim-Physical Measurements and Signatures in Remote Sensing*, Courchevel, France, ESA SP-319:347-350.

Surdyk, S. and M. Fily. 1991. Comparison between the observed microwave spectral signatures over the antarctic ice sheet and a snow emissivity model. *Proceedings of the 5th International Colloquim-Physical Measurements and Signatures in Remote Sensing*, Courchevel, France, ESA SP-319:351-354.

Wiscombe, W. J. and S. G. Warren. 1981. A model for the spectral albedo of snow. I: Pure snow. *Journal of Atomospheric Sciences*, 37:2,712-2,733.

Astronomy, astrophysics, and upper-atmosphere research

Identification of the boundary layer as the entry point for high-latitude dayside Pc3-4 magnetic pulsations

M.J. Engebretson and J.R. Beck

Department of Physics, Augsburg College
Minneapolis, Minnesota 55454

R.L. Rairden and S.B. Mende

Palo Alto Research Laboratory
Palo Alto, California 94304

R.L. Arnoldy

Institute for the Study of the Earth, Oceans, and Space
University of New Hampshire
Durham, New Hampshire 03824

L.J. Cahill, Jr.

School of Physics and Astronomy
University of Minnesota
Minneapolis, Minnesota 55455

T.J. Rosenberg

Institute for Physical Science and Technology
University of Maryland
College Park, Maryland 20742

A continuing question in ground-based studies of ionospheric and space physics concerns the source of the 15- to 50-millihertz frequency oscillations in the earth's magnetic field commonly observed during dayside local times, especially at high latitudes. These waves, known as Pc3-4 pulsations, are often assumed to have their ultimate source at or upstream of the earth's bow shock, where the solar wind first meets the boundary of the earth's magnetic field cavity, or magnetosphere. Despite two decades of study, it is not clear how these waves, which are strongest at high latitudes, reach the ground.

Recent studies have shown that Pc3-4 magnetic pulsations observed at the Amundsen-Scott South Pole Station, Antarctica (about 74° invariant latitude) within several hours of local magnetic noon are often accompanied by roughly simultaneous pulsations in 427.8 nanometer wavelength auroral light, as detected by a zenith-viewing photometer (Engebretson et al. 1990, 1991). These observations suggested that a modulation of electron precipitation at Pc3-4 frequencies, the cause of the pulsations in auroral light, might be involved in the production of at least some of the magnetic pulsation activity seen on the ground.

As a follow-up to these observations, we have undertaken additional studies of pulsation data from magnetometers and photometers at the South Pole and have also compared these with data from an all-sky auroral imaging camera at the South Pole in an attempt to determine what part of the auroral region might be responsible for these optical pulsations. Magnetic field

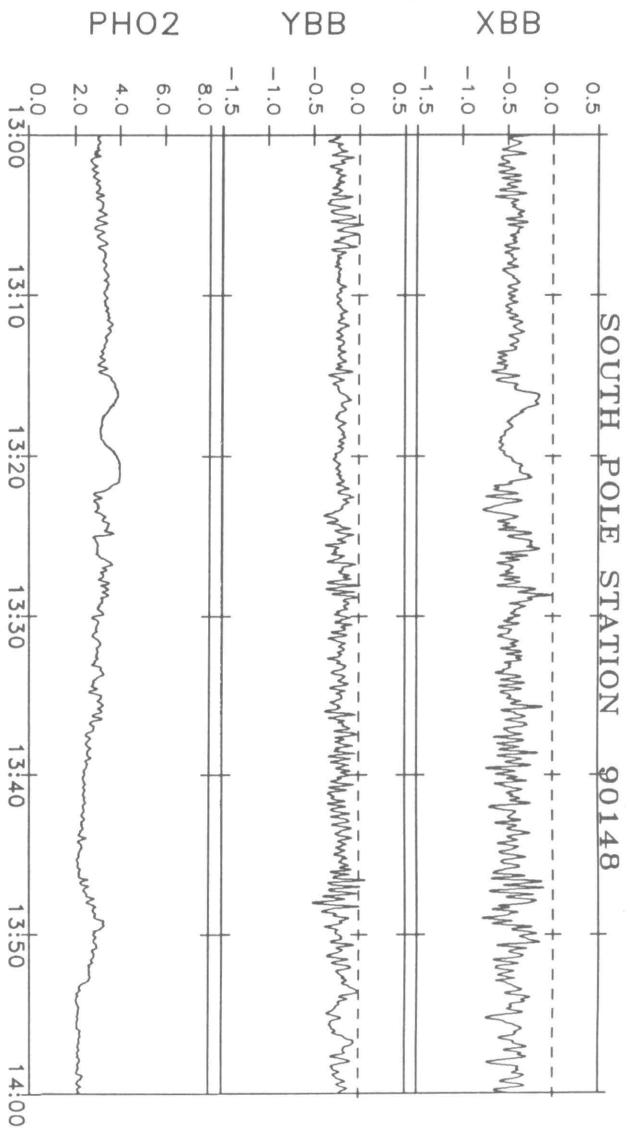

Figure 1. Time series plot of data from the Amundsen-Scott South Pole Station, Antarctica, 1300 to 1400 UT 28 May1990. From top to bottom, the panels display search coil magnetometer data (XBB and YBB, in nanoTesla/second) and zenith-viewing photometer data (427.8 nanometers, in kiloRayleighs).

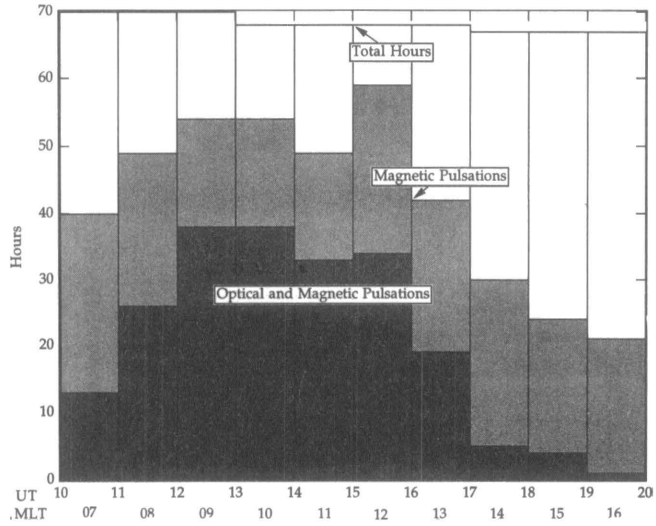

Figure 2. Hourly occurrences of Pc3-4 pulsations in magnetic and optical signals at the Amundsen-Scott South Pole Station during a 70-day period May-July1990, as a function of universal time (UT) and magnetic local time (MLT). There were no cases in which optical Pc3-4 pulsations were observed without magnetic pulsations.

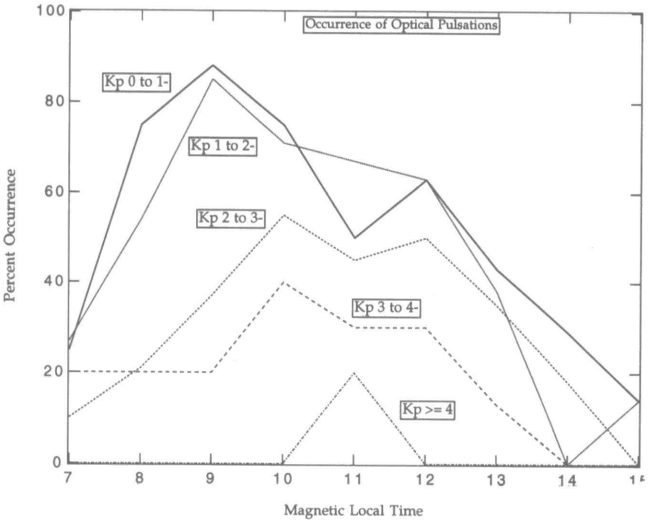

Figure 3. Percentage occurrence rates of simultaneous Pc3-4 magnetic and optical pulsations at the Amundsen-Scott South Pole Station as a function of local time for several ranges of the Kp magnetic activity index.

data are recorded continually at the South Pole throughout the year, and auroral emissions at 427.8 nanometer and 630.0 nanometer wavelengths are routinely recorded at the South Pole during austral winter (May to September) by both all-sky imagers, recording one image per minute, and zenith-viewing photometers with 55° full angle field of view, recorded each second. We analyzed magnetometer and photometer data for 70 days during the 1990 austral winter (May-July) and used these to compile a data base of pulsation occurrence as a function of time and level of global auroral activity (using the planetary Kp magnetic disturbance index). Pulsation activity (in magnetometer or photometer signal) was listed for a given hour if any narrowband Pc3-4 activity was evident during that hour.

Figure 1 shows typical pulsation activity in magnetic field and auroral light for a 1-hour period from 1300 to 1400 universal time (UT) 28 May1990. Packets of simultaneous Pc3-4 pulsations in all three traces are clearest from 1300 to 1308, near 1314, between 1322 and 1330, and from 1346 to 1348 UT. Other variations in the signals shown mainly result from local, more irregular auroral sources. On this day the all-sky images showed some auroral activity poleward of the Amundsen-Scott South Pole Station after 1300 UT and becoming fainter after 1400 UT.

Data from the all-sky images showed that, when optical pulsations were observed, there was usually a low level of 630.0-nanometer emissions and no appreciable 427.8 nanometer emissions. The proportion of these emissions indicates that the electrons impinging on the upper atmosphere to produce these auroral emissions have the relatively low energies characteristic of the regions near or outside the magnetospheric boundary. In addition, the brightest auroral emission was poleward of the observing station during times when both magnetic and optical emissions were observed. This location suggests that at these times the Amundsen-Scott South Pole Station was situated on magnetic field lines connected to the "boundary layer," just earthward of the magnetospheric boundary.

A statistical study of the magnetic and optical data supports the same conclusion. Figure 2 shows the occurrence of Pc3-4 pulsations as a function of universal time (from 1000 to 2000) and magnetic local time (MLT; bins are centered on times from 0700 to 1600 MLT). Both magnetic and optical pulsations in this data set are clearly more frequent before local magnetic noon (1530 UT) than after. The distribution of optical pulsations is consistent with the earlier results of Wu and Rosenberg (1992), who used a computer-based identification of optical pulsation activity in 10-minute intervals. It is significant that the occurrences of optical pulsations in every case formed a subset of the occurrences of magnetic pulsations; i.e., in no case during these 70 days did we observe a narrowband optical pulsation without simultaneously observing a narrowband magnetic pulsation (to within a few minutes).

Figure 3 shows occurrence rates of simultaneous Pc3-4 magnetic and optical pulsations as a function of the Kp magnetic disturbance index. The figure shows that optical pulsations are much less frequent for higher Kp values and are more common at pre-noon local times for all levels of Kp. It is well known from many earlier studies that the ionospheric foot of the magnetospheric boundary is approximately above or slightly poleward of the South Pole Station for low values of Kp and moves equatorward when Kp values increase. The sharp drop in occurrence of Pc3-4 optical pulsations as Kp increases suggests that a source region rather localized in latitude, probably the magnetospheric boundary layer, has moved away from the station.

Thus by two different means we infer that the electrons that cause the modulated auroral emissions come from the boundary layer, perhaps from plasma that has recently come from a quasi-parallel bow shock. Nonsteady penetration or diffusion of this shocked solar wind plasma onto closed field lines would place some electrons directly into "loss cone" orbits; these electrons would begin to travel along the magnetic field toward the ionosphere as soon as the plasma entered the boundary layer.

We conclude two things: First, because the auroral and magnetic pulsations are strongly linked to "upstream waves" impinging on the earth's magnetosphere from the solar wind, monitoring of auroral pulsations near the zenith provides an effective way of locating the position of the boundary layer from ground observatories. Secondly, our data are consistent with the hypothesis that Pc3-4 pulsations reach very high latitudes via modulated electron precipitation, which produces increases in the auroral

conductivity and currents (Engebretson et al. 1991). This work was supported by National Science Foundation grants DPP 89-13870, DPP 88-18229, and DPP 88-16825.

References

Engebretson, M. J., B. J. Anderson, L. J. Cahill, Jr., R. L. Arnoldy, T. J. Rosenberg, D. L. Carpenter, W. B. Gail, and R. H. Eather. 1990. Ionospheric signatures of cusp-latitude Pc3 pulsations. *Journal of Geophysical Research*, 95(A3):2,447-2,456.

Engebretson, M. J., L. J. Cahill, Jr., R. L. Arnoldy, B. J. Anderson, T. J. Rosenberg, D. L. Carpenter, U.S. Inan, and R. H. Eather. 1991. The role of the ionosphere in coupling upstream ULF wave power into the dayside magnetosphere. *Journal of Geophysical Research*, 96(A2): 1,527-1,542.

Wu, Q. and T. J. Rosenberg. 1992. High latitude pulsating aurorae revisited. *Geophysical Research Letters*, 19(1):69-72.

Images and energy spectra of an impulsive X-ray burst observed in the antarctic polar cap region

G. K. Parks, T. Freeman, M. McCarthy, and S. Werden

Geophysics Program
University of Washington
Seattle, Washington 98195

D. Smith and R. P. Lin

Physics Department and Space Sciences Laboratory
University of California
Berkeley, California 94720

In 1990 a balloon launched into a circumpolar trajectory from McMurdo Station, Antarctica, carried an X-ray pinhole camera and a high-energy-resolution germanium spectrometer. A circumpolar balloon is an ideal platform from which to study solar X-ray phenomenon (Smith et al. 1991). A circumpolar trajectory in Antarctica also covers a broad range of magnetic domains, from subauroral to polar cap regions, and thus offers scientists a unique opportunity to study energetic electron precipitation phenomenon on magnetic lines of force that contain different plasma populations. The balloon floated at an altitude of about 3.6 grams per square centimeter atmospheric depth for about 9 days.

The X-ray camera detects atmospheric bremsstrahlung X-rays in the energy range of about 20-120 kilo-electron volts, obtaining images over a field of view that corresponds to a circle of about 100 kilometers in diameter with a spatial resolution of about 15-20 kilometers, for a source located at an altitude of 100 kilometers. On-board data processing provides either imaging (216 pixels) or energy-spectral (255 channels) data. The germanium spectrometer detects X-rays from 20 to 2.5 million electron volts with a

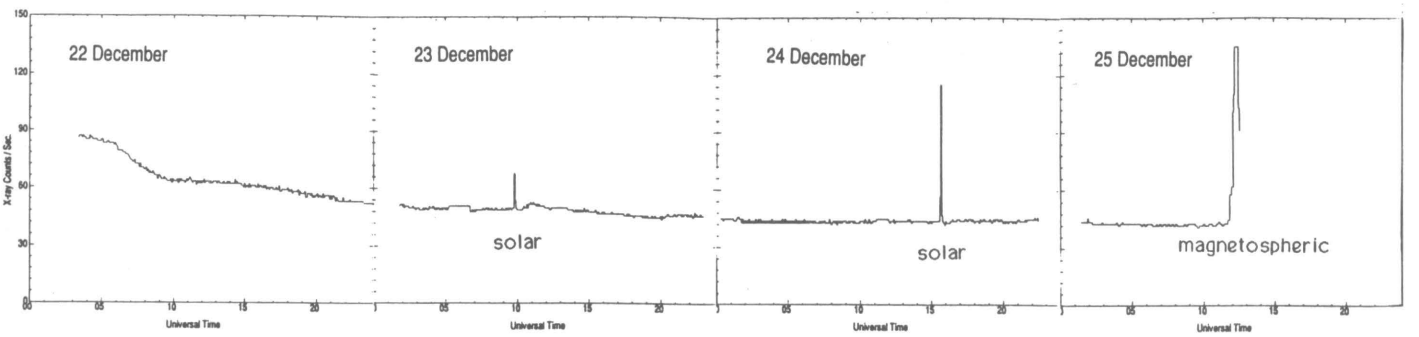

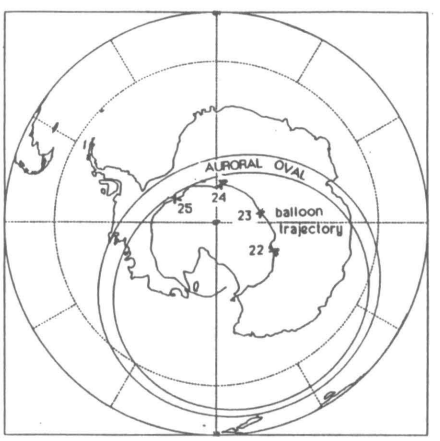

Figure 1. The top panels show the summary data of X-rays detected on 23, 24, and 25 December 1990. The bottom panel shows the trajectory of the balloon superimposed on the antarctic continent and the predicted position of the auroral oval.

resolution of greater than or equal to 1 kilo-electron volt full width at half maximum.

Impulsive X-ray events were detected on 23, 24, and 25 December 1990 (figure 1, top panel). All were observed on the dayside, inside the polar cap region and to the south of the predicted auroral zone but fairly close to the southward boundary (figure 1, bottom panel). The first two bursts are solar X-ray events and will be reported on in another paper. The impulsive burst on 25 December is associated with the earth's magnetospheric activity. Figure 2 shows raw images that represent two-dimensional contours of constant X-ray fluxes at the position of the detector plane (about 40 kilometers in altitude). These images indicate that electron precipitation can be beamlike and can occur over a small region, about 15-20 kilometers. That dimension is close to the limit of the instrument's capability suggests that the actual spatial region could be even smaller.

The germanium spectrometer recorded an X-ray spectrum showing precipitation activity during a 15-minute period just before data were collected by the X-ray camera. The emission appeared to come from a region located 26(+10,-11) degrees above the horizon, outside the field of view of the X-ray camera. The spectrum corrected to the top of the atmosphere is shown in the top panel of figure 3. The error bars represent statistical error and the solid lines represent the error due to uncertainty in the elevation angle. The bottom panels show X-ray energy spectra obtained by the X-ray camera. The best fit power law for the germanium spectrometer has an index of m = -3.70 (+0.41,-1.13). The three indices for the camera data (preliminary) are 0.57 (±-0.16), 0.46 (± -0.22), and 0.76 (± -0.18). The combined University of California at Berkeley and University of Washington data indicate that the energy spectrum hardened as the source moved overhead. Note that no precipitation was detected before the spectrum of figure 3 by the UCB spectrometer observations are unavailable for the time of the pinhole camera data.

A possible source of this burst is an independent polar cap source or a source that is associated with energetic electrons from the outer magnetosphere. A balloon located close to the southern boundary of the auroral oval could detect precipitated electrons from near the trapping boundary. We have reached no definite conclusion, however, about causes or relationships of the observed X-rays to auroral and magnetospheric activity.

Previous studies of auroral electrons have identified two sources of precipitation. A low-latitude source active in the ionosphere that accelerates electrons along the magnetic field direction is believed to be the primary source of less than 10 kilo-electron volts (Evans 1974; Mozer et al. 1977). A distant magnetospheric source that operates in and beyond synchronous altitudes is believed to be the source of higher-energy (greater than 20 kilo-electron-volts) electrons (Parks and Winckler 1968). Auroral images in the visible to the ultraviolet come from a mixture of the two electron sources. Because both of the sources are active at the same time, one cannot discern from the emission data alone which of the two sources is contributing or how their temporal and spatial features are related.

X-ray images, however, can provide important clues as to how the energetic magnetosphere sources work. X-rays with energies of about 20-120 kilo-electron-volts have been detected over the South Pole (Matthews et al. 1988), but our observations from the polar cap region provide the first quantitative small-scale X-ray images and simultaneous energy spectra. Our X-ray pinhole camera reveals new information on energetic electron precipitation phenomenon.

The duration of the X-ray burst on 25 December was about 15 minutes. Similar types of X-ray bursts have been observed from

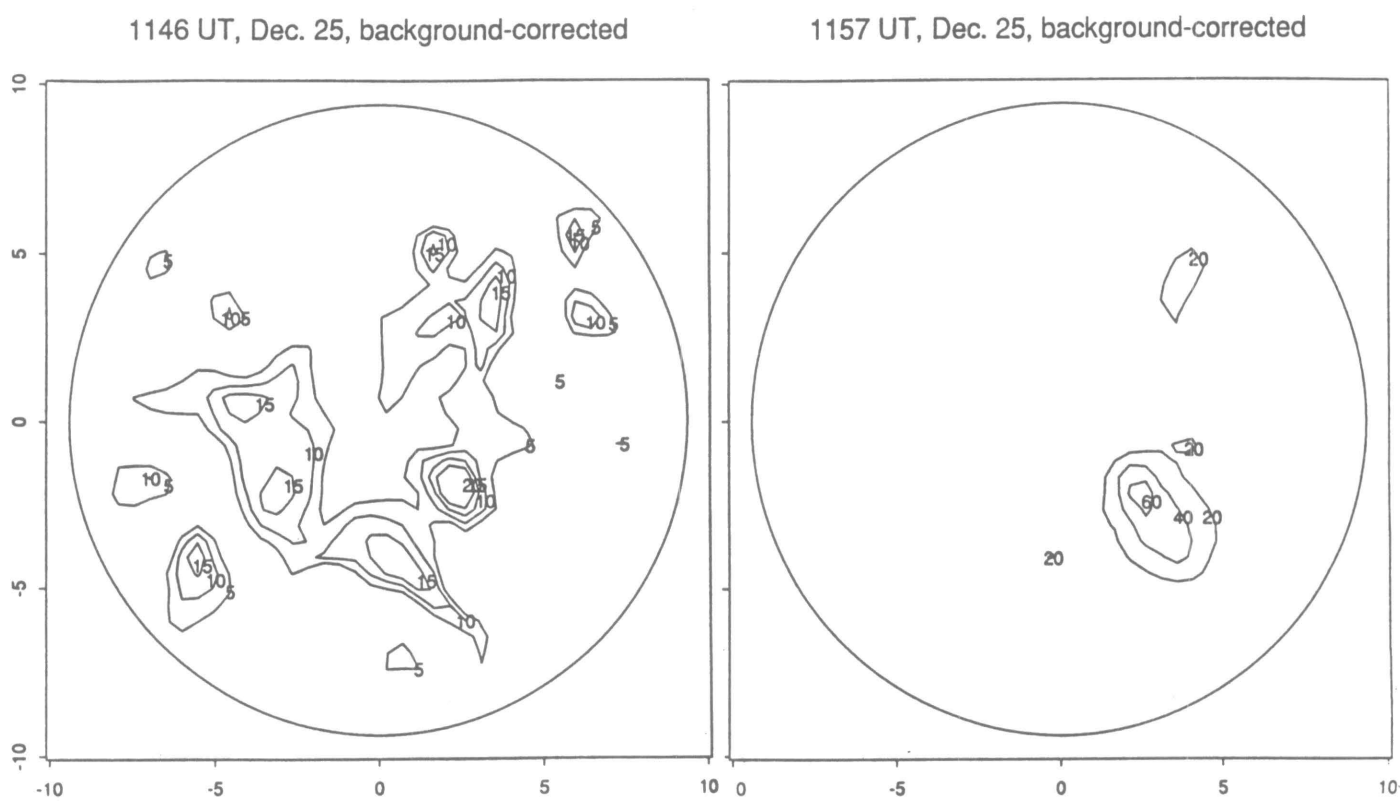

Figure 2. The two panels show the X-ray images obtained by the camera for the 25 December impulsive burst.

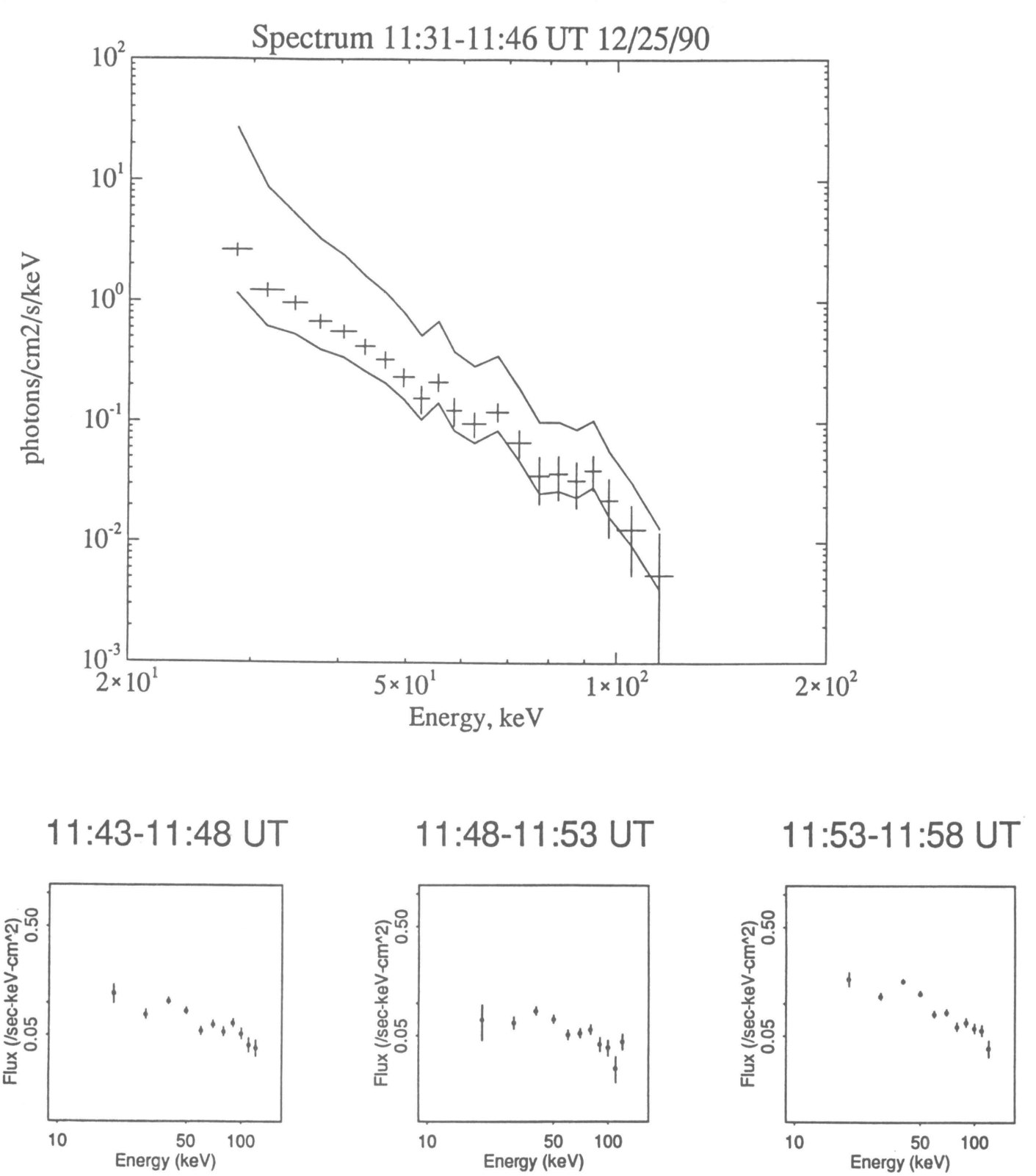

Figure 3. The top panel shows the differiential energy spectrum obtained by the UCB high-energy-resolution germanium spectrometer. The bottom panels show the energy spectra obtained by the UW X-ray camera. Note that the preliminary spectra obtained by the UW detector is much harder than the spectrum obtained by the UCB spectrometer.

the South Pole (private communication with T. Rosenberg and E. Bering 1992). The polar bursts seem shorter than the typical auroral precipitation, which has a duration of less than or equal to 30 minutes. Basic questions about the nature of electron precipitation sources include the following: What is the source of polar cap energetic electrons? Are polar sources independent of auroral sources? Could the impulsive bursts be the polar manifestation of auroral substorms? Could the apparent motion we observed be associated with the expansion phase of substorms? these questions cannot be answered without systematic research and require further study.

This work was supported in part by National Science Founda-

tion grants DPP 87-18586, DPP 87-17481, and DPP 91-18500. The instruments were launched on a National Aeronautics and Space Administration balloon as part of the long duration balloon developmental program.

References

Evans, D. 1974. Precipitation electron fluxes formed by a magnetic field aligned potential difference. *Journal of Geophysical Research*, 79:2,853-2,858.

Matthews, D., T. Rosenberg, J. Benbrook, and E. Bering. 1988. Dayside energetic electron precipitation over the South Pole (latitude = 75°). *Journal of Geophysical Research*, 93:12,941-12,945.

Mozer, F., C. Carlson, M. Hudson, R. Torbert, B. Paraday, J. Yatteau, and M. Kelly. 1977. Observations of paired electrostatistic shocks in the polar magnetosphere. *Physical Review Letters*, 38:292-295.

Parks, G. and J. Winckler. 1968. Acceleration of energetic electrons observed at the 6.6 equatorial plane during magnetosphere substorms. *Journal of Geophysical Research*, 73:5,786-5,791.

Smith, D., R. Lin, K. Hurley, and K. Anderson. 1991. Hard X-ray bursts observed on a long duration balloon flight in Antarctica (abstract). *EOS Transactions*, American Geophysical Union, 72:370.

Intense 2.3 hertz electric field pulsations in the stratosphere at high auroral latitudes

E. A. Bering, J. R. Benbrook, and B. Liao

Department of Physics
University of Houston
Houston, Texas 77204-5504

This paper reports results from the analysis of ultra-low-frequency (ULF) fluctuations observed by electric field detectors flown on stratospheric balloon payloads from the South Pole. This research is difficult to place in context since most investigators who have studied the ionospheric electric field using balloon-borne sensors have been interested in phenomena with time scales of tens of minutes or longer.

Few papers have considered fluctuations in balloon electric-field data at frequencies above 10 millihertz, and only one study that we are aware of reported signals in the vicinity of about 1 hertz (D'Angelo et al. 1983). These authors reported high magnetic latitude observations of broadband incoherent noise in their electric field data. The frequency of this noise ranged up to 1 hertz and had an amplitude of a few millivolts per meter. D'Angelo et al. did not state the bandwidth of their detector. However, the appearance of the published spectrogram suggests a cutoff at 1 hertz. These signals had an occurrence rate of 1-3 percent. D'Angelo et al. attributed these signals to polarization fields occurring within regions of turbulent variation in stratospheric conductivity. In this paper we report on observations of similar signals above the South Pole. The wider bandwidth and better ambient diagnostic data available from our payloads has enabled us to understand these events better.

The electric field data were acquired during the 1985-1986 South Pole balloon campaign (Bering et al. 1987) in which eight balloon payloads carrying three- axis double-probe electric field detectors were launched sequentially from the South Pole. The noise level of the electric field instrument was about 0.4 millivolts per meter, the digitization increment was 0.1 millivolts per meter, and the data were sampled at 8 hertz. We determined balloon payload attitude from an on-board magnetometer. We measured ambient air temperature with a thermistor that was shielded from direct sunlight and Earth albedo and was sampled at a 1-hertz rate. We obtained the data discussed here during flight 3, which reached float altitude around 2345 universal time on 21 December 1985.

We observed narrow bandwidth pulsations in the horizontal component of the electric field with an amplitude of about 40 to 60 millivolts per meter at a frequency of 2.3 hertz. The vertical component had similar signals, with amplitudes of about 70 to 200 millivolts per meter. The waves occurred in bursts of 5 to 15 seconds in duration at irregular 1- to 2-minute intervals. The event began around 0015 universal time on 22 December 1985 and lasted about 3 hours. Figure 1 shows an example of one of these wave bursts. A prominent burst of quasi-sinusoidal noise can be seen in all three components, starting at 0233:18 universal time and lasting for about 12 seconds. For this burst, maximum amplitude in the eastward component was about 60 millivolts per meter. The signal in the vertical component was initially unipolar, with a total amplitude roughly equal to the peak-to-peak amplitude in the horizontal component.

The power spectra of the horizontal component signals had three peaks at 2.2, 2.32, and 2.45 hertz. Long-term analyses incorporating many bursts show narrow, relatively stable bands (not shown). On the other hand, spectra of individual bursts show spectra that have broader peaks with time variation in

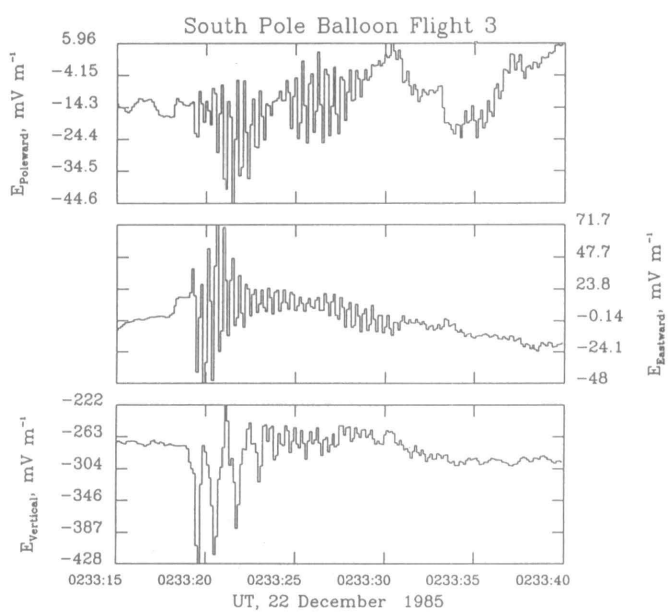

Figure 1. Three components of the electrical field measured by a balloon payload at an altitude of 32 kilometers above South Pole on 22 December 1985. The field is plotted in earth-fixed local geomagnetic coordinates. The three panels show the poleward, eastward, and vertical components, respectively. The data are plotted as a function of universal time at a rate of 8 samples per second.

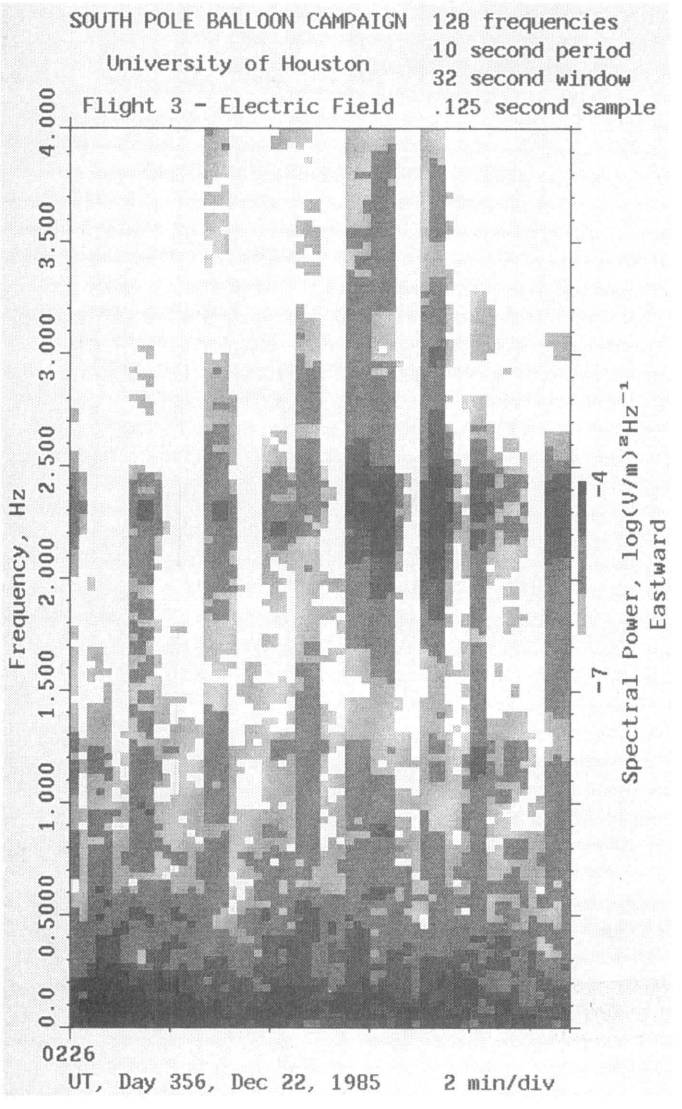

Figure 2. Gray-scale spectrogram of the power spectrum of the eastward component of the electric field. In this plot, the ordinate is frequency from 0 to 4 hertz, the abscissa is universal time, and the spectral power is plotted as intensity of gray, as shown in the calibration bar on the right. Ten minutes of spectra are shown. The spectra were computed using a 32-second window moved forward 10 seconds per step. The data were smoothed by frequency averaging, using a three-point moving average.

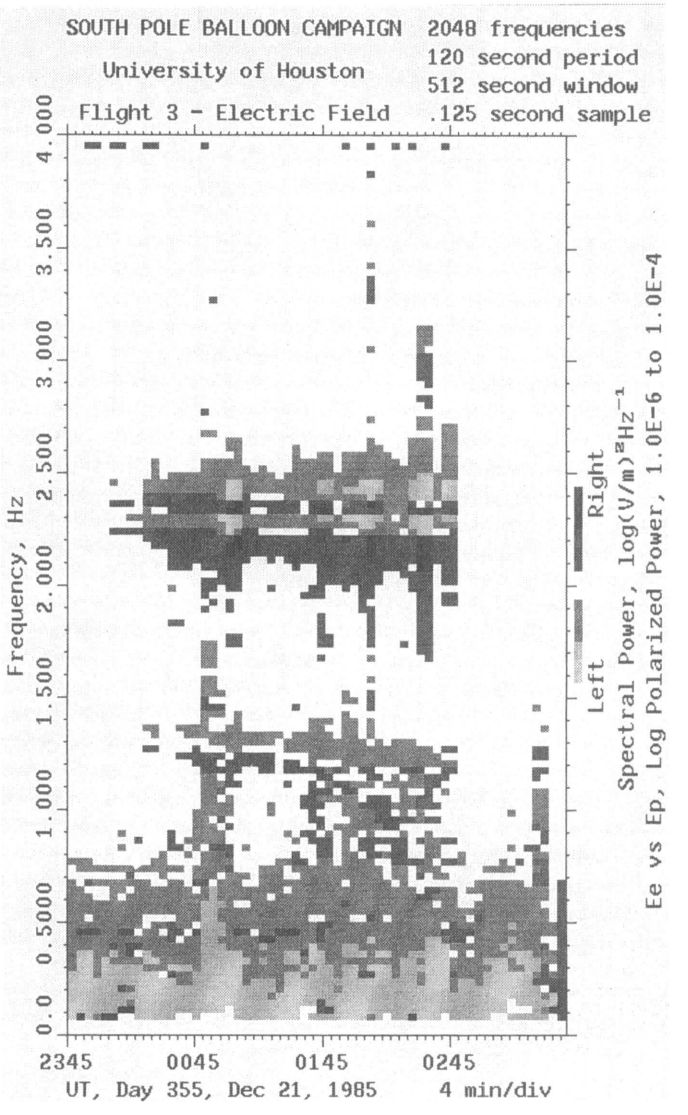

Figure 3. Gray-scale spectrogram of the circular polarization on the horizontal plane. In this figure, the gray scale has been split into two halves, with the lighter part showing left-handed polarization and the darker showing right-handed polarization. Four hours of data are shown. The spectra were computed with a 512-second window moved forward two minutes per step. The spectra were smoothed with 16-point frequency averaging.

central frequency. For example, figure 2 is a dynamic power spectrum of the eastward component, showing 10 minutes worth of data. The spectrum of the burst shown in figure 1 is the second of the two prominent bursts just to the right of center. Signatures of eight bursts appear, spaced irregularly through the interval shown. Spectrum analysis of the vertical component shows the 2.32 hertz peak and a falling tone that started at 1.35 hertz and descended to 1.2 hertz by the end of the event. This falling tone can be seen as a weak signal in figure 3. The difference in dominant frequencies in figure 1 is confirmed by spectral analysis of the vertical component, where this falling tone is the strongest signal.

Figure 3 shows a polarization power spectrum of the horizontal components for the entire period spanning the noise burst events. The polarization analysis shown in this figure indicates that the 2.2-hertz band was nearly 100 percent right-hand polarized, while the 2.32- and 2.45-hertz bands were nearly 100 percent left-hand polarized.

The waves were not seen in the search coil magnetometer data from the South Pole. They were also not seen in any of the other signals from the balloon payload, including the housekeeping data, the ambient temperature, or the ambient pressure.

What was the source of these unusual signals? Both ionospheric and atmospheric mechanisms are possible, including ionospheric plasma waves, thunderstorms or electrified clouds, aliased detection of Schumann resonance signals, mechanical motions of the payload or booms, charging of the payload or motions of the balloon ion wake, convecting conductivity fluctuations, or clear-air electrification and payload electronic noise.

Ionospheric plasma waves are a possible explanation, because the ion density is high enough to produce the observed amplitude and the ionosphere is nearby. Furthermore, an ionospheric source could produce the observed polarization and bandwidth. Also, ionospheric plasma waves are a common occurrence at high latitudes.

This model has problems because existing ionosphere-to-balloon mapping calculations predict some attention at this frequency. Since the observed amplitude is already unusually large for most ionospheric waves, atmospheric sources should be considered.

Thunderstorms or electrified clouds are possible explanations, because there would be enough charge present if the bad weather was nearby. Furthermore, this model accounts for the large vertical component of the signal. However, National Oceanic and Atmospheric Adminstration 9 satellite photographs and surface pressure analysis indicate that the nearest bad weather to the South Pole was about 1,600 kilometers away. At this distance, the signal amplitude implies an oscillation in total storm dipole moment of 10,000 Coulombs per kilometer if we were observing the electrostatic near field (D'Angelo et al. 1983). This estimate is prohibitively large. Another possibility, that we were under-sampling a Schumann mode, i.e., resonant electromagnetic waves, can be ruled out as an explanation because the polarization was wrong. The Schumann resonance propagates as a transverse magnetic mode and cannot have a horizontal component to the electric field (Schumann 1952). Furthermore, the frequency, bandwidth, and amplitude of our signals are all inconsistent with prior Schumann resonance observations (Sentman 1987; Sentman and Fraser 1991).

Most of the other explanations can also be ruled out. Since similar waves have been reported by others, we rule out instrumental causes. Mechanical motions require magnitude of E to be constant, which it was not. Charging of the payload, motions of the balloon wake, and electronic noise should produce signals that are coherent in all three components, contrary to observation. Convecting conductivity fluctuations should appear in the data as measured conductivity, air temperature, and pressure fluctuations. None of these could be found in the data.

Intense quasi-sinusoidal fluctuations in the electric field have been observed in the high latitude stratosphere. These "waves" are probably the same phenomena as reported by D'Angelo et al. (1983). We attribute the differences in frequency and amplitude to the narrower bandwidth of the previous payloads. The emissions are characterized by large amplitude, narrow bandwidth, and complicated polarization. The power spectrum of the vertical component peaks at a lower frequency than does the horizontal component. The most intense peaks in the spectra of the horizontal components are not harmonics of the major peak in the vertical component spectrum. No available model is fully satisfactory. An ionospheric source or a small nearby electrified cloud that was not noticeable in the satellite photographs remains the best possibility.

This research was supported by National Science Foundation grants DPP 84-15203, DPP 86-14092, and DPP 90-19567. We thank Dr. Mark Engbretson for analysis and useful comments regarding the South Pole search coil magnetometer data.

References

Bering, E. A., III, J. R. Benbrook, J. M. Howard, D. M. Oro, E. G. Stansbery, J. R. Theall, D. L. Matthews, and T. J. Rosenberg. 1987. The 1985-1986 South Pole balloon campaign. *Memoirs of the National Institute for Polar Research in Japan* (Proceedings of the Nagata Symposium on Geomagnetically Conjugate Studies and the Workshop on Antarctic Middle and Upper Atmosphere Physics), 313-317.

D'Angelo, N., I. B. Iversen, and M. Mohl Madsen. 1983. Low-frequency ($f \leq$ 1Hz) stratospheric electrical noise measured by balloon-borne sensors. *Journal of Geophysical Research*, 88:5,441-5,450.

Schumann, W. O. 1952. Uber die strahlungslosen Eigenschwingungen einer leitenden Kugel, die von einer Luftschicht und einer Ionospharenhulle umgeben ist. *Z. Naturforsch*, 7a:149.

Sentman, D. D. 1987. Magnetic elliptical polarization of Schumann resonances. *Radio Science*, 22:595.

Sentman, D. D. and B. J. Fraser. 1991. Simultaneous observations of Schumann resonances in California and Australia: Evidence for intensity modulation by the local height of the *D* region. *Journal of Geophysical Research*, 96:15,973-15,984.

Surface observations of global atmospheric electric phenomena at Amundsen-Scott South Pole Station

A. A. Few and G. A. Morris

Space Physics and Astronomy
Rice University
Houston, Texas 77251-1892

E. A. Bering, J. R. Benbrook, and R. Chadwick

Department of Physics
University of Houston
Houston, Texas 77204-5504

G. J. Byrne

NASA
Johnson Space Center
Houston, Texas 77058

Instruments for measuring the atmospheric electric field and current were deployed at South Pole Station in January 1991. The data acquired at 3 meters above the antarctic plateau surface are directly related to the global electric circuit parameters, in particular the ionospheric potential. The data allow us to continuously monitor the global electrical circuit from surface measurements.

Instrumentation. In January 1991 instruments for measuring atmospheric electrical current and field were deployed at two research sites at Amundsen-Scott South Pole Station, Antarctica. The instruments, deployment, and early results are described in Byrne et al. (1991) and Bering et al. (1991b). A discussion of the scientific value and merits of these measurements in the overall research of the global atmospherical electrical circuit and ionospheric electrodynamics can be found in Bering et al. (1991a). Only a very brief description of the instruments and the scientific rational are provided here.

Two instruments are deployed at each of the two research sites that are separated by 600 meters, which is characteristically greater than the thickness of the planetary boundary layer. This arrangement should provide each site with independent local environments. The parameters measured by the instruments are the vertical atmospheric electric field, E_z, and the vertical atmospheric Maxwell current density, J_z, where the subscript z denotes the altitude. Only steady-state conditions are considered here; therefore, the Maxwell current equals the conduction current. Other measured and derived parameters are recorded at the sites but will not be discussed here. All instruments are fixed at 3 meters above the local surface; hence the measured quantities are E_3 and J_3. These parameters are related by Ohm's law:

$$J_z = \sigma_z E_z \text{ and } J_3 = \sigma_3 E_3 \quad (1)$$

where σ_z and σ_3 are the atmospheric electrical conductivities at altitudes z and 3 meters respectively. E_z decreases approximately exponentially with altitude with an e-folding height about 6 kilometers; whereas, σ_z increases approximately exponentially with altitude with the same e-folding length. Under steady-state conditions J_z is invariant with altitude making it an ideal parameter for characterizing the global electric circuit. For example, we can make direct quantitative comparisons of J_z measurements at the surface with aircraft and balloon measurements.

The global electrical circuit. One scientific objective of our research is to obtain high time resolution (~ 1 second) measurements of the global electrical circuit. A recent review paper (Roble and Tzur 1986) provides details on the global electrical circuit; only the bare essentials are described here. Current flows from the tops of electrified clouds (thunderstorms predominately) upward to the ionosphere where it is distributed globally (some by traveling through the magnetosphere along magnetic field lines). Current flows from the ionosphere to the earth over the entire surface (a low resistance path the large cross-sectional area), and the current returns to the cloud through the earth and then by lightning and corona processes below the cloud. The effective resistance of this global current path is at least an order of magnitude smaller than the effective resistance of local current paths in the cloud environment, except possibly during intracloud lightning processes. This result is due to the exponential increase in atmospheric electrical conductivity with altitude. The current flowing to the global electrical circuit depends primarily upon the characteristics of the electrified cloud and is independent of the passive part of the global electrical circuit. The approximately 1,000 to 2,000 active electrified clouds over the earth at any given time act as independent current sources to the ionosphere and the global electrical circuit.

The earth surface and the ionosphere at 100 kilometers have high, approximately equal, conductivities ($10^{-2}\,\Omega^{-1}\,m^{-1}$). The lower atmosphere and the air inside clouds have conductivities ~10^{12} times smaller ($10^{-14}\Omega^{-1}m^{-1}$). The traditional model for this system is a capacitor formed by the earth and the ionosphere, C (~1 F). (The capacitance is difficult to specify because the charge is not on the ionosphere but distributed throughout the atmosphere; values for C range from 0.05 F to 2 F depending upon the application.) The whole atmosphere acts as a parallel resistor, R (~ 200 Ω), producing an RC time constant for the system of ~200 seconds. Without the continual generation of current by the global electrified clouds, the atmosphere would discharge in a matter of a few minutes. Ionospheric (~100 km) time constants are ~10^{-5} seconds; therefore, changes in currents to the ionosphere will be distributed globally within a few tens of microseconds. The global electrical circuit integrates the output of all of the earth's electrically active clouds into a single parameter I (~1000 A), the global current, and the system responds rapidly, enabling us to monitor the global current with high time resolution. I responds to the total global electrified cloud activity and has regular diurnal and seasonal variations. We expect it will also exhibit event-related responses such as the enhanced output from large mesoscale convective complexes, which produce prodigious lightning activity.

The global current, I, flowing across the atmospheric resistor, R, drives the ionosphere to a potential V (~200 kV)

$$V = R*I \quad (2)$$

R should exhibit diurnal and seasonal variations because it will be influenced by global cloudiness; however, *R* is frequently assumed constant in discussions of the global circuit. Because of the high conductivity in the ionosphere, *V* is treated as position invariant in the ionosphere.

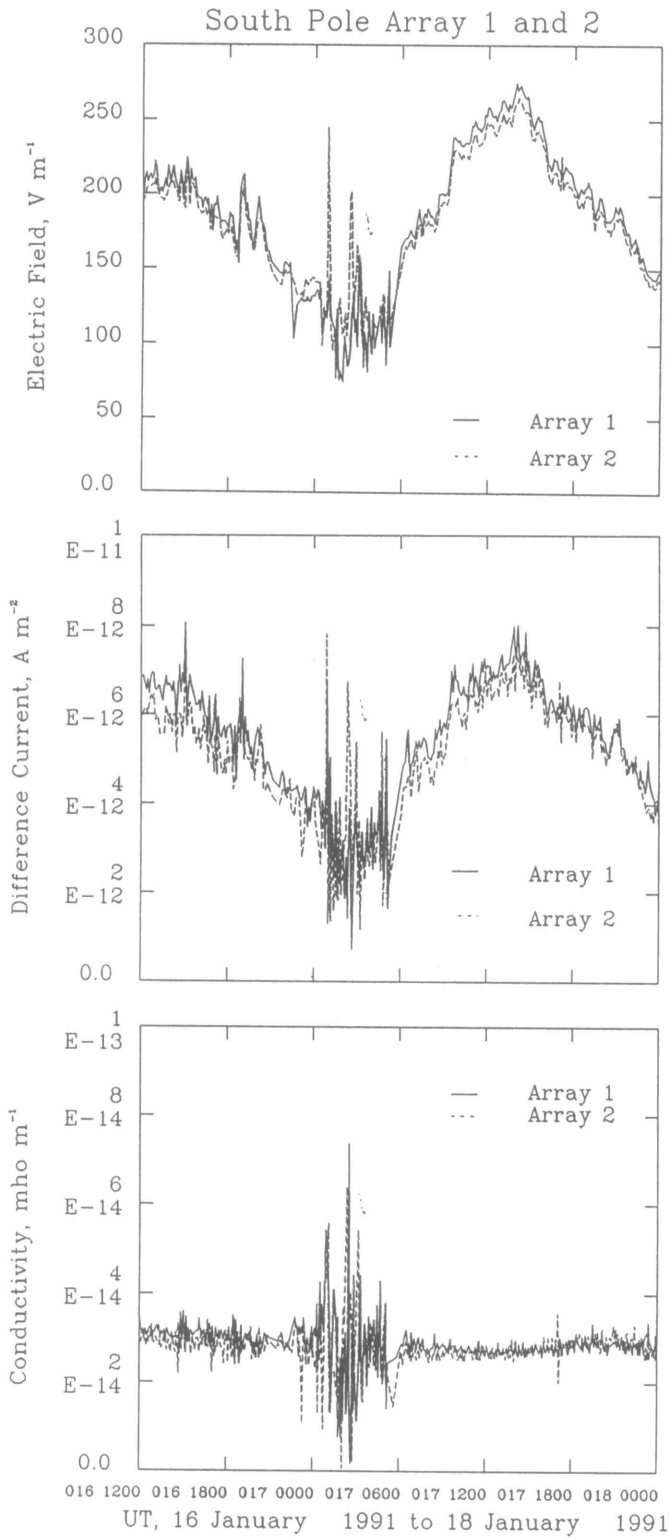

Figure 1. A 36-hour sample of atmospheric electrical measurements at Amundsen-Scott South Pole Station. The top graph shows the vertical electric field at two sites. The middle graph shows the current density at two sites. The bottom graph shows the computed conductivity at two sites (see equation 6). There is a disturbed weather period in the morning of 17 January 1991.

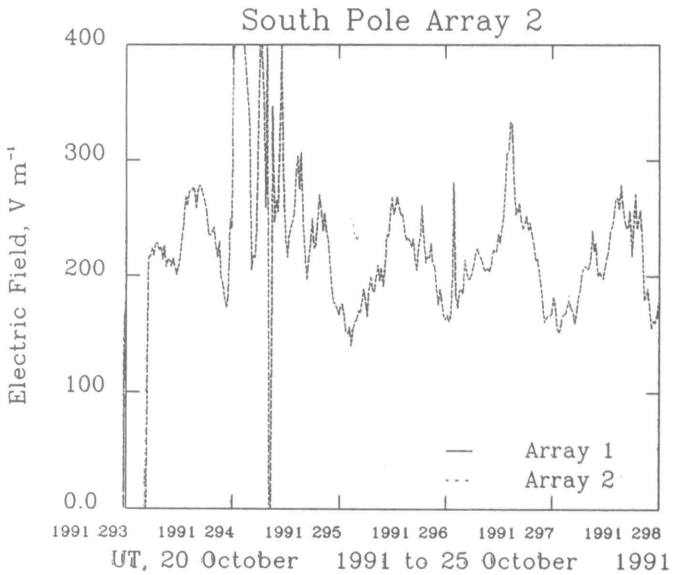

Figure 2. Five consecutive days of electric field measurements at Amundsen-Scott South Pole Station. The first half of day 294 is disturbed, but other periods clearly show global circuit variations.

Surface measurements related to global circuit parameters. In order to relate our measurements of E_3 and J_3 to the global circuit parameters I, R, and V, we need to define the columnar resistance, r_z, which is the resistance of a unit area between the altitude z and the ionosphere (~100 km); the units are Ωm^2. The complimentary columnar resistance between the surface and the altitude z is r_s-r_z where s is the altitude of the local surface. Owing to the inverse relationship between resistivity and conductivity, r_z decreases exponentially with altitude. The current density in a column of air is determined by rs following Ohm's law

$$J_z = V/r_s \quad (3)$$

Since J_z is invariant with altitude, we have for steady-state situations

$$J_3 = V/r_s = (R/r_s)I \quad (4)$$

Our measured current J_3 is directly proportional to the ionospheric potential. Furthermore, on the antarctic plateau, r should not experience diurnal variations; hence, equation 4 may be used to research diurnal variations of the ionospheric potential from our surface measurements. Additional discussion of the advantages of the antarctic plateau for this research is given in Byrne et al. (1991) and Few et al. (1992). Under the assumption that *R* is constant, our surface measurements can be related to *I*, but additional research is needed to understand the diurnal variations in *R*.

Equations 1 and 4 can be used to derive a similar set of relationships between E_3 and the global circuit parameters.

$$E_3 = V/(r_s\sigma'_3) = (R/r_s\sigma_3)I \quad (5)$$

We see in Equations 4 and 5 that either instrument can be used to research the global circuit. The electric field measurement has another parameter, σ_3, in its relationship; however, like r_s, σ_3 should not experience diurnal variations on the antarctic plateau.

In addition to providing one level of redundancy, the two instruments provide the more important functions of validating instrument performance and evaluating local environmental conditions. An example of these functions can be found from equation 1, which is used to find σ_3 from our measurements.

$$\sigma_3 = J_3/E_3 \tag{6}$$

If both measurements, E_3 and J_3, exhibit significant changes throughout the day, but their ratio, σ_3, remains steady with the correct magnitude, then we can be confident that the instruments are performing correctly. Figure 1 clearly demonstrates this function of validation of instrument performance.

The function of environmental evaluation is also demonstrated in the conductivity curves of figure 1. There is a period of disturbed weather in the morning of 17 January 1991. When the conductivity curve shows this disturbance, we know that the electrical data cannot be used for global electrical research. In the periods before and after the disturbance the conductivity at both sites are equal and constant indicating a return to a steady electrical state. We believe that this state of constant conductivity is also accompanied by a constant columnar resistance. Had the data in figure 1 been acquired outside the Antarctic Circle, where diurnal heating of the surface produces convective turbulence, we would see that the conductivity would also show diurnal variations and the disturbed state would dominate the data record. Figure 2 is a 5-day continuous record of the electric field at Array 2 at South Pole Station. There is an obvious disturbed period on the second day, but the global circuit diurnal signature is clearly evident in the remaining data.

Conclusions. Our instruments at South Pole Station are measuring the atmospheric electrical field and current at 3 meters above the antarctic plateau surface. These measurements are directly related to parameters of the global electrical circuit and allow continuous monitoring except during disturbed weather conditions. There is redundancy in the experiment design (two instruments at two sites) that allows us to validate instrument performance and explore the local electrical environment.

This research was supported by National Science Foundation grant DPP 89-17464. At Rice University additional support was provided by the Charles Conly Research Fund. A. A. Few acknowledges the support of the National Center for Atmospheric Research during a sabbatical leave of absence from Rice University and of the Charles L. Conly Research Fund of Rice University.

References

Bering, E. A., J. R. Benbrook, G. J. Byrne, and A. A. Few. 1991a. Measurement of vertical atmospheric electric current at a network of sites in Antarctica including manned stations and automatic geophysical observatories. *Publications of the Institute for Geophysics and Polar Academic Sciences,* D-35(238):119-135.

Bering, E. A., G. J. Byrne, A. A. Few, and G. A. Morris. 1991b. Initial results from measurements of atmospheric conduction currents and electric fields at the South Pole. *Antarctic Journal of the U.S.,* 26(5):294-296.

Byrne, G. J., E. A. Bering, A. A. Few, and G. A. Morris. 1991. Measurements of atmospheric conduction currents and electric fields at the South Pole. *Antarctic Journal of the U.S.,* 26(5):291-294.

Few, A. A., G. A. Morris, E. A. Bering, J. R. Benbrook, R. Chadwick, and G. J. Byrne. 1992. Maxwell current density measurements at South Pole: Evaluation of measurements and instrument performance. *Proceedings of the 9th International Conference on Atmospheric Electricity 1992.* St. Petersburg, Russia: Main Geophysical Observatory, 23-26.

Roble, R. G. and I. Tzur. 1986. The global atmospheric-electrical circuit. *The Earth's Electrical Environment.* Washington, D.C.: National Academy Press, 206-231.

Correlated bursts of AKR, VLF, and HF noise associated with an isolated dayside magnetic impulse

Surinder P. Singh and Theodore J. Rosenberg

Institute for Physical Science and Technology
University of Maryland
College Park, Maryland 20742

James LaBelle

Department of Physics and Astronomy
Dartmouth College
Hanover, New Hampshire 03755

Numerous investigations of auroral radio noise (ARN), involving ground and space observations, have covered a wide range of frequencies. These studies have been reviewed for the time period 1946-1967 by Ellyett (1969), and for the time period covering 1968-1988 by LaBelle (1989).

ARN in the extremely-low-frequency (ELF) to very-low-frequency (VLF) range (0.3-30 kilohertz), for example, chorus and auroral hiss, is fairly common (Morgan 1977). ARN at higher frequencies, particularly in the high-frequency (HF) to very-high-frequency (VHF) range (3-300 megahertz) is less common (Harang 1969; Nesmyanovich et al. 1976; Hartz, Reid, and Vogan 1956; Kellogg and Monson 1979; Osipov and Shevlev 1973). Even more uncommon are simultaneous noise emissions in the VLF and HF bands (Nishimuta, Ose, and Sinno 1969; Harang 1969; Benson and Desch 1991). It should also be noted that the reality of ARN in the HF to VHF range is often questioned, the experimental observations sometimes being ascribed to interference from locally-generated or propagated noise associated with human activity.

The past studies of ARN can be summarized as follows. Various papers have reported noise emission bursts. These bursts are sometimes broad band, often covering the full bandwidth of the instrument. Often these bursts are associated with cosmic radio noise absorption events, implying a possible connection to the precipitation of electrons of kiloelectronvolt energies, or higher. Most of the reported occurrences have been on the nightside. Sometimes identical bursts are observed at geo-

graphically distant stations. Correlated bursts in the VLF and HF bands are found but are not so common.

The present study attempted to identify correlated VLF/HF noise emission events using riometer and VLF data from South Pole Station. The riometer is an instrument that uses background HF cosmic radio noise to measure the opacity of the D and the E regions of the ionosphere. The incoming radiation is compared with the expected value at quiet conditions to yield the absorption. Data from most of 1984 and the beginning of 1989 were examined. From among the events discovered, the one presented here was most notable for its association with an auroral kilometric radiation (AKR) event. AKR is an intense electromagnetic radiation emitted from the earth towards outer space, and hence is not observable on the ground. The typical frequency range is from 100 to 700 kilohertz and the spectrum peaks between 200 and 300 kilohertz. The source region is believed to be situated at altitudes of 1,200 to 3,000 kilometers and is usually observed on the nightside (Wu 1985).

Figure 1 displays ground-based data recorded at South Pole station on 12 November 1984. From the top are the University of Maryland riometer data at two HF frequencies (a and b), three of the bandpass-filtered channels from the Stanford University ELF/VLF experiment (c, d, and e), and the three orthogonal components of magnetic variation measured by the AT&T Bell Laboratories fluxgate magnetometer (f, g, and h). The riometer starts showing an absorption pulse (voltage decrease) beginning approximately 1131 universal time (0801 magnetic local time), which is about 2 to 3 minutes after the start of the magnetic impulse as measured by the horizontal (H) component. Following the peak of the magnetic pulse, the ELF/VLF channels show a series of noise bursts, numbered 1 through 5 for the sake of reference.

The recovery of the absorption in the riometers is interrupted by a similar series of bursts. Burst number 1 is the most intense and occurs just after 1137 universal time, at the same time as in the VLF channels. It drives the 30 megahertz riometer to saturation (approximately 7 volts), but has been clipped at 4.25 volts for the sake of clarity. This burst in the 51.4 megahertz riometer is quite modest by comparison (approximately 1.17 volts). Burst 1 was also observed in the 51.4 and 30 megahertz riometer data at McMurdo Station which is about 1,300 kilometers from South Pole Station (McMurdo data not shown).

The bursts labeled 2, 3 and 4 appear in the 30 megahertz riometer as only slight level shifts above the background level prevailing prior to the event. These bursts are also closely correlated with those in the VLF channels. Burst 5 has no apparent presence in the riometers. In all of the channels displayed in figure 1, apart from the bursts, the data are remarkably quiet; even the digitization step is evident in the 31 to 38 kilohertz channel.

At the time of this event the Ampte/Irm satellite was in the ecliptic plane, near the bow shock at 16 earth radii from the centre of the earth on the morning side (0830 magnetic local time). The magnetic field changes recorded at the satellite just before the first burst in the ground observations indicate that either the bow shock has moved out, putting the satellite in the magnetosheath for about 3 minutes, or an interplanetary magnetic field discontinuity has passed by.

Figure 2 shows the satellite wave data in spectrogram representation and line plots of two selected frequency bands, together with ground data from the 30 megahertz riometer and the 11 to 13 kilohertz VLF channel. The ground level burst numbers on the 11 figure draw attention to the correlation with the ground data. At the instant of the first ground level burst there is an Auroral Kilometric Radiation (AKR) event. This burst occurs in the frequency range 200 to 700 kilohertz. Bursts 2 and 3 are also prominent in the AKR data. Burst 4 has a weak counterpart at 275 to 375 kilohertz in the satellite data. Burst 5 precedes a weak AKR burst by about a minute.

In summary, this paper describes a correlated VLF, HF, and AKR emission event occurring on the dayside of the magnetosphere during an isolated magnetic impulse. The origin of these noise emissions remains a topic of further study. Theoretical work has identified near-earth processes capable of explaining VLF noise (Maggs 1976) and AKR (Wu 1985), but not HF emissions. In the present instance, however, the Solar-Geophysical Data (1985a and 1985b) compilations for this day show that the HF emissions were due to a Type III solar radio noise burst. Specifically, these reports identify such a burst as occurring at 1137.2 universal time at the earth, precisely the time of the first and most intense of the riometers HF spikes. (The following, much weaker noise enhancements on the riometers were probably too weak in comparison to be identified as outstanding radio noise occurrences.)

The very close association of Type III solar noise with the AKR suggests the possibility of external stimulation, as was first suggested by Calvert (1981). The AKR, perhaps by way of modifying the magnetospheric electron velocity distribution, might in turn lead to the generation of the observed VLF emissions. The relationship of these correlated emission features to the occurrence of the magnetometer/riometer absorption impulse may be coincidental. On the other hand, the magnetospheric impulse may have preconditioned the ionosphere/magnetosphere to be susceptible to the external stimulation of the AKR by the solar radio noise burst.

We thank our colleagues U.S. Inan for supplying the ELF/VLF data, L. J. Lanzerotti for the magnetometer data, and R. Treumann for the AKR data. We thank C. S. Wu for useful discussions. This research has been supported by National Science Foundation grant DPP 88-18229.

References

Benson, R. F. and M. D. Desch. 1991. Wideband noise observed at ground level in the auroral region. *Radio Science*, 26(4):943-948.

Calvert, W. 1981. The stimulation of auroral kilometric radiation by Type III solar radio bursts. *Geophysical Research Letters*, 8(10):1,091-1,094.

Ellyett, C. D. 1969. Radio noise of auroral origin. *Journal of Atmospheric and Terrestrial Physics*, 31: 671-682.

Harang, L. 1969. Radio noise from aurora. *Planetary and Space Science*, 17:869-877.

Hartz, T. R., G. C. Reid, and E. L. Vogan. 1956. V.H.F. auroral noise. *Canadian Journal of Physics*, 34:728-729.

Kellogg, P. J. and S. J. Monson. 1979. Radio emissions from the aurora. *Geophysical Research Letters*, 6(4):297-300.

LaBelle, J. 1989. Radio noise of auroral origin: 1968-1988. *Journal of Atmospheric and Terrestrial Physics*, 51(3):197-211.

Maggs, J. E. 1976. Coherent generation of VLF hiss. *Journal of Geophysical Research*, 81(10):1,707- 1,724.

Morgan, M. G. 1977. Wide band observations of LF hiss at Frobisher Bay (L = 14.6). *Journal of Geophysical Research*, 82(16):2,377-2,386.

Nesmyanovich, A. T., S. I. Musatenko, V. A. Kravchenko, and V. V. Chmil'. 1976. Radio bursts from outer space near the earth in the meter-wavelength range. *Radiophysics and Quantum Electronics*, 19(8):1,101-1,105.

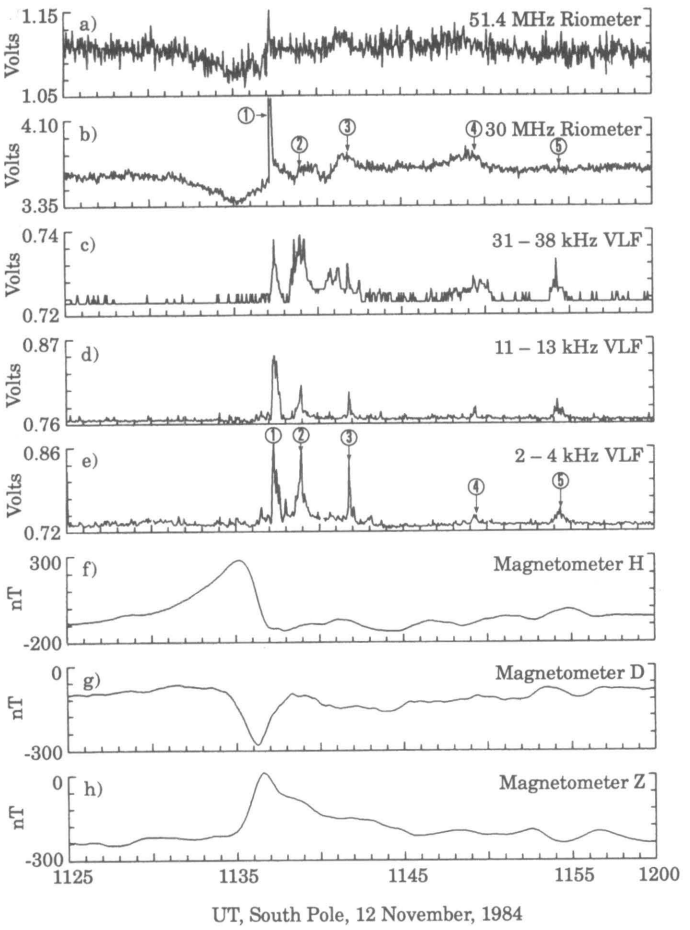

Figure 1. Ground riometer, VLF, and magnetometer data from South Pole station for 12 November 1984. Symbol nT stands for nanotesla, UT for universal time. H, D, Z represent horizontal, east-west, and vertical components of the magnetic field, respectively. The numbers 1 through 5 mark the occurrences of VLF noise bursts that are correlated with bursts of HF noise and the AKR emissions.

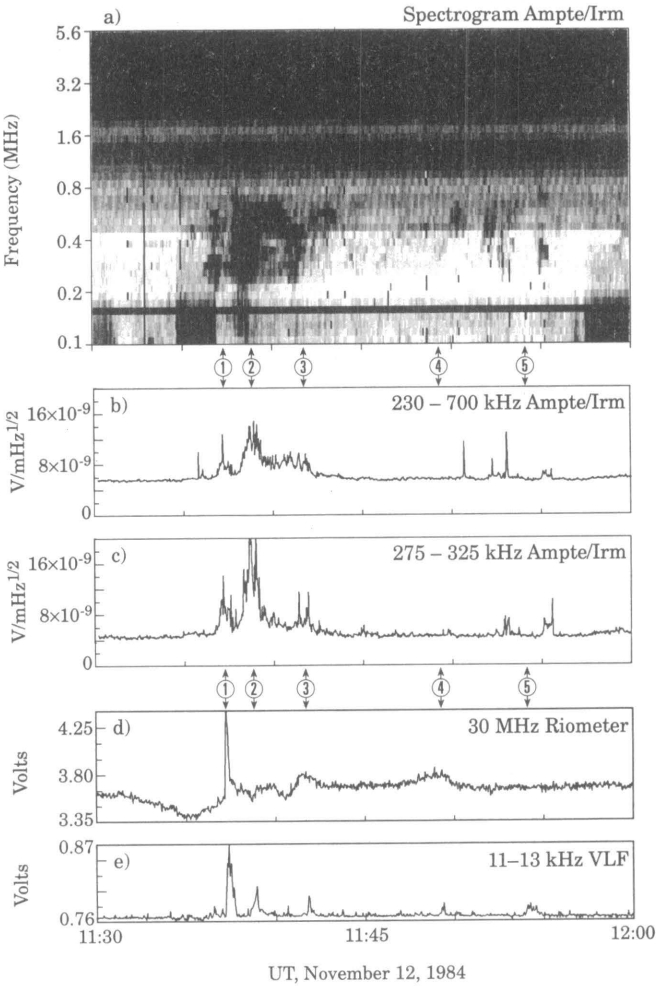

Figure 2. Ampte/Irm satellite data (top three panels), and South Pole station ground data (bottom two panels). Symbols are explained in the caption for figure 1.

Nishimuta, I., M. Ose, and K. Sinno. 1969. Abnormal enhancements of HF noise intensity at Syowa Station, Antarctica. *Journal of Geomagnetism and Geoelectricity*, 21(3):697-700.

Osipov, N. K. and Y. G. Shevelev. 1973. Two types of radio emissions of the auroral ionospheric disturbances. *Geomagnetism and Aeronomy*, 13:573-575.

Solar Geophysical Data. 1985a. Boulder, Colorado: U.S. Department of Commerce, 485(pt I):66.

Solar Geophysical Data. 1985b. Boulder, Colorado: U.S. Department of Commerce, 489(pt II):8.

Wu, C. S. 1985. Kinetic cyclotron and synchrotron maser instabilities: Radio emission processes by direct amplification of radiation. *Space Science Reviews*, 41:215-298.

Riometer signature of the cusp

ZHOU WANG AND THEODORE J. ROSENBERG

Institute for Physical Science and Technology
University of Maryland
College Park, Maryland 20742

A main theme of the Geospace Environment Modeling (GEM) program is to identify ionospheric signatures of the dayside cusp (Rosenberg 1989). The cusp is a funnel-shaped region through which there is nearly direct entry of solar wind and magnetosheath particles into the earth's magnetosphere (Newell and Meng 1988). Located near magnetic noon, it projects to the polar caps at low altitude as a region of approximately 1-2 degrees in latitudinal extent and approximately 30 degrees in longitudinal extent. Under conditions of moderate geomagnetic activity, the magnetic latitude of the low altitude cusp is approximately 74 degrees, the same as that of South Pole Station.

Motivated by the request to search for cusp ionospheric signatures in ground-based data, and to intercalibrate the signatures identified by different observing techniques (Crooker 1990), we asked the question: "Is there a riometer signature of the cusp?" One's initial guess might be to answer no because auroral cosmic noise absorption, as measured by riometers, is thought to arise from enhanced ionization in the D region and the cusp particle distribution is composed of electrons too low in energy to reach that depth (70-90 kilometers) in the atmosphere.

The result of our search, however, suggests that there is a riometer absorption signature of the cusp. The effect occurs in the F region at an altitude of approximately 250 kilometers and is related to the production in the cusp of patches of greatly enhanced ionization that subsequently drift into the polar cap.

In order to answer the question posed above one must determine by independent means when the cusp is within, or passing through, the riometer field of view. Our approach was to use a known or accepted cusp signature to determine when it was likely that the cusp was in the vicinity of South Pole Station. For this purpose, we examined the optical intensity ratio I(630.0 nanometers)/I(427.8 nanometers) using South Pole zenith photometer data covering the same approximately 60 degrees field of view as do the broadbeam riometers at the station. High values of this emissions ratio are produced by precipitating electrons with energies less than a few hundred electron volts and could indicate that South Pole Station was in the cusp.

Our procedure was to search the 1989 austral winter data for intervals when the optical intensity ratio exceeded 3 for durations longer than 5 minutes. The search was confined to the 8 hours centered on magnetic noon (1530 universal time at South Pole Station). Of the 150 days examined, 32 were selected as containing one or more time intervals when South Pole Station might have been in close proximity to the cusp. Note that a high I(630.0)/I(427.8) ratio does not uniquely identify the cusp, but might also indicate the cleft or polar cap, larger regions that border on the cusp. Hence we needed to examine additional data resources.

A comparison with Halley Bay PACE (Polar Anglo-American Conjugate Experiment) radar identifications of the cusp (Baker et al. 1990) within the radar's much larger field of view (which includes Amundsen-Scott South Pole Station) for the same 150-day period found 16 days in common with the South Pole "optical cusp" selection. A further comparison with Defense Meteorological Satellite Program (DMSP) particle identifications of the cusp produced a final set of 7 days when we could be reasonably confident that the cusp for a time was within 1 degree of the latitude of South Pole Station.

Figure 1 shows the average 38.2 megahertz riometer absorption and I(630.0)/I(427.8) optical intensity ratio for these 7 days as a function of universal time for the 8 hours centered on magnetic noon. It is seen that riometer absorption enhancements are positively correlated with high optical intensity ratios in the 2-hour interval from 1330 to 1530 universal time (1000-1200 magnetic local time), corresponding to the nominal location of the dayside cusp. This correlation was somewhat surprising in that riometer absorption and a high I(630.0)/I(427.8) ratio are usually associated with high- and low-energy electron precipitations, respectively, whereas the cusp is devoid of high-energy electrons.

Figure 2 illustrates the South Pole Station riometer and photometer data for one of the seven events. The second panel from the top gives the ratio of the optical intensities shown in the two lowest panels. On the ratio panel are indicated the times of three southern hemisphere passes of DMSP satellites through the cusp and the time interval when the PACE radar detected the cusp passing equatorward of South Pole Station. The latitudinal position of the cusp as found by satellite data is consistent with the position and motion of the cusp inferred from the radar data.

In figure 2 note especially the very high values of the optical ratio between 1450 and 1515 universal time, an interval terminated by an intense spike of 630.0 nanometer emission that occurred simultaneously with the PACE radar identification of cusp passage at South Pole Station. The top panel of the figure shows an enhancement of riometer absorption beginning about 1500 universal time when the cusp is overhead, reaching a peak

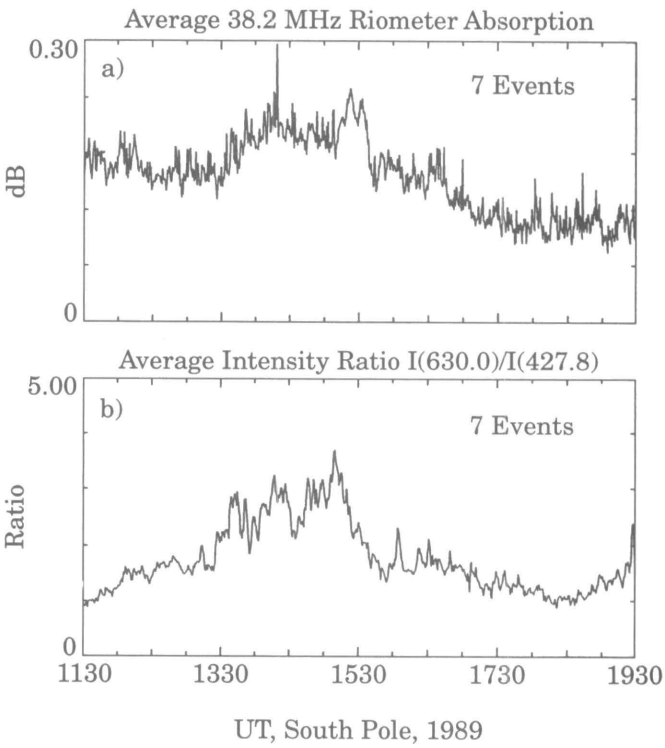

Figure 1. The average 38.2 megahertz riometer absorption and optical intensity ratio I(630.0)/I(427.8) for 7 occasions when the dayside cusp was determined to be within 1 degree of South Pole Station.

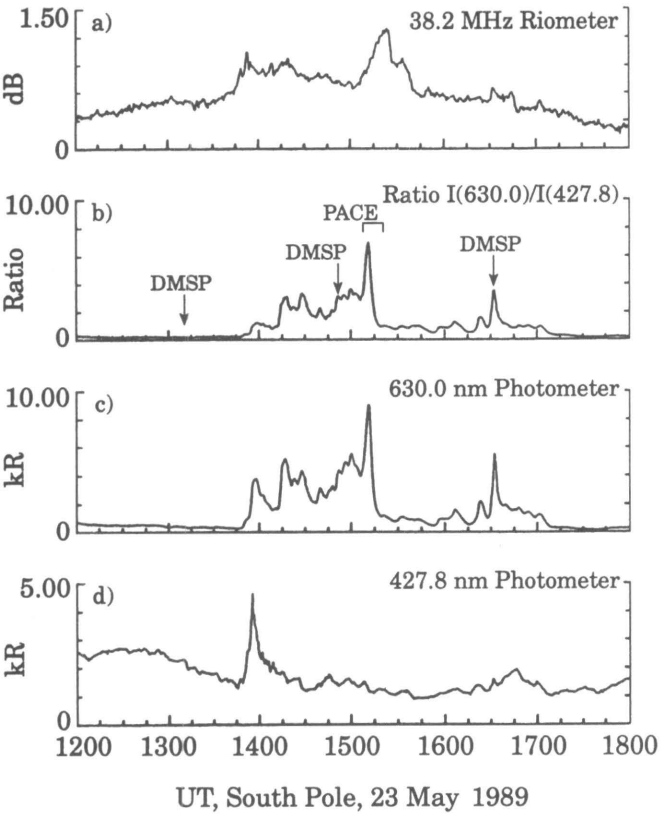

Figure 2. An example of broadbeam riometer and photometer response during a period when the cusp passed through the field of view of the South Pole instruments. *Arrows* depict three passes of the DMSP satellite which detected the cusp above 76-79 degrees magnetic latitude at 1308 universal time, at 73.5-75.5 degrees magnetic latitude at 1449 universal time and at 71.5 degrees magnetic latitude at 1631 universal time. The *bracket* indicates when the PACE radar detected the cusp over South Pole Station.

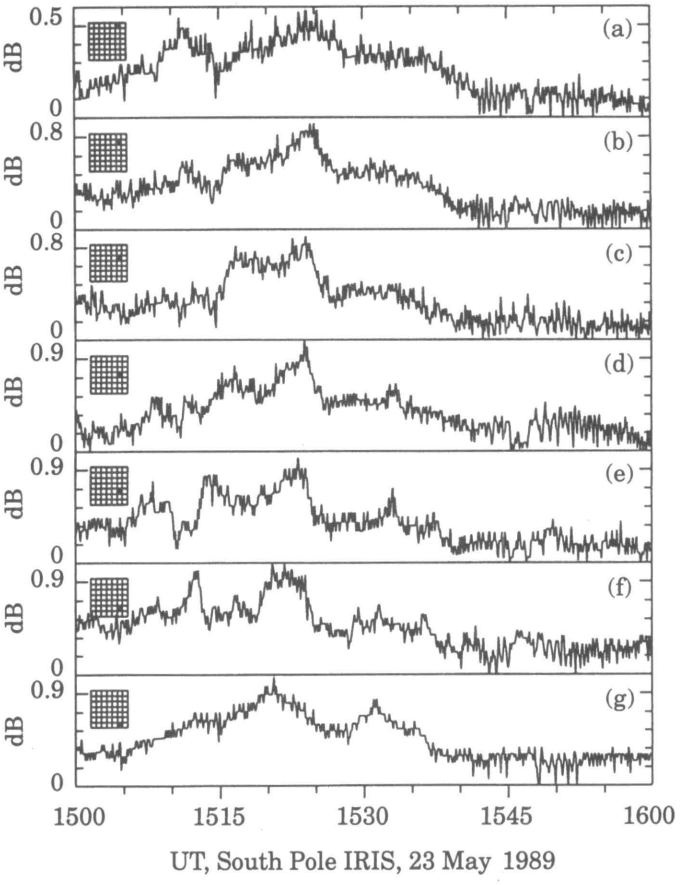

Figure 3. Absorption response in a column of IRIS beams oriented approximately along the geomagnetic south-north direction with south at the top. "dB" stands for decibels.

of 1.3 decibels shortly after the cusp has moved equatorward and beyond the field of view of the instruments at South Pole Station. This enhancement of riometer absorption, and earlier increases that occurred following the sudden commencement of a magnetic storm at 1346 universal time, are superimposed on a quasi-steady absorption level of 0.3 to 0.5 dB caused by solar-proton induced ionization.

This event and a number of others examined suggest that significant auroral absorption can occur on the dayside in the vicinity of the cusp in the apparent absence of electron precipitation with energies sufficient to cause the D-region ionization enhancements to which riometer absorption is usually attributed. In fact, other case studies (Wang et al. 1991, 1992) support the contention that the riometer response is caused by F-region absorption associated with a plasma patch formed in the cusp and propagating into the polar cap. Some evidence for this, in the event of figure 2, is suggested in figure 3 by the absorption variations observed along a south-north oriented set of riometer beams from the IRIS (Imaging Riometer for Ionospheric Studies) instrument at South Pole Station (Detrick and Rosenberg 1990). The signal variations are increasingly shifted to later times as the perturbed region moves poleward (from the bottom to the top panel).

We thank our colleagues K. B. Baker of the Applied Physics Laboratory/Johns Hopkins University and J. R. Dudeney and A. Rodger of the British Antarctic Survey for their analysis and interpretation of the Halley PACE radar data and P. T. Newell, also of APL/JHU, for contributing information on cusp location from the DMSP satellite data. This research was supported by National Science Foundation grant DPP 88-18229.

References

Baker, K. B., R. A. Greenwald, J. M. Ruohoniemi, J. R. Dudeney, M. Pinnock, P. T. Newell, M. E. Greenspan, and C. I. Meng. 1990. Simultaneous HF radar and DMSP observations of the cusp. *Geophysical Research Letters*, 17:1,869-1,872.

Crooker, N. 1990. *Geospace Environment Modeling Workshop Report on Intercalibrating Cusp Signatures.* Weston, Massachusetts: Northeastern University.

Detrick, D. L. and T. J. Rosenberg. 1988. IRIS: An imaging riometer for ionospheric studies. *Antarctic Journal of the U.S.*, 23(5):196-198.

Newell, P. T. and C. I. Meng. 1988. The cusp and the cleft/boundary layer: Low altitude identification and statistical local time variation. *Journal of Geophysical Research*, 93:14,549-14,556.

Rosenberg, T. J. 1989. *Geospace Environment Modeling Report of the Workshop on Ionosphere Signatures of Cusp, Magnetopause and Boundary Layer Processes.* College Park, Maryland: University of Maryland.

Wang, Z., D. L. Detrick, and T. J. Rosenberg. 1992. Imaging riometer measurements of F-region electron density structures. *Antarctic Journal of the U.S.*, 26(5):298-301.

Wang, Z., T. J. Rosenberg, P. Stauning, S. Basu, and Y. Zambre. 1992. Riometer absorption associated with F-region plasma structures: Observations and calculations. *Eos Transactions*, American Geophysical Union, 73(14):266.

Meteorological observations unique to the South Pole

G. Hernandez

Graduate Program in Geophysics
University of Washington
Seattle, Washington 98195

R. W. Smith

Geophysical Institute
University of Alaska
Fairbanks, Alaska 99775-0800

D. J. Belinne

Antarctic Service Associates
Englewood, Colorado 80112

Optical measurements of the meteorology of the upper atmosphere are regularly made near the South Pole at Amundsen-Scott Station in order to provide an understanding of the properties and behavior of this region of the atmosphere at high latitudes. Specifically, the natural radiation from hydroxyl (OH) molecular species at an altitude near 87 kilometers (Witt et al. 1979) is used as a tracer for the motion and temperature of the mesosphere. The motions and temperatures are determined from measurements of the Doppler shift and width of the $P_1(2)$ line of the hydroxyl emission at 8400 angstroms, using a high-resolving-power Fabry-Perot spectrometer (Hernandez 1988).

We obtained the measurements of the upper atmosphere during the austral winters of 1991 and 1992. The observations made during the month of August 1991 are typical of the results obtained at Amundsen-Scott Station and will be used here to illustrate the observed behavior. These observations are made by sequential examination of the sky, at an elevation of 30° above the horizon, in eight directions 45° apart in longitude, starting at 30° geographical longitude. A local zenith observation is made after the eight azimuths observations. Effectively, these observations provide information on the winds and temperatures of the mesosphere at 87-kilometer altitude at a distance of 1.5° away in latitude from the South Pole.

Figure 1 shows the observed winds and temperatures at 87 kilometers for the first 500 hours of measurement during August 1991. This figure shows the wind observations at 210° longitude and illustrates the short- and long-term variations in both the winds and temperatures. A modified power spectral analysis, or periodogram (Lomb 1976; Scargle 1982), of the winds and temperatures for this period shows the presence of statistically significant winds at a number of frequencies; however, unexpectedly, the winds are not accompanied by significant variations of the temperature at the same frequency. An example of this behavior is given in figure 2 for the power spectral analysis in the frequency near 0.1/hour or 10.1 hour periodicity. In addition, the time when maximum wind occurs at a given longitude, or phase progression, indicates that the observed motions consist of the effects of a single wave motion rotating in the zonal direction

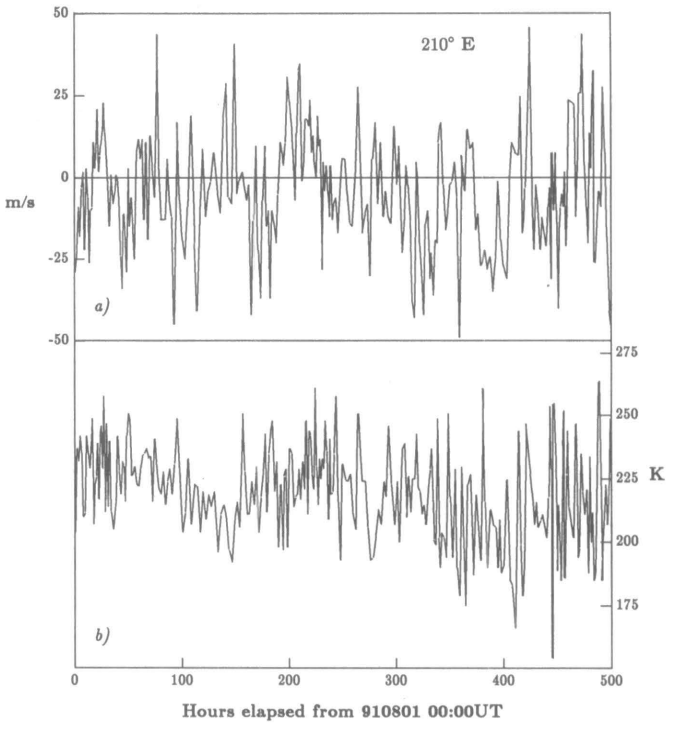

Figure 1. South Pole optical data determined in the 210° E longitude direction: (*A*) Wind; (*B*) kinetic temperature. The data series cover the first 500 hours of measurements for the period 1 August 1991 to 25 August 1991.

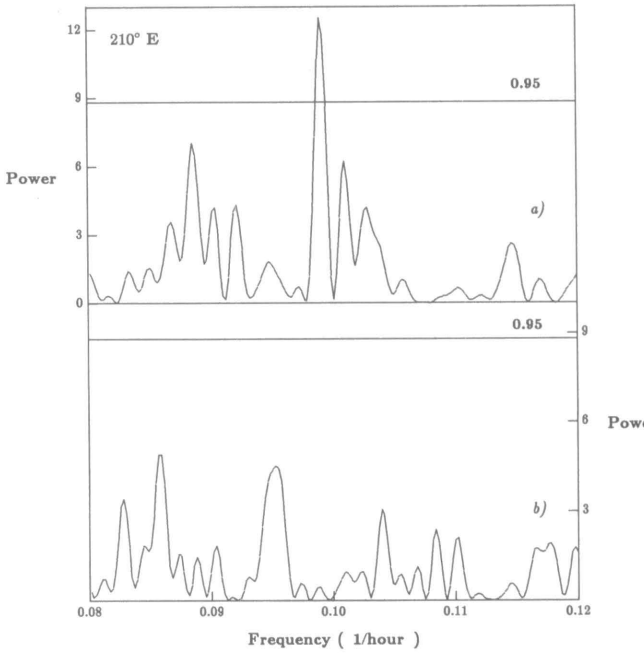

Figure 2. Lomb-Scargle periodogram for the South Pole data of figure 1: (*A*) The neutral motions; (*B*) the kinetic neutral temperature. The periodicities covered by the frequency scale are from 13.33-hour to 8.0-hour. Null-hypothesis 95-percent significance levels are indicated in both panels.

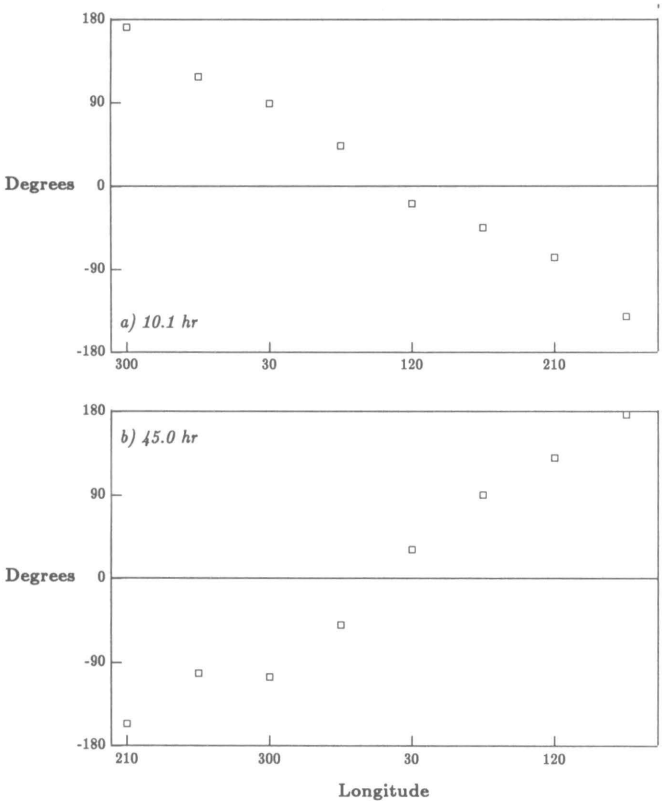

Figure 3. (*A*) Phase progression of the 10.1-hour oscillation observed at the South Pole as a function of azimuth; (*B*) same as (*A*), except for the 45-hour oscillation.

about the South Pole once per period, or a wavenumber one oscillation. Figure 3 shows this behavior, with the time normalized as longitude. Note that the 10.1-hour periodicity wave progresses westward while the 45-hour periodicity wave progresses eastward, but in both cases the phase progression indicates a wavenumber one, or one maximum (at a given longitude) per period.

The absence of other wavenumber waves, other than wavenumber one, indicates that the usual atmospheric oscillations (Andrews et al. 1987), such as the strong 12-hour periodicity zonal wavenumber two tides found elsewhere (Forbes 1982), have nearly vanished near the geographic pole. Examination of the behavior of waves near the geographic poles shows there is a fundamental reason for the absence of high-wavenumber motions at these locations (Hernandez et al. 1992). This can be done by expansion of the variables in a power series in $\sin\theta$, where θ is the co-latitude, and substitution into the linearized equations for the wave motions; the leading terms of the equations show the behavior close to the poles. If s is the zonal wavenumber, then near the poles the pressure and temperature will vary as $(\sin\theta)^s$, and only for zonal wavenumber zero they can be large; physically, they cannot vary with longitude without being discontinuous at the poles. On the other hand, horizontal winds vary as $(\sin\theta)^{|s-1|}$, and zonal wavenumber one winds will be observed at the poles. A wind that is continuous and blows across the poles resolves into a wavenumber one component. Therefore, tidal winds for which the predominant zonal modes have wavenumber two would be negligible at the poles and increase with distance away from them (Hernandez et al. 1992).

This result is of general application to neutral atmospheric wave motions in the neighborhood of the geographic poles, and it is independent of pressure level, or height. Our mesospheric observations have brought to light this general global property of the high-latitude atmospheric motions; they indicate the uniqueness of the Amundsen-Scott Station for meteorological and upper atmosphere investigations.

This investigation was supported by National Science Foundation grants DPP 90-17484 and ATM 89-22206.

References

Andrews, D. G., J. R. Holton, and C. B. Leovy. 1987. *Middle Atmosphere Dynamics*. Orlando, Florida: Academic Press.

Forbes, J. M. 1982. Atmospheric tides 2. The solar and lunar semidiurnal components. *Journal of Geophysical Research*, 87:524-552.

Hernandez, G. 1988. *Fabry-Perot Interferometers*. Cambridge: Cambridge University Press.

Hernandez, G., R. W. Smith, G. J. Fraser, and W. L. Jones. 1992. Large-scale waves in the upper atmosphere at antarctic high-latitudes. *Geophysical Research Letters*, 19:1,347-1,350.

Lomb, N. R. 1976. Least-squares frequency analysis of unequally spaced data. *Astrophysics and Space Science*, 39:447-462.

Scargle, J. D. 1982. Studies in astronomical time series analysis.II. Statistical aspects of spectral analysis of unevenly spaced data. *Astrophysical Journal*, 263:835-853.

Witt, G, J. Stegman, B. H. Solheim, and E. J. Llewellyn. 1979. A measurement of the O_2 atmospheric band and the OI(^{1}S) green line in the nightglow. *Planetary and Space Sciences*, 27:341-350.

South Pole anisotropy measurements of the cosmic microwave background radiation at 1 degree using a 25-35 gigahertz (GHz) HEMT receiver

JOSHUA GUNDERSEN, JEFFREY SCHUSTER, AND TODD GAIER

Department of Physics
University of California
Santa Barbara, California 93106

Anisotropy measurements of the cosmic microwave background radiation (CMBR) provide a critical test for cosmological theories and have been placing ever greater constraints on theories of large-scale structure formation in the universe. Recently, significant levels of anisotropy have been found in the large angular scale measurements from the Cosmic Background Explorer (COBE) satellite's differential microwave radiometer (DMR) experiment (Smoot et al. 1992). Measurements at smaller angular scales are of special interest since they provide a probe of large-scale structures that could have formed inside the horizon size of the universe at the time of decoupling, roughly a few hundred thousand years after the Big Bang. Figure 1 shows the recent upper limits on CMBR anisotropies, including our 1988-1989 and 1990-1991 South Pole results, and the COBE DMR detection.

During the austral summer of 1990-1991 we took three instruments to the South Pole Station to study anisotropy in the CMBR. These three instruments were designed to measure anisotropies in the CMBR at seven different frequencies, ranging from 15 gigahertz (GHz) to 90 GHz, and at 3 different angular scales ranging from 30 minutes to 10 degrees. The most sensitive data has come from the four channel homodyne receiver, shown in figure 2, which incorporates an ultralow noise High Electron Mobility Transistor (HEMT) for direct amplification of the CMBR between 25 and 35 GHz (8-12 millimeters). The HEMT amplifier is cooled to 6 K in a ^{4}He cryostat and operates with a receiver noise temperature of 30 K. The signal is detected full band and is also split into four 2.5 GHz bands using an array of circulators and bandpass filters. This type of multifrequency measurement is necessary in order to discriminate between intrinsic CMBR fluctuations and confusing foreground sources.

This receiver was coupled to the Advanced Cosmic Microwave Explorer (ACME) platform, which is a 1-meter, off-axis Gregorian telescope with a nutating elliptical secondary capable of arc minute stabilization (Meinhold et al. 1991). The nutating secondary moves the microwave beam back and forth on the primary creating a sinusoidally chopped beam response on the sky. The total power measured in one beam position is then subtracted from the measured power in the other beam position and the difference is then integrated over a complete nutation cycle. When the 25-35 GHz system is in place on ACME, the beam width ranges between 1.3 degrees and 1.8 degrees at full width at half maximum (FWHM). The beam throw of the nutating elliptical secondary was 2.1 degrees on the sky. We observed for 500 hours between 16 December 1990 and 12 January 1991. From this 500 hours of data, 250 hours were considered usable. Much of the unusable data was removed due to weather/atmosphere or other systematic cuts that we implemented. During the 250 hours we performed sun scans, to check our beam, moon scans to check the calibration, galaxy scans to characterize galactic emission, zenith scans to characterize the atmosphere, and a variety of overlapping, deep CMBR scans to measure anisotropies.

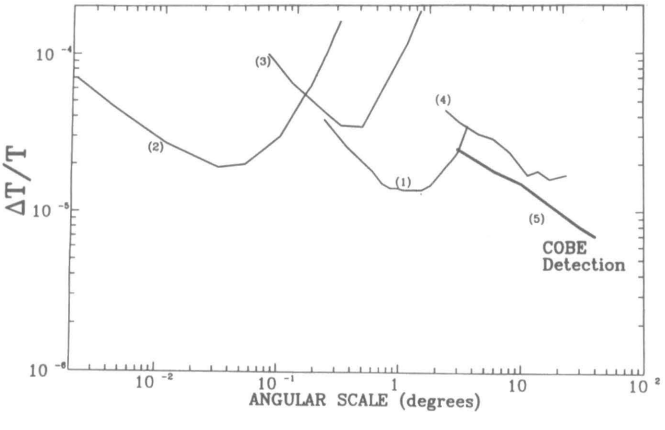

Figure 1. Gaussian autocorrelation limits on anisotropy in the Cosmic Microwave Background Radiation and the COBE detection. (1) Gaier et al. South Pole 1990-1991 (2) Readhead et al. 1989 (3) Meinhold and Lubin, South Pole 1988-1989 (4) Meyer, Cheng, and Page 1991 (5) Smoot et al. 1992.

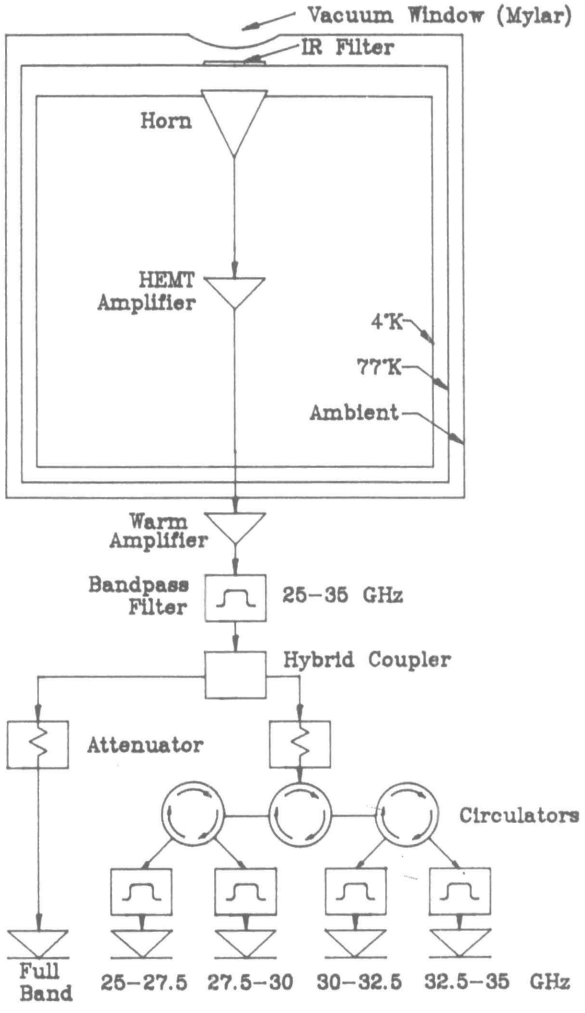

Figure 2. Schematic of the 25-35 gigahertz HEMT receiver.

The network of deep CMBR scans consisted of a raster scan of 9 positions in azimuth, each position separated by 2.1 degrees on the sky, repeated at six elevations, each separated by 45 minutes in declination. In addition, we performed an overlapping 13-point scan in azimuth at the lowest declination and an overlapping 15-point scan in azimuth at the second to highest declination. Each of these eight scans in azimuth obtained data with error bars less than 50 microkelvin (μK) per channel and two of the scans have error bars between 20 and 30 μK per channel. This compares to our 1988-1989 South Pole data, which had a single channel and a single scan with 50 μK error bars and compares to COBE's DMR which has obtained 50 μK error bars in its most sensitive pixels for its 53 GHz channel. The 1990-1991 measurements represent the most sensitive measurements of CMBR anisotropy to date.

The data from one of the elevations in the nine point raster scan has been analyzed in detail, as shown in figure 3. The lower frequencies have strong detections present, while the higher frequencies do not. This type of spectrum is not indicative of CMBR fluctuations. The 32.5-35 GHz channel imply a 95 percent confidence upper limit of $\Delta T/T \leq 1.4 \times 10^{-5}$ for gaussian fluctuations in the CMBR, shown in figure 1. This represents a factor of 7 improvement over previous limits at the angular scale $\theta_c = 1.2°$ (Timbie and Wilkinson 1990). The details of the analysis are presented in Gaier et al. 1992. Work is proceeding on the analysis of the rest of the raster scan region and the adjoining larger 13 and 15 point scans.

This project would have not been possible without the Center for Particle Astrophysics and the support and encouragement of Bernard Sadoulet. The remarkable cryogenic HEMT amplifier was supplied by Mike Balister and Marian Pospiezalski at NRAO. This work was supported by National Science Foundation grant DPP 89-20578, the National Aeronautics and Space Administration under grant NAGW-1062, and the National Science Foundation's Center for Particle Astrophysics under grant NSF UCB AST88-0916. Much of the hands-on support came from other members of our lab group including Dr. Peter Meinhold, Tim Koch, Mike Seiffert, Mark Lim, Alex Wuensche, and Dr. Philip Lubin. Finally we would like to thank Bill Coughran and the entire Antarctic Support Associates staff for their work at the South Pole during the 1990-1991 austral summer.

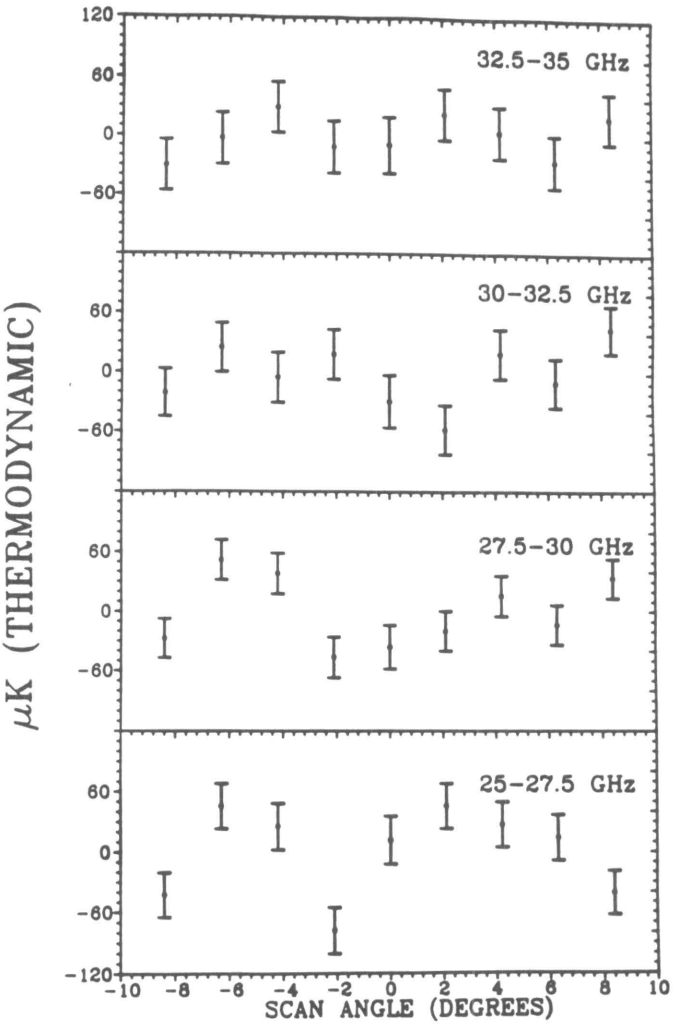

Figure 3. Binned data for the 25-35 gigahertz HEMT receiver from the nine-position scan centered at a = 0.5^h, d = -62.25°. A linear component has been removed as a function of scan position. The error bars displayed are ± 1 σ.

References

Gaier, T., J. Schuster, J. Gundersen, T. Koch, P. Meinhold, M. Seiffert, and P. Lubin. A degree scale measurement of anisotropy of the cosmic background radiation. *Astrophysical Journal Letters*, submitted.

Meinhold, P. and P. Lubin. 1991. A medium scale measurement of the cosmic microwave background at 3.3 millimeters. *Astrophysical Journal Letters*, 370:L11.

Meinhold, P., A. Chingcuanco, J. Gundersen, J. Schuster, P. Lubin, D. Morris, and T. Villela. 1991. A balloon borne millimeter-wave telescope and stabilized platform for measurements of anisotropy in the cosmic background radiation. *Astrophysical Journal*, submitted.

Meyer, S., E. Cheng, and L. Page. 1991. A measurement of the large scale cosmic microwave background anisotropy at 1.8 millimeter wavelength. *Astrophysical Journal Letters*, 371:17.

Readhead, A., C. Lawrence, S. Myers, W. Sargent, H. Hardebeck, and A. Moffett. 1989. A limit on the anisotropy of the microwave background radiation on arc minute scales. *Astrophysical Journal*, 346:566.

Smoot, G., C. Bennett, A. Kogut, E. Wright, J. Aymon, N. Boggess, E. Cheng, G. DeAmici, S. Gulkis, M. Hauser, G. Hinshaw, C. Lineweaver, K. Loewenstein, P. Jackson, M. Janssen, E. Kaita, T. Kelsall, P. Keegstra, P. Lubin, J. Mather, S. Meyer, S. Moseley, T. Murdock, L. Rokke, R. Silverberg, L. Tenorio, R. Weiss, and D. Wilkinson. 1992. Structure in the COBE DMR First Year Maps. *Astrophysical Journal Letters*, submitted.

Timbie, P. and D. Wilkinson. 1990. A search for anisotropy in the cosmic microwave radiation at medium angular scales. *Astrophysical Journal*, 353:140.

Cosmic ray trajectories in the Tsyganenko magnetosphere

JOHN W. BIEBER, PAUL EVENSON, AND ZHONGMIN LIN

Bartol Research Institute
University of Delaware
Newark, Delaware 19716

The cosmic rays impacting earth do not arrive with equal intensity from all directions. Rather, the flow of cosmic rays in earth's vicinity is anisotropic to a degree ranging from the hundredths of percent level in some components of the steady-state galactic anisotropy to highly anisotropic, beamlike distributions observed during some solar energetic particle events. With suitable analysis, the detailed character of measured anisotropies can serve as a sensitive probe of cosmic-ray transport and scattering processes in the local interplanetary medium (Bieber, Evenson, and Pomerantz 1986; Bieber and Chen 1991).

In order to analyze anisotropies detected with ground-based instrumentation, one must take account of the effect of the geomagnetic field and magnetosphere. Generally one is interested in the "asymptotic direction" of the particle, i.e., its direction of approach before it encountered earth's magnetosphere. To determine asymptotic direction, the particle's trajectory is numerically traced backwards through a model magnetosphere until it crosses the magnetopause. The results of such computations are available in the form of tables such as those presented by Gall et al. (1982), which list asymptotic directions for vertically incident particles as a function of station location, particle rigidity, and time of day. The use of tables, however, necessarily involves a number of compromises. For example, the Gall et al. tables are computed only for a geodipole "tilt angle" (the instantaneous angle between earth's magnetic dipole and a plane oriented normal to the earth-sun direction) of zero, and they take no account of varying levels of geomagnetic activity. Furthermore, one must invariably interpolate between table entries when analyzing actual data. The present paper describes our efforts to eliminate the need for such tables through implementation of an accurate trajectory-tracing code in a realistic new model of earth's magnetosphere.

The Tsyganenko magnetosphere. Our trajectory code employs the most recent and comprehensive of the global quantitative magnetosphere models developed by Tsyganenko (1989; private communication 1992). Independent studies by Flückiger et al. (1991) have concluded that the Tsyganenko model significantly improves the reliability of geomagnetic corrections for ground-based cosmic ray data. We combine Tsyganenko's representation of the external field with the International Geomagnetic Reference Field for epoch 1990 to represent the contribution of earth's internal field. We employ the correct value of the geodipole tilt angle as a function of season and time of day. The Tsyganenko model accommodates varying levels of geomagnetic activity by providing seven (in the most recent version) independent parameter sets corresponding to different ranges of the geomagnetic Kp index, a readily available, global index of the level of geomagnetic disturbance .

Figure 1 illustrates the configuration of the Tsyganenko magnetosphere at two different times on 22 October 1989. The tilt angle is near 0° in panel *a* and near -22° in panel *b*. In both panels

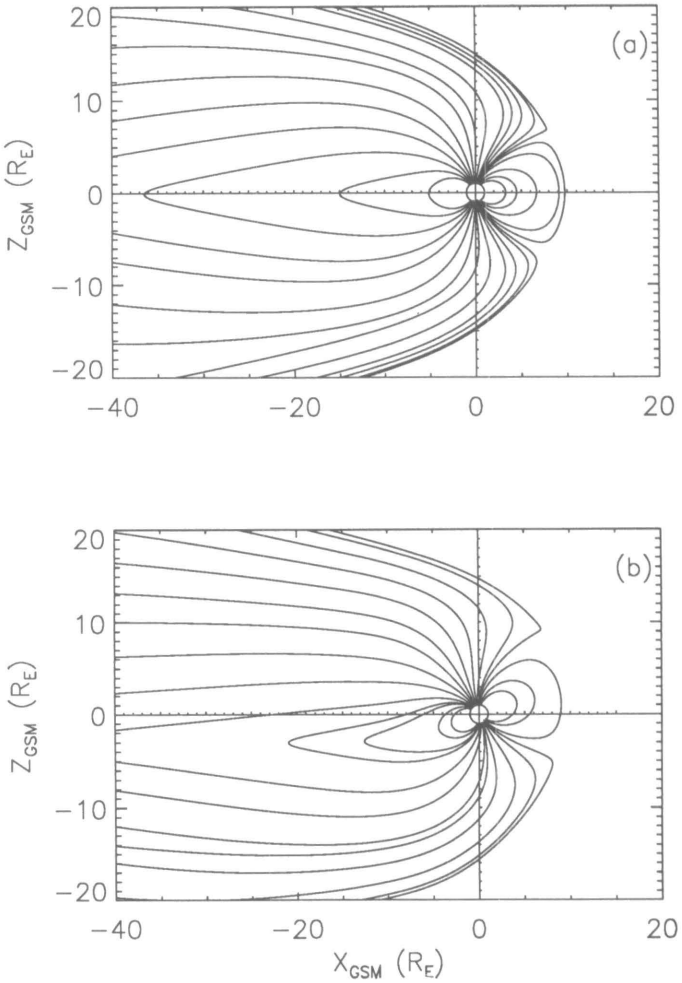

Figure 1. Depiction of magnetic field lines in the Tsyganenko model of earth's magnetosphere on 22 October 1989 (*A*) at 1800 universal time when the dipole tilt angle was near zero, and (*B*) at 0400 universal time when the dipole tilt angle was -22.4 degrees. Both plots show results for high (Kp = 5) geomagnetic activity and display field lines in the noon-midnight meridional plane of the geocentric solar magnetospheric (GSM) coordinate system. The sun is to the right, and the units are earth radii (R_E).

the solar wind flow, coming from the right, compresses the magnetic field on the dayside of earth and stretches the field into a tail-like configuration on the nightside. As earth rotates, the cosmic rays incident on a given location must pass through different regions of this highly asymmetric configuration. Hence, the asymptotic directions will be a function of the time of day.

Asymptotic directions: dependence on geomagnetic activity and time of day. Figure 2 displays on a map of earth's surface the asymptotic longitude and latitude of protons arriving vertically over South Pole, as computed from the Tsyganenko model. Results are shown for two different levels of geomagnetic activity at 3-hour intervals of universal time. The proton rigidity is 10^9 volts, corresponding to an energy of 433 million electron volts.

The inner trace, which represents low geomagnetic activity (Kp = 0), is reasonably consistent with the tabulated results of Gall et al. (1982). As the day progresses, the asymptotic direction traces a roughly circular pattern in a counter-clockwise direction. Qualitatively similar behavior occurs for high geomagnetic activity (Kp = 5), shown by the outer trace, but the universal time dependence is considerably greater. Between 0300 and 1800 hours universal time, for example, the asymptotic latitude ranges

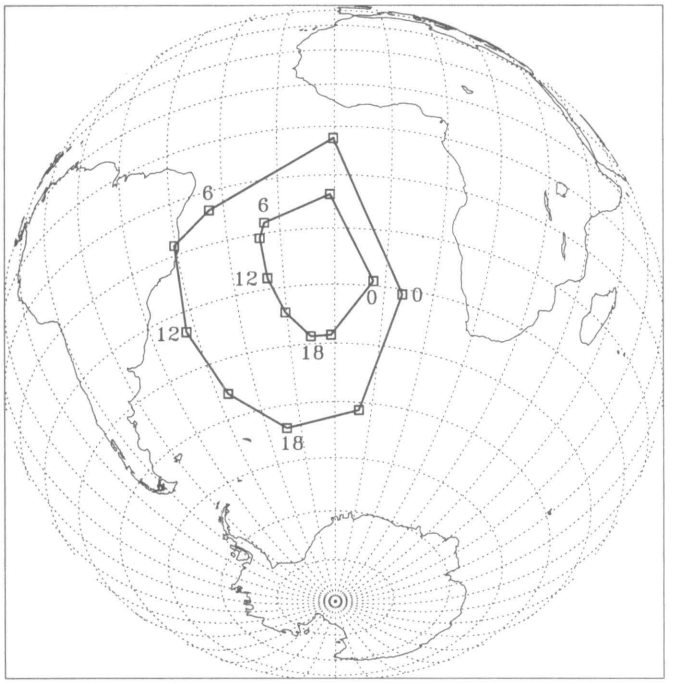

Figure 2. Time dependence of the asymptotic direction of protons with rigidity 10^9 volts arriving vertically over the South Pole on 22 October 1989. Results are shown both for low geomagnetic activity (Kp = 0, inner trace) and high geomagnetic activity (Kp = 5, outer trace) using the Tsyganenko model of the magnetosphere. Squares display results at 3-hour intervals and are labeled in hours universal time.

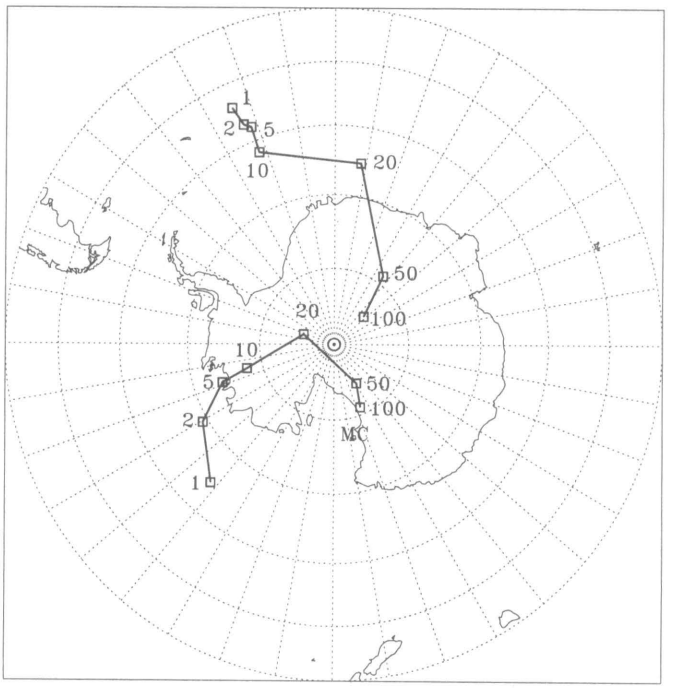

Figure 3. Rigidity dependence of the asymptotic direction of protons arriving vertically over the South Pole (upper trace) and McMurdo (lower trace) at 1800 hours universal time on 22 October 1989. Squares display results for different rigidities and are labeled in units of 10^9 volts. The computation employed the Tsyganenko model for the correct (Kp = 5+) level of geomagnetic activity at this time. "MC" denotes the location of McMurdo Station.

over 25° during low geomagnetic activity and over 51° during high activity.

Asymptotic directions: dependence on particle rigidity. The variation of asymptotic direction with particle rigidity is illustrated in figure 3 for protons vertically incident over South Pole (upper trace) and McMurdo stations (lower trace). The time displayed is 1800 universal time on 22 October 1989, which is when a huge, anisotropic "spike" of solar cosmic rays was observed by neutron monitors at these two stations (Bieber, Evenson, and Pomerantz 1990a,b). The plot employs the Tsyganenko model with Kp = 5+, which is the level of geomagnetic activity actually measured at this time.

We see that the asymptotic direction gradually approaches the station position as the particle rigidity increases. This is as expected, since the highest energy particles experience the least amount of deflection in the geomagnetic field. Comparing with figure 2, we see that the time of day and the geomagnetic activity level conspired to push the South Pole viewing direction unusually far south at the time of the 22 October 1989 solar particle event, an important point to consider in modeling this highly unusual event. In summary, we conclude that use of the Tsyganenko magnetosphere model in particle trajectory-tracing codes will significantly advance our capability to make high accuracy measurements of cosmic ray anisotropies.

This work was supported by National Science Foundation grants DPP 88-18586 and ATM-9014806.

References

Bieber, J. W. and J. Chen. 1992. A three-dimensional perspective on cosmic ray anisotropies. *Antarctic Journal of the U.S.,* 26(5):305-306.

Bieber, J. W., P. A. Evenson, and M. A. Pomerantz. 1986. Focusing anisotropy of solar cosmic rays. *Journal of Geophysical Research,* 91(A8):8,713-8,724.

Bieber, J. W., P. Evenson, and M. A. Pomerantz. 1990a. A barrage of relativistic solar particle events. *EOS Transactions,* American Geophysical Union, 71(33):1,027-1,035.

Bieber, J. W., P. Evenson, and M. A. Pomerantz. 1990b. Unusual cosmic ray spike. *Antarctic Journal of the U.S.,* 25(5):277-278.

Flückiger, E. O., E. Kobel, D. F. Smart, and M. A. Shea. 1991. A new concept for the simulation and visualization of cosmic ray particle transport in the earth's magnetosphere. *Proceedings 22nd International Cosmic Ray Conference* (Dublin), 3:648-651.

Gall, R., A. Orozco, C. Marin, A. Hurtado, and G. Vidargas. 1982. Tables of approach directions and points of entry of cosmic rays for higher latitude cosmic rays stations. Mexico City: Universidad Nacional Autonoma de México, 1982.

Tsyganenko, N. A. 1989. A magnetospheric magnetic field model with a warped tail current sheet. *Planetary and Space Science,* 37: 5-20.

Flight of the MAGPIE: Measuring the isotopic composition of the cosmic ray ion group

M. H. Salamon, J. W. DeFord, and S. Rice

Physics Department
University of Utah
Salt Lake City, Utah 84112

S. P. Ahlen and D. Loomba

Physics Department
Boston University
Boston, Massachusetts 02215

We designed the Magnetic Passive Isotope Experiment (MAGPIE) to measure the isotopic composition of the iron-group nuclei (manganese through nickel) in the cosmic radiation within the energy interval 0.1-1.0 billion electron volts per nucleon (Salamon et al. 1991). Given large statistics and sufficient mass resolution, such a measurement would yield rich information on the nucleosynthesis, acceleration, and propagation of nuclear cosmic rays within our galaxy.

It is believed that first-order Fermi acceleration at supernova shock fronts is responsible for the acceleration of most cosmic rays (Ellison et al. 1990). It is not known, however, whether the source material is the ejecta of supernovae, whose strong shock fronts promptly accelerate the freshly synthesized cosmic rays, or instead is simply several-billion-year-old interstellar matter that is entrained and accelerated by passing shock fronts. Measurements of the elemental abundances in the cosmic rays provide only limited information on this and other outstanding questions in particle astrophysics, as various atomic selection effects may significantly alter the observed elemental composition (Meyer 1985). Isotopic abundance measurements within a given element are relatively free from these distortions and provide additional data which can further constrain models of synthesis and acceleration.

The iron-group nuclei are particularly informative in this regard, as their isotopic composition is very sensitive to the stellar-core environment just before and during stellar collapse, during which explosive nucleosynthesis of these nuclei occur (Woosley 1976). Should measured iron-group cosmic-ray isotopes be similar in composition to that of our solar system, then it is likely that the cosmic-ray source is interstellar matter that is undergoing slow chemical evolution. Should dramatic differences exist, then we are probably detecting fresh ejecta from supernovae, whose constitution would provide a new and exciting window on explosive nucleosynthesis.

A "smoking gun" that would prove that cosmic rays are freshly produced and accelerated in supernovae would be the observation of one or more of the electron-capture isotopes nickel-56, cobalt-57, and nickel-59 in the cosmic-ray iron-group. These isotopes decay via electron-capture but are stable against positron decay. With electron capture lifetimes of 6.1 days (nickel-56), 270 days (cobalt-57), and 80,000 years (nickel-59), these isotopes would have decayed long ago in the interstellar matter (Simpson 1983). Only if these isotopes were to be accelerated to relativistic energies very shortly after their synthesis, thereby stripping the nuclei of all their atomic electrons (preventing electron capture), could they survive without decay for periods comparable with the mean cosmic-ray propagation time of about 10 billion years. Detection of these rare (if extant) isotopes amidst populous neighboring mass peaks requires stringent mass resolution.

A number of cosmic-ray iron isotope experiments have been flown in the past (Leske et al. 1992), but none have achieved the mass resolution required for unambiguous identification of rare isotopes, which is roughly 0.2 atomic mass unit, or a fractional mass resolution of less than 0.4 percent. MAGPIE was designed

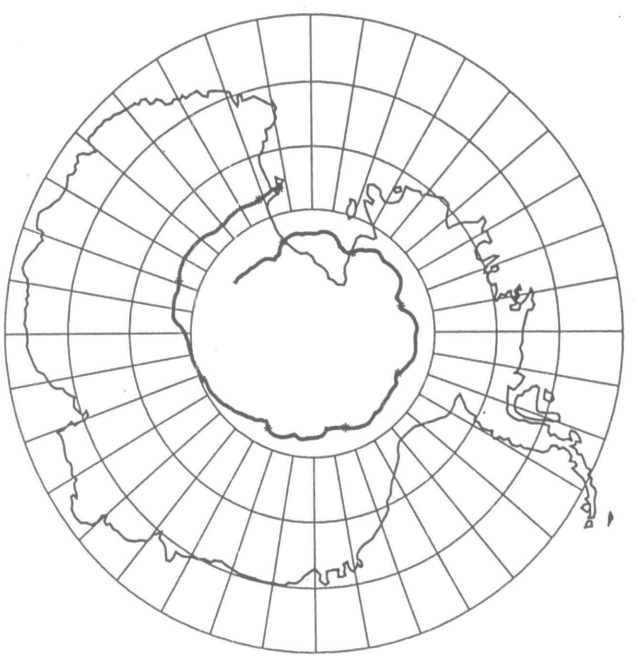

Figure 1. MAGPIE's flight path. From NASA presentation by H. Needleman of NASA/Wallops.

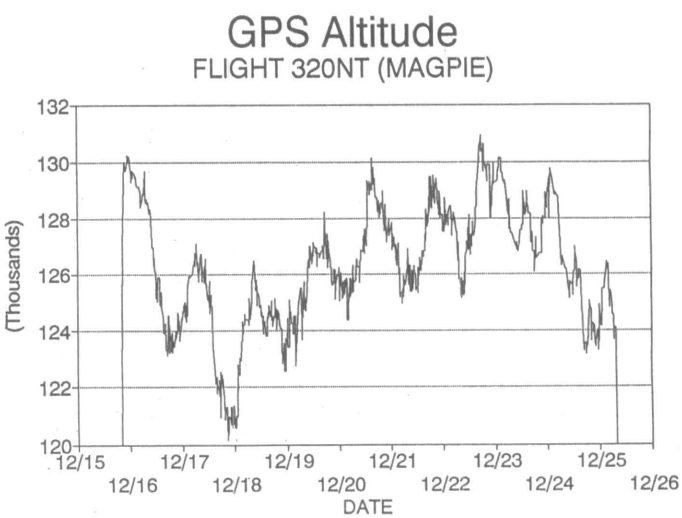

Figure 2. MAGPIE's altitude profile (thousands of feet). From R. Nock of NASA/Wallops.

to achieve this requisite mass resolution, with an event rate of about 100 iron-group cosmic-ray nuclei per day of flight. The instrument measures particle mass by determining its rigidity (momentum/charge) with a magnetic spectrometer, and particle charge and velocity with a range stack of about 200 sheets of nuclear-track-detecting plastic (CR-39, Ahlen et al. 1981). It is optimized to detect iron-group nuclei in the energy interval 0.1-1.0 billion electron volts per nucleon, in which region the cosmic-ray iron flux is maximal. (For such an experiment, being near one of the two geomagnetic poles is essential; at lower latitudes, the Earth's magnetic field acts as a rigidity filter, preventing lower energy cosmic rays from reaching the upper atmosphere. In this regard the Antarctic is an ideal location, as the cosmic-ray iron-group flux there is maximal. The magnetic spectrometer consists of a superconducting magnet with three sheets of CR-39 that act as particle hodoscopes. Rigidity is determined by measurement of the particle's trajectory curvature in the magnetic field to an accuracy of tens of microns. The thin (0.25 millimeter) sheets of CR-39 comprising the range stack detect highly ionizing particles (such as relativistic iron) by the polymer damage that occurs along the particle trajectory in the plastic (Fleischer et al. 1975). After etching in a solution of sodium hydroxide, microscopic "tracks" (etch pits) appear along particle trajectories on the plastic surface; measurement of their size gives the particle charge and velocity. By observing the slowing of the particle in the stack as it loses energy by ionization, one can uniquely determine both its charge and entry velocity. (As the particle slows, its ionization energy loss increases, producing larger track structures in the plastic.) About one million etch pits must be measured for this experiment; these will be analyzed by a fully automated microscope system with imaging hardware/software that is capable of automated track pattern recognition.

The Antarctic provides a unique opportunity to achieve long-duration balloon flights. Because the sun never sets in the austral summer season, balloons do not suffer usual day-night altitude loss of mid-latitude flights. Because the winds drive the payload into a circumpolar trajectory, flights do not have to be terminated prematurely as at mid-latitudes, when winds may carry payloads out to sea, over mountain ranges, or over populated areas. The net effect is that, in contrast to the one to two days of flight usual for mid-latitude launches, heavy payloads can now be kept aloft for one, two, or more weeks, thus dramatically increasing the statistical significance (and science return) of these balloon-borne experiments.

Our payload, with a scientific weight of 907.19 kilograms, was flown with a 8,991,600-meter balloon in December 1991 from Williams Field, near McMurdo Station in the Antarctic. It quickly reached its float altitude of about 3 grams per square centimeter, remaining for 9 days at this altitude before the flight was terminated, having made its planned single circumnavigation of the Pole. Figure 1 shows MAGPIE's flight path, and figure 2 its altitude profile. Had the superconducting magnet's dewar been designed for greater liquid helium storage, there is no indication in the altitude profile data that MAGPIE could not have flown for many more days. An initial attempt to recover the payload with a C-130 Hercules transport failed because of the very high altitude (3,505.2 meters) of the landing site on the glacial plateau. Recovery of the payload was finally achieved with two flights of a Twin Otter based at the South Pole.

Analysis of the data from the MAGPIE flight is presently under way. Chemical processing and microscopic measurement of the range stack data will take a little over one year, with new results on the cosmic-ray iron-group isotope composition being expected shortly afterwards.

We thank the field members of the National Scientific Balloon Facility and the National Aeronautic and Space Administration's long duration balloon group for their outstanding support. This research was supported by NASA Space Physics Division grant NAGW-1999 and National Science Foundation grant DPP 90-03850.

References

Ahlen, S. P. et al. 1992. Track recording solids. *Physics Today,* 34:32.

Ellison, D. C. et al. 1990. First order fermi particle acceleration by relativistic shocks. *Applied Journal,* 360:702.

Fleischer, R. L., P. B. Price, and R. M. Walker. 1975. *Nuclear tracks in solids.* University of California Press.

Leske, R. A. et al. 1992. The isotopic composition of iron-group cosmic rays. *Applied Journal,* 390:199.

Meyer, J. P. 1985. Solar-stellar atmospheres and energetic particles, and galactic cosmic rays. *Applied Journal Supplimental,* 57:173.

Salamon, M. H. et al. 1991. MAGPIE: A magnetic passive isotope experiment to measure the cosmic ray iron group isotope abundances. *Proceedings of the 22nd International Cosmic Ray Conference,* Dublin, Ireland, 2:583.

Simpson, J. A. 1983. Elemental and isotopic composition of the galactic cosmic rays. *Annual Review of Nuclear Particle Science,* 33:323.

Woosley, S. E. 1976. Importance of isotopic composition of iron in the cosmic rays. *Astrophyical Space Science,* 39:103.

Helioseismology from the South Pole: Surprises from near the solar surface

S.M. Jefferies and M.A. Pomerantz

Bartol Research Institute
University of Delaware
Newark, Delaware 19716

J.W. Harvey

National Solar Observatory
Tuscon, Arizona 85726

T.L. Duvall, Jr.

Laboratory for Astronomy and Solar Physics
National Aeronautics and Space Administration
Goddard Space Flight Center
Greenbelt, Maryland 20771

Helioseismology is the study of the properties of the solar interior through measurement of the sun's natural acoustic oscillations. These oscillations are observed at the solar surface as upward and downward motions and also as intensity variations. The periods of the ~10^7 various oscillations peak at 5 minutes but range from about 15 minutes to less than 3 minutes, and the spatial scales range from the entire solar circumference to about 1 megameter. Different oscillations probe different depths and latitudes of the interior. The oscillation spectrum is crowded, and accurate measurement requires good resolution in both temporal and spatial frequency. The South Pole is a uniquely advantageous site for obtaining helioseismology measurements because long-duration observations interrupted only by poor weather are possible during the austral summer. This advantage has been used frequently since 1979.

In our previous work, we used observations made during the austral summers of 1981, 1987, 1988, and 1990-1991 to probe the intermediate and deep solar interior. We studied the mean structure, asphericity, and rotation of the interior and variations of these quantities with the solar activity level. The same observations, surprisingly, provide information about conditions near the solar surface. A traditional helioseismic analysis of near-surface layers involves accurate measurements of the properties of small-spatial-scale waves. However, we found that high- and low-frequency waves of large and intermediate spatial scale also prove to be powerful diagnostics of conditions near the sun's surface.

At low frequencies, our observations of the solar oscillation spectrum show that spectral features associated with trapped modes are asymmetric in frequency (see figure 1). In collaboration with Y. Osaki (Tokyo University), we modeled this asymmetry after a Fabray-Perot etalon, familiar from optics. The observations can be reproduced if the acoustic source of the waves is quite shallow—about 50 kilometers below the visible surface. The asymmetry results from the interference of waves that travel directly from the source to the surface with those that travel downward, are trapped in an acoustic cavity, and are seen at the surface only as leakages from the cavity. Other investigations, some using our observations, have suggested that the source of the solar oscillations lies a few hundred kilometers deeper than our analysis indicates. An extensive discussion of this result is given by Duvall et al. (1992).

The early observations made after solar oscillations were discovered in 1962 were of small areas on the solar surface. Such

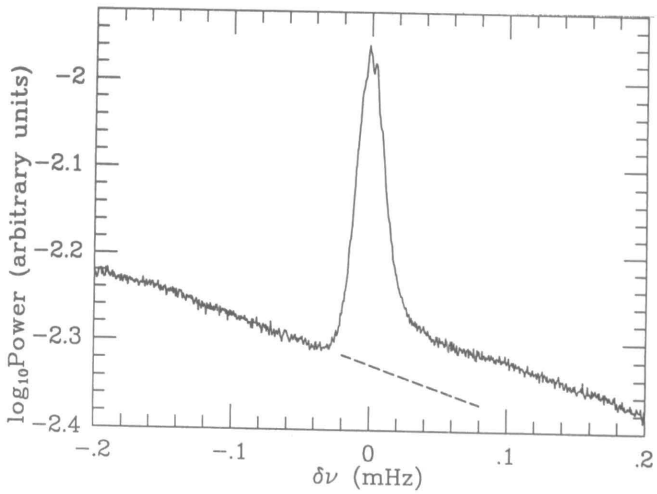

Figure 1. Asymmetry of the spectral line profile of solar oscillation modes (1988 South Pole data). This is the average power spectrum as a function of the frequency offset of modes of radial order 2, degrees 157-221, and all azimuthal orders. Line-center frequency offsets were removed before averaging. The asymmetry is indicated by the mismatch of the low- and high-frequency backgrounds. Fits to spectra of this sort indicate that the acoustic noise that generates the solar oscillations is located about 60 kilometers beneath the sun's surface.

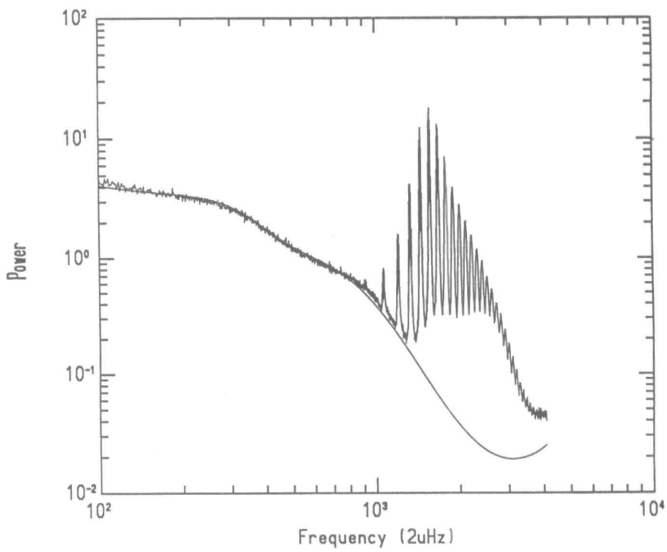

Figure 2. Evidence for 3-minute-period oscillations appears in this average power spectrum of solar oscillations for degrees 100-105 (1988 South Pole data). Abscissa units are 2 microhertz, and ordinates are arbitrary units. The 3-minute feature is the broad rightmost upward bump in the lower envelope of the oscillations (centered at 2500 on the abscissa scale). The smooth line is a model of the background due to nonperiodic solar fluctuations and instrumental noise.

observations made higher and higher in the solar atmosphere showed a change in the dominant period from 5 minutes toward 3 minutes. One explanation of this is that a resonant cavity (with a characteristic period of 3 minutes) exists in the atmosphere above the solar surface (Leibacher and Stein 1971). This cavity was calculated to be quite different from the one that traps waves beneath the surface. Other explanations have also been offered (e.g., Fleck and Schmitz 1991; Worral 1991). It has been surprising that the more recent helioseismic observations of large areas of the solar surface have showed no evidence for existence of the 3-minute-period oscillations (e.g., Woodard and Libbrecht 1991; Fernandes et al. 1992). This puzzle is now solved by our observations, which clearly show a broad 3-minute-period spectral feature (Harvey et al 1992). The surprise, and one reason that it was elusive in recent observations, is that it affects the spectral background more strongly than the average or peak spectral power levels (see figure 2).

Additional studies of near-surface conditions using our observations include first measurements of phase shifts associated with the absorption of wave energy by sunspots (Braun et al. 1992a) and surprising indications of subsurface magnetic structures (Braun et al. 1992b). The latter result offers the possibility (if the first results are confirmed) of predicting where and when activity may erupt onto the solar surface.

This work was supported in part by National Science Foundation grant DPP 89-17626, the Solar Physics Branch of the Space Physics Division of the National Aeronautics and Space Administration, and the National Solar Observatory.

References

Braun, D. C., T. L. Duvall, Jr., B. J. LaBonte, S. M. Jefferies, J. W. Harvey, and M. A. Pomerantz. 1992a. Scattering of p-modes by a sunspot. *Astrophysical Journal*, 391:L113.

Braun, D. C., C. A. Lindsey, Y. Fan, and S. M. Jefferies. 1992b. Local acoustic diagnostics of the solar interior. *Astrophysical Journal*, 392:739.

Duvall, T. L., Jr., S. M. Jefferies, J. W. Harvey, Y. Osaki, and M. A. Pomerantz. 1992. Asymmetries of solar oscillation line profiles. *Astrophysical Journal*, submitted.

Fernades, D. N., P. H. Scherrer, T. D. Tarbell, and A. M. Title. 1992. Observations of high frequency and high wavenumber solar oscillations. *Astrophysical Journal*, 392:736.

Fleck, B. and F. Schmitz. 1991. The 3-min oscillation of the solar chromosphere: A basic physical effect? *Astronomy and Astrophysics*, 250, 235.

Harvey, J. W., S. M. Jefferies, M. A. Pomerantz, and T. Duvall, Jr. 1992. Global observations of chromospheric oscillations. *Bulletin of the American Astronomical Society*, 24:753.

Leibacher, J. W. and R. F. Stein. 1971. A new description of the solar five-minute oscillation. *Astrophysics Letters*, 7:191.

Woodard, M. F. and K. G. Libbrecht. 1991. Is there an acoustic resonance in the solar chromosphere? *Astrophysical Journal*, 374:161.

Worral, G. 1991. Oscillations of the solar atmosphere: The 5-min peak as a consequence of wave reflection at the photosphere. *Monthly Notices of the Royal Astronomical Society*, 251:427.

Automatic geophysical observatories prepared for the polar cap network

JOHN H. DOOLITTLE

Lockheed Palo Alto Research Laboratory
Palo Alto, California 93404

Deployment of a network of six unmanned automatic geophysical observatories (AGOs) is planned on the antarctic polar plateau. Coordinated investigations of the high-latitude ionosphere and magnetosphere will be carried out by several identical experiments operated synchronously at each site. A consortium of institutions has responsibility for the experiments, including a fluxgate magnetometer (AT&T Bell Laboratories), a search-coil magnetometer (Tohoku University), a very-low-frequency receiver (Stanford University), a low-frequency/high-frequency receiver (Dartmouth College), an imaging riometer (University of Maryland), and an auroral all-sky camera (Lockheed Palo Alto Research Laboratory). To support flight operations, weather measurements, including air temperature, wind speed and direction, and barometric pressure, will be made available in near real time through the ARGOS satellite data-retrieval system.

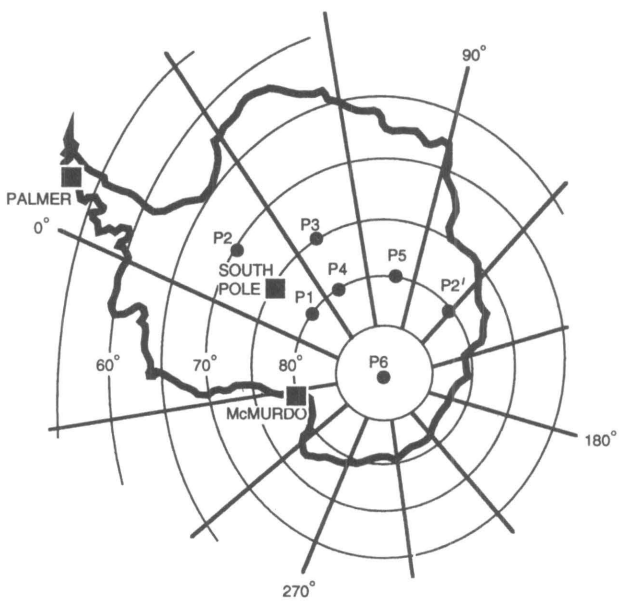

Figure 1. Planned locations of the six AGOs shown in invariant geomagnetic coordinates. The geographic coordinates are (P1) 83.9 S 130.1 E; (P2) 85.7 S 46.5 W; (P3) 82.8 S 47.5 E; (P4) 82.0 S 97.2 E; (P5) 75.7 S 89.2 E; and (P6) 74.1 S 128.8 E. At a later date, one AGO may be moved to (P2') 69.5 S 98.8 E.

Figure 2. The AGO shelter was designed to take advantage of the carrying capacity of the LC-130 Hercules aircraft. Field deployment and recovery is done without tractor support.

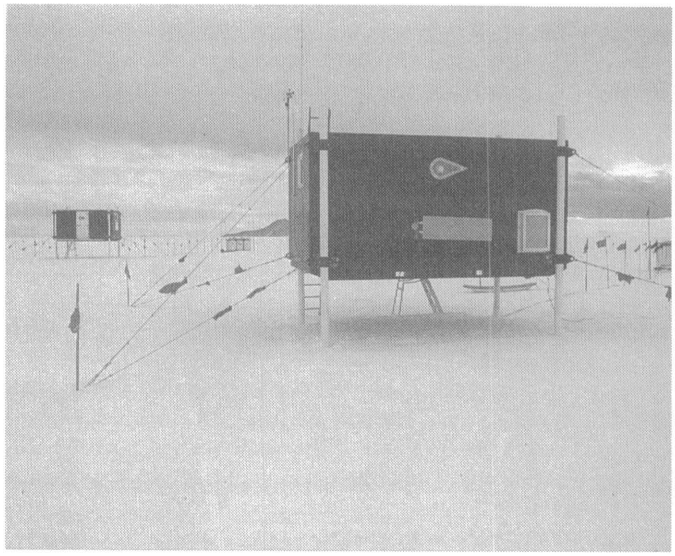

Figure 3. Two AGOs set up for trial operation on the Ross Ice Shelf near McMurdo Station. The shelter is elevated on struts to minimize snow drifting. Propane is delivered in fuel sleds of interconnected cylinders that are limited in size by transportation requirements.

Planned locations for the AGOs, shown in figure 1, were selected to provide a meridional array from the geomagnetic pole (near Dome C) through South Pole Station, another meridional array one-and-a-half hours in geomagnetic time to the east, and an arc of AGOs along the 80-degree invariant magnetic latitude. The polar cap network will include several manned stations where similar experiments are on-going.

As host to the experiments, the AGO provides power, heat, shelter, and data acquisition. The design is driven by requirements to provide 50 watts of power in an enclosure that is temperature-regulated near 20 °C while the outside temperature varies between -10° and -85 °C. On-board recording is required for 2.4 gigabytes of data. Deployment and service calls to the AGOs will be supported by ski-equipped LC-130 Hercules aircraft and must be accomplished within two flights per site each year.

Lockheed Palo Alto Research Laboratory has developed the AGO around a Teledyne Energy Systems propane-fueled thermoelectric generator that produces, with no moving parts, more than 60 watts of electric power. Advantage has been taken of the hauling capability of the Hercules aircraft (figure 2) and the 2 kilowatts of usable heat from the generator to provide a large 16′ × 8′× 8′ shelter that houses the experiment electronics and data acquisition system and also provides crew living quarters and work space for up to four annual visitors. Figure 3 shows two AGOs set up near Williams Field near McMurdo Station during trial operations in 1990. The shelter is fabricated from fiberglass laminated panels with a 4-inch-thick polyurethane foam core to give both strength and insulation in a very lightweight structure. In order to minimize snow drifting, the shelter is supported on struts that allow it to be elevated above the surface.

In trial operations in Antarctica during the 1992 winter, the AGOs demonstrated normal operation at temperatures below -70 °C and in winds in excess of 80 kilometers per hour. This follows two previous years of field trials in which performance discrepancies were seen under extreme antarctic conditions requiring modifications to be made to the design. The final configuration was tested to a temperature of -55 °C in a cold chamber at the U.S. Army Aberdeen Proving Ground prior to the start of the 1992 antarctic field trials.

A trial integration of the experiments into an AGO was done in May 1992 at a remote Lockheed test facility in the Santa Cruz Mountains in California in order to identify and correct all sources of self-generated electromagnetic interference. Several weeks of unmanned operation there has shown that the experiments and AGO are now ready for the first deployment on the polar plateau in November 1992.

This work is supported by National Science Foundation contract DPP 88-14294.

Gamma-ray and hard X-ray spectroscopy on a long-duration balloon flight

P. T. Feffer and R. P. Lin

Physics Department and Space Sciences Laboratory
University of California
Berkeley, California 94720

Solar flares, which are explosions in and near sunspots, are the most powerful natural particle accelerators in our solar system. The balloon-borne High-Resolution Gamma-ray and Hard X-ray Spectrometer (HIREGS) is designed to detect photons from ~20 kiloeclectron volts (keV) to ~17 million electron Volts (MeV) with an energy resolution of 1.5 to several keV. Collisions of flare-accelerated more than 20 keV electrons with the solar atmosphere produce hard X-ray and gamma-ray continuum through the bremsstrahlung process. These electrons often appear to carry a significant fraction of the total energy released in a flare (Lin and Hudson 1971, 1976). Interactions of flare-accelerated more than 10 MeV ions with the ambient solar atmosphere produce gamma-ray lines, the strongest of which are at 2.223 MeV from neutron capture in hydrogen, 0.511 MeV from positron annihilation, and 6.129, 4.438, 1.634, 1.369, 1.779, and 0.847 MeV from oxygen-16, carbon-12, neon-20, magnesium-24, silicon-28, and iron-56 de-excitations, respectively (Ramaty et al. 1975; Ramaty and Murphy 1987). The high-resolution measurements of HIREGS will thus provide detailed information on the distribution of accelerated particles in flares and their interactions with the solar atmosphere. Long-duration balloon flights in Antarctica during austral summer provide the coverage (24 hours per day for 8 to 14 days) required to have a high probability of catching large solar flares (Lin 1989). HIREGS is part of the Max '91 campaign organized to obtain coordinated observations of solar flares over as wide a range of the electromagnetic spectrum as possible during this solar maximum.

Experimental details. HIREGS consists of an array of twelve 6.7-centimeter-diameter × 6.1 centimeter-long-segmented *n*-type germanium (Ge) coaxial detectors, cooled by liquid nitrogen and enclosed on the sides and bottom by a 5-centimeter-thick bismuth germanate (BGO) anticoincidence shield. A 10-centimeter-thick drilled cesium iodide (CsI) collimator in front provides a ~24° FWHM field of view. Additional passive collimation reduces the field of view to ~3° × 12° for hard X-rays (less than 300 keV). Only four of the 12 detectors were flown in this first flight; the full array will be flown in the second flight scheduled for December 1992/January 1993.

The 1,700-kilogram payload (figure 1) was launched from Williams Field (McMurdo) on an 830,000-cubic-meter, helium-filled balloon on 10 January 1992. The balloon and payload circumnavigated the antarctic continent in 13 days and 17 hours, travelling about 5,500 kilometers at an average altitude of 39 kilometers (figure 2). A total of 173 hours of observations were obtained. HIREGS observed the sun 75 percent of the time and divided the remaining time between background observations and the galactic center.

When the balloon was no longer within line of sight of Williams Field, data were stored on board and then transmitted to a

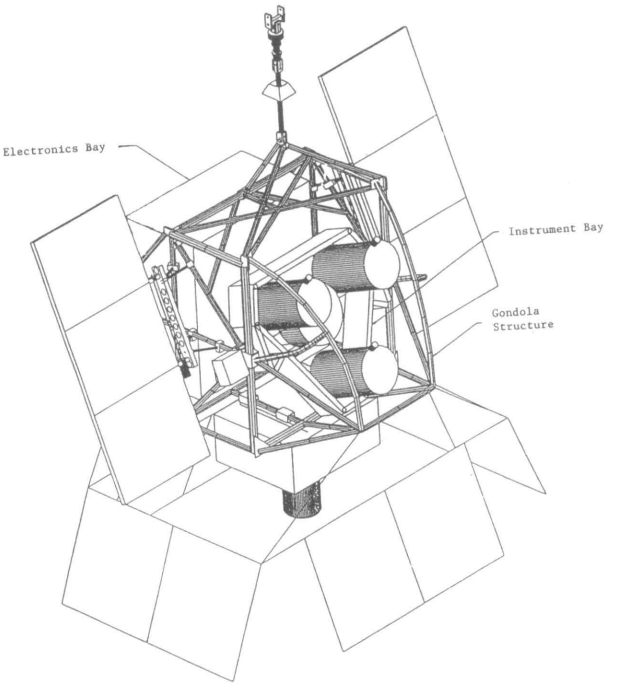

Figure 1. The HIREGS flight system ready for launch. The instrument is surrounded by an aluminized mylar thermal enclosure and is held within a gondola that points the detectors to within a fraction of a degree. The panels to the side and bottom are solar cells for producing power.

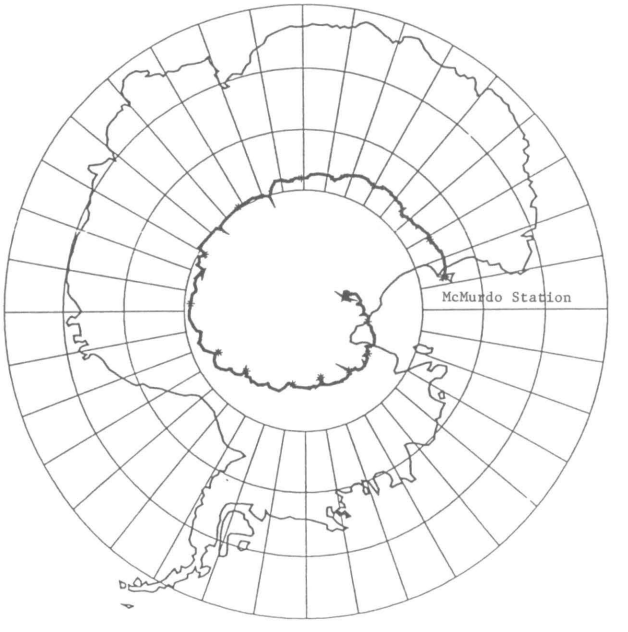

Figure 2. HIREGS circumnavigated Antarctica 10 to 24 January 1992.

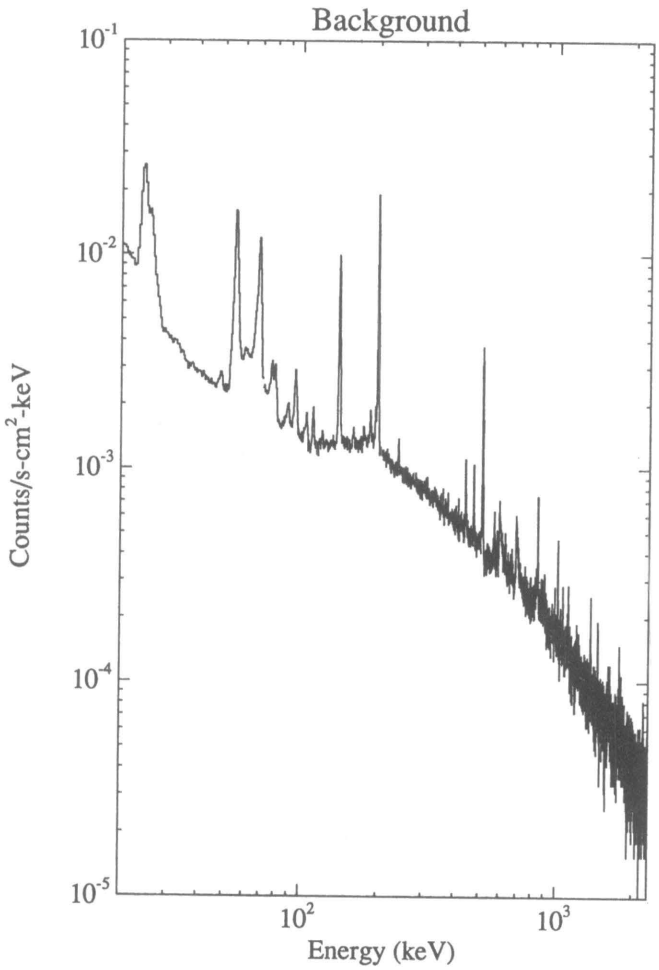

Figure 3. A typical HIREGS background spectrum containing 140 minutes worth of accumulated counts.

Hercules LC-130 aircraft flown under the balloon on three occasions during the flight. The instrument was cut down about 900 kilometers south of McMurdo on the Antarctic Plateau. Several days later, a small Twin Otter airplane was flown to the landing site where the instrument was disassembled and all but the gondola recovered.

Preliminary results. In 128 hours of solar observations, HIREGS did not find any intense hard X-ray and/or gamma-ray bursts from solar flares. The coverage included an M-class flare, detected in soft X-rays by the GOES spacecraft at 1913 UT (maximum) 13 January, but HIREGS saw no increase in hard X-rays or gamma-rays above background. This flare may have been located over the limb of the sun since it was also not detected by the Owen's Valley Radio Observatory. The rest of the data is currently being analyzed for smaller flare bursts.

Galactic center. Over the past two decades, the many observations of the galactic center and plane have described a region with multiple variable gamma-ray and hard X-ray sources, a variable narrow electron-positron annihilation line at 511 keV, a possible orthopositronium continuum below the line, and other features not yet well understood. HIREGS made measurements near the galactic center, and a detailed analysis is under way.

Gamma-ray background. Figure 3 shows a typical HIREGS background spectrum. The background consists of several components: atmospheric and cosmic gamma-rays produced by cosmic-ray interactions with the atmosphere that enter the detector aperture and leak through the shield; elastic-scattering of energetic neutrons off Ge atoms in the detector; and β-decays of radioactive nuclei produced within the detector itself (Gehrels 1985). The lines are produced by neutron activation, spallation products of Ge, and the natural radioactivity of materials in or near the detectors. In Antarctica, the gamma-ray background is several times higher than at mid-latitudes because the lower geomagnetic cut-off rigidity admits a higher cosmic-ray flux.

Acknowledgments. The HIREGS investigation is a collaborative effort involving the University of California, Berkeley; University of California, San Diego; the Centre d'Etude Spatiale des Rayonnements in Toulouse, France; with theory and data analysis support from Goddard Space Flight Center and the Paris Observatory in Meudon. We are grateful for the efforts of all field participants—S. McBride, J. H. Primbsch, K. Youssefi, G. Zimmer, R. Pehl, N. Madden, D. Malone, P. Luke, C. Cork, M. Pelling, D. Schickele, F. Duttweiler, J. Billups, S. Slassi, F. Cotin, G. Vedrenne, J. Lavigne, and G. Rouaix. This research was supported in part by NASA grant NAG8-830.

References

Gehrels, N. 1985. Instrumental background in balloon-borne gamma-ray spectrometers and techniques for its reduction. *Nuclear Instruments and Methods in Physics Research,* A239:324-349.

Lin, R. P. 1989. Cosmic and solar gamma-ray, X-ray and particle measurements from high altitude balloons in Antarctica. Astrophysics in Antarctica. In D. J. Mullan, M. A. Pomerantz, and T. Stanev (Eds.), *Astrophysics in Antarctica* (AIP Conference Proceedings 198). New York: American Institute of Physics, 157-165.

Lin, R. P. and H. S. Hudson. 1971. 10-100 keV electron acceleration and emission from solar flares. *Solar Physics,* 17:412-435.

Lin, R. P. and H. S. Hudson. 1976. Non-thermal processes in large solar flares. *Solar Physics,* 50:153-178.

Ramaty, R., B. Kozlovsky, and R. E. Lingenfelter. 1975. Solar gamma rays. *Space Science Reviews,* 18:341-388.

Ramaty, R. and R. J. Murphy. 1987. Nuclear processes and accelerated particles in solar flares. *Space Science Reviews,* 45:213-268.

Psychological aspects of polar living

PETER SUEDFELD AND G. DANIEL STEEL

The University of British Columbia
Vancouver, British Columbia

LAWRENCE A. PALINKAS

University of California, San Diego
La Jolla, California

The importance of psychology to polar expeditions was explicitly recognized as early as the second Scott expedition (Cherry-Garrard 1922 and 1965). Explorers have always maintained that the personality of each member is the single most important factor in the success or failure of the project. The right group may be able to overcome the most adverse conditions and the worst luck. The wrong group, however, can turn the easiest tasks into a disaster.

To identify the right people, the organizer of the expedition interviewed volunteers, looking for physical robustness, a strong but pleasant manner in social interaction, relevant experience and skills (including military or naval service), an adventurous and persevering spirit, and sometimes the ability to contribute financially to the expedition.

The scientific selectors, who took over since the International Geophysical Year, rely on biographical checklists, tests of psychiatric adjustment, peer ratings, and leader evaluations, with interviews as a backup source of information. But the criteria are not dramatically different. Polar psychiatrists have identified a triumvirate of indispensable traits: stability (good emotional health), compatibility (the ability to get along well with others), and ability (the training, experience, and skills to perform one's particular job well).

More recently, the emphasis has been expanded to more basic research on why some people are attracted to unusual environments, such as the polar regions, space, and underwater habitats; what they expect to experience in these environments; how they adapt to the situation; their reactions during and after their stay; how they differ from those who are not drawn into such activities; and why some people keep going back, while others do not, and so on. The goal is a deeper understanding of an interesting aspect of human behavior—the challenge and fascination of remote, novel, unique, and harsh environments. The Polar Psychology Project (PPP) (Suedfeld, Bernaldez and Stossel 1989) is a multinational, long-term, transpolar program to study these issues.

During the austral summer of 1991-1992, two researchers from the PPP distributed almost 200 sets of questionnaires and conducted about 50 interviews at McMurdo Station and Scott Base. Not all of the data are available at this time. Some results have not been analyzed, and some questionnaires will not be collected until the end of austral winter.

We have analyzed the results from the NEO Five Factor Inventory (FFI), a short version of the Five Factor Personality Inventory (Costa and McCrae 1989), which yields scores for what are now considered to be the five most basic and theoretically important personality traits: neuroticism, extraversion, openness to experience, conscientiousness, and agreeableness. Of these, neuroticism and agreeableness are closely related to stability and compatibility, respectively. Conscientiousness applies to job-related factors (working hard, getting things done on time). Openness to experience is unrelated to the polar triumvirate but was predicted to be strong among those who venture to the Poles. Extraversion has to do with positive emotions, emotional warmth, and activity level, traits that may be both positive and negative in a polar context: people high on this scale are friendly and gregarious, but in the restricted social life of an isolated station may be perceived as intrusive and demanding of attention.

To date, we have 57 complete NEO-FFI forms from personnel at McMurdo Station. There were no statistically significant differences between the antarctic sojourners and the representative U.S. sample on which the test was normed, except that the former were significantly lower on neuroticism (mean scores of 12.95 versus 18.70 for the norm group, p less than .0001). This difference held for both the 44 men in our sample (mean = 12.07, male norm = 16.89, $p = .006$) and the 13 women (mean = 15.92 versus the 20.50 female norm). The latter, however, did not reach statistical significance because of the small sample size.

It appears from this early finding that either the recruitment (i.e., self-selection) or the selection procedures, or both, are successful in bringing to McMurdo Station a group that is emotionally stable: not depressed nor anxious. This is an interesting contradiction of a popular speculation that polar life attracts those who cannot fit well into "normal" society. The lack of similar differences on the other factors, however, is somewhat surprising and will be investigated further.

This work was supported by National Science Foundation grant DPP 90-19131.

References

Cherry-Garrard, A. [1922] 1965. *The worst journey in the world: Antarctic 1910-1913.* Harmondsworth, England: Penguin.

Costa, P. and R. McCrae. 1989. *The NEO five factor inventory.* Lutz, Florida: Psychological Assessment Resources.

Suedfeld, P., J. P. Bernaldez, and D. Stossel. 1989. The Polar Psychology Project (PPP): A cross-national investigation of polar adaptation. *Arctic Medical Research,* 48:91-94.

National Science Foundation Young Scholars antarctic research experience—First science cruise of R/V *Nathaniel B. Palmer* (92-2)

M. N. Darling

Princeton University
Princeton, New Jersey 08544

B. Castillo

University of Chicago
Chicago, Illinios 60615

C. R. Griffith

University of California-Irvine
Irvine, California 92715

E. Morales

Massachusetts Institute of Technology
Boston, Massachusetts 02115

R. Swayzer

Xavier University
New Orleans, Louisianna 70125

On 22 June 1992 five young scholars and four of their former high school teachers set foot on land in Punta Arenas, Chile after having spent a little over a month in the Weddell Sea aboard the research vessel *Nathaniel B. Palmer*. This was the final step in a process that began in the fall of 1990 when the students initially applied for the program after completing various Young Scholars programs (for high school students) across the country.

As part of their antarctic experience the students and teachers followed the progress of the new ice breaking vessel *Nathaniel B. Palmer* through various stages of construction. Trips were made to Edison Chouest Offshore, Inc., of Galliano, Louisiana in May and October of 1991 where they had the opportunity to see the ship under construction and walk through unfinished corridors to rooms that would become cabins and science laboratories. In May the ship was still in two parts: the hull was upside-down in one part of the ship yard while the superstructure was being worked independently. The hull was flipped in August and when the participants next saw the ship in October it was in one piece with the name *Nathaniel B. Palmer* inscribed on the hull. The inside was still unfinished with wires running everywhere and construction workers busy drilling and welding. Seeing the vessel docked in Punta Arenas, on 16 May 1992 after returning from its first trip to the ice, it was hard to believe that it was the same ship. Painted a bright red with a cream yellow superstructure and green decks, the ship looked sleek and new. The crew was already touching up with fresh paint the few places where the bow had scratched against ice. The interior was brightly finished with computers and scientific instruments installed and operating.

Prior to the mission, each young scholar was assigned to a principal investigator with whom they would do research on board the new vessel. The cruise in which the students and teachers were involved was the recovery cruise of Ice Station Weddell #1 (ISW-1) and the research performed on the ship related to the work done at the ice camp. (Gordon and Lukin this issue; Gordon and Huber this issue; Ackley and Lytle this issue; and Ackley and Lytle et al. this issue, for overviews of the science programs). Elizabeth Morales, from El Paso, Texas and Carolyn Griffith, from Torrance, California, worked with Arnold Gordon's physical oceanography team out of Columbia University's Lamont-Doherty Geological Observatory (LDGO). Carolyn Griffith also worked on a project designed by George Hunt, a seabird ecologist from the University of California at Irvine. Brett Castillo, from Escondido, California and Naomi Darling from Holliston, Massachusetts worked with the sea-ice team under the direction of Stephen Ackley from the Cold Regions Research and Engineering Laboratory (CRREL), while Robert Swayzer, from Winnsboro, Louisiana worked with a biology research team under the direction of Cornelius Sullivan from the University of Southern California. During the summer of 1991, the students visited with their principal investigators for 2 weeks to learn about the work they would be doing on the ship.

For the first time, high school teachers were also involved in the National Science Foundation Young Scholars Antarctic Research Experience. Initially their role was only to accompany the students to Louisiana and observe the ship construction. However, as the program evolved, four of the five teachers nominated by their students were able to go to the Antarctic. A successful outcome of having teachers participate in this program is that they will be able to take their experience back into the classroom and interest greater numbers of students in polar science. The teachers will be developing curriculum materials to use in their own classrooms and, hopefully, in classrooms around the coun-

Figure 1. The Young Scholars in front of the mess hall at Ice Station Weddell #1. From left to right: Brett Castillo, Carolyn Griffith, Elizabeth Morales, Naomi Darling, and Robert Swayzer.

try. The teachers involved were Ruthanne Thomas, a professor in the Department of Chemistry at the University of North Texas, Richard Schwartz, a chemistry teacher at Torrance High School, John Cavanaugh, a physics teacher at San Pasqual High School in Escondido, California and Peter Amati, a biology teacher at Holliston High School. Michael Clay, a calculus teacher at Winnsboro High School at the time of the nomination, was not able to join his student in the Antarctic but did participate in the ship visits and antarctic orientation.

On board the ship, students and teachers worked with researchers to collect data, take measurements, and keep records. Elizabeth Morales and Dr. Thomas collected water samples from the conductivity-temperature-depth (CTD) casts to be used for chlorofluorocarbon analysis. These freons can be used as markers to trace ocean water masses. Carolyn Griffith and Richard Schwartz worked on the bridge of the ship during daylight hours keeping a record of all the birds, seals, and whales observed. Brett Castillo, Naomi Darling, John Cavanaugh, and Peter Amati worked with the sea-ice team. (Ackley and Gow et al. this issue). They maintained an hourly record of ice observations and an iceberg log from the bridge of the *Nathaniel B. Palmer* while the ship was traveling through ice (see Darling, Lytle, and Ackley this issue). The sea-ice team also occupied 15 ice stations during the cruise at which time the students and teachers surveyed ice and snow elevations along surface elevation profile lines and took measurements of snow thickness (see Lytle and Ackley this issue). In addition, ice cores were collected for physical and chemical analysis (see Gow et al. this issue). Robert Swayzer assisted in the ice observations and iceberg log as well as working with Sullivan's biology team on ice-core sections. Sections of core when melted and subjected to several chemical and biological tests, such as total chlorophyll content and nutrient assays, assist in the understanding of relationships between ice structure and the biology contained within the ice (see Sullivan et al. this issue).

From 5 June to 9 June the *Nathaniel B. Palmer* assisted in the recovery of ISW-1. At the Ice Station, everyone worked together to take the camp down and load everything onto the *Palmer* and *Akademik Federov.* Scientists, teachers, students, and Antarctic Support Associates (NSF's civilian support contractor for the U.S. Antarctic program) personnel all worked together shoveling snow, taking down weatherports, and hauling fuel drums.

Of his experience, Robert Swayzer writes, "There is no single word that can describe the sense of accomplishment that one gets from being a participant in the United States Antarctic Program. From the travel through South America to the recovery of Ice Station Weddell #1, every aspect has been marvelous." Carolyn Griffith writes that "the sacred, ineffable beauty of countless icy scenes have been ingrained in my mind forever. My antarctic experiences will inspire my study of science for the rest of my life."

Antarctica is a land that touches the soul. Her raw savage beauty and untouched desolate wonders have the power to change people's lives.

For these Young Scholars returning from the Antarctic is just the beginning. In the summer of 1992 following the cruise, Brett Castillo worked with Sullivan's team on ice core analysis and Naomi Darling worked with Steve Ackley's team on ice conditions observed in the western Weddell Sea. Carolyn Griffith will be working further with George Hunt to analyze the bird data collected during the cruise.

We would like to thank the National Science Foundation for making this experience possible. Jane Dionne of the Office of Polar Programs and Elmima Johnson of the Young Scholars Program made a dream come true with their untiring energy and enthusiasm. We are also grateful to our Principal Investigators Stephen Ackley, Dr. Sullivan, and Dr. Gordon for their patience, dedication and support of the program. Thanks are also extended to Vicky Lytle, Dr. Gow, Bruce Huber, Calvin Mordy, and Preston Sullivan for working closely with us and coordinating our scientific activity on the ship. ASA personnel John Evans, Kevin Wood, and Mike Darrah as well as the captain and crew of the *Nathaniel B. Palmer* also helped to make this experience as terrific and unforgettable as it was. Thank you!

References

Ackley, S. F., V. I. Lytle, B. Elder, and D. Bell. 1992. Sea ice investigations on Ice Station Weddell #1: I. Ice dynamics. *Antarctic Journal of the U.S.*, this issue.

Ackley, S. F. and V. I. Lytle. 1992. Sea ice investigations on Ice Station Weddell #1: II. Ice thermodynamics. *Antarctic Journal of the U.S.*, this issue.

Ackley, S. F., A. J. Gow, V. I. Lytle, M. N. Darling, and N. E. Yankielun. 1992. Sea ice investigations on *Nathaniel B. Palmer:* Cruise 92-2. *Antarctic Journal of the U.S.*, this issue.

Darling, M. N., V. I. Lytle, and S. F. Ackley. 1992. Ice observations in the western Weddell Sea (*Nathaniel B. Palmer* 92-2). *Antarctic Journal of the U.S.*, this issue.

Gordon, A. L. and V. V. Lukin. 1992. Ice Station Weddell #1- Overview. *Antarctic Journal of the U.S.*, this issue.

Gordon, A. L. and B. A. Huber. 1992. Ice Station Weddell #1: Thermohaline stratification. *Antarctic Journal of the U.S.*, this issue.

Gow, A. J., V. I. Lytle, D. Bell, and S. F. Ackley. 1992. Ice core studies in the western Weddell Sea (*Nathaniel B. Palmer* 92-2). *Antarctic Journal of the U.S.*, this issue.

Lytle, V. I. and S. F. Ackley. 1992. Snow properties and surface elevation profiles in the western Weddell Sea (*Nathaniel B. Palmer* 92-2). *Antarctic Journal of the U.S.*, this issue.

Sullivan, C. W., C. H. Fritsen, and C. W. Mordy. 1992. Microbial production in antarctic pack ice: Time series studies at the U.S.-Russian drifting ice station. *Antarctic Journal of the U.S.*, this issue.

Mapping the McMurdo Station sewage plume

JAMES P. HOWINGTON, GORDON A. MCFETERS, AND JAMES J. SMITH

Department of Microbiology
Montana State University
Bozeman, Montana 59717

JAMES P. BARRY

Monterey Bay Aquarium Research Institute
Pacific Grove, California 93950

We investigated the spatial distribution and movement of the sewage plume from McMurdo Station, Antarctica. We also examined ocean currents to determine their effect on the movement of the plume. Samples of seawater were obtained and analyzed for coliform bacteria, high densities of which were found along the circa-1- kilometer shoreline of McMurdo Station and the plume extended 200 - 300 meters seaward. Relocating the outfall from a surface configuration to the subsurface had little influence on the distribution of the plume, which sometimes reached the seawater intake station 400 meters to the south. Ocean current measurements in the study area confirmed that although the prevailing advection was to the north and away from the intake area, episodic reversals of flow at some current-meter stations coincided with pulses of sewage that moved into the intake.

The spatial distrubution of the McMurdo Station sewage plume was determined by sampling the water column for coliform densities. Samples were collected within the plume and at pristine control locations, miles away from the sewage plume, during three different periods. Coliform numbers were determined using membrane filtration techniques. All of the methods used are widely accepted and are described in the American Public Health Association 1989. Current Patterns were also determined in the study area using InterOcean S4 current meters. These highly sensitive electronic meters were able to detect currents as weak as 0.1 centimeters per second.

The sample periods coincided with three different configurations of the McMurdo Station sewage outfall. During the initial sampling period (17 to 28 October 1991), the outfall was located fifty feet from the shore and submerged in seventeen feet of water during low tide. At that time, 23 sample sites as well as the seawater intake were tested. Water samples were collected just below the ice and at the bottom of the water column. During the second sampling period, 20 to 29 November 1991, the outfall was relocated to the surface, as it had been during the 1990-1991 season. This arrangement was needed to allow the addition of twenty feet of pipe to the subsurface outfall. Samples were collected from 17 sites and the seawater intake. The final sampling period (16 to 18 December 1991) occurred after the outfall pipe had been extended an additional twenty feet, with the discharge end of the pipe in thirty-eight feet of water during low tide. Samples were collected at 18 locations as well as the seawater intake. The information in figure 1 demonstrates that the sewage plume occupied an area that encompassed the entire region from the intake jetty to Hut Point and extended at least 200 to 300 meters seaward, with some localized areas of higher sewage pollution. Samples taken from most of the stations indicated that the sewage was relatively well mixed (vertically) in the water column. On all occasions, the coliforms were detected in the desalination intake water. Their numbers ranged from a high of 523 per 100 to a low of 7 per 100, with an average count over the entire sample period of 187 coliforms per 100 milliliters. The large fluctuations in coliform numbers isolated from the intake station probably resulted from occasional current reversals, discussed below, rather than the outfall configuration. These periodic southern currents likely carried parcels of sewage toward the source-water intake. Repeated sampling at other locations also demonstrated the periodic movement of more concentrated pulses of sewage within the study area.

During October to December 1991, currents were measured at eight locations near the shoreline adjacent to McMurdo Station in

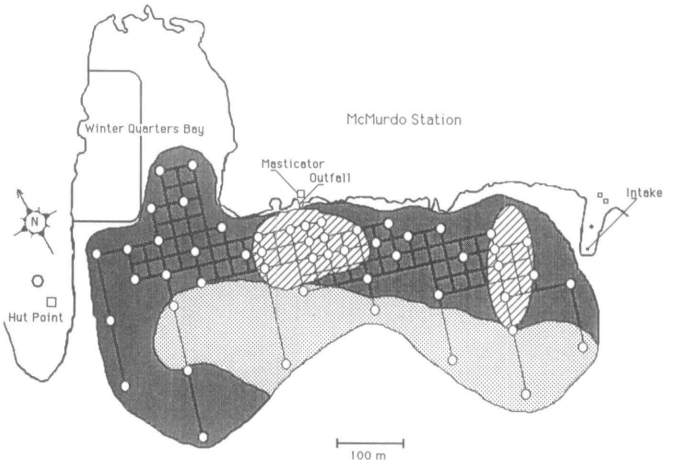

Figure 1. Representative map of coliform bacterial densities near McMurdo Station, Antarctica. The sampling grid is represented by lines overlying the sewage plume, and sampling locations are shown as circles on the grid. Coliform densities are indicated as areas that are *stippled* (<100/100 milliliters), *shaded* (100-1,000/100 milliliters), and *crosshatched* (>1,000/100 milliliters).

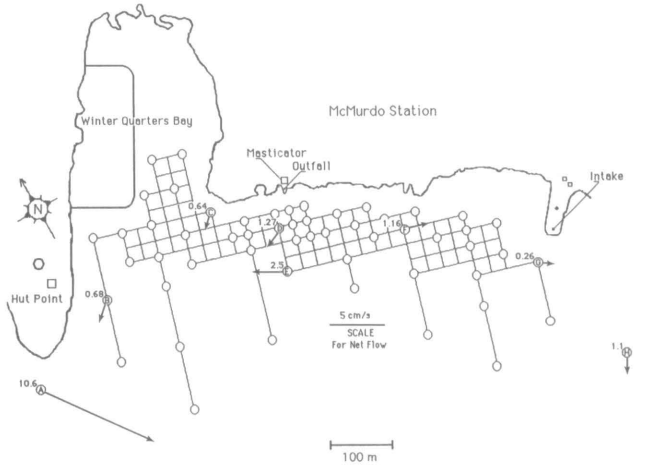

Figure 2. Map of the McMurdo Station vicinity showing the location of current-meter measurement stations. Arrows indicate the direction and magnitude of the net motion of the currents. Numbers indicate the current speed (in centimeters per second). A 5-centimeter-per-second bar is shown.

conjunction with the collection and measurement of coliform bacteria presumably released from the McMurdo Station wastewater outfall. Measurements continued for periods of 9 to 75 days. Preliminary analyses indicate several features of currents in the near-shore environment at McMurdo Station, including periodic flow patterns related to daily tidal changes, net transport, and episodic flow reversals in some areas. These features have important implications for the advection of the sewage plume from the McMurdo Station sewage outfall.

The general patterns of advection are shown in figure 2, which also shows station locations and a current vector that is indicative of the direction and magnitude of each net flow. This vector indicates the average direction and rate of the flow at each station during the measurement period but does not indicate any variation in flow, although at some stations, the variation was considerable. This flow pattern, which involves a strong southward flow near Hut Point and a small counterclockwise gyre in Winter Quarters Bay reaching at least as far south as the outfall station, is probably typical, as documented in other studies (e.g., Raytheon report circa 1983). Near the sea-ice transition (station F) the net flow was slow and toward the southeast, along the coast. This station may be southeast of the gyre mentioned above, or advection may be related to its shallow depth. The net flow near the jetty was very sluggish, with somewhat higher speeds toward the south at station H.

The most important implication of this preliminary analysis of the data on advection in the vicinity of the outfall is that although the flow generally carries the sewage plume offshore and toward the west (away from the intake area), there are episodes of current reversal when the plume may be advected toward the intake pipe. We plan to undertake continuing studies to consolidate our understanding of the distribution and movement of sewage from McMurdo Station in the antarctic marine environment.

This work was supported by National Science Foundation grant DPP 90-19059.

References

American Public Health Association. 1989. *Standard methods for the examination of water and wastewater*, 17th ed. Washington, D.C.: APHA.

Raytheon Service Company. 1983. Report on the McMurdo Station water quality study. Unpublished technical report to ITT Antarctic Services.

The *Bahia Paraiso* spill in Arthur Harbor, Anvers Island

M.C. Kennicutt II, S.J. McDonald, and Stephen T. Sweet

Geochemical and Environmental Research Group
Texas A&M University
College Station, Texas 77845

Enroute to resupply an Argentine antarctic base, the *Bahia Paraiso* ran aground on 28 January 1989, approximately 2 kilometers from Palmer Station, an U.S. antarctic research station. The *Bahia Paraiso* had just completed a sight-seeing visit to the station and was exiting Arthur Harbor when the accident occurred. The vessel contained a cargo of diesel fuel arctic (DFA), jet fuel, gasoline, and compressed gas cylinders totaling more than 250,000 gallons. A 30-foot tear in the ship's hull began to discharge petroleum into the waters of the surrounding bays almost immediately. Within 4 days of the accident 100 square kilometers of sea surface was covered by an oil slick and an estimated 600,000 liters of diedel fuel arctic (DFA) had been released.

The first evidence of ecological damage was observed in the intertidal zone. Invertebrate mortality, mostly dead and moribund limpets, was observed as early as 1 February, with thousands of dead individuals being observed by 4 February (Kennicutt et al. 1990). Comparative qualitative evidence suggested as much as 50 percent of the littoral population perished within a 2 kilometer radius of the wreck. Limpet mortality was heaviest in coves that retained oiled waters or were persistently replenished with oil due to the prevailing winds (Stockton, personal communication.). Well-drained intertidal pools more distant from the spill were less affected.

The earliest evidence of lethal exposure of sea birds was noted on 1 February when dead, oiled Adélie penguins and blue-eyed shags were found in Biscoe Bay adjacent to Palmer Station (Fraser personal communication). The mortality rate during the spill was less than 300 individuals over a 3-week period, with 89 percent being penguins and shags. The actual rate may have been higher due to an underestimate of mortality caused by the severe weather conditions, the efficiency of scavengers and predators, and the abandonment of breeding colonies. A breeding failure—caused by natural factors—among shags and south polar skuas coincided with the spill.

In response to the grounding of the *Bahia Paraiso* a series of intertidal, subtidal, and bay sampling sites were established to determine the fate and effect of the released petroleum (figure). Tissue, sediment, and water samples were collected over a 6-week period after the spill and standard stations were established for reoccupation in subsequent years. Hydrocarbon analyses confirmed that macroalgae, limpets, and beaches were repeatedly stained with diesel fuel and the greatest contamination was in intertidal areas (Kennicutt et al. 1991a and b). Intertidal limpets were "oiled" over a 6- to 7-week period. Two weeks after the first spillage PAH contamination was reduced by a factor of three to five. After 6 to 7 weeks contamination was nearly an order of magnitude lower than during the most intense "oiling" (Kennicutt et al. 1991a). Sediments and cobble beaches in the intertidal were contaminated over a period of several weeks and took anywhere from days to weeks to be cleansed.

The diesel fuel rapidly evaporated, was diluted with seawater, and much of the residue was flushed from the immediate area by wave and current action. Several factors contributed to limiting the impact of the spill including the volatility of the released product, the relatively small volume of material released, the

Summary of total PAH[a] detected in intertidal limpet tissues in Arthur Harbor at various times after the *Bahia Paraiso* spill (modified after Kennicutt et al. 1990a)

Island	Approx. distance from the Bahia Paraiso, km	2/1/89	2/4/89	2/2/89	3/17/89	3/22/90	3/31/91 to 4/15/91
DeLaca	0.2	698	125147	1260	3893	1001	177
Janus	0.3	1029	4120	1272	1882	*b*	32
Litchfield-A	0.8	527	21203	4996	2791	1070	382
Torgersen	1.2	549	10162	1819	*b*	523	186
Litchfield-B	1.3	329	78248	9639	2111	276	248
Bonaparte Point	1.4	164	3673	17653	2094	919	276
Litchfield-C	1.4	194	2178	227	2264	259	43
Humble-A	1.7	571	15495	1090	1861	233	198
Humble-B	1.8	1542	36395	3267	2511	324	36
Norsel Point	2.1	1399	1723	76	780	*b*	54
Hero Inlet	2.1	677	5387	6262	473	544	57
Christine-A	3.5	21959	17211	4279	925	*b*	174
Christine-B	3.6	35775	11322	2749	1198	1181	337
Hermit	4.0	16969	24874	3244	2138	907	528
Limitrophe-A	4.1	75301	23833	1722	2413	672	471
Limitrophe-B	4.2	2687	15946	1683	901	*b*	84
Laggard	4.4	2707	1888	1242	515	21	68
Jacobs	4.7	5648	25856	3077	--	*b*	71
Comorant-A	5.7	1440	48993	54347	1203	622	35
Comorant-B	6.0	1403	628	1315	460	*b*	80

[a]In ppb dry weight. [b]Below detection limit (~10 ppb).

weather conditions, the offshore winds and currents, and the lack of low energy intertidal areas for fuel to accumulate.

One year after the spill several areas exhibited continued contamination due to chronic low-level leakage from the ship (table). Subtidal sediments and distant intertidal locations contained no detectable PAH. Exceptions were two beaches on Hermit and Cormorant Island and limpets in close proximity to the wreck (i.e., Janus Island, DeLaca Island, and Bonaparte Point). Sediments near the docking facilities at Palmer Station are contaminated due to station and boating activities. Diesel fuel and combustion-related PAH contamination are present in sediments and limpets in close proximity to the station (Kennicutt et al. this issue).

Two years after the release of DFA into Arthur Harbor, little spill-related contamination could be detected in intertidal and subtidal limpets (table). Periodic releases of small amounts of material randomly contaminated nearby islands; in particular the intertidal areas of Christine, Limitrophe, and Humble Islands. Subtidal sediment contamination was primarily due to other local inputs. A few beaches were anomalously contaminated 2 years after the spill. Quiescent weather conditions, occasional releases from the wreck, and prevailing winds and currents tended to concentrate contaminants in these relatively low-energy environments. The intertidal limpets collected along these beaches were also contaminated.

These studies were supported by National Science Foundation grants DPP 89-12497, DPP 89-15015, and DPP 90-22346. We would also like to acknowledge the field support of Jim Jobling, Anthony Tripp, Tim Wilkinson, and Elsa Haubold. Laboratory and data support was provided by numerous GERG staff scientists.

References

Kennicutt, M. C. II, et al. 1990. Oil spillage in Antarctica: Initial report of the National Science Foundation-sponsored quick response team on the grounding of the *Bahia Paraiso*. *Environmental Science and Technology*, 24:620-624.

Kennicutt, M. C. II, S. T. Sweet, W. R. Fraser, W. L. Stockton, and M. Culver. 1991a. The grounding of the *Bahia Paraiso*, Arthur Harbor, Antarctica—I. Distribution and fate of oil spill related hydrocarbons. *Environmental Science and Technology*, 25:509-518.

Kennicutt, M. C. II, S. T. Sweet, W. R. Fraser, W. L. Stockton, and M. Culver. 1991b. The fate of diesel fuel spilled by the *Bahia Paraiso* in Arthur Harbor, Antarctica. *Proceedings, 1991 International Oil Spill Conference*, 594-600.

Kennicutt, M. C. II, T. J. McDonald, and S. S. McDonald. 1992. Hydrocarbon contamination in Arthur Harbor, Anvers Island. *Antarctic Journal of the U.S.*, this issue.

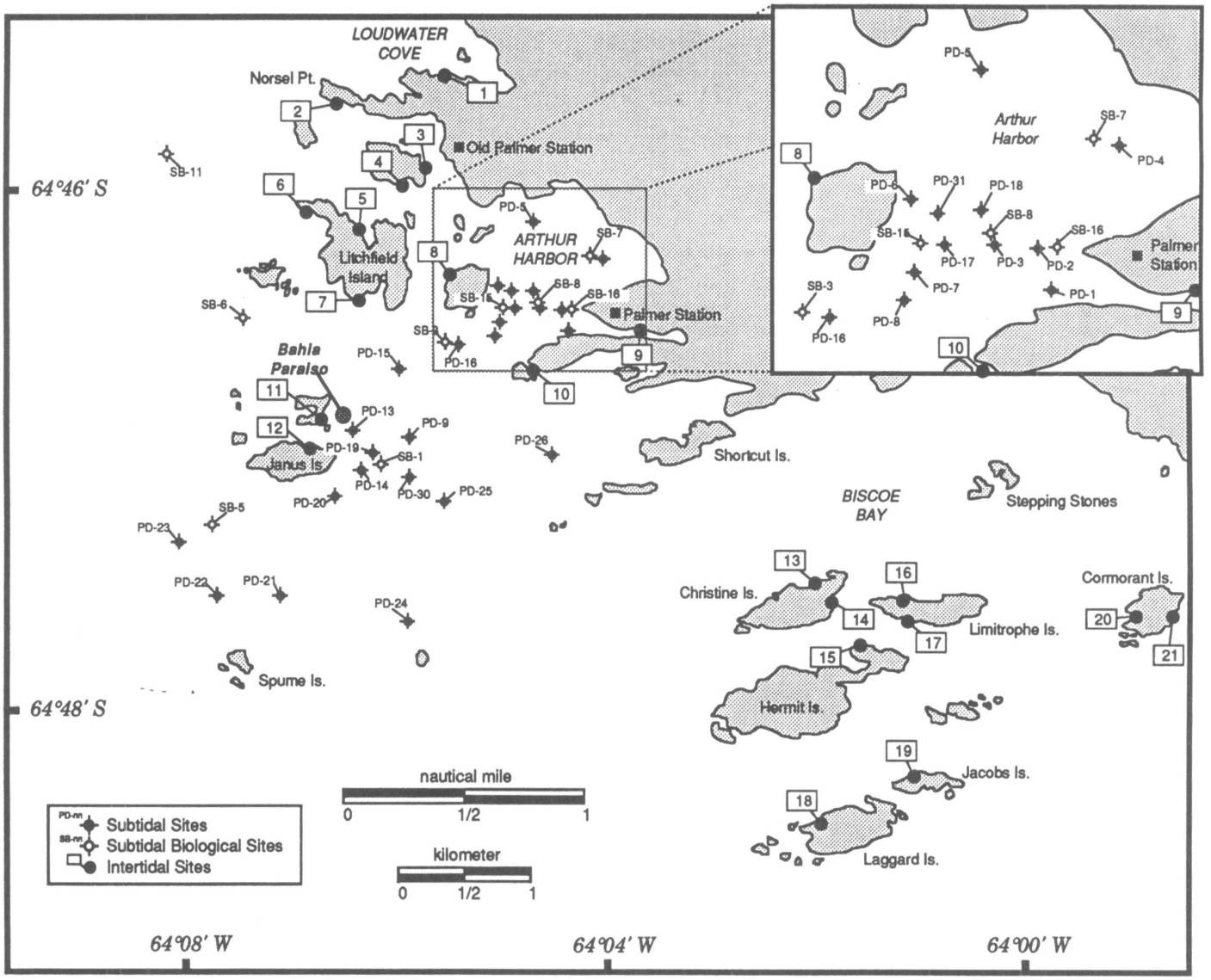

The location of intertidal and subtidal sampling locations for limpets and sediments in the vicinity of Arthur Harbor, Antarctica.

Polynuclear aromatic hydrocarbon exposure in antarctic fish

SUSANNE MCDONALD, MAHLON KENNICUTT II, AND KATE FOSTER-SPRINGER

Geochemical and Environmental Research Group
Texas A&M University
College Station, Texas 77845

MARGARET KRAHN

National Marine Fisheries Service
Northwest Fisheries Science Center
Seattle, Washington 98112

Antarctica is considered to be one of the last remaining pristine environments. Consequently, much interest has been generated concerning the influence of humans on the antarctic environment. Recent studies have documented the presence of petroleum-related hydrocarbons in sediments and tissues sampled near Palmer Station and the *Bahia Paraiso* wreckage (Kennicutt et al. 1990, 1991a, b, and c this issue).

A study was undertaken to assess polynuclear aromatic hydrocarbon (PAH) exposure in fish. Fish enzymatically convert PAH into a variety of metabolites not detected by conventional techniques so measuring tissue concentrations in fish can underestimate PAH exposure. The metabolism of PAH is catalyzed by enzymes concentrated in the liver. Subsequently, metabolites can be excreted into bile for eventual elimination. The induction of mixed-function oxidase (MFO) enzyme activity has been widely used as a sensitive bioassay technique for the detection of organic contamination. The activity of ethoxyresorufin O-deethylase (EROD), a MFO enzyme, is commonly measured to suggest PAH

Table 1. Concentration of PAH metabolites in the bile of fish captured near Palmer Station, *Bahia Paraiso* wreck and remote sites

Site	Species	Naphthalene (ng g^{-1} wet wt.)	Phenanthrene (ng g^{-1} wet wt.)
Palmer Station	*Notothenia croiiceps neglecta*	51000 ± 9000 (n=6)	6000 ± 1500 (n=6)
Old Palmer Station	*Notothenia croiiceps neglecta*	21000 ± 6000 (n=2)	2500 ± 210 (n=2)
Bahia Paraiso	*Notothenia croiiceps neglecta*	69000 ± 61000 (n=16)	9000 ± 10000 (n=16)
Low Island	*Notothenia croiiceps neglecta*	38000 ± 14000 (n=9)	5000 ± 2000 (n=9)
Low Island	*Chaenocephalus aceratus*	l9000 ± 13000 (n=8)	3000 ± 2000 (n=8)
Low Island	*Notothenia gibberfrons*	20000 ± 6000 (n=8)	2400 ± 930 (n=8)
Dallman Bay	*Notothenia gibberfrons*	36000 ± 17000 (n=6)	4000 ± 2200 (n=6)

Table 2. Biliary PAH metabolite concentrations in *Notothenia croiiceps neglecta* captured near the *Bahia Paraiso* wreck and Palmer Station

	Biliary PAH metabolites			
	Fluorescent aromatic hydrocarbons (ng g^{-1} wet wt.)		GC/MS (ng g^{-1} wet wt.)	
	Naph	Phen	290/335 nm Naph	260/350 nm Phen
Bahia Paraiso				
Fish 1	37000	2800	<LOD	<LOD
Fish 2	42000	4600	12	20
Fish 3	150000	18000	450	244
Fish 4	36000	3900	26	< LOD
Fish 5	35000	700	<LOD	<LOD
Fish 6	270000	37,000	1746	838
Palmer Station				
Fish 1	50000	8100	66	46
Fish 2	64000	8000	49	55
Fish 3	38000	6400	101	51

LOD = Limit of detection

exposure. Other techniques used to estimate PAH exposure in fish include measuring the concentration of metabolites in bile by high performance liquid chromatography (HPLC)/fluorescence detection and sequenced selected ion monitoring (SSIM) gas chromatography mass spectrometry (GC/MS) (Krahn et al. 1984, 1986, and 1992). The HPLC/fluorescence detection technique estimates metabolite concentrations by summing the integrated areas of all compounds eluting between specified elution times; whereas, GC/MS identifies and quantifies individual metabolites.

The bile of *Notothenia croiiceps neglecta* captured near Palmer Station and the *Bahia Paraiso* wreck and *Notothenia croiiceps neglecta*, *Notothenia gibberfrons*, and *Chaenocephalus aceratus* captured near remote sites (Low Island and Dallmann Bay) was screened by HPLC/fluorescence detection. The presence of metabolites fluorescing at naphthalene and phenanthrene wavelengths was detected in all samples (table 1). Higher than expected concentrations of metabolites were measured in the bile of fish sampled from remote sites. Therefore, the bile of selected fish was analyzed by GC/MS to confirm the presence of PAH metabolites. Individual PAH metabolites were identified by GC/MS in four fish captured near the wreck and in three captured near Palmer Station (table 2). The HPLC and GC/MS techniques both detected high concentrations of metabolites in two fish trapped near the *Bahia Paraiso* wreck. Additionally, the composition of metabolites is similar to that found in a *Notothenia gibberfrons* injected with diesel fuel. The three fish captured near Palmer Station contained low concentrations of individual metabolites indicating low-level exposure. GC/MS was unable to confirm

Table 3. Biliary PAH metabolite concentrations in fish captured near Low Island and in Dallman Bay

		Biliary PAH metabolites			
		Fluorescent aromatic hydrocarbons (ng g^{-1} wet wt.)		GC/MS (ng g^{-1} wet wt.)	
Site	Species	Naph	Phen	290/335 nm Naph	260/350 Phen
Dallman Bay	*Notothenia gibberfrons*	40000	4300	<LOD	<LOD
Low Island	*Notothenia croiiceps neglecta*	17000	2400	<LOD	<LOD
Low Island	*Notothenia gibberfrons*	22000	2200	<LOD	<LOD
Low Island	*Chaenocephalus aceratus*	24000	3200	<LOD	<LOD

LOD = Limit of detection

the presence of PAH metabolites in the bile of fish capture at remote sites (table 3). Furthermore, hepatic EROD activity was low (less than 50 pmol min^{-1} mg^{-1}) and did not appear to be induced in *Notothenia croiiceps neglecta* captured in Dallmann Bay. This suggests that these fish were not exposed to PAH. Apparently, compounds other than the analytes of interest fluoresce at the excitation/emission wavelengths selected to monitor naphthalene and phenanthrene metabolites.

Biliary metabolite concentrations indicate that fish captured near Palmer Station and the *Bahia Paraiso* wreck are exposed to PAH. Exposure near Palmer Station is most likely the result of chronic low-level input from boating/shipping and station activities (Kennicutt et al. this issue). Evidence for exposure in fish trapped near the wreck was variable. The variability in metabolite concentrations most likely reflects the heterogeneous distribution of contaminants in the sediments, episodic leakage from the wreck, and/or the mobility of the fish. Assessing PAH exposure in antarctic fish by screening bile using HPLC/fluorescence detection is useful but must be confirmed by other techniques to minimize the false positive indications of exposure caused by spectral interferences noted in some bile samples.

This study was supported by National Science Foundation grant DPP 90-22346. The field assistance of Jim Jobling, Tony Tripp, Tim Wilkinson, and Elsa Haubold is acknowledged. Laboratory assistance was provided by Michelle Bingham and Yu Yanhui.

References

Kennicutt, M. C. II, et al. 1990. Oil spillage in Antarctica: Initial report of the National Science Foundation-sponsored quick response team on the grounding of the *Bahia Paraiso*. *Environmental Science and Technology*, 24:620-624.

Kennicutt, M. C. II, S. T. Sweet, W. R. Fraser, W. L. Stockton, and M. Culver. 1991a. The grounding of the *Bahia Paraiso*, Arthur Harbor, Antarctica—I. Distribution and fate of oil spill related hydrocarbons. *Environmental Science and Technology*, 25:509-518.

Kennicutt, M. C. II, S. T. Sweet, W. R. Fraser, W. L. Stockton, and M. Culver. 1991b. The fate of diesel fuel spilled by the *Bahia Paraiso* in Arthur Harbor, Antarctica. *Proceedings, 1991 International Oil Spill Conference*, 594-600.

Kennicutt, M. C. II, S. T. Sweet, T. J. McDonald, and G. J. Denoux. 1991c. Oil spills in polar climates. The *Bahia Paraiso* accident. *Proceedings 23rd offshore technology conference*, OTC paper No. 6526, 249-256.

Krahn, M. M., M. S. Meyers, D. C. Burrows, and D. C. Malins. 1984. Determination of metabolites of xenobiotics in the bile of fish from polluted waterways. *Xenobiotica*, 14:633-646.

Krahn, M. M., L. D. Rhodes, M. S. Meyers, L. K. Moore, W. D. MacLeod, and D. C. Malins. 1986. Association between metabolites of aromatic compounds in bile and the occurrence of hepatic lesions in English sole (*Parophyrs vetulus*) from Puget Sound, Washington. *Archives of Environmental Contaminations and Toxicology*, 15:61-67.

Krahn, M. M., D. G. Burros, G. M. Ylitalo, D. W. Brown, C. A. Wigrin, T. K. Collier, S. L. Chan, and U. Varanasi. 1992. Mass spectrometric analysis for aromatic compounds in bile of fish sampled after the *Exxon Valdez* oil spill. *Environmental Science and Technology*, 26:116-126.

Hydrocarbon contamination in Arthur Harbor, Anvers Island

M. C. Kennicutt II, T. J. McDonald, and S. J. McDonald

Geochemical and Environmental Research Group
Texas A&M University
College Station, Texas 77845

The presence of humans in remote areas can lead to the introduction of contaminants to otherwise pristine areas. It is often suggested that due to its remoteness, Antarctica should be one of the last remaining areas relatively free of the impact of human activities. However, human presence dates back to the early 1900s and has greatly increased in the last several decades (Platt and Mackie 1979; Clarke and Law 1981; Dayton 1972; Platt 1978, 1979; Lenihan et al. 1990). Localized contamination has been documented at several locations and in most instances is related to petroleum products (Cripps and Priddle 1991; Kennicutt et al. 1990; Lenihan et al. 1990; Risebrough et al. 1990). Petroleum, and its by-products, contain numerous compounds that have toxicological and carcinogenic effects. Due to the epidemiology of polynuclear aromatic hydrocarbons (PAH), they are commonly monitored in studies of anthropogenic pollution. Few studies have systematically documented the distributions, sources, and fate of contaminants in Antarctica (i.e., Kennicutt et al. 1990, 1991a, b, and c; Risebrough et al. 1990; Lenihan et al. 1990; Cripps 1990, 1991; Cripps and Priddle 1991).

The Antarctic Peninsula is a focus of human activity due to the concentration of bird and mammal populations, its mild climate, and its accessibility from South America. Many nations have located their scientific stations along the peninsula and the area attracts the majority of tourism activities in Antarctica. World attention was focused on pollution along the Antarctic Peninsula in 1989 when the Argentine supply ship the *Bahia Paraiso* ran aground in Arthur Harbor, Anvers Island (Kennicutt et al. 1990, 1991 a, b, and c). This incident highlighted the consequences of a catastrophic release of hydrocarbons (Kennicutt et al. this issue). Point source releases, such as spills, are dramatic events. However, a more insidious problem is long-term, sublethal exposure of marine ecosystems to contaminants due to everyday activities. We report the initial findings of a study of hydrocarbons in the organisms and sediments adjacent to Palmer Station, Anvers Island.

The major source of hydrocarbon contamination in subtidal samples near Palmer Station is diesel fuel spillage and leakage related to ship and boating activities (figure1). Combustion-derived PAH were present in subtidal sediments seaward of abandoned incineration sites at Palmer and Old Palmer Station (figures 1 and 2). Soil from various locations around Palmer Station was stained with weathered diesel fuel, lubricating oil, and hydraulic fluid. Subtidal sediments near Old Palmer Station were also contaminated with diesel fuel, apparently leaching from the shore. Diesel fuel was stored as a fuel cache and for heating fuel at Old Palmer Station. Spillage has contaminated soils and runoff transports a portion of this material to subtidal sediments. Soil and intertidal contamination was lower at Palmer Station than at Old Palmer Station even though Old Palmer Station has been inactive for years. This suggests that op-

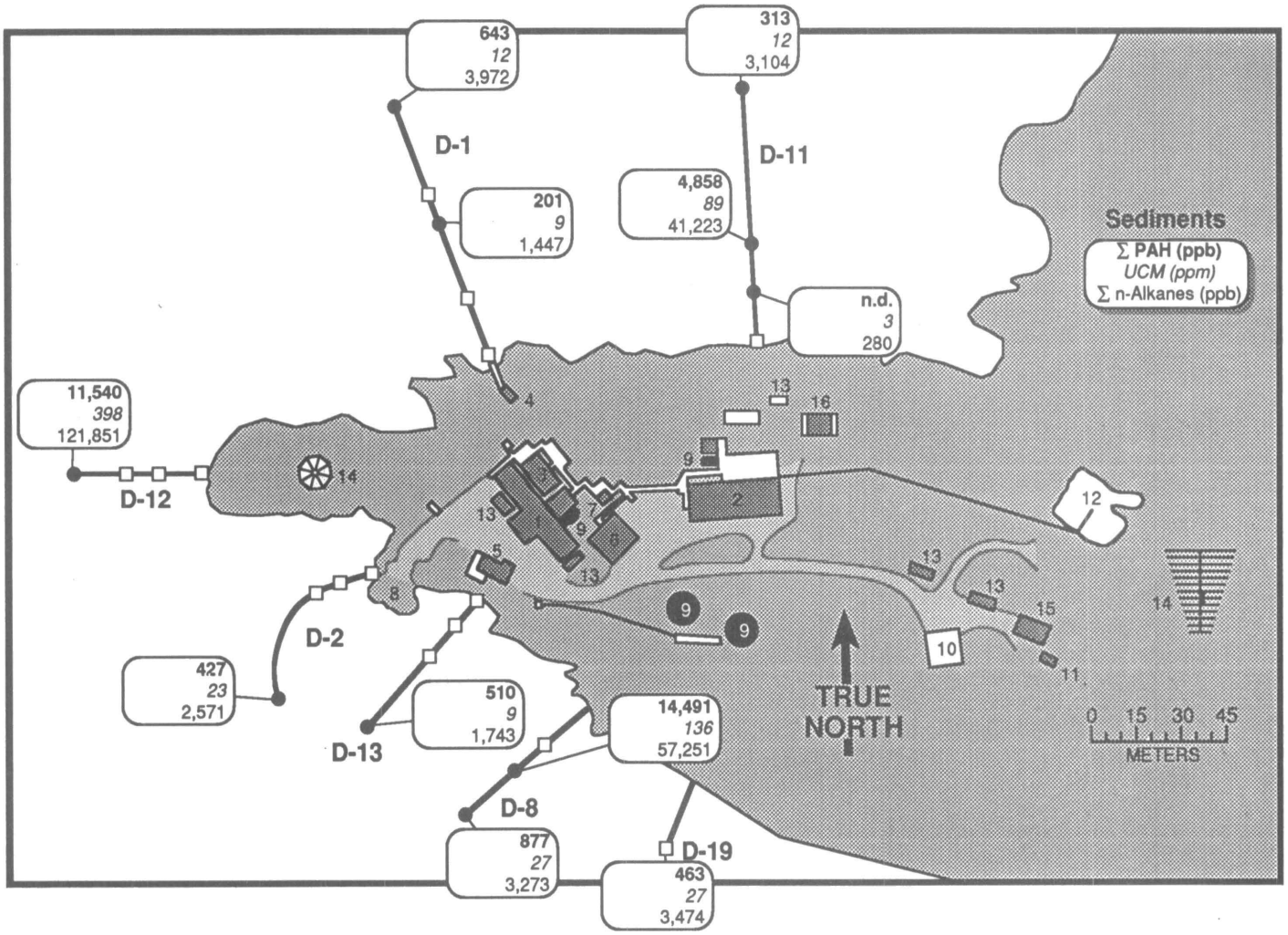

Figure 1. Concentration polycyclic aromatic hydrocarbons (ÂPAH, ppb dry wt.), the unresolved complex mixture (UCM, ppm dry wt.), and normal alkanes (Ân-alkanes, ppb dry wt.) in subtidal sediments collected adjacent to Palmer Station, Anvers Island.

erational practices have helped limit contamination at Palmer Station. Scouring by currents and ice redistributes contaminants throughout the harbor. Little, if any, subtidal contamination could be directly attributed to the *Bahia Paraiso* spill.

Contamination of marine environments is also monitored by analyzing tissues for contaminants. Contaminant concentrations in sediment and water do not always indicate faunal exposure. Intertidal and subtidal limpets (*Nacella concinna*) collected near Palmer and Old Palmer Stations contained measurable quantities of PAH (figure 3). Contamination was highest in the intertidal and decreased with increasing distance from shore. The highest concentrations of tissue contaminants were found in intertidal areas adjacent to high levels of onshore soil contamination. Limpets preferentially incorporated more water soluble aromatic compounds, suggesting exposure to dissolved contaminants in runoff rather than particulate or slick-derived materials. This was in contrast to subtidal sediments which were primarily contaminated with freshly spilled diesel fuel. While contamination is detectable in limpets in the vicinity of Palmer Station, the concentrations observed were one to two orders of magnitude lower than the contamination caused in intertidal limpets by the *Bahia Paraiso* diesel fuel spill. While a "halo" of hydrocarbons can be detected both in sediments and limpets adjacent to an existing and an abandoned station the contamination is low level. The contamination rapidly decreases with distance from the source and is virtually nondetectable one-half kilometer from the Station.

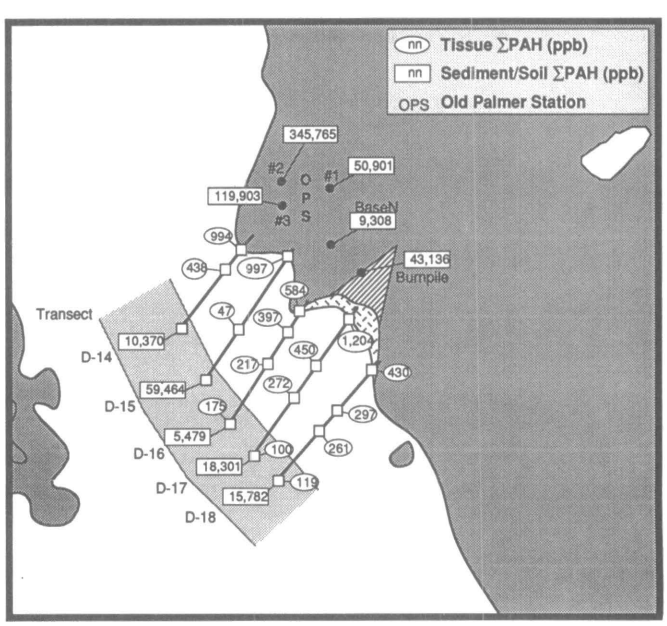

Figure 2. ÂPAH (ppb dry wt.) in sediments and tissue extracts collected in the vicinity of Old Palmer Station adjacent to Arthur Harbor.

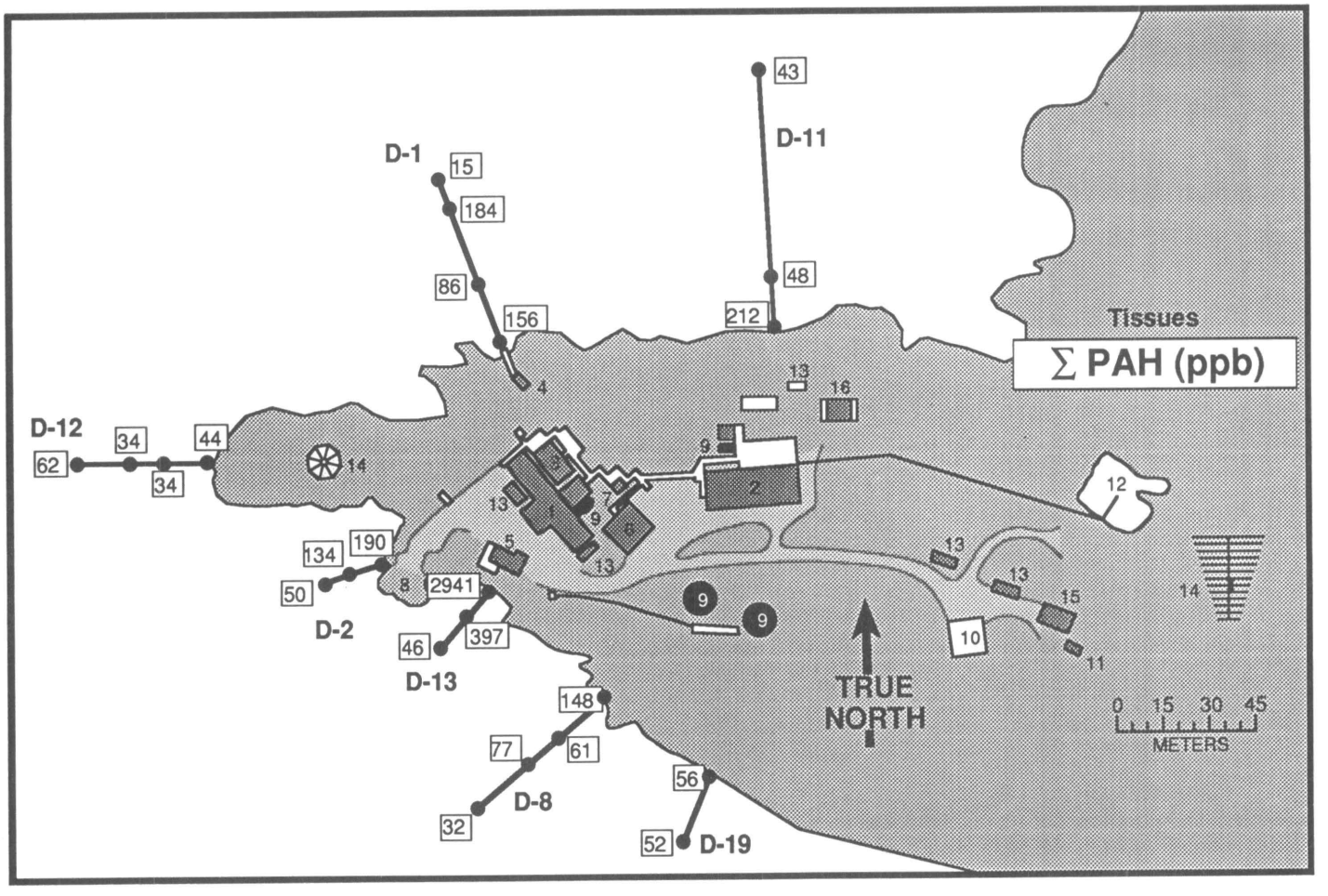

Figure 3. Polycyclic aromatic hydrocarbon concentrations (ÂPAH ppb dry wt.) in limpet tissues collected along transects near Palmer Station, Anvers Island, Antarctic Peninsula.

These studies were supported by National Science Foundation grants DPP 89-12497, DPP 89-15015, and DPP 90-22346. We would also like to acknowledge the field support of Jim Jobling, Anthony Tripp, Tim Wilkinson, and Elsa Haubold. Laboratory and data support was provided by numerous GERG staff scientists.

References

Clarke, A. and R. Law. 1981. Aliphatic and aromatic hydrocarbons in benthic invertebrates from two sites in Antarctica. *Marine Pollution Bulletin*, 12:10-14.

Cripps, G. C. and J. Priddle. 1991. Hydrocarbons in the antarctic marine environment. *Antarctic Science*, 3:233-250.

Cripps, G. C. 1990. Hydrocarbons in seawater and pelagic organisms of the southern ocean. *Polar Biology*, 10:393-402.

Cripps, G. C. 1991. Problems in the identification of anthropogenic hydrocarbons against natural background levels in the Antarctic. *Antarctic Science*, 1:307-312.

Dayton, P. K. 1972. Toward an understanding of community resilience and the potential effects of enrichment to the benthos at McMurdo Station, Antarctica. In B. C. Parker (Ed.), *Proceedings of the Colloquium on Conservation Problems in Antarctica.* Laurence, Kansas: Allen Press, 81-95.

Kennicutt, M. C. II, et al. 1990. Oil spillage in Antarctica: Initial report of the National Science Foundation-sponsored quick response team on the grounding of the *Bahia Paraiso*. *Environmental Science and Technology*, 24:620-624.

Kennicutt, M. C. II, S. T. Sweet, W. R. Fraser, W. L. Stockton, and M. Culver. 1991a. The grounding of the *Bahia Paraiso*, Arthur Harbor, Antarctica—I. Distribution and fate of oil spill related hydrocarbons. *Environmental Science and Technology*, 25:509-518.

Kennicutt, M. C. II, S. T. Sweet, W. R. Fraser, W. L. Stockton, and M. Culver. 1991b. The fate of diesel fuel spilled by the *Bahia Paraiso* in Arthur Harbor, Antarctica. *Proceedings, 1991 International Oil Spill Conference*, 594-500.

Kennicutt, M. C. II, S. T. Sweet, T. J. McDonald, and G. J. Denoux. 1991c. Oil spills in polar climates: The *Bahia Paraiso* accident. *Proceedings 23rd Offshore Technology Conference*, OTC Paper No. 6526, 249-256.

Lenihan, H. S., J. S. Oliver, J. M. Oakden, and M. D. Stephenson. 1990. Intense and localized benthic marine pollution around McMurdo Station, Antarctica. *Marine Pollution Bulletin*, 21:422-430.

Platt, H. M. 1978. Assessment of the macrobenthos in an antarctic environment following recent pollution abatement. *Marine Pollution Bulletin*, 9:149-153.

Platt, H. M. 1979. Ecology of King Edward Cove, South Georgia: Macrobenthos and the benthic environment. *Bulletin British Antarctic Survey*, 49:231-238.

Platt, H. M. and P. R. Mackie. 1979. Analysis of aliphatic and aromatic hydrocarbons in antarctic marine sediment layers. *Nature* (London), 280:576-578.

Risebrough, R. W., B. W. Lappe, and C. Younghans-Haug. 1990. PCB and PCT contamination in Winter's Quarter Bay, Antarctica. *Marine Pollution Bulletin*, 21:523-529.

High-resolution ultraviolet spectral irradiance monitoring program in polar regions: Five years (and growing) of data available to polar researchers in ozone- and ultraviolet-related studies

CHARLES R. BOOTH, TIMOTHY B. LUCAS, AND JOHN H. MORROW

Biospherical Instruments
San Diego, California 92110-2621

In the fall of 1987, responding to the serious ozone depletion reported in Antarctica, the Office of Polar Programs of the National Science Foundation called for the establishment of an ultraviolet monitoring system in Antarctica. This network was brought on-line in 1988, and we present the details of its operation and examples of recent data products here. This network is the first automated, high-resolution ultraviolet (UV) scanning spectroradiometer network installed in the world. It has been largely successful in operation in the harshest environments of Antarctica and the Arctic and is currently returning data to researchers studying the effects of ozone depletion on terrestrial and marine biological systems; in addition, it is being used in development and verification of models of atmospheric light transmission.

Spectroradiometers were installed in four locations between February and November 1988; a fifth instrument located at Barrow, Alaska, was installed in December 1990. The table lists the positions and the period of data referred to in this report for these sites.

The spectroradiometer is based on a temperature-stabilized double-scanning monochromator coupled to a photomultiplier tube (PMT) detector (figure 1.) The system is optimized for operation in the UV. A vacuum- formed Teflon diffuser serves as an all-weather irradiance collector and is heated by the system to discourage ice and snow buildup. The instrument has wavelength and intensity calibration lamps for automatic calibrations at programmed intervals (typically two to four times per day). A data acquisition system accompanies the instrument, and an IBM-compatible computer is used to control the system and log the data. (See figure 1.) The system hardware is divided into two sections. The first section, consisting of the irradiance collector,

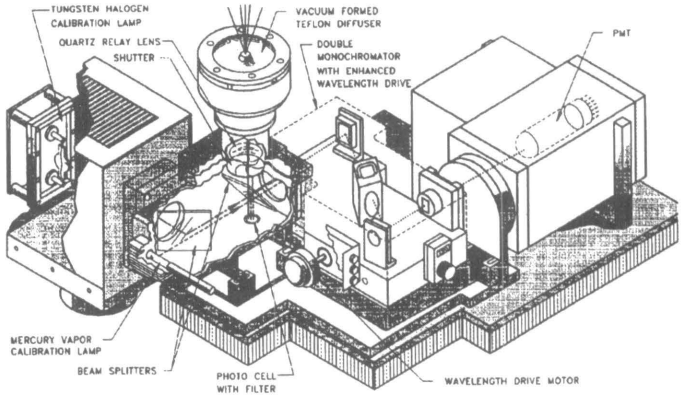

Figure 1. Cutaway diagram of monochromator and collection optics.

monochromator, PMT, and calibration sources, is housed in a fully weatherproof enclosure built into the roof of a building at the site. Located up to 15.24 meters away, typically on a laboratory bench, is the remainder of the system, consisting of power supplies, temperature controllers, electronic interfaces, and the personal computer. In addition to the internal, automatically controlled sources for wavelength and sensitivity calibration, a separate calibration fixture mounted above the irradiance collector is provided for periodic manual calibrations, typically every 2 weeks.

The f/3.5, 0.1-meter, double monochromator is the heart of the system; it is configured with 167-micron input/output slits and a 250-micron intermediate slit. The holographic gratings have 1,200 grooves/millimeter blazed at 250 nanometers and driven by a stepping motor with a step size of 0.05 nanometer. The spectral bandwidth is a nominal 0.75 nanometer. The photomultiplier tube is a 28-millimeter diameter, 11-stage device with a bialkali cathode and a quartz window. It is housed in a cooled enclosure, maintained at approximately 0 °C, to reduce dark current and noise. Temperature of the monochromator is carefully monitored and controlled and is typically stable to 0.5 °C. In addition to the frequent calibrations with the internal standards, periodic calibration of the system uses an optical standard traceable to the National Institute of Standards and Technology.

Data scans are conducted on an hourly basis when the sun is above the horizon. Data are collected on a reduced schedule at night. This provides a complete history of the operation of the instrument throughout a complete temperature cycle. Background data (Eppley sensors and instrument temperature) are collected over 24 hours at 5-minute intervals. At sites inside the arctic or antarctic circles, the instrument is operated on a reduced scan schedule during the winter darkness.

There are several classes of data that are available to the

Installation sites

ID #	Site	Longitude	Latitude	Established	Normal Season
1	McMurdo, Antarctica	166.40° E	77.51° S	March 1988	August-April
2	Palmer, Antarctica	64.03° W	64.46° S	May 1988	Year-round
3	South Pole, Antarctica	0.00°	90.00° S	February 1988	September to March
4	Ushuaia, Argentina*	68.00° W	54.59° S	November 1988	Year-round
5	San Diego, California**	117.00° W	32.00° N	1990	Testing facility, no reported data
6	Barrow, Alaska***	156.47° W	71.18° N	December 1990	January to November

*CADIC: Centro Austral de Investigaciones Cientificas, Argentina.
**Full-time data available after November 1992.
***UIC/NARL: Ukpeagvik Inupiat Corporation/(formerly) Naval Arctic Research Laboratory.

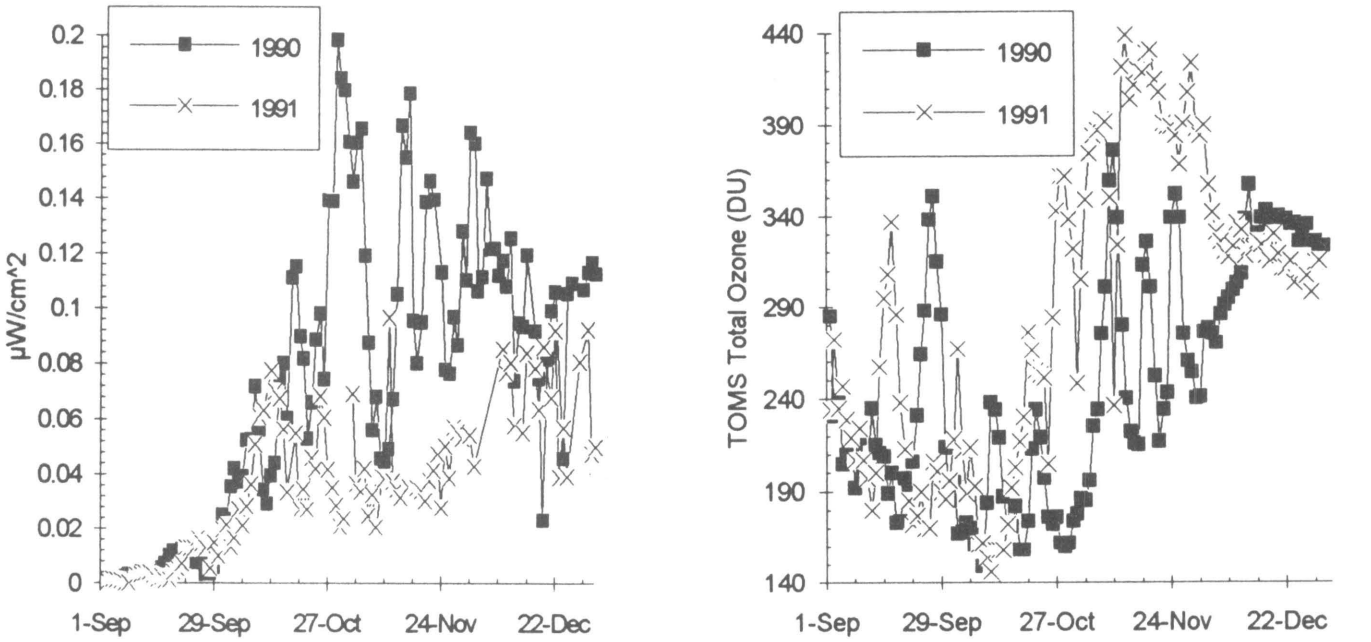

Figure 2. (*A*) NASA TOMS ozone data (left). 1990 readings are significantly lower than those in 1991 and correspond to the higher levels of observed UV. (*B*) Example time series of dose-weighted irradiance at McMurdo available from the network. In this example, Setlow's (1974) dose weighting has been used to calculate the dose-weighted irradiance.

various segments of the research community. Level 1 data are in their original binary form and are uncorrected for offsets or wavelength errors. These data are only available to approved NSF- sponsored researchers. Level 2 data have been referenced to calibration constants determined at the beginning of the season and have been corrected for wavelength errors and daily changes in responsivity, based on daily scans of the internal lamp wavelength and instrument responsivity. Level 2 data is available in near real time at most sites for NSF-sponsored researchers conducting research at that site. These data are provisional, and investigators are cautioned to check with Biospherical Instruments before any final conclusions or publications are made using these data, as they are subject to revision. Level 3 data are referenced to both beginning and end-of-season calibration events in order to compensate for system changes, long-term drifts, such as calibration lamp aging, or other effects. Furthermore, Level 3 data include corrections for instrument and ambient-temperature fluctuations, as well as other retrospective corrections. Level 3 data are distributed on a CD-ROM and are generally available to any researcher (request data through NSF). Level 3 data are normally made available during the summer for the period covering the previous 12 months.

Data are processed in microwatts per square centimeter per nanometer and are available in two forms: Database data where time series of parameters of interest are collected into data files that are readily computer-readable and individual files with full spectral resolution for each hourly scan. There are three types of data bases: spectral integrals including dose weightings (figures 3 and 6), irradiances at selected wavelengths (figures 4a, 4c, and 5), and quality control data bases. Data at the full spectral resolution (figure 5) are available as individual data files for each scan segment. Because of the large number of these files (up to 30,000 per site per year), these files are distributed on a ISO9660 CD-ROM in ASCII comma separated values format (CSV). Small numbers of these full- resolution files are also available by other means of electronic distribution. (Contact Biospherical Instruments for details.)

Over the past 5 years this network of instruments has provided data for the support of several research programs, the details of which may be found in the following references: Lubin and Frederick (1990, 1991, 1992), Lubin et al. (1989, 1992), Smith et al. (1990, 1991, 1992), and Stamnes et al. (1990, 1991, 1992). Examples of data recently obtained are shown in the following figures.

Figures 2 and 3 contrast the 1990 and 1991 austral spring seasons at McMurdo Station. In 1990 there was considerably greater ozone depletion (figure 2), and this was reflected in higher 1990 levels of biologically active UV irradiance (figure 3).

Figure 3 examines the irradiance environment at the South Pole for the period 15 September to 15 December 1991. The major feature in the time series of irradiance for 300 nanometers, where ozone strongly absorbs (figure 3a), coincides with a reduction and subsequent increase in ozone concentration (figure 3b). This is in contrast with the 400-nanometer irradiance, where ozone is transparent (figure 3d). UV-B, spanning the spectral region of 280-320 nanometers, is also ozone-sensitive (figure 3c). Between 11 and 17 November 1991 the total column ozone concentration over the South Pole doubled. The change in the UV-B spectral irradiance between these two dates is shown in figure 5. With this high-resolution spectral data, we are able to use Setlow's (1974) dose weighting to calculate the change in biologically active radiation, as shown in figure 6. Integration under these curves shows a 67 percent decrease in instantaneous dose-weighted irradiance.

In figures 4a and 4b the effect of ozone depletion over the South Pole can be clearly seen. The irradiance at 400 nanometers (figure 3c) regularly increased during the season as the sun approached solstice (barring clouds and occasional shading of the instrument by other apparatus). To increasingly greater degree with decreasing wavelength, the time course of irradiance

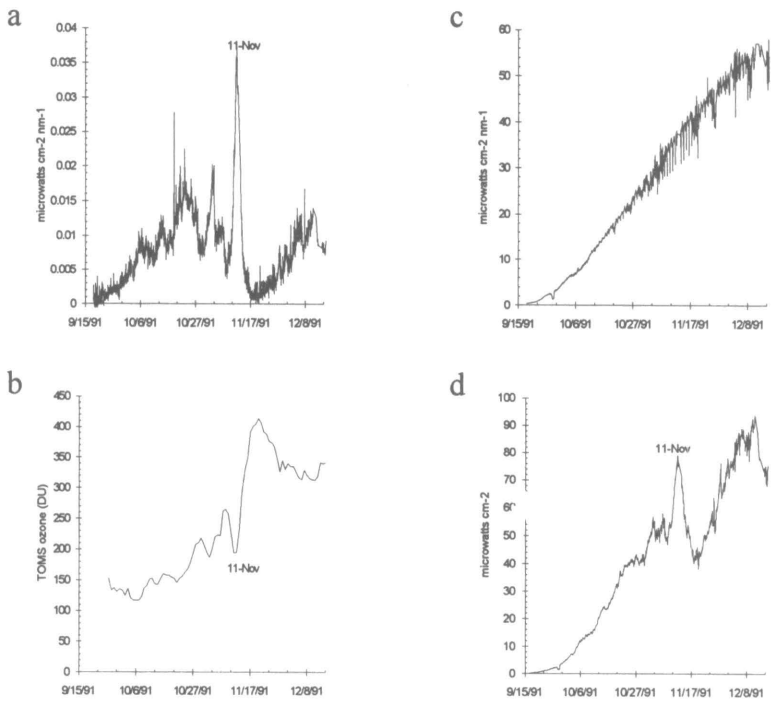

Figure 3. (*A*) Time series of irradiance at 300 nanometers at the South Pole. (*B*) Time series of ozone as reported by TOMS. Units are Dobson Units. (*C*) Irradiance at 400 nanometers. During part of the year the collector was shaded, causing daily dips. (*D*) Time series of integrated UV-B (280-320 nanometers) irradiance.

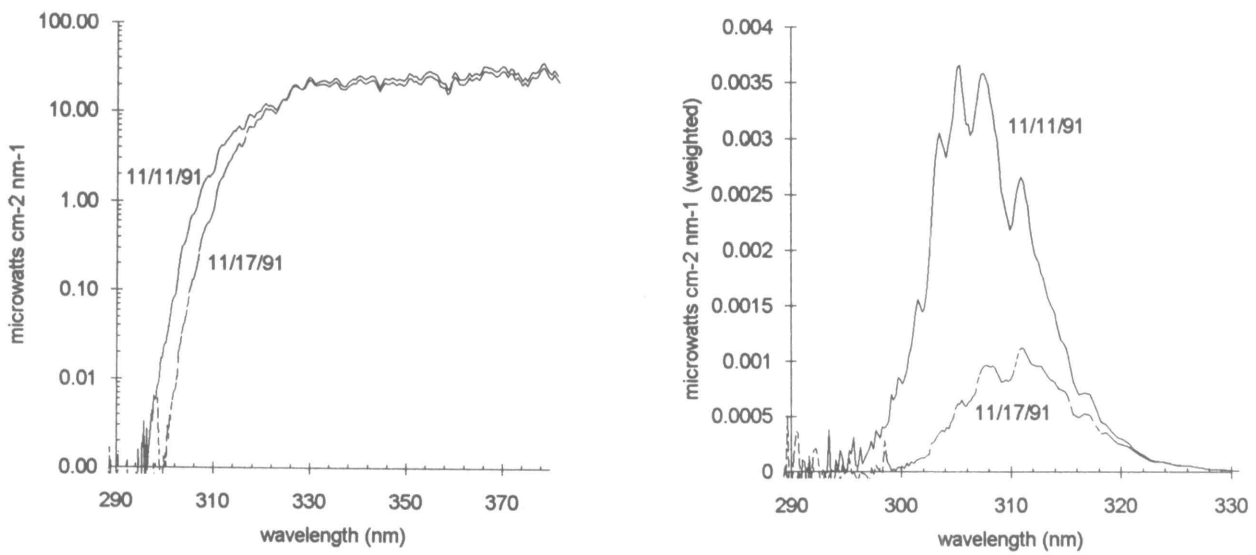

Figure 4. (*A*) Spectral irradiance over the South Pole (top) on 11 and 17 November 1991. (*B*) Spectral irradiance (bottom) from (*A*) with Setlow's dose weighting applied.

resembles the inverse of the ozone concentration, particularly when the sun is high, showing the strong correlation between lower ozone and higher UV irradiance.

The need for the rapid set up of the UV-monitoring program was established by Dr. Peter Wilkniss, Director, Office of Polar Programs, National Science Foundation. We thank a variety of contributors to this effort, including Sue Weiler, Steve Kottmeier, John Gress, Susana Diaz, David Norton, Dan Endres, Chris Churylo, Tanya Mestechkina, John Tusson IV, and David Neuschuler. TOMS (Total Ozone Mapping Spectrometer) are from the Toms Update CD-ROM (TOMS 1992). Data from the NSF UV spectroradiometer network is available to researchers on CD-ROM. Consult the authors for details.

This is an ongoing Technical Project, #T-313, and the participants are subcontractors to the Antarctic Support Associates.

References

Lubin, D. and J. E. Frederick. 1992. Observations of ozone and cloud properties from NSF ultraviolet-monitor measurements at Palmer Station, Antarctica. *The Antarctic Journal of the U.S.*, 25(5):241-242.

Lubin, D. and J. E. Frederick. 1990. Column ozone measurements at Palmer Station, Antarctica: Variations during the austral springs of 1988 and 1989. *Journal of Geophysical Research*, 95:13,883-13,889.

Lubin, D. and J.E. Frederick. 1989. Ultraviolet monitoring program at Palmer Station, spring, 1988. *Antarctic Journal of the U.S.*, 24(5):172-174.

Lubin, D., J. E. Frederick, C. R. Booth, T. Lucas, D. Neuschuler. 1989. Measurements of enhanced springtime ultraviolet radiation at Palmer Station, Antarctica. *Geophysical Research Letters*, 16:783-785.

Lubin, D. and J. E. Frederick. 1991. The ultraviolet radiation environment of the Antarctic Peninsula: The roles of ozone and cloud cover. *Journal of Applied Meteorology*, 30:478-493.

Lubin. D., B. G. Mitchell, J. E. Frederick, A. D. Alberts, C. R. Booth, T. Lucas, D. Neuschuler. 1992. A contribution toward understanding the biospherical significance of antarctic ozone depletion. *Journal of Geophysical Research*, in press.

Smith, R. C., Z. Wan, and K. S. Baker. 1990. Ozone depletion in Antarctica: Satellite and ground measurements, and modeling under clear-sky conditions. *Journal of Geophysical Research*, in press.

Smith, R., B. Prezelin, R. Bidigare, D. Karentz, S. MacIntyre. 1991. Ice Colors '90: Ultraviolet radiation and phytoplankton biology in antarctic waters. *The Antarctic Journal of the U.S.*, 288-290.

Smith, R. C., B. B. Prezelin, K. S. Baker, R. R. Bidigare, N. P. Boucher, T. Coley, D. Karentz, S. MacIntyre, H. A. Matlick, D. Menzies, M. Ondrusek, Z. Wan, K. J. Waters. 1992. Ozone depletion: Ultraviolet radiation and phytoplankton biology in antarctic waters. *Science*, 256: 952-959.

Smith, R., K. Baker, D. Menzies, K. Waters. 1991. Biooptical measurements from the Ice Colors '90 cruise 5 Oct -21 Nov 1990. SIO Ref 91-13.

Smith, R. C. and K. S. Baker. 1989. Stratospheric ozone, middle ultraviolet radiation and phytoplankton productivity. *Oceanography*, November 1989, 4-10.

Stamnes, K., J. Slusser, and M. Boden. 1991. Derivation of total ozone abundance and cloud effects from spectral irradiance measurements. *Applied Optics*, 30:4,418-4,426.

Stamnes, K., J. Z. Jin, J. Slusser, C. Booth, and T. Lucas. 1992. Several-fold enhancement of biologically effective ultraviolet radiation levels at McMurdo Station Antarctica during the 1990 ozone hole. *Geophysical Research Letters*, in press.

Stamnes, K., J. Slusser, M. Bowen, C. Booth, and T. Lucas. 1990. Biologically effective ultraviolet radiation, total ozone abundance, and cloud optical depth at McMurdo Station, Antarctica, September 15, 1988 through April 15, 1989. *Geophysical Research Letters*, 17:2,181-2,184.

Setlow, R. B. 1974. The wavelengths in sunlight effective in producing skin cancer: A theoretical analysis. *Proceedings of the National Academy of Science*, 71(9):3,363-3,366.

TOMS (Total Ozone Mapping Spectrometer). 1992. TOMS Update CD-ROM. Available from the National Space Science Data Center (NSSDC), Goddard Space Flight Center.

The Antarctic Marine Geology Research Facility 1991-1992

JONATHAN R. BRYAN

Department of Geology
Florida State University
Tallahassee, Florida 32306

The 1991-1992 project year (1 June to 31 May 1992) was a time of change for the National Science Foundation's Antarctic Marine Geology Research Facility at Florida State University (FSU). Dennis S. Cassidy, curator of the facility for 28 years, retired at the end of September 1991, and a new curator was hired by the FSU Department of Geology. Cassidy's outstanding leadership and organization of the facility made for a smooth transition. The mission and activities of the facility continued with little interruption and are summarized below.

From the extensive collection of cored, dredged, trawled, and grabbed sediments at the facility, a total of 1,129 samples were distributed to 21 geoscientists representing 17 institutions and 4 countries. The curator received requests for samples taken from the following cruises and drilling projects:

- USNS *Eltanin*: 879 samples from over 200 piston cores and 85 trigger cores;
- ARA *Islas Orcadas*: 16 samples from 2 piston cores;
- USCGC *Glacier*: 74 samples from 10 piston cores;
- Cenozoic Investigations of the Ross Sea (CIROS) 1 and 2: 96 samples; and
- R/V *Polar Duke*: 64 samples from 3 piston cores.

Two shipments of cores were received. These include 2 piston cores from the February - March 1990 cruise of the R/V *Polar Duke* to the Ross Sea/McMurdo Sound area (Anderson and Bartek 1990) and 8 piston cores, 8 trigger cores, and 4 gravity cores from the January 1991 cruise of the same vessel around the northern Antarctic Peninsula (Anderson 1991).

Over 250 paleomagnetic samples from various *Eltanin* and *Islas Orcadas* piston cores were returned by Michael T. Ledbetter (California State University). Numerous cores are on loan to Rice University for X-ray analysis. These include 43 piston cores (15 *Eltanin*, 19 *Glacier*, 9 *Polar Duke*), 19 trigger cores (15 *Eltanin*, 4 *Glacier*), 2 Phleger cores (*Eltanin*), 2 trawled samples (*Eltanin*), and 3 cores from the Ross Ice Shelf Project.

The facility hosted several visiting scientists during the project year. Most of the investigators were obtaining samples; others were inspecting the collections for their prospective research. The following 15 geoscientists visited the facility on the following dates: 9-11 July 1991: Scott E. Ishman (Byrd Polar Research Center, Ohio State University) and Andrew Stein (Hamilton College); 14-17 August 1991: David M. Harwood (University of Nebraska), Xin Ke Jiang (University of Nebraska), and Gary S. Wilson (Antarctic Research Centre, Victoria University of Wellington, New Zealand); 28 February 1992: Valesca Maria Portilla Eilert (Universidade Federal do Rio Grande do Sul, Brazil); 9 March 1992: Rusty Lotti (Lamont-Doherty Geological Observatory); 26-31 May 1992: John B. Anderson (Rice University), Laura Branfield (Rice University), Stephanie Shipp (Rice University), Phil Bart (Rice University), Fernando Siringan (Rice University), John Andrews (University of Colorado, Boulder), Anne Jennings (University of Colorado, Boulder), and Kerstin Williams (University of Colorado, Boulder).

Complete sediment descriptions for the 1985, 1986, and 1987 austral summer cruises of the USCGS *Glacier* (Anderson 1985; Anderson et al. 1986; Jeffers and Anderson 1986; Anderson et al. 1987) and the 1986 cruise of the NSF-chartered research vessel *Polar Duke* (Jeffers 1987) were near completion at the time of Cassidy's retirement. The first order of business for the new curator was the publication of this material. The facility is currently entering all core and other sediment descriptions, including gra-

phic logs, into a computer data base in an effort to expedite the production of core description volumes. The Deep Freeze 1985 volume was recently completed (Bryan et al. 1992) and is available to all interested geoscientists, prospective users of the facility, and libraries upon request to the curator. Additional volumes for the remaining cruises will be forthcoming. Initial descriptive work on material from the 1988, 1989, 1990, and 1991 R/V *Polar Duke* cruises (Anderson 1988; Domack 1988; Lawver and Villinger 1989; Anderson and Bartek 1990; Anderson 1991) is in progress.

In addition to descriptive work for publication, a new initiative at the facility is the entry of all core data into the National Geophysical Data Center (NGDC) data bank. It is hoped that the inclusion of the facility's cores in that data base will promote wider recognition of, access to, and of the outstanding collection utilization.

Prior to his departure, Cassidy completed a unique bibliographic data base consisting of all published articles making reference to materials curated at the facility (Cassidy 1990). The data base is regularly updated and is available to all interested parties by request to the curator. Researchers who have used or are using samples from the facility are reminded to please send reprints to the curator as soon their work is completed and published.

As a service-oriented institution, the facility participates in a number of activities as a courtesy to the general antarctic community and to the local community in Tallahassee, Florida. Inquiries about materials published by the facility are frequently received from researchers and libraries. Requests for maps and other references are fulfilled from the facility's outstanding library. Recently, several publications and photographs were sent to the new International Antarctic Centre in Christchurch, New Zealand, for an educational visitor display case. The antarctic facility is also regularly visited by local schools and geology classes, and members of its staff are producing an educational exhibit on antarctic geology that will be displayed in the FSU Geology Department.

The curatorship of antarctic collections at Florida State University is supported by National Science Foundation grant DPP 75-19723.

References

Anderson, J. B. 1985. Preliminary results from the USC *Glacier* 1985 cruise. *Antarctic Journal of the U.S.*, 19(5):81-85.

Anderson, J. B. 1988. Marine Geophysical survey of the Antarctic Peninsula continental shelf (63° W to 68° W): Preliminary results. *Antarctic Journal of the U.S.*, 23(5):91-94.

Anderson, J. B. 1991. Preliminary results of high resolution seismic and coring surveys in the Antarctic Peninsula region. *USAP 91 marine geology-geophysics cruise report and R/V* Polar Duke *equipment status*, Department of Geology and Geophysics, Rice University, Houston.

Anderson, J. B. and L. R. Bartek. 1990. Preliminary results of a high-resolution seismic reflection survey of the Ross Sea continental shelf. *Antarctic Journal of the U.S.*, 25(5):61-63.

Anderson, J. B., L. R. Bartek, and D. E. Reid. 1987. Preliminary results of a 1986-1987 austral summer marine geological survey of the western Ross Sea. *Antarctic Journal of the U.S.*, 22(5):120-122.

Anderson, J. B., D. J. DeMaster, and C. A. Nittrouer. 1986. Preliminary results from marine geological cruises aboard the U.S. Coast Guard icebreaker *Glacier*. *Antarctic Journal of the U.S.*, 21(5):144-148.

Bryan, J. R., C. Kelly, X. Liu, and C. Painter (Eds.). 1992. Descriptions of sediments recovered by the USCGC *Glacier*, USARP Operation Deep Freeze 1985, South Orkney Plateau, South Shetland Shelf, Bransfield Strait, Marguerite Bay, and Pine Island Bay. *Contribution no. 54, Sedimentology Research Laboratory*, Department of Geology, Florida State University, Tallahassee.

Cassidy, D. S. 1990. A bibliographic database for project collections of the Antarctic Marine Geology Research Facility and core library. *Antarctic Journal of the U.S.*, 25(5):288-290.

Domack, E. W. 1988. Depositional environments of the antarctic continental shelf: Fjord studies from the R/V *Polar Duke*. *Antarctic Journal of the U.S.*, 23(5):96-102.

Jeffers, J. D. 1987. Preliminary results of marine geological and geophysical investigations in the Bransfield Strait, Antarctic Peninsula. *Antarctic Journal of the U.S.*, 22(5):131-134.

Jeffers, J. D. and J. B. Anderson. 1986. Sedimentation and tectonics in the Bransfield Strait: A preliminary report. *Antarctic Journal of the U.S.*, 21(5):141-143.

Kennedy, D. S. and J. B. Anderson. 1986. Preliminary results of marine geologic investigations, Marguerite Bay, Antarctic Peninsula. *Antarctic Journal of the U.S.*, 21(5):149-151.

Lawver, L. A. and H. Villinger. 1989. North Bransfield Basin: R/V *Polar Duke* cruise PD VI-88. *Antarctic Journal of the U.S.*, 24(5):117-120.

Surveying and mapping in Antarctica

Roy R. Mullen and Jerry L. Mullins

U.S. Geological Survey
Reston, Virginia 22092

The U.S. Geological Survey's (USGS) Antarctic Surveying and Mapping Program focused its activities during the 1991-1992 season on the acquisition of global positioning system (GPS) geodetic mapping control, Doppler satellite surveying, seismology, Doppler satellite tracking, and an international GPS campaign.

During 1991-1992 field season the USGS's geodetic control crews employed GPS positioning as the means of establishing geodetic mapping control in Antarctica. As part of the international GPS campaign, the USGS team of Gordon H. Shupe, Jon C. Campbell, and Frank J. Kenney established GPS base stations at McMurdo, South Pole, and Byrd stations.

Additionally, supported by the USC *Polar Sea*, the team established new mapping control stations along the Marie Byrd Land coast, Mount Siple, and Pine Island Bay areas. In the Mount Siple area, new stations were established on Maher Island (Station Campbell), Burtis Island (Station Tootie), and Lovill Bluff (Station Zimmerman).

In the Pine Island Bay area eight new control stations were established and five existing stations reoccupied. The stations reoccupied were part of USGS's 1960s land traverse which covered much of the area adjacent to Pine Island Bay. The new positions acquired for these old stations will allow them to be used for mapping in the current satellite datum.

The USGS participated in the third phase of the antarctic GPS observing campaign. The objectives of the international GPS campaigns are to determine the relative motion between the antarctic tectonic plates and the adjoining plates and to establish

a baseline between existing and proposed antarctic very long baseline interferometry sites.

The USGS team, with teams from other participating countries, conducted simultaneous observations at antarctic stations from 14 December 1991 to 22 January 1992. The campaign obtained a quality data set from a network of globally distributed stations that will assess the use of GPS for long baseline geodetic surveys in Antarctica. The antarctic continent-wide GPS operations were coordinated by the Australian Survey and Land Information Group in Canberra, Australia, a member of the Scientific Committee On Antarctic Research (SCAR) Working Group on Geodesy and Geographic Information. The USGS team collected GPS data continuously at the McMurdo, South Pole, and Byrd stations using a dual-frequency carrier phase GPS receiver. Agencies from Australia, Germany, Italy, Spain, Chile, Argentina, and the United States deployed GPS receivers at stations throughout the continent. The GPS data collected at these stations are being processed in Australia and the United States.

A primary goal of the GPS campaign was to continue our work and investigations to improve GPS observations on the continent of Antarctica. The project offers an opportunity to evaluate the practical aspects of GPS survey operations in polar regions. The experience is being used to assess the use of integrating GPS surveys, conducted in support of potential scientific projects, with observations at GPS fiducial reference stations located in Antarctica. The results will identify key areas for further improvement in tracking instrumentation, field procedures, and data analysis.

The objective of the SCAR Working Group on Geodesy and Geographic Information is to acquire high-quality geodetic data to study geodynamics affecting the antarctic and adjoining tectonic plates. Other programs, notably the west antarctic sheet ice initiative and the National Oceanic and Atmospheric Administration's Climate and Global Change Program, will be supported by the SCAR project. Also, the team established eight new Doppler satellite stations and reoccupied two previously established stations in the vicinity of the proposed Pegasus runway on the McMurdo Ice Shelf. These 10 stations will be reoccupied in subsequent field seasons to monitor the direction and velocity of ice movement in support of the Cold Regions Research and Engineering Laboratory's proposed Pegasus blue-ice runway project.

In January 1992 the USGS team conducted a geodetic survey to establish the position of the true South Pole marker at Amundsen-Scott Station. Based on this season's observations and data from previous surveys, the ice sheet at the South Pole continues to move approximately 10 meters per year in a northwesterly direction. The team installed a permanent brass marker identifying the 1991-1992 austral summer position.

The USGS has operated a Doppler satellite receiving station year-round at Amundsen-Scott South Pole Station since the 1972-1973 season. The USGS South Pole team of Roger A. Barlow and Michael J. Starbuck wintered over during the 1991-1992 season. The team collected satellite tracking data to establish precise ephemerides of geodetic satellites. Also, the USGS operates and maintains seismometers at the South Pole. The South Pole Station provides essential azimuth control for determination of epicenters for disturbances that occur in the southern latitudes and serves as a vital station in the Worldwide Standardized Seismological Network.*

These programs were funded by National Science Foundation grant DPP 91-14787.

** In addition, the USGS operates and maintains seismometers for University of California at Los Angeles ultralong period seismic program. Data from this program are used in the study of earth tides.*

Integrated offshore studies on antarctic Cenozoic history, glaciation, and sea-level change: The ANTOSTRAT project

A.K. Cooper

U.S. Geological Survey
Menlo Park, California 94025

P.N. Webb

Department of Geology
Ohio State University
Columbus, Ohio 43210

The Antarctic Offshore Acoustic Stratigraphy project (ANTOSTRAT) is a recent international cooperative effort to coordinate and integrate all existing acoustic and geologic sample data from the antarctic continental margin to study Cenozoic glacial history and the offshore geologic impacts of the antarctic ice sheet. Five segments of the antarctic continental margin that have thick glacial sedimentary deposits (Ross Sea, Wilkes Land, Prydz Bay, Weddell Sea, and Antarctic Peninsula) have been targeted for detailed studies of existing seismic and geologic data by regional working groups. The desired result of ANTOSTRAT studies is a unified model for circumantarctic glaciation and global sea-level changes. The model would be the basis for future testing by scientific drilling of the antarctic continental margin.

Much of what is currently known about the antarctic continental margin is derived from acoustic data (e.g., high- and low-resolution seismic-reflection, bathymetry, and side-scan data) that have been collected since the 1960s. At least five areas of the antarctic continental shelf are underlain by Cenozoic sedimentary sequences that are many kilometers thick and have prograded the continental shelf up to 85 kilometers (figure 1a)(e.g., Hinz and

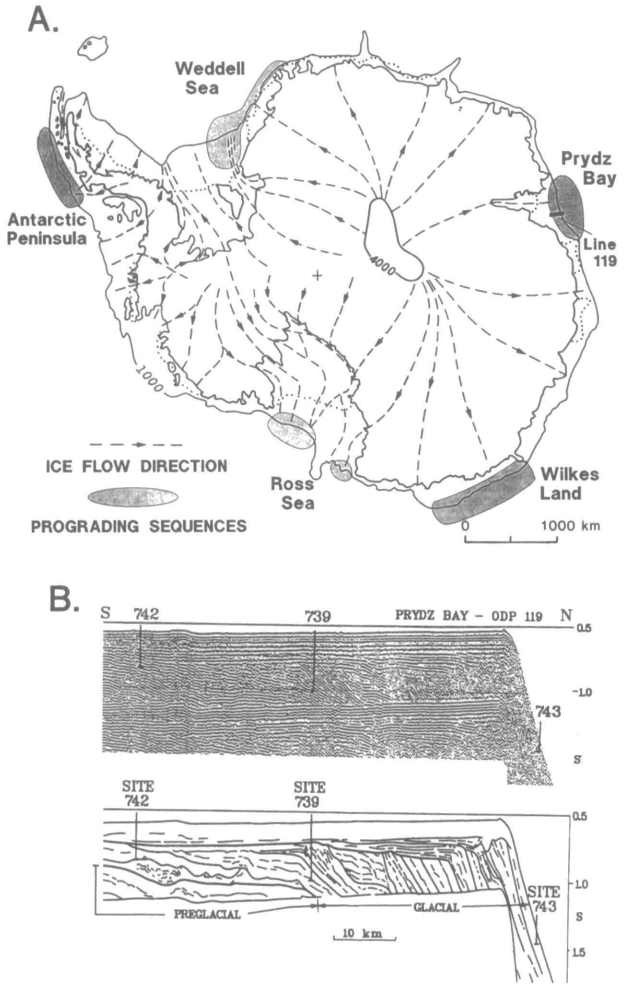

Figure 1. (*A*) Antarctic map showing ice-flow directions during last glacial maximum and locations of prograding sedimentary sequences; and (*B*) a profile across the prograding sedimentary sequences that were drilled in Prydz Bay on ODP Leg 119 (modified from Cooper et al. 1991b).

Block 1984; Haugland et al. 1985; Larter and Barker 1989; Cooper et al. 1991a). The Cenozoic sequences have been drilled on the continental shelves of the Ross Sea and Prydz Bay (figure 1b) and are composed of glacial-marine rocks, some of which are at least as old as early-Oligocene age.

The Cenozoic sequences have acoustic signatures suggesting that the grounded antarctic ice sheet has episodically advanced to the continental shelf edge, and retreated, many times during the Cenozoic. The geologic records left on the continental shelf by the waxing and waning of the ice sheet provide proximal information on ice volumes and paleoclimates (Barrett 1991). Deciphering these records and their correlation with the records of global sea-level variations (e.g., Webb et al. 1984; Bartek et al. 1991; figure 2) is the underlying goal of the ANTOSTRAT project.

The location and internal geometry of the offshore Cenozoic sequences are controlled by many factors including tectonics, supply, distribution, and compaction of sediments, crustal flexure and sediment redistribution by fluctuating grounded ice sheets, and sea level change. All factors must be considered to separate and ascertain the absolute sea-level record (Anderson et al. 1983; Cooper et al. 1991a). For example, as a result principally of ice erosion and limited sediment supply, most parts of the antarctic continental shelf lie in water depths greater than 400 meters, which is too deep to expose the shelf to subaerial erosion during common sea-level fluctuations of 100-300 meters. Yet, such sea-level fluctuations may be directly linked to the size and extent of the antarctic ice sheets, which can reach thicknesses sufficient to erode even the deepest parts of the continental shelf.

In April 1989 the ANTOSTRAT project was initiated under the auspices of the Scientific Committee on Antarctic Research (SCAR) Group of Specialists on the Evolution of Cenozoic Paleoenvironments of the Southern High Latitudes. The purpose of the project was to facilitate the coordination of existing and future acoustic and geologic data from the antarctic continental margin, and to achieve a better understanding of the relationships between Cenozoic terrestrial and marine glacial-interglacial histories, and between Cenozoic ice-volume and global sea-level variations. The project is overseen by a nine-member international steering committee guided by advice from the geoscience community. ANTOSTRAT functions in advisory and coordinating roles to assist national antarctic-geoscience programs. Scientific interchange within ANTOSTRAT is achieved through workshops and regional working group meetings and cooperative projects. Although many data com-pilations exist for Antarctica (e.g., Hayes 1991), ANTOSTRAT is the first major effort to combine existing data (many unpublished), to help coordinate future studies, and to work toward answering important Cenozoic questions (e.g., Webb 1990).

The first ANTOSTRAT workshop was held in June 1990 to display existing data holdings and discuss factors controlling the deposition of offshore Cenozoic glacial strata (Cooper and Webb 1990). Working groups with regional coordinators were established for five regions of the Antarctic continental margin (Antarctic Peninsula, Ross Sea, Wilkes Land, Prydz Bay, and Weddell Sea; figure 1a) to facilitate multinational data compilations and investigations of regional problems.

The second ANTOSTRAT workshop was held in April 1991 to discuss and design procedures for the use and dissemination of antarctic multichannel seismic reflection data (MCS)(figure 3), which are critical for defining the detailed structure and evolution of the earth's crust. By consensus, a new Antarctic seismic data library system (SDLS) for cooperative research was designed (and later adopted by the October 1991 Antarctic Treaty Consultative Meeting as Resolution XVI-12), and will make MCS data openly available for viewing at library branches worldwide. Initially, two branches will be in the U.S. at Menlo Park, California and Reston, Virginia.

Under SDLS guidelines (Cooper et al. 1992) MCS data can be used in cooperative studies with data collectors 4 years after the time of data collection, with some restrictions, and MCS data will be available for unrestricted use eight years after data collection. SDLS time guidelines do not supersede U.S. or other national guidelines, which may require shorter times for dissemination of data.

A third ANTOSTRAT workshop was held September 1991 to design procedures for compilation and coordination of data sets and for making offshore stratigraphic maps in the five targeted regions of the antarctic continental margin. Techniques and locations for possible scientific drilling, sea-floor coring, and dredging were outlined to lay the groundwork for acquiring data on ages and on depositional environments of the Cenozoic prograding sequences.

Future thematic workshops are planned. Geoscience researchers who wish to contribute data and ideas are encouraged to participate. The greatest benefits to antarctic Cenozoic geosci-

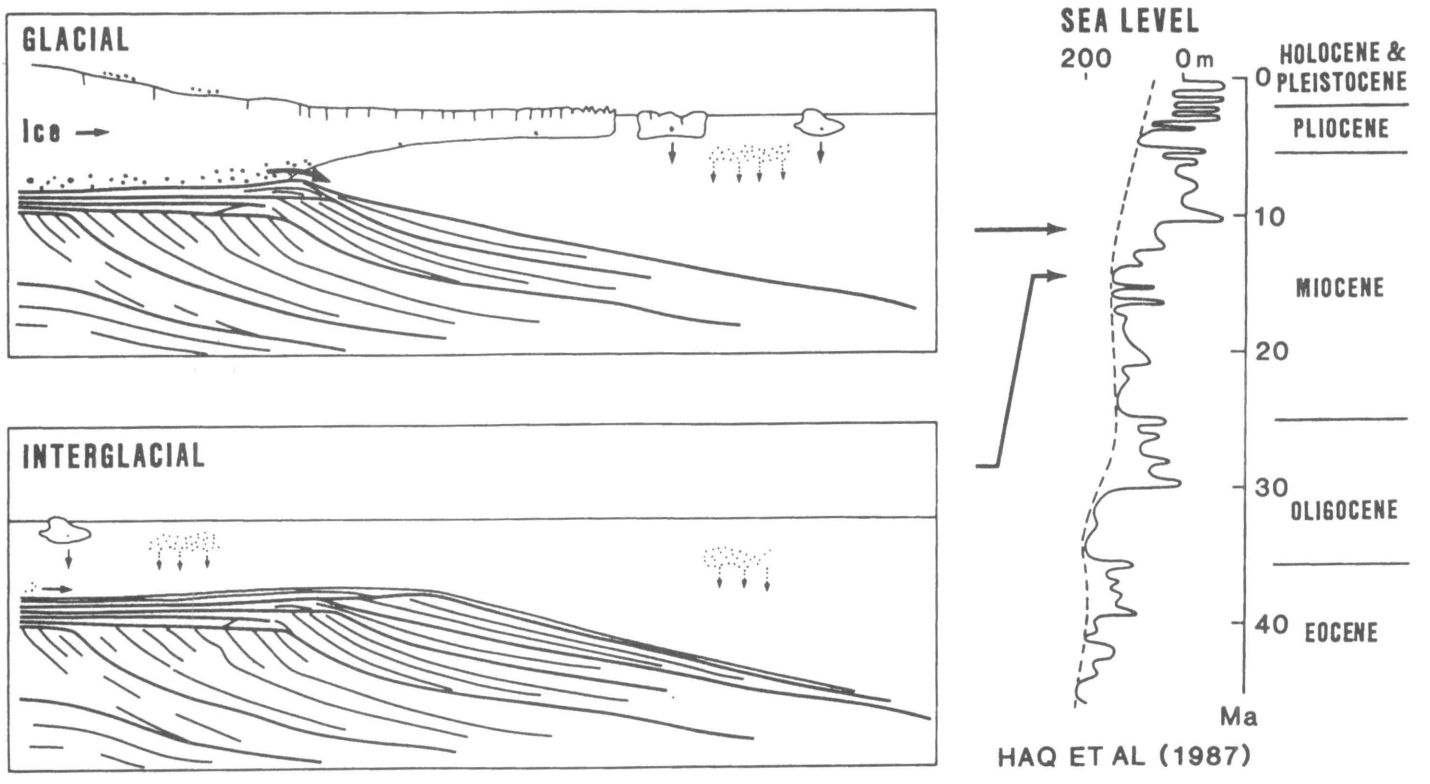

Figure 2. Model for deposition of prograding sedimentary sequences by grounded ice sheets and their inferred relationship to global sea-level fluctuations (from Cooper et al. 1991a).

ence will come from coordinated studies, which ANTOSTRAT advocates and hopes to facilitate. This research was partly supported by National Science Foundation grant DPP 90-10852.

References

Anderson, J. B., C. Brake, E. Domack, N. Myers, and R. Wright. 1983. Development of a polar glacial-marine sedimentation model from antarctic Quaternary deposits and glaciological information. In B. Molnia (Ed.), *Glacial Marine Sedimentation*, 233-265.

Barrett, P. J. 1991. Antarctica and global climate change—a geological perspective. In B. Harris and B. Stonehouse (Eds.), *Antarctica and Global Climatic Change*. Cambridge: Scott Polar Research Institute and Belhaven Press, 35-50.

Bartek, L. R., P. R. Vail, J. B. Anderson, P. A. Emmet, and S. Wu. 1991. The effect of Cenozoic ice sheet fluctuations in Antarctica on the stratigraphic signature of the Neogene. *Journal of Geophysical Research*, 96 B4:6,753-6,778.

Behrendt, J. C. 1990. Multichannel seismic reflection surveys over the antarctic continental margin relevant to petroleum resource studies. In B. St. John (Ed.), *Antarctica as an Exploration Frontier—Hydrocarbon Potential, Geology, and Hazards*. Tulsa: American Association of Petroleum Geologists, 69-76.

Cooper, A. K. and P. N. Webb (Eds.). 1990. International Workshop on Antarctic Offshore Acoustic Stratigraphy (ANTOSTRAT): Overview and Extended Abstracts. *U.S. Geological Survey Open-File Report 90-309*, Menlo Park, 290.

Cooper, A. K., P. J. Barrett, K. Hinz, V. Traube, G. Leitchenkov, and H. M. J. Stagg. 1991a. Cenozoic prograding sequences of the antarctic continental margin: A record of glacio-eustatic and tectonic events. *Marine Geology*, 102:175-213.

Cooper, A. K., H. M. J. Stagg, and E. Geist. 1991b. Seismic stratigraphy and structure of Prydz Bay, Antarctica: Implications from Leg 119 drilling. In J. Barron and B. Larson et al. (Eds.), *Proceedings of the Ocean Drilling Program, Scientific Results*, V.119. College Station, Texas, 5-25.

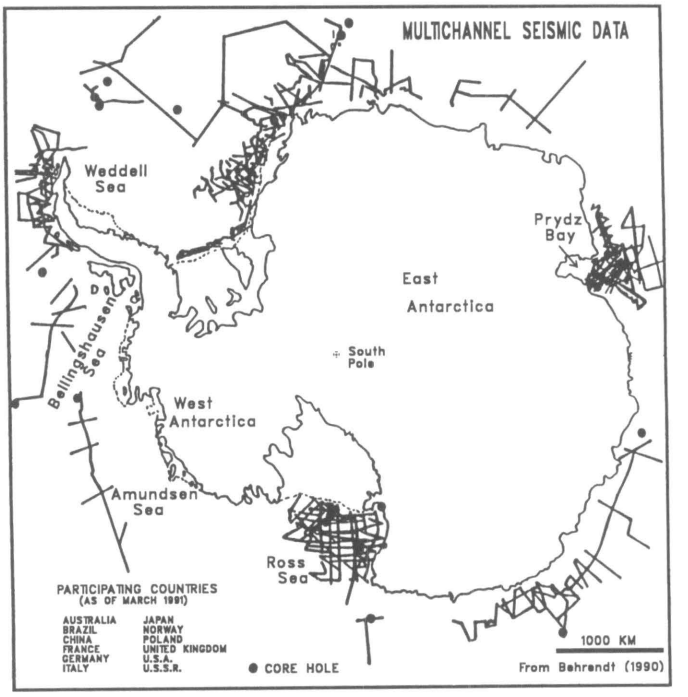

Figure 3. Map of multichannel seismic-reflection profiles across the antarctic continental margin.

Cooper, A. K. and the ANTOSTRAT Steering Committee. 1992. A SCAR seismic data library system for cooperative research: Summary report of the international workshop on antarctic seismic data. *SCAR Report* No. 9, August 1992. Cambridge, England: Scott Polar Research Institute.

Haugland, K., Y. Kristoffersen, and A. Velde. 1985. Seismic investigations in the Weddell Sea embayment. *Tectonophysics*, 114:293-313.

Haq, B. H., J. Hardenbol, and P.R. Vail. 1987. Chronology of fluctuating sea levels since the Triassic. *Science*, 235(4793):1,156-1,167.

Hayes, D. (Ed.). 1991. Marine Geological and Geophysical Atlas of the Circum-Antarctic to 30 degrees south. *Antarctic Research Series*, V. 54. Washington, D.C.: American Geophysical Union.

Hinz, K. and M. Block. 1984. Results of geophysical investigations in the Weddell Sea and in the Ross Sea, Antarctica. *Proceedings of 11th World Petroleum Congress*, London, England, PD 2, 279-291.

Larter, R. D. and P. F Barker. 1989. Seismic stratigraphy of the Antarctic Peninsula Pacific margin: Record of Pliocene-Pleistocene ice volume and paleoclimate. *Geology*, 17:731-734.

Webb, P. N. 1990. The Cenozoic history of Antarctica and its global impact. *Antarctic Science*, 2(1): 3-21.

Webb, P. N., D. M. Harwood, B. C., McKelvey, J. H. Mercer, and D. Stott. 1984. Cenozoic marine sedimentation and ice-volume variation on the east antarctic craton. *Geology*, 12:287-291.

Index of Authors

Ackley, S. F., 87, 89, 91, 93, 95, 109, 111
Andreas, Edgar L., 115
Adriani, Alberto, 274
Ahlen, S. P., 320
Alley, Richard, 50
Amos, A. F. 175, 228, 230
Anderson, John, 71
Arakelian, T., 296
Arnoldy, R. L., 299
Azam, Farooq, 125, 127
Babenko, A. N., 43
Baker, Karen S., 250, 253
Balois, J. Y., 187
Barry, James P., 330
Beaulieu, S., 183
Beck, J. R., 299
Behrendt, John C., 40
Bell, D., 89, 111
Belinne, D. J., 314
Benbrook, J. R., 304, 307
Bengtson, John L., 213
Benoit, Paul H., 28
Bentley, C. R., 43
Bering, Edgar A., 304, 307
Berkman, Paul A., 134
Berthelot, B., 202
Bidigare, Robert R., 119
Bieber, John W., 318
Bindschadler, Robert A., 47
Booth, Charles R., 338
Borns, Harold W. Jr., 51
Boroughs, T. J., 30
Bosch, Isidro, 121
Boucher, Lisa D., 2
Boucher, Nicholas P., 242
Boveng, Peter L., 213
Braaten, David A., 282
Brody, E., 160
Bromwich, David H., 289, 291
Browne, David W., 134
Brown-Leger, Susan, 263
Buchanan, D., 30, 31
Burgett, J., 166, 177
Butcher, Theresa L., 145
Butler, J. H., 269
Bryan, Jonathan R., 341
Byrne, G. J., 307
Cahill, L. J. Jr., 299
Carlson, R. W., 296
Carrasco, Jorge F., 289
Casco, Stella M., 223
Castillo, B., 328
Chadwick, R., 307
Chappell, Mark A., 145
Christian, James R., 170
Claffey, Keran J., 115
Clarke, T. S., 43
Close, Ann R., 131
Cochlan, William P., 225
Cole, Brian E., 127
Cooper, A. K., 343
Crockett, Elizabeth L., 143
Croll, Donald A., 213
Cullen, John J., 122
Cummings, S. O., 269
Danielson, Alice, 85
Darling, M. N., 87, 91, 328
DeFord, J. W., 320
DeMaster, David J., 74, 77
Demer, David A., 210
Denton, George H., 55
Deschamps, P. Y., 187, 197
Deshler, Terry, 274
Detrich, H. William III, 139
Deuzé, J. L., 191, 197, 199
Devaux, J. C., 193
DiTullio, Giacomo R., 131, 135
Doolittle, John H., 323
Domack, Eugene W., 63, 64, 66, 71
Dore, J. E., 164, 166, 177
Douglas, Hector D., 213
Dreschoff, G. A. M., 282
Du, Yang, 291
Dunbar, Robert B., 79
Dunlap, Walter C., 121
Duvall, T. L. Jr., 322
Elder, B., 111
Elkins, J. W., 269
Engebretson, M. J., 299
Etnier, Shelly, 131
Evenson, Paul, 318
Fastook, J. L., 35
Faure, Gunter, 11, 30, 31
Feffer, P. T., 325
Feldmann, Rodney M., 19, 20
Fernandes, Luiz, 226
Ferrario, Martha, 158
Few, A. A., 307
Filkorn, Harry F., 20
Fitzgerald, Paul G., 12
Foster-Springer, Kate, 333
Fraser, W. R., 249
Frazer, Thomas K., 137, 249
Freeman, T., 301
Fritsen, C. H., 113
Frouin, R., 187, 191, 193, 195, 197, 199, 202, 205
Gaier, Todd, 316
Gautier, Catherine, 276
Geren, M., 166
Ghidella, Marta E., 68
Goebel, Michael E., 213
Goehringer, Dale D., 263
Goldstone, Jed, 122
Goloub, Philippe, 191, 197, 199
Gonzales, A., 183
Gordon, Arnold L., 97, 99, 100
Gordon, Louis I., 72
Gow, A. J., 87, 89
Griffith, C. R., 328
Grootes, P. M., 57
Grunow, A. M., 14
Gundersen, Joshua, 316
Gunn, John T., 108
Haberman, Karen L., 244
Hacecky, Karen L., 244
Hagen, E. H., 31
Hall, B. D., 269
Hall, Brenda L., 55
Hammer, William R., 1
Handley, Phil, 253
Harvey, J. W., 322
Harvey, R. P., 26
Harwood, David M., 3
Heine, John, 129
Helbling, E. Walter, 217, 219, 221, 223
Herman, M., 187, 191, 197, 199
Hermanto, Rony, 195
Hernandez, G., 314
Heuberger, Renate, 278
Hewitt, Roger P., 209, 210
Hickerson, William J., 1
Hofmann, Eileen E., 239
Hollibaugh, James T., 125, 127
Holm-Hansen, O., 153, 154, 160, 175, 219, 221, 223
Holt, Rennie S., 209
Houlihan, T., 166
Houston, Brent R., 249
Howes, Brian L., 263
Howington, James P., 330
Huber, Bruce A., 99, 100
Huntley, M. E., 153, 172, 175, 179, 181, 183
Hwang, Kelley K., 250
Ishman, Scott, 64
Ivanov, Boris V., 115
Jacobel, Robert W., 47
Jacobson, Aubrie, 131
Janes, Donald N., 145
Janosy, Robert J., 9
Janssen, John, 142, 213
Jeffries, M. O., 83, 85
Jeffries, S. M., 322
Jiang, Xinhe, 3
Johnson, K., 31
Johnson, K. S., 11
Kang, Sung-Ho, 119
Karentz, Deneb, 121
Karl, D. M., 164, 166, 168, 170, 175, 177
Kaupp, S., 172
Keimel, B. M., 148
Keller, Randall A., 22
Kennicutt, Mahlon II, 331, 333, 335
Khalil, M. A. K., 267
Kjome, Norman T., 279
Klinck, John M., 239
Können, G. P., 293
Krahn, Margaret, 333
Kyle, Philip R., 271
LaBelle, J., 309
LaBrecque, John L., 68
Lascara, Cathy M., 239
Lavender, M. K., 228
Lesser, Michael P., 122
Letelier, R., 166, 177
Leventer, Amy, 79
Levine, Murray D., 105
Liao, B., 304
Lin, R. P., 301, 325

Lin, Zhongmin, 318
Lipschutz, Michael E., 25
Liu, C., 43
Lizotte, Michael P., 259
Loeb, Valerie, 173, 214, 217
Loomba, D., 320
Lopez, M. D. G., 172, 181, 183
Lord, N., 43
Lucas, Timothy B., 338
Lubin, Dan, 276
Lukin, Valery V., 97
Lytle, V. I., 87, 89, 91, 93, 109, 111
Macheret, Y. Y., 43
Magaard, U., 166
Makshtas, Aleksandr, 115
Manley, Scott W., 213
Martin, P., 148
Martinson, Douglas G., 99, 102, 103
Mashiotta, T. A., 66
Mathieu, G., 117
McCarthy, M., 301
McClennen, Charles, 71
McClintock, James B., 129
McDonald, S. J., 331, 333, 335
McDonald, T. J., 335
McFeters, Gordon A., 330
McPhee, Miles G., 102, 103
Mende, S. B., 299
Mensing, T. M., 11
Menzies, David, 250
Miller, Gary D., 148, 150
Mitchell, B. G., 160, 162
Moline, Mark, 242, 245
Morales, E., 328
Mordy, C. W., 113
Morehead, Mark D., 108
Morison, James H., 102, 103
Morris, G. A., 307
Morris, K., 83
Morrison, John M., 77
Morrow, John H., 338
Morse, D. L., 59
Moylan, Thomas, 137
Muench, Robin D., 108
Mullen, Roy R., 342
Mullins, Jerry L., 342
Mulvaney, R., 38
Murcray, F. J., 278
Neale, Patrick J., 122
Nelson, David M., 72
Nelson, K. E., 47
Newberger, Timothy, 244, 253
Nittrouer, Charles A., 74, 77
Nordhausen, W., 179, 181
Novick, A. N., 43
Oglesby, R. J., 35
Oltamans, S. J., 279
Ondrusek, Michael E., 119
Padman, Laurie, 102, 105
Palinkas, Lawrence A., 327
Panouse, M., 185, 187, 193
Parks, G. K., 301
Parish, Thomas, 287
Parrish, G., 166, 177
Paterson, Donna R., 249
Pearse, John S., 132
Pearse, Vicki B., 132
Peel, D. A., 38
Perl, P. J., 183
Pierson, Geoffrey H., 74, 77
Place, Allen R., 147
Polk, Scott M., 131
Pomerantz, M. A., 322
Pook, Michael, 284
Pope, Robert H., 74
Prentice, M. L., 35, 51
Prezelin, Barbara B., 242, 244, 245
Priddle, J., 187
Priscu, John C., 257, 259, 260
Quetin, Langdon B., 137, 235, 244
Rairden, R. L., 299
Rasmussen, R. A., 267
Raymond, Charles, 38
Redfield, Thomas F., 12
Reynolds, Stephen J., 12
Rice, S., 320
Roby, Daniel D., 147
Rosen, James M., 279
Rosenberg, Jane E., 209
Rosenberg, Theodore J., 299, 309, 312
Ross, Robin M., 137, 235, 244
Roth, Joyce, 28
Ruzicka, James J., 140
Sala, Livio O., 217
Salamon, M. H., 320
Sar, Eugenia, 158
Schreer, Jason F., 152
Scheppe, Kai, 242, 245
Schere, Eric, 71
Schlezinger, David R., 263
Schlosser, Peter, 117
Schuster, Jeffrey, 316
Schutt, J. W., 26
Sears, Derek W. G., 28
Sears, Hazel, 28
Seydel, Keith, 242, 245
Sharp, Thomas R., 257
Shoemaker, Vaughan H., 145
Sidell, Bruce D., 143
Siegel, Volker, 214
Silva S., Nelson, 219
Singh, S. P., 309
Slattery, Marc, 129
Smethie, William M. Jr., 117
Smith, D., 301
Smith, David C., 125, 127
Smith, James J., 330
Smith, Raymond C., 236, 250, 253
Smith, R. W., 314
Smith, Walker O. Jr., 131, 135
Smoak, Joseph M., 74
Smythe, W. D., 296
Sosik, Heidi M., 162
Stearns, Charles R., 280, 285
Steel, G. Daniel, 327
Steig, E. J., 57
Stephens, Elise, 242
Steward, Greig F., 125, 127
Strelin, Jorge A., 22
Stroeven, Arjen P., 51
Stump, Edmund, 12
Suedfeld, Peter, 327
Sullivan, C. W., 113
Swanson, T. H., 269
Swayzer, R., 328
Sweet, S. T., 331
Szyper, J. P., 166, 168, 177
Taylor, Edith L., 2
Taylor, Jan R. E., 147
Taylor, Thomas N., 2
Testa, J. Ward, 152
Thomas, N., 2
Tien, G., 166, 177
Thompson, T. M., 269
Trivelpiece, Wayne Z., 249
Venkatesan, M. I., 66
Vernet, M., 154, 157, 160, 162, 175
Verwaerde, Claude, 187
Villafañe, Virginia E., 221, 223
Waddington, E. D., 59
Wallace, G. E., 148
Wang, Zhou, 312
Waters, Kirk J., 236, 250
Webb, P. N., 343
Weertman, B. R., 38
Weidner, George A., 280, 285
Wendler, Gerd, 284
Weppernig, Ralf, 117
Werden, S., 301
Weston, James, 129
Whillans, Ian M., 45
Wilson, Terry J., 6, 9
Wong, Patricia S., 127
Wormuth, John H., 226
Yankielun, N. E., 87, 95
Yeager, Marilyn, 226
Zhou, M., 179
Zreda-Gostynska, Grazyna, 271

U.S. ANTARCTIC RESEARCH PROGRAM
1991-92
LOCATIONS OF MAJOR ACTIVITIES

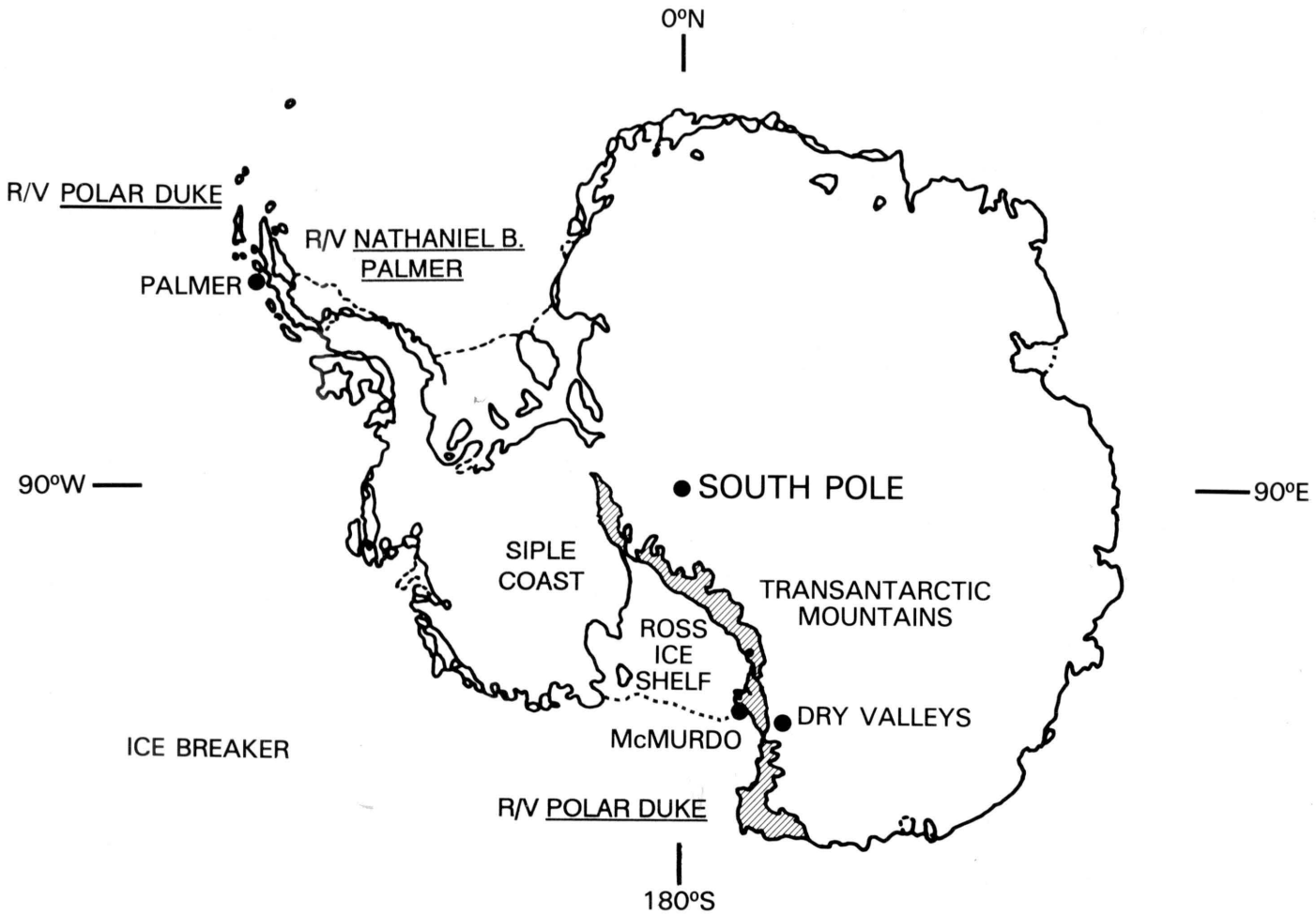

Back cover. East Base on Stonington Island near the Antarctic Peninsula was built in 1940 by the U.S. Antarctic Service Expedition. The oldest remaining U.S. station in Antarctica, it was declared an historic monument by representatives of the Antarctic Treaty Consultative Parties in 1989. As the second phase of the U.S. effort to clean-up and reclaim this historic site, archaeologists and historians from the National Science Foundation (NSF) and the National Park Service, along with employees of NSF's antarctic support contractor, went to Stonington Island in March 1992 to document the artifacts remaining at the site and restore the buildings that still stand there. Their work included organizing and setting up an interpretive display, designed to help visitors to the base understand the types of research conducted at the station. (NSF photograph by Noel Broadbent, Office of Polar Programs.)

NATIONAL SCIENCE FOUNDATION
WASHINGTON, D.C. 20550

NSF 93-84